



New generation of "bulk" catalyst precursors for hydrodesulfurization synthesized in supercritical fluids

Manuel Théodet

► To cite this version:

Manuel Théodet. New generation of "bulk" catalyst precursors for hydrodesulfurization synthesized in supercritical fluids. Material chemistry. Université Sciences et Technologies - Bordeaux I, 2010. English. NNT : 2010BOR14092 . tel-00559113

HAL Id: tel-00559113

<https://theses.hal.science/tel-00559113>

Submitted on 24 Jan 2011

HAL is a multi-disciplinary open access archive for the deposit and dissemination of scientific research documents, whether they are published or not. The documents may come from teaching and research institutions in France or abroad, or from public or private research centers.

L'archive ouverte pluridisciplinaire **HAL**, est destinée au dépôt et à la diffusion de documents scientifiques de niveau recherche, publiés ou non, émanant des établissements d'enseignement et de recherche français ou étrangers, des laboratoires publics ou privés.



Distributed under a Creative Commons Attribution - NonCommercial - NoDerivatives 4.0 International License

THÈSE

présentée à

L'UNIVERSITÉ BORDEAUX I

ÉCOLE DOCTORALE DES SCIENCES CHIMIQUES

Par **Manuel THEODET**

Ingénieur ENSCPB

POUR OBTENIR LE GRADE DE

DOCTEUR

SPÉCIALITÉ : Physico-Chimie de la Matière Condensée

NOUVELLE GENERATION DE PRECURSEURS « BULK » DE CATALYSEUR
D'HYDRODESULFURATION SYNTHETISES EN MILIEU FLUIDE SUPERCRITIQUE

NEW GENERATION OF « BULK » CATALYST PRECURSORS FOR
HYDRODESULFURIZATION SYNTHESIZED IN SUPERCRITICAL FLUIDS

Co-superviseurs de recherche : Cristina Martínez & Cyril Aymonier

Soutenue le 03 Novembre 2010

Après avis favorable de :

M. E. PALOMARES, *Professor, UPV, Valencia, Spain*
M. M. TÜRK, *Professor, KIT, Karlsruhe, Germany*

Rapporteurs

Devant la commission d'examen formée de :

M. C. DELMAS, *Directeur de Recherche, CNRS, Bordeaux, France*
M. J. ETOURNEAU, *Professeur émérite, Université Bordeaux I, Bordeaux, France*
M. C. AYMONIER, *Chargé de Recherche, CNRS, Bordeaux, France*
M. F. CANSELL, *Professeur, IPB, Bordeaux, France*
M. A. CORMA, *Professor, ITQ, UPV-CSIC, Valencia, Spain*
Mme. C. MARTINEZ, *Tenured scientist, ITQ, UPV-CSIC, Valencia, Spain*
M. E. PALOMARES, *Professor, UPV, Valencia, Spain*
M. M. TÜRK, *Professor, KIT, Karlsruhe, Germany*
M. D. UZIO, *Chercheur R&D, IFP, Lyon, France*

Président
Rapporteur
Examineurs

**Il faut
parfois savoir
sauter dans
l'inconnu!**



General Summary

Acknowledgements 7

Introduction 13

References 18

I - Hydrodesulfurization and SCFs opportunities 21

I.1. Hydrodesulfurization (HDS): a general overview 25

I.2. Supercritical fluids 56

I.3. Conclusion..... 76

I.4. References 78

II - Synthesis of HDS catalyst precursors in SCFs..... 103

II.1. Experimental section..... 107

II.2. Results..... 114

II.3. Conclusion 161

II.4. References..... 163

III - Catalytic tests..... 167

III.1. HDS: experimental setup and parameters 171

III.2. Catalytic activity checking 185

III.3. Experiments with HDS-specific reactor 188

III.4. Tests on real feed..... 203

III.5. Conclusion 209

III.6. References 210

Conclusion 213

Appendices 219

Appendix I. Process families in a refinery plant 223

Appendix II. Process providing hydrotreatment feedstocks..... 224

Appendix III. Hydrodesulfurization 228

Appendix IV. Characterization techniques..... 232

References 245

Acknowledgements

So this is the time for a personal word. During those 3 years and 10 months of PhD at the **Institut de Chimie de la Matière Condensée de Bordeaux** and at the **Instituto de Tecnología Química** de Valencia (not that I counted the days but...) I have met a lot of people outside and inside the work sphere that contributed to make this adventure possible and enjoyable. So the purpose of these pages (probably the most read pages) is to say thank you to every single person who took part in the success of this work.

In the first place, I am anxious to thank **Mr. Claude DELMAS**, director of the **ICMCB**, for welcoming me within his institute in Bordeaux and for having accepted to preside at the assessment committee of my defense.

In the same manner, I would like to express my sincere gratitude to **Mr. Avelino CORMA**, director of the **ITQ**, for having provided me with this enriching opportunity to collaborate with him in Valencia, for his interest and precious advice and ideas all along my stays in Spain.

I am also grateful toward **Mr. Eduardo PALOMARES** and **Mr. Michael TÜRK** for taking the time to assess my manuscript. Your advices for some final corrections were greatly appreciated. My regards also go to **Mr. François CANSSELL**, my research director who even though hardly present always had an interest in my work or a kind encouraging word and **Mr. Denis UZIO** for making me the honor of being members of my assessment committee.

I feel deeply obliged toward **Mr. Jean ETOURNEAU**, not only for accepting to be in my assessment committee but mostly for enabling the collaboration between the two institutes and the existence of this project via the Functional Advanced Materials Engineering network of excellence (**FAMEnoe**, today's **European Multifunctional Materials Institute**). I am proud having been part of the EMMI family, during the thesis but also the few months following the defense.

My heartiest thanks go to my two supervisors, **Mr. Cyril AYMONIER** and **Mme. Cristina MARTÍNEZ**. Cyril, thank you for welcoming me in your group, giving me the opportunity to develop this experience abroad and for letting me idle hands to work on extra-thesis time consuming associative projects. Your constant enthusiasm and confidence in my work allowed me to push through and complete this thesis. Cristina, being in the chaos of moving

from a place to another, completely unknown in the first time, be it from the language, the city, the lab or the scientific field, is a tough challenge you helped me to get through with your natural kindness and constant cheering, and overcoming with you those numerous difficulties we encountered in such a short time has been enriching experience. Finally I want to thank both of you since in the last months of this project, your writing skills and diligence for the corrections of my manuscript helped relieve many writing blocks.

Although doing a PhD is somehow a lonely process, you need many people to collaborate with, whose skills allow the project to mature, all the more when such a project is carried out between two labs from different countries and different scientific culture. Christine, Dominique, Eric, Laëtitia, Patrick and Sonia (ICMCB), Estefanía, Amparo, Maria-Jesús, Maria-Isabel (ITQ), your help in characterizing and analyzing my materials, your ideas, techniques and positive vibrations were greatly appreciated. Stan, I thank you for your time, patience and considerate attitude. I deeply appreciate your help overcoming my ignorance in Rietveld refinement. Mélanie as well as Jérôme, a shared *laissez* to thank you both for your precious help and advices not only concerning microscopy but also in the manner completing and valorizing my work, drawing my attention on the most important and valuable results, plus a special wink at Daïky. I also want to thank Elisabeth (CREMEM) for her energetic help in microscopy and Odile (ISM) for her kind help and our everyday life discussions.

There are always people who act their own way to make your research conditions as comfortable as possible. Fabien, Bernard (x2), Daniel, Paulo, Sandrine, Carole, Juan, Javier (x2), Maria-Jesus, Bixente, Ricardo, thank you for facilitating my life all along those years at the two institute, and to you Jacques, who had to support me and my whims.

It was a pleasure to share doctoral studies, life and morning rituals of the coffee with all people from the group 7 and more particularly David who is my twin of thesis, one and only officemate, Cathel, Popo, Elsa, Sabine, Cédric (x2), Anne-Claire, Marion, Arnaud, Maxime, Antoine, Yves, Carole, Anne, Sam and all the trainees that worked with us, especially Rudy and Nico.

I cannot forget Lydia (twin sister), Stéph (vieux Toulou), Graziella (mother in law), Mona, Etienne, Marie-Hélène, Jean-Louis, Manu, Marianne, Laurent, Fernando who helped me go through this work by their encouragements, backup and precious advices, and Lance for

reading and correcting my English grammars and vocabulary making this thesis easier to read and of more acceptable quality.

I have been fortunate to come across many funny & good friends, sometimes best friends, without whom life would be bleak. However, when come the time of the acknowledgements, I sometimes feel cursed! I could write pages of anecdotes for each of you guys! Jeannot, Charly, Grego (my bear roomy), our Asian tours will always be engraved in my mind as well as all those good time shared from the very beginning of the thesis. My dear friends Dawid and Math, roller skating on the quays of Bordeaux and evenings at the “Cave belge” or “Titi twister” are just perfect souvenirs. To all friends I met at the ICMCB: Sandrine, Alex, Jerem, Sam, Kevinou, Cécile, Manu, Elias, Aurélien, Cinta, Aurélie, Guillaume, Math, Annelise, Seb, Oliv’, Lionel, Tib, Rémy, Cindy, Nico L, etc... to all friends I met at the ITQ: Rut, Imma, Ernest, Yannick, Younes, Manu, Piotr, Froso, Michael, Bastian, Belen, Rebeca, Stefi, Selene, Salva, Victor, Matthias, Richard, etc... to all friends met thanks to the two student associations I took part during my thesis, ADoC and Aquidoc, especially, Adrien, Flu, Benjamin (where is my vine stock?), Pascal, Charles, Mathilde, Claire, Marion, and many, many more, I wish to express my deep feelings.

I finally want to address special thanks and love to my very close friends from the Pimousse Team™: Romain, Iona, Nico, Etienne, Cécile, Clémence, Nico nico, Seb and the very good friends gravitating around and of course my family and especially my mother, father and sister.

Looking back, I am surprised and at the same time very grateful for all I have received and wonderful people I met throughout these years. It has certainly shaped me as a person and has led me where I am now. All these years of PhD studies are full of such gifts... It is now high time to turn over a new leaf of my life and write the first lines of a new adventure...

Introduction

The Kyoto Protocol of 1998 to the United Nations Framework Convention on Climate Change strengthens the international response to this particular issue. The developed countries committed themselves to reduce their collective emissions of six key greenhouse gases by at least 5 %, a target to be achieved during the period 2008-2012 and measured against either a 1990 or 1995 baseline [1]. Despite the failure of the Copenhagen accord in unifying the member states of the United Nations on clear reduction objectives in 2009 [2], the will to urgently combat climate change is still topical. Road vehicles are increasingly reliant upon catalytic after-treatment devices to attain the emissions limits taken against air pollution. The adverse effect of sulfur in petrol and diesel fuels on the effectiveness of catalytic exhaust gas after-treatment technologies is well established [3-7]. Accordingly a reduction in the sulfur content of petrol and diesel fuels is likely to have a larger impact on exhaust emissions than changes to the other fuel parameters.

Therefore, increasingly stringent environmental regulations will require significant reductions in sulfur in distillate fuels. For example, according to the Directive 98/70/EC of the European Parliament and of the Council relating to the quality of petrol and diesel fuels and its amendments and evolutions [8-13], the proposed sulfur limit for distillate fuels to be marketed in the European Union for the year 2011 is 10 wppm or less. Similar measures are taken in Japan (10 wppm) and in North America (15 wppm). Such levels correspond to the removal of +99.99 % of sulfur from typical crude containing 1.5 wt% sulfur, and the removal process has been termed **deep or ultra-deep hydrodesulfurization (Deep-HDS)**.

The final report of the Commission of the European Communities concerning the Directive 98/70/EC and dated from 2008 concludes on the observation that the monitoring of fuel quality in 2006 shows the specifications for petrol and diesel laid down in Directive 98/70/EC are in general met and very few overrun were identified [14]. However, as the supply of low sulfur, low nitrogen crudes decreases, refineries are processing crudes with greater sulfur and nitrogen contents at the same time that environmental regulations are mandating lower levels of these heteroatoms in final products. Given the refining industry's cyclical margin, refineries are today looking into more innovative ways of maintaining reasonable margins to quickly recover the investment they made and justify additional investment to cope with changes. Consequently, to meet the ultra-low sulfur requirements without expensive modifications to existing refineries, it will be necessary to design a new generation of catalysts with very high desulfurization activity, particularly for distillate fuels at low to medium pressure, catalysts to be run in the existing process units.

In this context, our objective was: a) to propose an original and innovative method to synthesize a new generation of HDS catalysts using supercritical fluids (SCFs), and b) to investigate the catalytic properties of these new materials. The idea was to take advantage of the specific properties of SCFs in material science to achieve the synthesis of a contaminant-free “bulk” HDS catalyst with a defined composition and developing a high specific surface area. The materials - as HDS catalyst precursors - were elaborated in France with the group “supercritical fluids” of the Institut de Chimie de la Matière Condensée de Bordeaux (ICMCB-CNRS) based at the Université de Bordeaux I (UB1), whereas the tests of their catalytic activity were carried out in Spain at the Instituto de Tecnología Química (ITQ-CSIC) located at the Universidad Politécnica de Valencia (UPV). This international and multidisciplinary collaboration was made possible thanks to the former Functional Advanced Materials Engineering Network of Excellence (FAMEnoe) granted by the EU 6th Framework Program and at the origin of the actual European Multifunctional Materials Institute (EMMI).

The multidisciplinary dimension of this project brings us to propose in the first chapter of this document a detailed description of: a) hydrodesulfurization (HDS) catalysis, from its function and process to the description of classical catalysts of the reaction, and b) chemistry in supercritical fluids for the design of advanced nanostructured materials and particularly the opportunities it provides for the design of oxides. This chapter permits to identify the issues the refinery industry faces today and highlight weaknesses in existing solutions that SCF technology is able to address and will outline this PhD project.

The second chapter presents the study of the synthesis using supercritical fluids of nanostructured NiMoO_4 and CoMoO_4 which are classical HDS catalyst precursors (the actual HDS catalysts being the sulfide form obtained by reduction of these oxides). This chapter falls into 3 main parts with first a description of our general synthesis and characterization approach, followed by the determination of our operating parameters illustrated by the presentation of our material NiMoO_4 . The last part investigates the influence of some experimental parameters over the characteristics of our powders: nature of the solvent (particularly choice of alcohol), cations ratio (excess of either Mo or Ni), and nature of the promoter (Ni or Co).

The third and last chapter deals with catalytic tests performed in parallel of the synthesis study. We first present our testing strategy explaining the choice and composition of a model feedstock simulating an oil fraction that could classically undergo deep-HDS and the detection techniques used to evaluate the catalytic activity of our materials. The considered model feedstock contains 500 wppm of sulfur (classical concentration of deep-HDS feedstock) and contains what we consider to be our reference compounds for this evaluation: dibenzothiophene (DBT) and 4,6-dimethyldibenzothiophene (4,6-DMDBT) which are among the most refractive sulfur compounds regarding HDS. This chapter investigates the influence of the composition of the powders, of a thermal pretreatment and of the promoter nature (Ni or Co) before opening the way for real feedstocks treatment, initiate by the hydrodesulfurization of a Light cycle oil.

References

- [1] United-Nations. Kyoto protocol to the united nations framework convention on climate change **1998**
- [2] United-Nations. Copenhagen accord to the united nations framework convention on climate change **2009**
- [3] Summers, J. C. and Baron, K. "The effects of SO₂ on the performance of noble metal catalysts in automobile exhaust." *Journal of Catalysis* **1979**. vol. 57, no. 3, 380
- [4] Lyons, J. S. M., Lax, D., and Welstand, S. "Investigation of sulfur sensitivity and reversibility in late-model vehicles." *Society of Automotive Engineers, Special Publication* **1999**. vol. SP-1478, 123
- [5] Engström, P., Amberntsson, A., Skoglundh, M., Fridell, E., and Smedler, G. "Sulphur dioxide interaction with NO_x storage catalysts." *Applied Catalysis B: Environmental* **1999**. vol. 22, no. 4, L241
- [6] Sedlmair, C., Seshan, K., Jentys, A., and Lercher, J. A. "Studies on the deactivation of NO_x storage-reduction catalysts by sulfur dioxide." *Catalysis Today* **2002**. vol. 75, no. 1-4, 413
- [7] Corro, G. "Sulfur impact on diesel emission control - a review." *Reaction Kinetics and Catalysis Letters* **2002**. vol. 75, 89
- [8] European Communities. 98/70/EC. Tech. rep. **1998**. Official Journal of the European Union L 350 dated from 28.12.1998, p. 58
- [9] European Communities. 2000/71/EC. Tech. rep. **2000**. Official Journal of the European Union L 287 dated from 14.11.2000, p. 46
- [10] European Communities. 2003/17/EC. Tech. rep. **2003**. Official Journal of the European Union L 76 dated from 22.3.2003, p. 10
- [11] European Communities. Regulation (EC) N° 1882/2003. Tech. rep. **2003**. Official Journal of the European Union L 284 dated from 31.10.2003, p. 1
- [12] European Communities. 2008/50/EC. Tech. rep. **2008**. Official Journal of the European Union L 152 dated from 11.6.2008, p. 1
- [13] European Communities. 2009/30/EC. Tech. rep. **2009**. Official Journal of the European Union L 140 dated from 5.6.2009, p. 88
- [14] European Communities. Report from the commission to the council and the European parliament Quality of petrol and diesel fuel used for road transport in the European Union: Fifth annual report (Reporting year 2006). Tech. rep. **2008**

Chapter I

Hydrodesulfurization and SCFs opportunities

I. Hydrodesulfurization and SCFs opportunities.....	21
I.1. Hydrodesulfurization (HDS): a general overview	25
I.1.1. HDS: place in today's refinery process.....	25
I.1.1.1. Petroleum refining and HDS feedstocks origin	27
I.1.1.2. Sulfur compounds in HDS feedstocks	29
I.1.2. Hydroprocessing	31
I.1.2.1. Hydrotreating	31
I.1.2.2. Hydrodesulfurization (HDS)	33
<i>I.1.2.2.1. General HDS reaction mechanisms</i>	<i>33</i>
<i>I.1.2.2.2. Deep-Hydrodesulfurization.....</i>	<i>36</i>
I.1.3. HDS catalysts	39
I.1.3.1. Conventional HDS catalysts	39
<i>I.1.3.1.1. Role of the support</i>	<i>40</i>
<i>I.1.3.1.2. Active phase and structure of supported HDS catalysts</i>	<i>41</i>
<i>I.1.3.1.3. Active sites and deactivation</i>	<i>44</i>
I.1.3.2. Deep-HDS issue.....	46
I.1.3.3. Advances in HDS catalyst	48
<i>I.1.3.3.1. Supported sulfide catalysts.....</i>	<i>48</i>
<i>I.1.3.3.2. Bulk catalysts.....</i>	<i>50</i>
I.1.3.4. Alternatives to HDS.....	53
I.1.4. Conclusion on HDS overview	54
I.2. Supercritical fluids	56
I.2.1. Definition and generalities	57
I.2.2. Synthesis of nanomaterials in SCFs	60
I.2.2.1. Formation of nanostructures in SCFs from a chemical reaction: principle ...	64
I.2.2.2. Process and operation parameters.....	67
I.2.2.3. Opportunity	71

I.2.3. Focus on oxides	73
I.2.4. Conclusion on SCFs opportunities.....	75
I.3. Conclusion.....	76
I.4. References	78

I.1. Hydrodesulfurization (HDS): a general overview

I.1.1. HDS: place in today's refinery process

The oil refining industry has considerably grown during the 20th century to become an important part of everyday modern activity. One of the main objectives of processing crude oil is to reduce their very high carbon/hydrogen ratio. Nowadays, there are many oil fields in the world and each of them produces crude oil of different quality based on different characteristics and presence of impurities (Table I.1).

Table I.1: Feedstock origin and properties [1]

	Crude oil					Commercially hydrotreated gas oil
	Nigeria Forcados	Brent	Syrian Light	Oural	Arabian Heavy	
Classification of crude	Naphthenic	Paraffinic	Paraffin	Intermediate	Aromatic	
<i>Properties</i>						
Boiling range, °C, (5–95%)	296–380	301–405	296–382	298–400	293–399	220–380
S-content (wt.%)	0.25	0.43	0.61	1.18	2.10	0.076
N-content (ppm by wt.)	359	343	271	509	421	60
Aromatic C ^a (%)	17	11	11	12	16	–
Density (g/ml)	0.882	0.857	0.849	0.877	0.879	0.840

Crude oil is a mixture of literally hundreds of hydrocarbon compounds ranging in size from the smallest, methane, with only one carbon atom, to larger compounds containing 200 or more atoms of carbon (Figure I.1 a). Not all compounds contained in the crude oil are pure hydrocarbons. The crude oil also contains certain impurities such as sulfur (Figure I.1 b), nitrogen, oxygen, and metals. By far the most common of these impurities are the organic sulfur compounds called mercaptanes. The sulfur compounds with more complicated structure also exist such as disulfides, thiophenes, benzothiophenes, dibenzothiophenes and their substituted analogues [2], compounds that particularly attract our attention for this project.

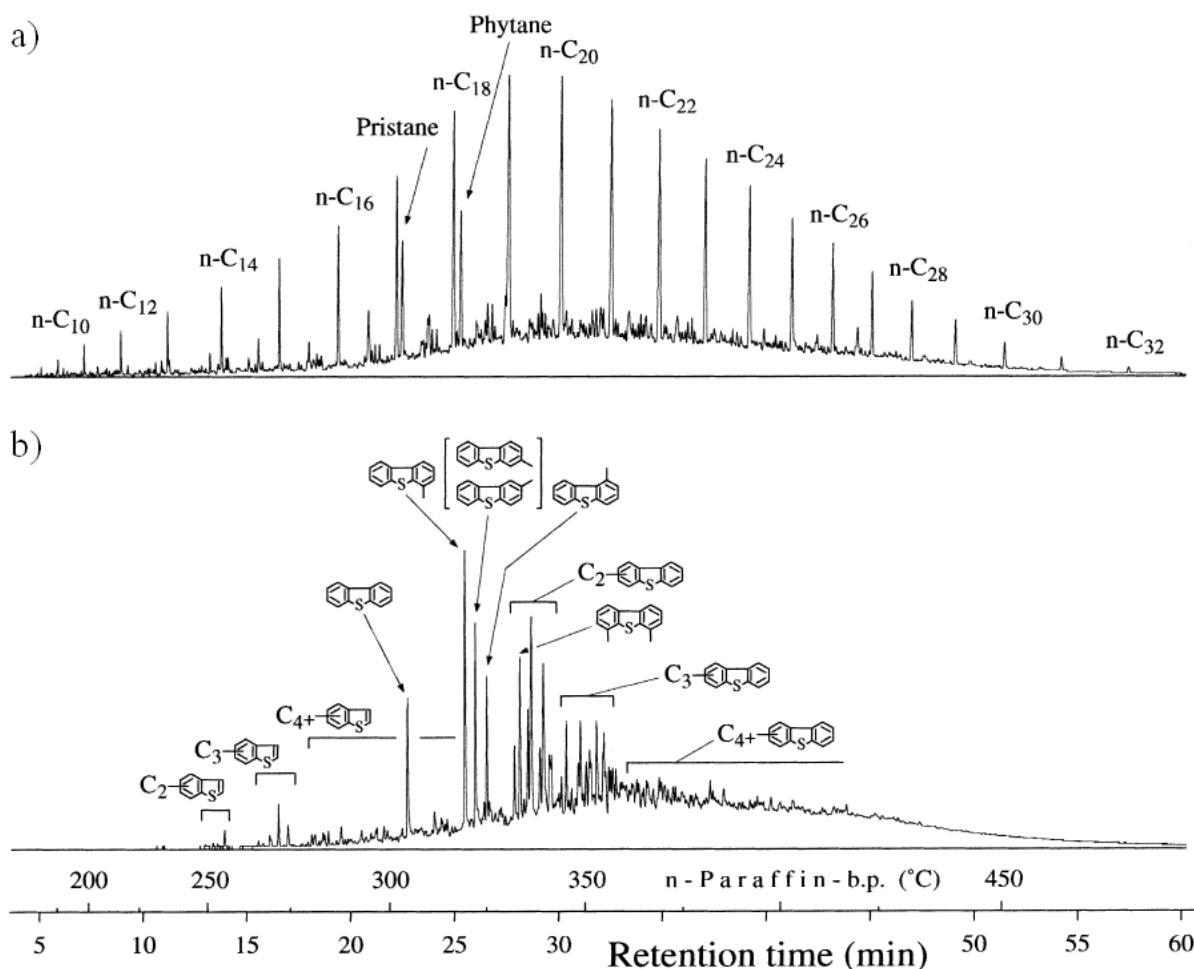


Figure I.1: Profile of the Brent heavy gas oil (see Table I.1) a) carbon-specific chromatogram & b) sulfur-specific chromatogram [1]

Other organic impurities are unsaturated hydrocarbons. Olefins, which are usually not present in the original crude oil, but are often formed during the refining process, are unstable and readily combine with themselves or other similar compounds to form polymers, resulting in insoluble gums and cause major problems within gas-station deposits. Another group of unsaturated hydrocarbons, aromatics, are usually very stable and they are a source of concern mainly because of their environmental and health effects. Although organic chloride compounds are not usually removed from crude oil as a product, the corrosive effect of these compounds on parts of refinery plants is always a source of concern. The last troublesome compounds for the refinery industry to be mentioned are the metals contained in the crude oil, typically nickel, iron and vanadium. Because of their low volatility, they are found in the heavier products of crude oil. They only become a concern in certain cases when they can affect further processing of the oil.

Very complex procedures are required to refine crude oil and there are many individual processes for obtaining marketable products of high quality. The hydrodesulfurization process intervenes at different stages of the refinery and on different byproducts of the crude oil. To better visualize its place and importance in a refinery flow scheme and understand its role, we briefly describe the general refinery system and the processes providing feedstock to hydrotreaters. We will elaborate upon hydrotreating technology, focusing our attention on HDS, from its concept to its evolution.

I.1.1.1. Petroleum refining and HDS feedstocks origin

The petroleum refining industry converts crude oil into more than 2500 refined products that can be divided into 7 groups:

- Volatile products (propane and butane Liquefied Petroleum Gas, light naphtha),
- Light distillates (gasoline, heavy naphtha, kerosene and jet fuels),
- Middle distillates (automotive diesel, heating oil, gas oil),
- Fuels oil (marine diesel, bunker fuels),
- Lubricating oils (motor, spindle, machine oil),
- Waxes (food and paper coating grade, pharmaceutical grade),
- Bitumen (asphalt, coke).

Products in these groups are processed to meet certain specifications, result of a compromise between desired performance characteristics in the product and the ability to make such product from the available crude oil and the processing facilities at hand.

Oil refining is a very complex procedure and there are many individual processes for obtaining the desired products previously mentioned. It exists in hundreds of different configurations for the refinery's processing flow scheme. The choice of a configuration is largely determined by the composition of the crude oil feedstock and the chosen slate of petroleum products. The example of refinery flow scheme presented in [Figure I.2](#) shows a general processing arrangement used by refineries. The arrangement of these processes will vary among refineries, and few, if any, employ all of these processes. In orange are the hydrotreating processes that are of particular interest in our project.

Figure I.2: Example of refinery flow diagram

The three major families of processes that transform crude oil into petroleum products are separation processes (S), conversion processes (C) and treatment processes (T). As clearly illustrated in Figure I.2, hydroprocessing plays a major role in the treatment process. Most of separating and conversion processes provide hydrotreaters with feedstocks for hydrotreatment. These feedstock are principally jet fuel, gas oil (Diesel), kerosene and naphtha coming from atmospheric distillation process (1) as well as vacuum gas oil coming

from vacuum distillation process (2). Naphtha and diesel recovered from Fluid Catalytic Cracking (FCC) (3) and coker reactors (4) may also undergo further HDS. All these processes we mentioned are described in more details in the [appendices I and II](#).

Most oil streams in a refinery plant have to undergo hydrotreatment at some moment of their processing which makes hydrotreating a process of paramount importance in any refinery by means of total amount of feedstock treated.

Depending on their origin and physical properties, the HDS feedstocks do not contain the same sulfur compounds as explained in the next paragraph.

I.1.1.2. Sulfur compounds in HDS feedstocks

From a general consideration, a HDS feedstock is an oil fraction containing sulfur compounds to be removed either prior to further processing in the refinery or to meet with commercial standards of end products. The low-boiling crude oil fractions (light naphtha) mainly contain aliphatic organosulfur compounds namely thiols, thioethers and disulfides. They are very reactive and can easily be removed. The higher boiling fractions, such as heavy straight-run naphtha, straight-run diesel (gas oil) and light FCC naphtha, contain thiophenes, benzothiophenes and their alkylated derivatives. These compounds are more difficult to convert via hydrotreating. The heaviest fractions blended to the gasoline and diesel pools (bottom FCC naphtha, coker naphtha, FCC and coker diesel) contain mainly alkylbenzothiophenes, dibenzothiophenes and alkyldibenzothiophenes. The higher boiling fractions of crude oil contain relatively more sulfur compounds and a higher molecular weight as illustrated in [Figure I.3](#).

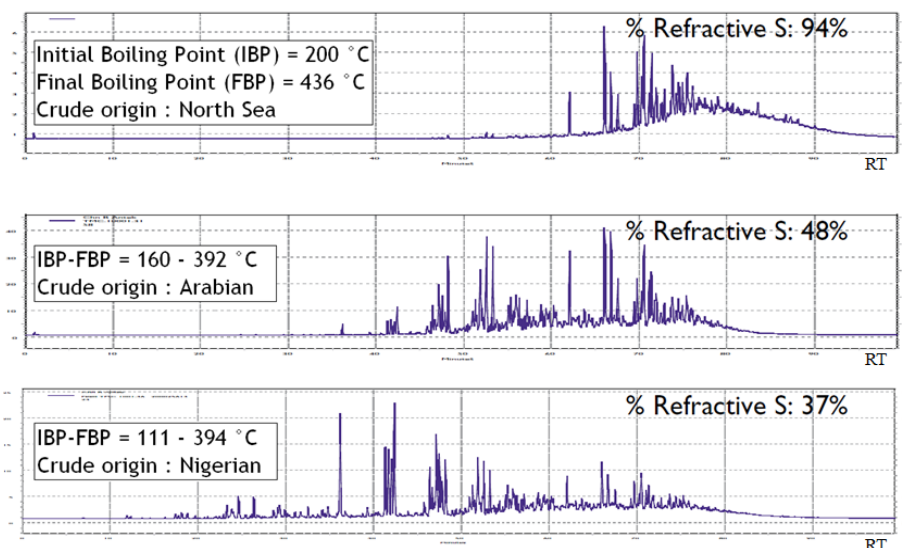


Figure I.3 : Percentage of refractive sulfur compounds in feed as a function of boiling point (adapted from [3])

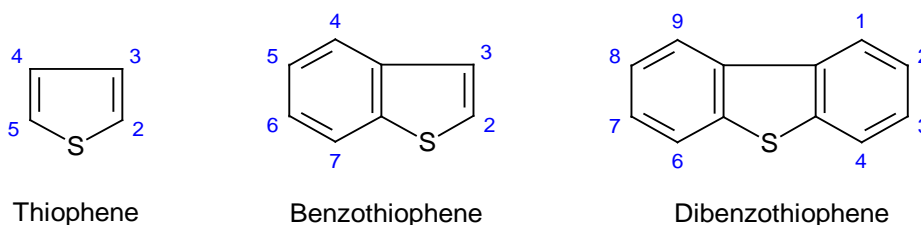


Figure I.4 : classical sulfur-containing refractive compounds (conventional atoms numbering)

The relative reactivity of sulfur compounds in HDS follows the order thiophene > alkylthiophene > benzothiophene > alkylbenzothiophene > dibenzothiophene > alkyldibenzothiophene without substituent at the 4- or 6- position > alkyldibenzothiophene with one substituent at either the 4- or 6- position > 4,6-dialkyldibenzothiophene [4].

The numerous types of oil fractions that require hydrotreatment and their various origins within the plant explain the increasing interest in any improvement of hydrotreating yield and efficiency.

Each of the above mentioned HDS feedstocks require specific conditions to be treated from their sulfur compounds. However, the general hydrotreating process used remains the same and is described in the following section.

I.1.2. Hydroprocessing

There are several key engineering processing associated with hydroprocessing, including hydrocracking and hydrotreating [2].

Hydrocracking is an established and reliable method for transforming low value heavy oil fractions into valuable products. In the hydrocracking process, low cost heavy oil fractions are reacted with hydrogen at high temperature (350-400 °C) and pressure (9-20 MPa) in the presence of an optimized catalyst system to yield high value products: diesel, jet fuel and naphtha for either gasoline production or as chemical feedstock [5].

While a significant change in molecular weight occurs during hydrocracking, hydrotreating usually implies only small changes in overall molecular structure. This process Which we will describe in more details is another well established refinery process for improving products qualities, and hydrodesulfurization is a common reaction encountered in this process.

I.1.2.1. Hydrotreating

Hydrotreating process saturates olefins and removes a significant amount of the impurities present in the raw distillate streams by reaction with hydrogen. They are therefore of paramount importance regarding the regulations previously mentioned which stipulate that oil products must be purified to diminish air-polluting emissions of sulfur and nitrogen oxides which contribute to acid rain. Furthermore, from a processing point of view, another important reason for removing sulfur from the streams within a petroleum refinery is that sulfur, even in extremely low concentrations, poisons the noble metal catalysts (platinum and rhenium) in the catalytic reforming units that are subsequently used to upgrade the octane rating of the naphtha streams, for example. Consequently, this process is one of the largest applications of industrial catalysis on the basis of the amount of material (oil fraction) processed per year. Based on the amount of catalyst sold per year, hydrotreating catalyst constitutes the third largest catalyst business after exhaust gas catalysts and fluid cracking catalysts [6].

Although there are significant variations from region to region, it is clear that environmental regulations will pose a major driving force for introducing more hydrotreating

capacity in refineries. Deep-hydrodesulfurization and aromatics reduction become increasingly important and as a result, a majority of all refinery streams undergo hydrotreating today. These new challenges have a very strong impact on current refining facilities and will continue to have effects in the near future on what triggers an increased interest in both basic and applied research within hydrotreating catalysis.

As mentioned earlier, the impurities removed during hydroprocessing are mainly metals and compounds containing sulfur, nitrogen and oxygen. The sulfur is the most common, but at the same time the least tolerable of these impurities. However, because of the steep increase in the consumption of the refined products from crude oil, crude oils of lower quality have to be processed and that requires, in addition to hydrodesulfurization (HDS), the removal of metals (hydrodemetalization, HDM), nitrogen (hydrodenitrogenation, HDN) and in some cases also oxygen (hydrodeoxygenation, HDO). Another possible way to obtain hydrotreated products of desired quality could be hydrotreating of blends of several distillate fractions. A study of the effects of catalytic hydrotreating on diesel quality using feedstocks prepared with different oil blends was undertaken by Ancheyta-juárez et al. [7,8]. Their results show that diesel specifications in sulfur content and cetane number could be reached through single step hydrotreating of these blends at moderate hydrotreating operation conditions. The deeper understanding of hydrotreating and need for products of better quality also led to the development of the processing of crude oil using two reaction stages: the same team [9] shows that crude oil quality can be substantially improved by hydroprocessing in two stages with different catalyst in each: the result of the first stage reaction was removal of metals while hydrodesulfurization was a main reaction in the second stage. A similar idea, but for hydrodesulfurization only, was presented by Reindhoudt et al. [10], where the application of a separate HDS reactor followed the conventional HDS process and in which a tailor-made catalyst for the effective removal of the remaining (most refractory) sulfur compounds could be applied. This is what is called Deep-HDS and the objective of our project work is to synthesize efficient catalysts of this specific reaction.

The term “hydrotreating” is often used as a synonym for hydrodesulfurization because the removal of sulfur remains the main goal of the hydrotreating process.

The following part aims at describing in depth the reaction of hydrodesulfurization with both industrial and scientific considerations.

I.1.2.2. Hydrodesulfurization (HDS)

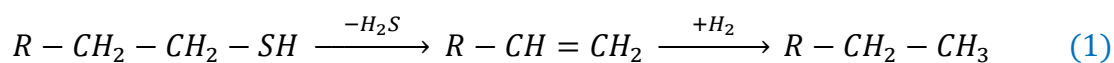
The reactivity of organosulfur compounds strongly depends on their structure. Substituent groups adjacent to the S atom generally retard HDS. Methyl substituents in the ortho- and para- positions promote C-S bond cleavage compared to those in meta-position. Using molecular orbital calculations, this has been interpreted in terms of the effect of the electron-donating properties of the substituent (inductive effect) and its position in the ring on the lability of the C-S bond. Those adjacent to the S atom decrease reactivity mainly through steric effects. The latter effect is especially marked for dibenzothiophene, the 4,6-dimethyl compound being roughly ten times less active than the compound without methyl groups [11 and ref therein]. This is important for the processing of real feeds as it has been found that dialkyldibenzothiophenes substituted in the 4,6-carbon positions remain intact until the final stages of HDS.

Our compound of reference to evaluate our material for its catalytic properties in this project is one of the most refractive sulfur compound: 4,6-dimethyldibenzothiophen (4,6-DMDBT).

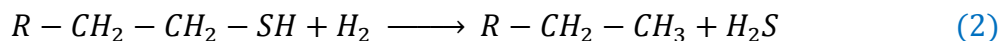
The hydrotreating process in an industrial refinery, from the general setup to reaction conditions and operating variables are given in more details in the [appendix III](#). In the following section, we aim to present what the hydrodesulfurization reaction is.

I.1.2.2.1. General HDS reaction mechanisms

Aliphatic and aromatic thiols are intermediates in ring-opening reactions of cyclic sulfur-containing compounds. They have a high reactivity, and the sulfur atom can be easily removed, which explains why they do not appear in oil. Aliphatic thiols may react through elimination and hydrogenation ([eq. 1](#)):

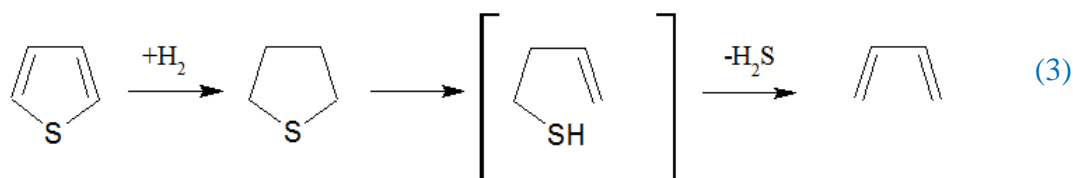


and through hydrogenolysis (eq. 2):

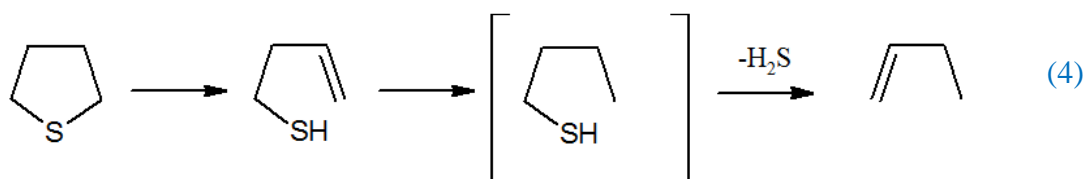


As will be described further, hydrodesulfurization is a heterogeneously catalyzed reaction. Supported transition metal sulfides have been found to be the best catalysts for the HDS reaction. Elimination takes place via well established acid-base reactions catalyzed by the surface of the metal sulfide. The reaction is an example of the Hofmann-type β -hydrogen elimination reaction [12-14]. Hydrogenation and hydrogenolysis take place at the metal sulfide surface via C-S and H-H bond scissions and C-H and S-H bond formation [15]. Aliphatic thiols which contain a β -H atom undergo elimination at a faster rate than hydrogenolysis [16]. Aliphatic thiols without β -H atoms, such as methanethiol [17], must undergo hydrodesulfurization through hydrogenolysis. Hydrodesulfurization of thiophenol mainly gives benzene [18] and may also occur by hydrogenolysis.

The reaction mechanism with sulfur compounds containing aromatic ring(s) is not as simple as presented in the previous equations but can proceed through several reaction pathways. While the HDS mechanism of thiophene at low pressure is still under debate, at elevated H_2 pressures its major reaction path is via hydrogenation of thiophene to tetrahydrothiophene [18]. This intermediate can react to give butadiene through two successive β -H eliminations or to give n-butane through two hydrogenolysis steps (eq. 3):

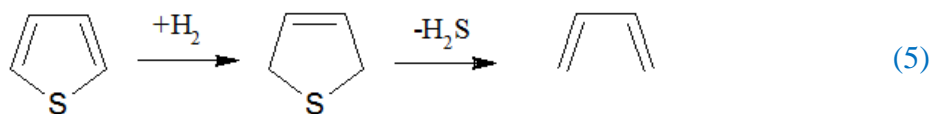


At high H_2 pressure, butadiene quickly reacts further to *cis*- and *trans*-but-1-ene and -2-ene and eventually to n-butane and is, therefore, difficult to observe. A direct route to butene may be as follows (eq. 4):



Neither 4-mercaptobut-1-ene nor butanethiol have ever been observed as a reaction intermediate in the gas phase. Once formed, they probably react directly at the catalyst surface. Indeed, the hydrogenation of olefins over HDS catalysts is fast, even though their equilibrium constants for adsorption on the catalyst surface are small. 4-Mercaptobut-1-ene, on the other hand, should have a high adsorption constant and also a high hydrogenation rate, thus making its detection in the gas phase very unlikely.

As already said, the HDS of thiophene at atmospheric pressure is still under debate after several decades of investigation [19]. Some authors have argued that the mechanism is in principal the same as at high pressure, with tetrahydrothiophene as the main intermediate. Its very low concentration is then explained by fast ring opening and sulfur removal subsequent to the rate-determining hydrogenation of thiophene. Other authors believe that direct hydrogenolysis of thiophene to butadiene and H_2S is the main route at low H_2 pressure. Organometallic studies have suggested that a slightly different pathway via 2,5-dihydrothiophene (eq. 5) might also play a role [20].



In accordance with this suggestion, surface science studies of the reaction of 2,5-dihydrothiophene on a sulfided Mo catalyst surface have shown that butadiene is eliminated in an intramolecular process without the participation of a $\text{C}-\text{C}=\text{C}-\text{C}-\text{S}-\text{M}$ metal thiolate intermediate [21].

When hydrodesulfurization levels corresponding to the removal of +99.99 % of sulfur from typical crude containing 1.5 w% sulfur which correspond to the European Union attempts for the year 2011 (cf. [Introduction](#)), the removal of the more refractive sulfur compounds (dibenzothiophene and alkylated derivatives) become essential and the removal process take the name of deep or ultra-deep HDS.

I.1.2.2.2. Deep-Hydrodesulfurization

Deep-hydrodesulfurization of the fuels implies that more and more of the least reactive sulfur compounds must be converted. Deep-HDS thus principally applies to benzothiophene, dibenzothiophene and their alkylated derivatives. The highly refractive character of these compounds automatically implies the presence of a catalyst to undergo the HDS reaction.

The mechanism of the HDS of dibenzothiophene (DBT) has been well studied [4]. Biphenyl (BP) is formed through a twofold hydrogenolysis, and this so-called direct desulfurization (DDS (eq. 6)) is the major reaction pathway for this reaction (80-90%). It can also react by partial hydrogenation of one of the phenyl rings, forming tetrahydrodibenzothiophene (4H-DBT) and hexahydrodibenzothiophene (6H-DBT), followed by C–S bond scission by hydrogenolysis or by elimination and hydrogenation of the resulting double bond. The resulting arylthiol is desulfurized to cyclohexylbenzene (CHB), analogously to the desulfurization of thiophenol to benzene described above. This route is called the hydrogenation route (HYD (eq. 7)).

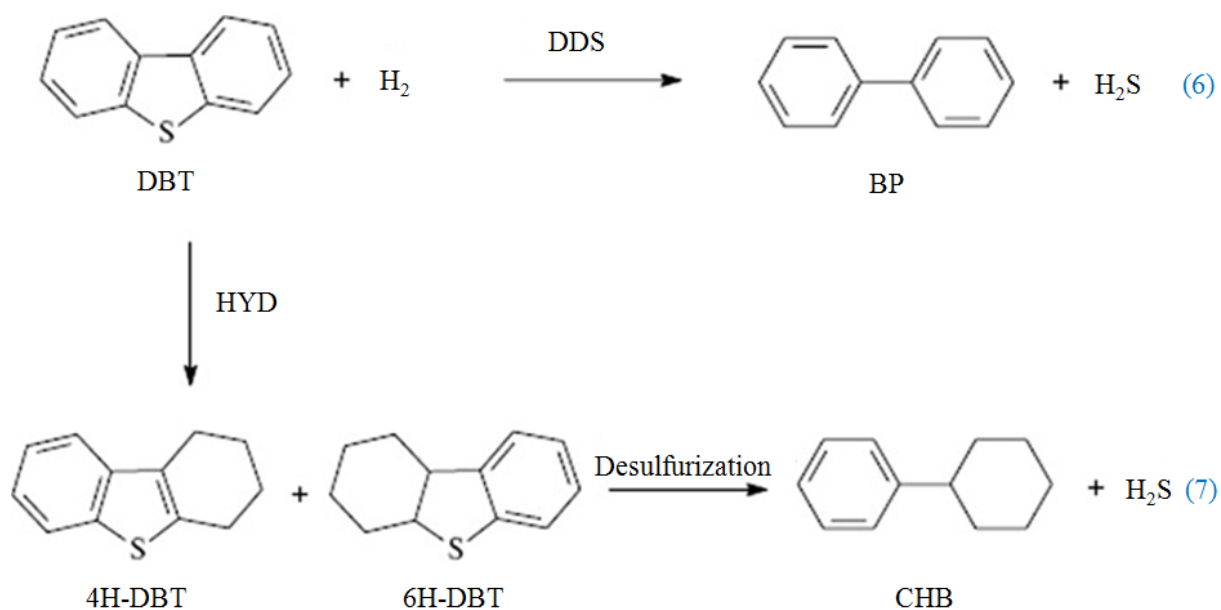


Figure I.5 : Reaction path network for HDS of DBT (taken from [22])

Alkyl groups next to the sulfur atom, as in 4,6-dialkyldibenzothiophene, sterically hinder the adsorption of the molecule perpendicular to the catalyst surface (Figure I.6). Consequently, no strong bond between the S atom of 4,6-dialkyldibenzothiophene and the active site at the catalyst surface can be established, and the removal of the S atom through the DDS route is strongly suppressed.

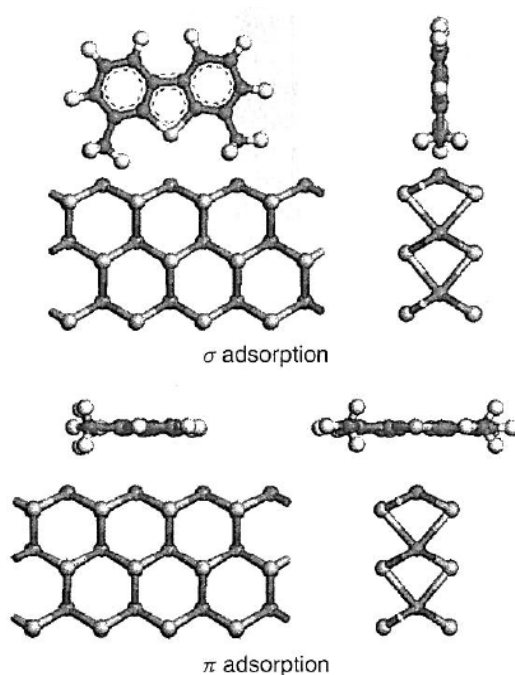


Figure I.6 : Adsorption of 4,6-dimethyldibenzothiophene in the σ and π modes [6]

The hydrogenation route (HYD) is almost equally fast for 4,6-dialkyldibenzothiophene as for dibenzothiophene, which can be explained by adsorption and reaction of the 4,6-dialkyldibenzothiophene parallel to the catalyst surface (Figure I.6). Because the DDS rate is fast for dibenzothiophene but slow for 4,6-dialkyldibenzothiophene, the HYD route is the minority route (10 – 20 %) for dibenzothiophene and the major (but equally slow) route for 4,6-dialkyldibenzothiophene. For these reasons, 4,6-dialkyldibenzothiophene molecules are among the most difficult to desulfurize.

Considerable work was carried out by Song et al. to understand the reaction steps involved in the HDS of the most common of the dialkyldibenzothiophenes: 4,6-dimethyldibenzothiophene (4,6-DMDBT). An identical desulfurization network as the one described for dibenzothiophene has been suggested (Figure I.7) [23,24]. Again, two main pathways are presented: DDS and HYD. An isomerization route has also been described, where the methyl groups migrate, but this is likely to operate in the presence of catalysts with

acidic supports [25,26]. The HYD route proceeds through hexahydrodimethyldibenzothiophene (6-H-DMDBT) and forms methylcyclohexyltoluene (MCHT). The DDS route produces 3,3'-dimethylbiphenyl. Interconversion between these products is believed to be slow. Further hydrogenation of MCHT leads to the ultimate product dimethylbicyclohexane (DMBCH), while the fully hydrogenated 12-hydro-dimethyldibenzothiophene (12H-DMDBT) is generally not observed.

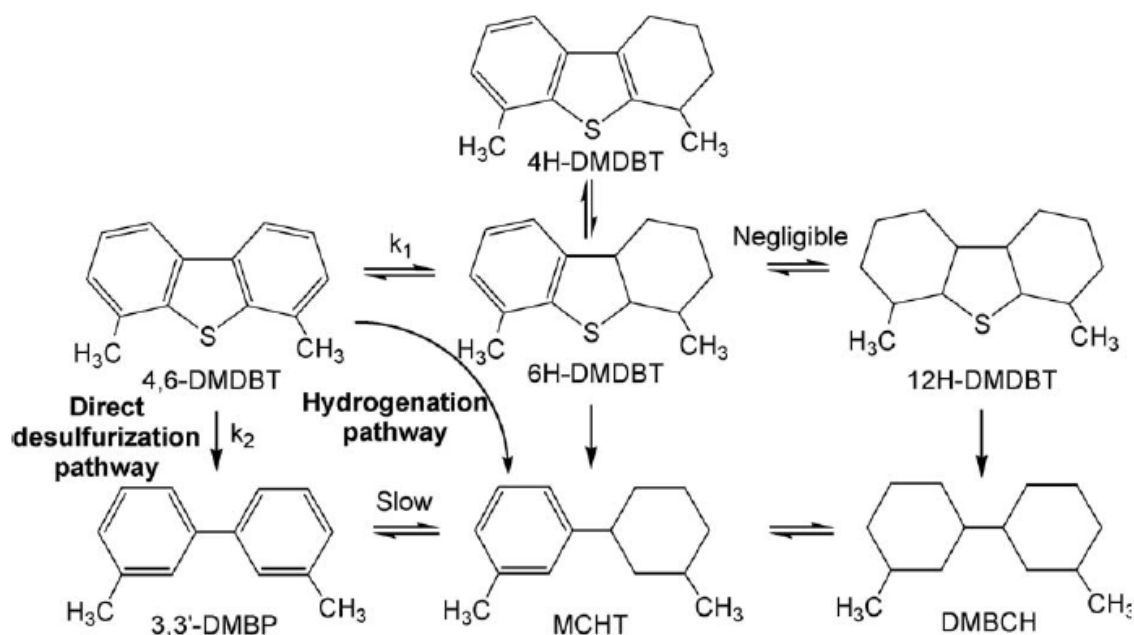
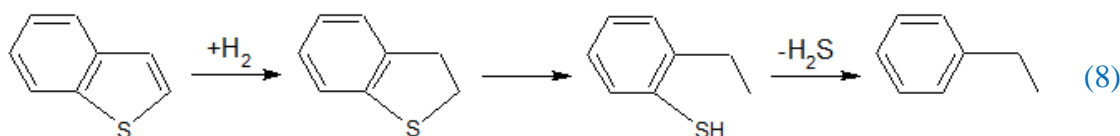


Figure I.7 : Reaction network for 4,6-DMDBT hydrodesulfurization [27]

Concerning the HDS of benzothiophene, it has been reported that the reaction mechanism is similar to the HYD route of dibenzothiophene [4]: hydrogenation to dihydrobenzothiophene first takes place previous to ring-opening hydrogenolysis and finally sulfur-removal hydrogenolysis (eq. 8).



Desulfurization of 4,6-DMDBT principally occurs via a hydrogenation step, suggesting the importance of the hydrogenation character of the catalyst to be used for this reaction.

Current regulations over sulfur content in automotive fuels force petroleum industries to systematically integrate deep-HDS in their overall process. As this reaction mainly concerns the most refractive sulfur compounds already mentioned, it does not go without catalytic consideration. Therefore, today's challenge in HDS becomes the search for catalysts with improved activity and selectivity that would avoid capital-intensive changes to the actual process. The following section focuses on HDS catalysts description and research advances.

I.1.3. HDS catalysts

The catalyst selection for a certain process is based on studies of activity, selectivity and lifetime. This is usually a very long and difficult task. Once the suitable catalyst giving the desired product quality at a reasonable cost is found, the search for a better catalyst starts immediately.

As aforementioned, hydrodesulfurization is a heterogeneously catalyzed reaction. The selection of a catalyst depends mainly on the required conversion and characteristics of the processed feedstock. Ideal hydrotreating catalysts should be able to remove sulfur, nitrogen and, in specific cases, metal atoms from the refinery streams. At the same time, they must improve other fuel specifications, such as octane/cetane number and aromatics content, essential for high quality fuel and meeting environmental legislation standards. We know that the characteristics of feed vary considerably and the amount of impurities and the physical properties thus determine the choice of the catalyst. This suggests that a universal catalyst or catalytic system suitable for hydroprocessing feeds from different sources does not exist. With respect to these chemical and physical properties, a wide range of hydroprocessing catalysts have been developed for commercial applications.

I.1.3.1. Conventional HDS catalysts

Any catalyst that exhibits hydrogenation activity will catalyze HDS to some extent. However, sulfide metals from the group VIB (chromium, molybdenum and tungsten) are particularly active for desulfurization, especially when promoted with metals from the group VIII (cobalt, nickel) [11]. The first industrial use of Mo-based hydrotreatment catalysts

appears to date from after the First World War [28]. For decades the basic metals engaged in the active phase have remained unchanged in spite of numerous efforts to replace them by more active or less expensive elements. Nevertheless, their performance has been greatly improved by the optimization of the synthesis of supports, by the addition of various adjuvant elements such as F, B and Si, and by the development of new methods of preparation [29].

A classical HDS catalyst is made of a supported active phase MoS_2 (usually over alumina) promoted by either Ni or Co. It is written as $\text{Co(Ni)Mo/Al}_2\text{O}_3$ and often referred as “CoMo” or “NiMo” depending on the promoting cation.

The next section throws a light on the way HDS catalysts are obtained and the importance and influence of the different constituents over their efficiency.

I.1.3.1.1. Role of the support

Although the chemical nature of the active sulfide phase has remained virtually the same for several decades, the quality of the support has been significantly optimized and its pore structure in particular has been adapted to the molecular weight of the feedstocks processed, especially where very heavy feeds are concerned.

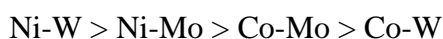
Luck [30] reviewed support effects on different reactions, and many other authors [31-36] have studied their role on HDS or hydrogenation. Alumina was found to be effective as a support for hydrotreating catalyst already in the beginning of the industrial application of the process and Ledoux et al. showed that the best support is $\gamma\text{-Al}_2\text{O}_3$ in term of HDS activity. They reported that the γ phase was the best one over η , θ , χ or amorphous alumina, principally due to the influence of its crystallinity and surface orientation on the anchorage of the active phase [37,38], and also to the enhancement it provides to the acidic properties of the sulfide phase thus improving its catalytic properties [39]. Almost all the surface area is found in the pores of the alumina (200 to $300\text{ m}^2.\text{g}^{-1}$) and the metals are dispersed in a thin layer over the entire alumina surface within the pores. This type of catalyst does display a huge catalytic surface for a small weight of catalyst. For this reason $\gamma\text{-Al}_2\text{O}_3$ is the most common support of conventional HDS catalysts.

Many researchers have explored ways of modifying $\gamma\text{-Al}_2\text{O}_3$ (e.g. $\text{SiO}_2\text{-Al}_2\text{O}_3$, $\text{P}_2\text{O}_5\text{-Al}_2\text{O}_3$, $\text{F-Al}_2\text{O}_3$, $\text{TiO}_2\text{-Al}_2\text{O}_3$, $\text{Pt-Al}_2\text{O}_3$) or have developed non-traditional supports for HDS. Examples are SiO_2 , $\text{ZrO}_2\text{-TiO}_2$, MgO , CeO_2 , carbon, zeolites, and mesoporous materials (e.g., MCM-41). Incorporation of a solid acid into the support helps adsorption and also promotes hydrogenation through protonation followed by hydride transfer. A solid acid may also isomerize substituted DBTs into non-substituted DBTs, thus speeding up sulfur removal on conventional catalysts. However, such acid-assisted catalysts are prone to coking and poisoning by organonitrogen.

In addition to the chemical nature of the catalyst, its physical structure (hence that of the support) is also important in determining the hydrogenation activity, particularly for heavy feedstock. When gas oils and residue are used, the feedstock is in the liquid phase under standard reaction conditions. Additional feedstock and hydrogen must diffuse through this liquid before reaction can take place at the inner surface of the catalyst particle. At high temperatures, reaction rates can be much higher than diffusion rates, and concentration gradients can develop within the catalyst particle. Therefore, the choice of catalyst porosity is an important parameter. High surface area (about $300\text{ m}^2\cdot\text{g}^{-1}$) and low- to moderate-porosity (from 12 \AA pore diameter in the case of crystalline acidic components to 50 \AA or more when based on amorphous materials) catalysts are used. With reactions involving high molecular weight feedstocks, pore diffusion can exert a large influence, and catalysts with pore diameters greater than 80 \AA are necessary for more efficient conversion.

I.1.3.1.2. Active phase and structure of supported HDS catalysts

Within the series of cobalt-promoted or nickel-promoted group VIB metal (Mo or W) based catalysts supported on $\gamma\text{-Al}_2\text{O}_3$, the ranking for hydrogenation is:



Even though nickel-tungsten is the best combination for hydrogenation, nickel-molybdenum is preferred as Mo is cheaper than W and easier to handle. Classically, hydrotreating catalyst precursors in their oxide form are industrially prepared by pore volume impregnation of $\gamma\text{-Al}_2\text{O}_3$ with an aqueous solution usually of $(\text{NH}_4)_6\text{Mo}_7\text{O}_{24}$ and $\text{Co}(\text{NO}_3)_2$ or

$\text{Ni}(\text{NO}_3)_2$, followed by drying or by co-impregnation of both salts followed by drying step after which hydrotreating catalysts are usually calcined in air at a temperature around 500 °C. Phosphate is often added as phosphoric acid or ammonium phosphate to enhance the solubility of molybdate by the formation of phosphomolybdate complexes. The sulfide form which is actually the hydrotreating catalyst can be obtained by sulfidation in a mixture of H_2 and H_2S , thiophene, CS_2 , dimethyldisulfide or an oil stream, depending on the considered process. The properties of the final sulfide catalyst depend to a great extent on the calcination and sulfidation steps. Optimum calcination and sulfidation temperatures for Al_2O_3 as a support are in the range 400-500 °C.

Since the 70's, several teams have worked on the structure of the $\text{CoMo}/\text{Al}_2\text{O}_3$ and different models (referring to interactions with the support as well as between Mo and the promoter) have been proposed: the mono-layer model [40-44], the intercalation model [45,46], the “pseudo-intercalation” model [11,47] and the contact synergy model [11,48-50]. The development of new characterization methods, like *in situ* Mössbauer spectroscopy, extended X-ray absorption fine structure (EXAFS) spectroscopy, and infrared spectroscopy however, enabled Topsøe and coworkers [51-58] to provide the most detailed structural description of “CoMo” catalysts and a new explanation of the promoting effect, widely accepted today. Cobalt may be present in three forms after sulfidation (Figure I.8), as Co_9S_8 crystallites on the support, as cobalt ions (Co^{2+}) in tetrahedral sites in the $\gamma\text{-Al}_2\text{O}_3$ lattice and the so-called Co-Mo-S phase was shown to be MoS_2 -like structures with the cobalt atoms located at the edges in five-fold coordinated sites (edge decoration model – Figure I.9).

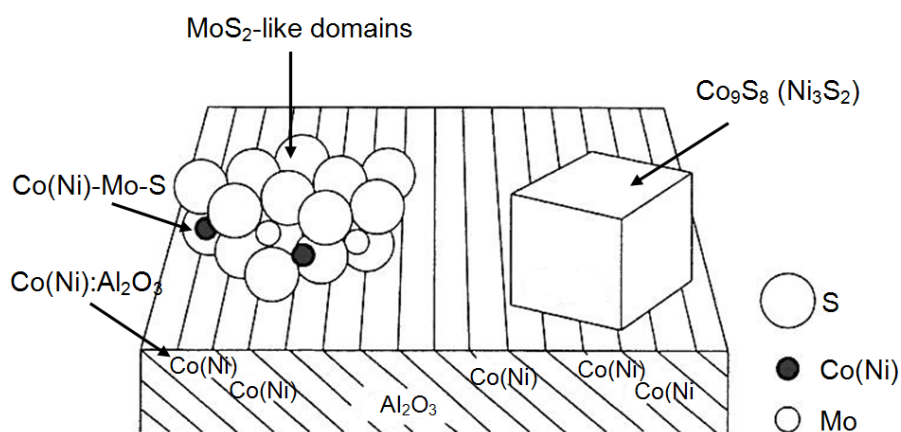


Figure I.8 : Schematic representation of the different phases present in typical supported catalyst (adapted from [59])

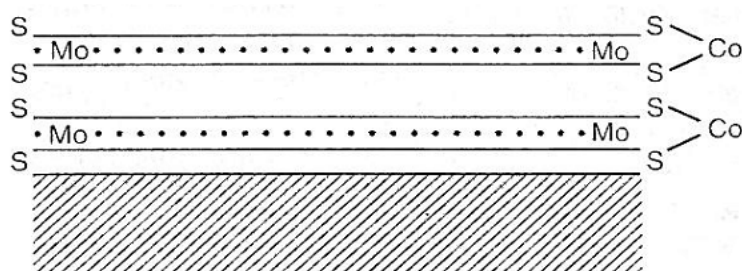


Figure I.9 : Edge decoration model of the structure of the Co atoms in sulfided Co-Mo/Al₂O₃ [6]

Since the Co₉S₈ (or Ni₃S₂) particles have a low catalytic activity and cover the MoS₂ particles, the HDS activity decreases at high Co/Mo ratios. The maximum activity is usually observed at a Co/Mo molar ratio of 0.3-0.5. This implies that the MoS₂ particles present on the Al₂O₃ support must be small enough to have a similar ratio of the number of Mo edge atoms (Mo_e) to the total number of Mo atoms (Mo_e/Mo similar to Co/Mo). Commercial catalysts usually contain Co/Mo or Ni/Mo molar ratios slightly above 0.5, at Mo loadings in the order of 10-15 wt%.

“CoMo” catalyst was used in the majority of hydrodesulfurization processes explaining the large amount of data obtained on the Co-Mo-S structure. However, nickel-promoted catalysts have been rediscovered as an interesting choice with regard to deep hydrodesulfurization. Similarities between “CoMo” and “NiMo” catalysts have been observed, particularly analogous promoting effect of Ni atoms and the Ni-Mo-S structure closely similar to Co-Mo-S [57]. However, small differences in the structure still exist. DFT (Density Functional Transform) calculations have furnished a wealth of information on the Co-Mo-S and Ni-Mo-S structures [60-66] (Figure I.10). The Mo atoms at the Mo edge are fully coordinated by six sulfur atoms in a trigonal prismatic arrangement. The Mo atoms are surrounded by four sulfur atoms, the outer two in bridge positions between the Mo atoms in a zigzag configuration, so that the Mo atoms are in distorted tetrahedral sulfur coordination. The most stable position for the Co and Ni promoter atom is at the edges of the MoS₂ particles. The Ni atoms are preferentially located at the metal edge and are not covered by sulfur atoms. As a result, the Ni atoms have square-planar sulfur coordination with open coordination positions. The Co atoms are preferentially situated at the S edges. Co atoms are also coordinated by four sulfur atoms, the outer two in bridge position but on the contrary of the Mo atoms case, the bridge positions are regular, leading to tetrahedral sulfur coordination.

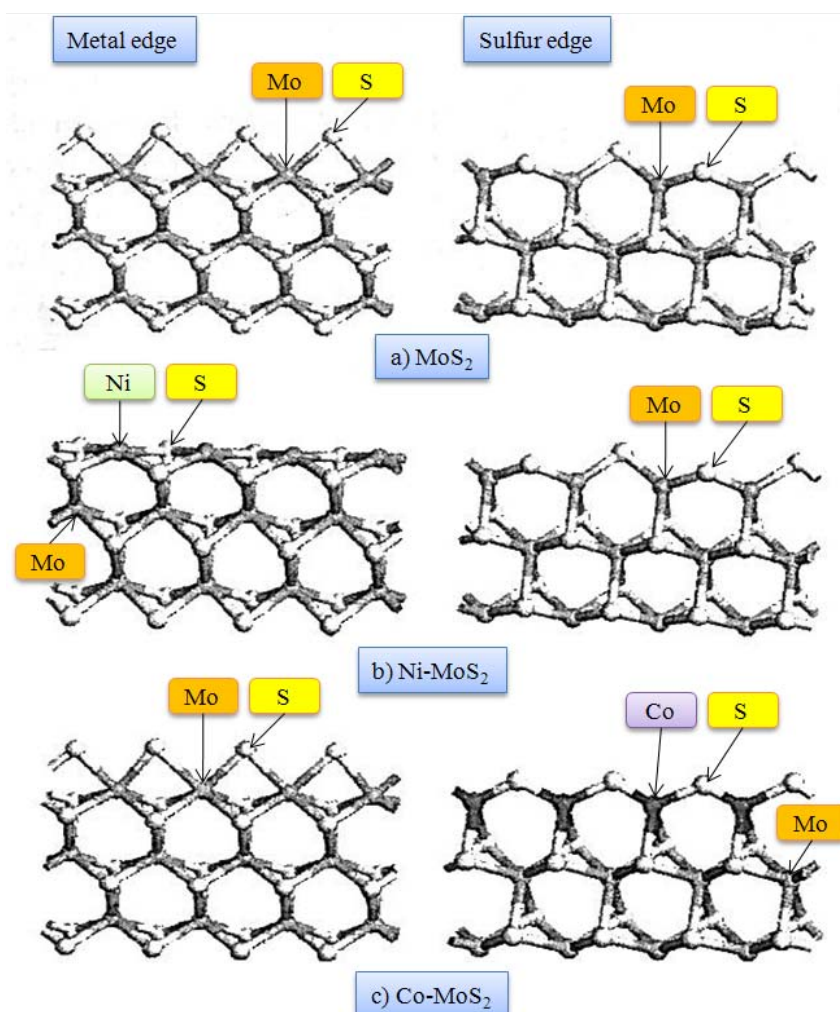


Figure I.10 : Structure of the metal and sulfur edges of MoS₂, Ni-MoS₂ and Co-MoS₂ under classical sulfidation conditions, as predicted by DFT calculations [6]

I.1.3.1.3. Active sites and deactivation

It has often been assumed that the catalytically active sites in a hydrotreating catalyst are Mo cations at the surface of MoS₂ crystallites with at least one sulfur vacancy so that the reacting molecule can chemically bond to the Mo cation [67,68]. Since sulfur anions in the basal planes of MoS₂ are more difficult to remove than anions at edges and corners, exposed Mo ions will be predominantly present at edges and corners and catalysis will occur at these positions [69]. The HDS activity of a MoS₂/Al₂O₃ catalyst increases substantially when Co or Ni is added. This effect is attributed to the promoter present in the Co(Ni)-Mo-S phase. The aforementioned DFT calculations suggest that a combined action of both metals is responsible for the catalysis [60-62]. It was shown that a sulfur atom bonded to a nickel or cobalt atom or between a nickel or cobalt atom and a molybdenum atom is less strongly bonded than a sulfur

atom between two molybdenum atoms and can be more easily removed creating a vacancy. The most active transition metal sulfides are those with the lowest metal-sulfur bond strength [70]. This suggests that the removal of sulfur from the catalysts is the rate-determining step in HDS. Studies performed with radioactive elements lead to the conclusion that upon adsorption of a sulfur-containing molecule on an anion vacancy at the catalyst surface, a nearby SH group adds a hydrogen atom and desorbs in the form of H_2S and, at the same time, creates a new vacancy.

Catalyst life depends on the feedstock properties and the degree of desulfurization desired. Some of the molecules present in industrial feedstock can act as inhibitors. Depending on its quality, the crude oil contains varying amounts of aromatics and components containing nitrogen and oxygen. Sulfur compounds can act as inhibitor as well. Moreover, H_2S (as well as NH_3 and H_2O) formed as a product of the hydrotreating reactions, also acts as inhibitor. All these compounds somehow influence the reactivity of individual sulfur compounds and thus the HDS efficiency. This is called the “matrix effect” [1,71].

HDS, HDN and demetallization occur simultaneously on the active sites within the catalyst pore structure, implying a competition between those reactions. Sulfur and nitrogen occurring in residue are converted to hydrogen sulfide and ammonia in the catalytic reactor.

Catalyst deactivation by coking is increased in the presence of basic nitrogen compounds and becomes even more important because the concentration of nitrogen compounds in the heavier feedstocks is much higher than in the straight-run distillates, and the acidic catalysts used in catalytic conversion are poisoned by those basic compounds. For this important consideration, nitrogen compounds are becoming of major concerns when it comes to hydrotreatment and more specifically to HDS and deep-HDS [72,73]. The poisoning effect of nitrogen can be offset to a certain degree by operating at a higher temperature. However, the higher temperatures tend to increase the production of compounds in the methane to butane range and decrease the operating stability of the catalyst in a way that it requires more frequent regeneration.

Removal of sulfur from the feedstock results in a gradual increase in catalyst activity, returning almost to the original activity level. As with ammonia, the concentration of the hydrogen sulfide can be used to control precisely the activity of the catalyst. Recycle gas scrubbing is employed in this view.

The metals in the feedstock are deposited on the catalyst in the form of metal sulfides, and cracking of the feedstock to distillate produces a laydown of carbonaceous material on the catalyst. Both events poison the catalyst and activity or selectivity suffers. The deposition of

carbonaceous material is a fast reaction that soon equilibrates to a particular carbon level and is controlled by hydrogen partial pressure within the reactors. On the other hand, metal deposition is a slow reaction that is directly proportional to the amount of feedstock passed over the catalyst. This last metals deposition is the only permanent poison to the catalyst causing permanent deactivation as they accumulate. However, this is usually of little concern, except when deasphalted oils are used as feedstocks, as most distillate feedstocks contain low amount of metals.

Providing that pressure drop buildup is avoided, cycles of 1 year or more and ultimate catalyst life of 3 years or more can be expected. The catalyst employed can be regenerated by normal stream-air or recycle combustion gas-air procedures. The catalyst is restored to near fresh activity by regeneration during the early part of its ultimate life. However, permanent deactivation of the catalyst occurs slowly during usage and repeated regenerations, so replacement becomes necessary.

I.1.3.2. Deep-HDS issue

Today, many desulfurized middle distillates have low total sulfur content but a disproportionately high concentration of refractory sulfur species. Desulfurizing these prehydrotreated distillates requires different catalysts and operating conditions than those used for HDS of raw distillates. Most existing distillate HDS processes have been optimized for treating raw distillates to meet the ancient 350-500 wppm specifications. Stretching today's technology to the ultralow sulfur regime requires overcoming the difficulty of desulfurizing 4-substituted and 4,6-disubstituted dibenzothiophenes. Most commercial catalysts were optimized for the HDS on non substituted DBTs to increase the reaction rate through a drastic enhancement of catalyst's hydrogenolysis functionality. When performing HDS, these catalysts do not consume much hydrogen.

A very different situation arises when it comes to the HDS of substituted DBTs, which mainly relies on the hydrogenation route. With the little hydrogenation power they possess, conventional catalysts generally require high hydrogen pressures or long contact times to attain an acceptable HDS rate. However, many refiners are limited by hydrogen pressure. Running HDS at too high temperature jeopardizes diesel quality. To minimize capital

investment and preserve crude slate flexibility, there is an enormous incentive to achieve deep HDS at low hydrogen partial pressures.

The development of a new generation of catalysts to achieve this objective of low nitrogen and sulfur levels in the processing of different feedstocks presents an interesting challenge in catalyst development.

Conventional “CoMo” catalysts are relatively better for desulfurization via the DDS pathway than via the HYD one since the “CoMo” hydrogenation activity is relatively low and, as a result, relatively little hydrogen is consumed. This makes “CoMo” catalysts attractive for the HDS of FCC naphtha which contains alkenes. “CoMo” catalysts are also used in the HDS of diesel fuel when high pressures cannot be used. In that case, one relies on longer residence times and higher temperatures. If the unit allows higher pressure, then “NiMo” catalysts can be used. They possess a high ability to saturate one of the aromatic rings of 4,6-dialkyldibenzothiophene and are therefore preferred for HDS of refinery streams that require extensive hydrogenation.

Zhang *et al.* [74] studied both the “NiMo” and the “CoMo” catalysts, and they report a better activity of the “NiMo” catalysts towards the substituted DBTs. This higher activity when compared to “CoMo” was attributed to the difference in the activity of both catalysts for the hydrogenation of aromatic rings of DBTs. It has already been mentioned that the refractory character of alkyldibenzothiophene comes from steric hindrance and the electronic effects of the substituents in certain position, and hydrogenation of the aromatic rings prior to sulfur removal is generally thought to decrease this steric hindrance and, therefore, facilitate the HDS reaction [75]. The hydrogenation pathway was found to be preferred in the case of hindered DBTs and this preference increases with the size of substituent in the 4- or 4,6-positions [76]. “NiMo” has evidently a higher hydrogenation activity and is thus more suitable for the HDS of hindered DBTs [77].

“NiMo” appears to be the best catalyst for the HDS of 4,6-DMDBT, which guided our choice of synthesizing this particular catalyst precursor in our project.

I.1.3.3. Advances in HDS catalyst

Improvements of conventional metal sulfide catalysts and the discovery of novel materials and supports are needed to meet the increasing demand of energy. Enhancement of catalysts activity and stability is required to increase refinery throughput and to upgrade low value feedstock to high value fuels. In addition, broad applicability of hydrotreating catalysts is desired to treat a wide range of feedstocks. These improvements must results in a refinery end-product that meets the mandates of environmental legislation and the shift in the automotive industry to high efficiency. Achievements of these demands will require catalysts with higher volumetric activity for HDS, HDN and aromatics saturation with minimal hydrogen consumption.

I.1.3.3.1. Supported sulfide catalysts

Considerable research in the past few years has concentrated on finding more active sulfide compositions, using new supports, exploring novel compounds and improving processes. Since our interest in this project work focuses on unsupported catalysts, we just summarize some papers and improvements in [Table I.2](#).

Table I.2 : Summary of recent advances in hydroprocessing with sulfides (adapted from [27])

Improvement of existing sulfides	
Review: Improving dispersion and morphology	+ Chianelli [78]
Sonochemical and CVD methods for high dispersion	+ Moon [79,80], Okamoto [81,82], Ramos [83]
Ultrasonic spray and pyrolysis for high dispersion	+ Suslick [84]
Microwave method for high dispersion	+ Liu, B. [85,86], Liu, X. [87]
Dispersing agent	+ Yoshimura [88], Okamoto [89], Escobar [90], Costa [91], Lélías [92], Rana [93,94]
Activation agents	+ Perot [95], Frizi [96]
Use of non-traditional elements	+ Fierro [97], Hubaut [98], Vít [99], Escalona [100,101], De los Reyes [102], Giraldo [103], Centeno [104]
New precursors with Mo-S bonds	+ Ishihara [105], Ho [106], Bensch [107,108], Cruz-Reyes [109]
Urea-matrix combustion method	+ Green [110-113]
Use of unsupported trimetallic compositions	+ Fuentes [114], Alonso [115], Huirache-Acuña [116,117], Nava [118]
Alternative or improved supports for sulfides	
Improvement of Al ₂ O ₃ with Ti, and Ga	+ Segawa [119,120], Ramírez [121,122], Vrinat [123,124], Zhao [125]
Improvement of Al ₂ O ₃ with B	+ Okamoto [126-128], Shimada [129], Centeno [130]
Improvement of Al ₂ O ₃ with B and P	+ Ferdous [131]
F ⁻ or PO ₄ ³⁻ bind to Al ³⁺ ions and reduce interactions	- Prins [132], Maity [133], Ding [134], Moon [135]
Basic additives (K, Li)	+ Diehl [136], Fan [137], Mizutani [138]
Composite supports (SiO ₂ -Al ₂ O ₃)	+ Van der Meer [139], Mochida [140], Kunisada [141], Ancheyta [142]
Composite supports (TiO ₂ -SiO ₂ , ZrO ₂ -Al ₂ O ₃)	+ Zhou [143], Zhang, Li [144]
Pure TiO ₂ supports for FeMo catalysts	+ Kraveva [145]
Hydroxyapatite modified by Zr and/or Al	+ Travert [146]
Carbon nanotubes, mesoporous clays	o Chen [147], Dalai [148], Shang [149], Song [150,151]
Mesoporous supports (MCM-41, SBA-15, Ti-HMS)	+ Klimova [152-154], Dhar [155,156], Li [157], Zepeda [158-161], Fierro [162], Rodríguez-Castellón [163], Silva-Rodrigo [164], Zeng [165]

+ : positive effect, - : negative effect, o : neutral or not applicable

I.1.3.3.2. Bulk catalysts

What is the real role in catalysis of the Alumina or of the support, speaking in more general terms? Traditionally, it has been thought that the role of the support is primarily to disperse and stabilize the MoS₂ based hydrotreating catalyst. This support effect is caused by a strong interaction between MoS₂ and the support itself. An additional function is making the catalyst less expensive by diluting the metal. The fundamental activity and selectivity resides in the sulfide phase. Because of the strong sulfide/support interaction the total activity of the catalyst is actually reduced per metal atoms as a result. Thus, it appears that historically the alumina supported catalyst arose because of reduced cost and improved stability of the unsulfided catalyst precursor which makes the material easier to transport, store and load in the reactor. However, unsupported catalysts with their high volumetric activity and unusual selectivity are the “wave of the future” in many hydrotreating and chemical applications [166,167].

In a catalyst, supports often interfere with the active phase and may reduce its potentiality. Moreover, it dilutes the active sites and large amounts of catalysts are needed to reach the desired fuel quality.

There are numerous papers in the open literature related to the chemical and physical properties of unsupported transition metal sulfides. Besides characterization studies, the performance of a large variety of mono-, bi- and multi-metallic materials in various test reactions has been examined. The performance studies identified several unsupported materials with higher activity and/or selectivity than the traditional γ -Al₂O₃ supported Ni/Co-Mo/W catalysts [168-172 and references therein]. This has resulted in numerous patents disclosing the preparation of unsupported transition metal sulfides and their use as hydroprocessing catalysts. Model-compound studies have indicated that bulk transition metal sulfides (TMS) tend to be more hydrogenation selective than supported catalysts.

The reported high activities of various types of unsupported catalysts can have different origins. The active sites in mixed Co(Ni)-Mo(W) sulfides are not necessarily different than those in the corresponding supported catalysts. However, the population of the active sites is much higher in unsupported catalysts and the total absence of metal/support interactions makes the unsupported Co(Ni)-Mo(W) sulfides an ultimate type of catalysts with a high intrinsic activity. Several noble metals (in particular Ru, Rh, Os and Ir) also have very

high intrinsic activities in different hydrotreating reactions [173-176]. Yet, the high prices of noble metals restrict their application in commercial hydrotreating. Ru is the cheapest of the noble metals, however, its price is still more than 40 times that of Mo and nearly 80 times that of W.

Despite the relatively large number of patents covering the different unsupported catalysts and their applications in hydroprocessing, there are only a few commercial bulk hydrotreating catalysts. Incorporating a catalyst with extremely high activity in existing refinery process equipment is all but straight forward. In most cases the process and the equipment was not designed for the heat release and H_2 consumption accompanying a very high activity catalyst. In addition to that, the price plays an important role even if the unsupported catalyst contains only Group VIII and Group VIB metals. High concentration of metals and higher density of unsupported, as compared to supported, catalysts will increase the reactor fill price significantly. There is one family of commercial bulk hydroprocessing catalysts that is being sold in sizable amounts in the present hydroprocessing market. This is the NEBULA[®] catalysts family. The NEBULA[®] catalyst family was developed in close cooperation between Albemarle Catalysts (former Akzo Nobel Catalysts) and ExxonMobil. The NEBULA[®] technology is patented and the catalyst preparation and composition are trade secrets of the Albemarle Catalysts Company [168].

Nevertheless, here are presented some strategies for preparing bulk TMS. A classical one is by thermal decomposition of metal amine thiomolybdates in which the promoter metals and Mo are molecularly associated with each other in different manners (in slurry, solutions...), using surfactants or not [177-179] and also catalysts derived from metal amine metallates that are heterometallic metal oxygen complexes of the formula $(ML)(MoO_4)$, where M is a divalent promoter metal such as Co or Ni, L is one or more polydentate chelating ligands with a total denticity of six [180].

It has been quite recently reported that bulk TMS can also be prepared by hydrothermal methods [181,182]. It implies two steps: the Mo oxide precursor was prepared hydrothermally in a stainless steel autoclave for 48 hours from an aged solution of ammonium heptamolybdate $[(NH_4)_4Mo_7O_{24} \cdot 4H_2O]$. The “NiMo” was prepared by impregnating nickel nitrate directly over the precursor MoO_3 by the initial impregnation method and was sulfided afterward with H_2S/H_2 (15 v% H_2S) at 400 °C for 2 hours.

In the citrate method, adequate amounts of $M(NO_3)_2 \cdot 6H_2O$ (M=Ni and/or Co) and $(NH_4)_6Mo_7O_{24} \cdot 4H_2O$ are dissolved separately in water. An excess of citric acid is then added to each solution. The obtained solutions are mixed together and the final solution is

concentrated in a rotary evaporator until formation of a viscous liquid, which is then heated at 80 °C for 20 hours in a vacuum oven. Once a powder has been obtained, the catalyst precursor is pre-calcined at 300 °C in a flow of dry air, in order to allow the decomposition of the citrate ion involving the formation of CO₂ and water. After the pre-calcination treatment, the catalyst precursor was calcined at 650 °C for 20 hours in a flow of dry air [183].

A quite original method consists in synthesis by Freeze-Drying: the starting Co-, Ni-, or Mo-containing solutions are prepared by dissolving their respective salts in distilled water. They are then combined to obtain (Co, Ni)-Mo source solutions. A small amount of nitric acid is added to the solution after mixture to ensure long-term stability of the solutions. Droplets of these solutions are flash frozen by projection onto liquid nitrogen and then freeze-dried at a pressure of 1-10 Pa and at a temperature of -45 °C in a Telstar Cryodos freeze-dryer. In this way, dried solid precursors are obtained as amorphous (X-ray diffraction) loose powders. Co_{1-x}Ni_xMoO₄ (0 ≤ x ≤ 1) samples were synthesized by thermal decomposition of the amorphous precursor solids [184].

In general, the weakness of bulk catalysts as compared to supported catalysts is that they have a much lower specific surface area (S_{BET}), 10 to 100 times lower than supported alumina catalysts. Some examples are given for comparison in Table I.3.

Table I.3 : Examples of BET surface area found in the literature

Catalysts	S _{BET} (m ² .g ⁻¹)	Examples of references
Examples of supported catalysts		
Al ₂ O ₃ support	~210	Review: Shyamal et al. [185]
TiO ₂ -Al ₂ O ₃ support	~250	
ZrO ₂ -Al ₂ O ₃ support	~230	
B ₂ O ₃ -Al ₂ O ₃ support	~290	
Unsupported catalysts		
Thermal decomposition method	10 - 80	Bai et al. [178], Soled et al. [179]
Metal amine metallates method	20 - 80	Ho et al. [166]
Hydrothermal method	20 - 50	Paraguay-Delgado et al. [181]
Citrate method	2 - 13	Maione et al. [183]
Freeze-drying method	20 - 40	Vie et al. [184]
Impregnation method	20 - 50	Olivas et al. [186]

An opportunity to increase the activity of HDS catalysts appears in the increase of their S_{BET} . Our project proposes an original way of synthesizing “NiMo” that permits attaining a higher S_{BET} .

I.1.3.4. Alternatives to HDS

Several alternative processes for the removal of sulfur from petroleum crudes have been developed or are being developed. For refractory molecules, the oxidative removal of sulfur from diesel by biodesulfurization, oxidative desulfurization and ultrasound-assisted oxidative desulfurization has been covered extensively in the literature (Table I.4). Instead of reducing sulfur compounds to form H_2S , these methods oxidize the sulfur species to their corresponding sulfoxides (1-oxides) and sulfones (1,1-dioxides). Refractory sulfur compounds such as DBT and 4,6-DMDBT are only slightly more polar than hydrocarbons of similar structure. However, sulfoxides and sulfones are substantially more polar, thus permitting thus their selective removal by following the selective oxidation step with solvent extraction or solid adsorption [27].

Other ideas to remove sulfur include reactive adsorption, adsorbent usually being transition metals supported on base oxides, typically Ni on ZnO, where Ni is the hydrodesulfurization site and ZnO is converted into ZnS by H_2S (for example [187-189]). Another alternative could be “non-destructive” adsorption where sulfur species are adsorbed as molecules as such. In this field, zeolites like 5X and 13A and active carbon have been reported as efficient sorbents [190]. The Irvad process could probably be mentioned as one of the first commercially oriented process [191].

IFP/Axens, in collaboration with BP, has developed and commercialized the OATS process (Olefin Alkylation Thiophenic Sulfur compounds) based on alkylation of thiophenic and mercaptan compounds which allows obtaining sweet and desulfurized naphtha without hydrogen consumption. The alkylation of sulfur compounds over an acid catalysts leads to a boiling point shift of the resultant product toward a diesel range. A simple fractional distillation reduces then the sulfur content in the gasoline range [192-194].

Physical separation methods can be rapidly mentioned like a membrane-based process, called S-Brane, proposed by Grace Davidson and CB&I [195], or an extractive distillation

process, GT-DeSulphTM [196]. Last intriguing referenced options, precipitation [197] and electrochemical polymerization [198] can be named.

Table I.4 : A summary of process improvements and new processes (adapted from [27] and completed [199])

Technology	Effect	References
Review: Recent developments in industry	o	Babich and Moulijn [200]
Biodesulfurization (BDS)	+	Liu [201], Towfighi [202], Kong [203], Xu [204], Mohebbi [205], Bassi [206], Li [207,208]
Oxidative Desulfurization (ODS)	+	Wang [209], Song [210], Sampanthar [211], Corma [212], Lu [213], Green [214], Collins [215], García-Gutiérrez [216,217]
Ultrasound-assisted oxidative desulfurization (UAOD)	+	Doraiswamy [218], Yen [219-221], Zhao [222]
Reactive adsorption	+	Malandra [187], Gislason [188], Khare [189]
“Non-destructive” adsorption	+	Salem [190], Irvin [191]
Alkylation	+	Huff [192], Alexander [193], Bourbigou [194]
Physical separation methods	+	Zhao [195], Kumar [196]
Precipitation	+	Shiraishi [197]
Electrochemical polymerization	+	Schucker [198]

+ : positive effect, - : negative effect, o : neutral or not applicable

Although these processes are viable alternatives to remove sulfur, they require capital investment for new unit operations. As a result, refinery industries keep focusing on HDS and Deep-HSD. The discovery of new catalysts and implementation into existing hydrotreating reactors is the most promising option for achieving deep HDS.

I.1.4. Conclusion on HDS overview

Hydrodesulfurization intervenes at multiple levels in the general refinery process which makes it a leading step in crude oil processing. Current and future regulations toward sulfur concentrations in automotive fuels, together with the lower and lower quality of the available crude oils, ask for innovative and efficient solutions for oil desulfurizing. Numerous

alternative to HDS are proposed, however, as they imply costly modifications of the existing equipments, solutions that improve hydrotreatment are preferred.

What raises problems in HDS are the refractive sulfur compounds such as 4,6-DMDBT that ask more stringent conditions to be converted and today's challenge is to develop a new generation of catalysts to achieve Deep-HDS. The open literature revealed that 4,6-DMDBT is easier to convert after hydrogenation of one of its rings suggesting that a catalyst with good hydrogenation activity is required. Among the well known HDS catalysts, "NiMo" has this specific ability over "CoMo" and is therefore preferred when referring to Deep-HDS.

Having the HDS active phase supported does not really provide with more efficient catalyst due to metal/support negative interactions and the dilution of the active sites. The new trend is to work with bulk catalysts and numerous patents already exist proposing various synthesize solutions. However, bulk catalysts usually develop low specific surface area (S_{BET}). Increasing this S_{BET} appears to be a very interesting lead in the development of a new generation of catalysts. Supercritical fluids technology is known to be efficient in the synthesis of oxide nanopowders of high S_{BET} . Therefore, we propose in this project a new and original solution to achieve such an objective by synthesizing "NiMo" bulk catalyst precursors of high S_{BET} using supercritical fluid technology.

The following part presents generalities concerning Supercritical Fluids (SCFs) and material synthesis using this unconventional media and the advantages it can provides in the synthesis of our catalyst precursors of "NiMo".

I.2. Supercritical fluids

The interest of considering supercritical fluids as a media for chemical reactions has been recognized for years. Studies led within the ICMCB consolidate the know-how to elaborate nanostructures in SFCs and revealed not only the relevance of using them regarding the final characteristics of the synthesized materials but also that it permits overcoming the drawbacks of more classical solution chemistry approaches [223,224]:

- a versatile method to synthesize materials of different nature: metals, oxides, semi-conductors or even nitrides,
- well crystallized materials at relatively low temperatures (often lower than 400 °C),
- materials with original and controlled structures and microstructures, morphology and composition,
- materials with high specific surface areas,
- formation of nanocomposites by modification of the surface or volume of materials.

In 1972 the first United Nations conference on the human environment in Stockholm was held. It was here that the concept of sustainability describing an economy "in equilibrium with basic ecological support systems" was born [225]. Then in 1987, the United Nations released the Brundtland Report which defines sustainable development as "development which meets the needs of the present without compromising the ability of future generations to meet their own needs" [226]. In this context, as supercritical fluids (SCFs) are considered as a sustainable technology, they have attracted a deep interest and undergone important developments over recent years, and appear as serious alternatives to more classical material synthesis and design methods and better meet environmental guidelines.

Historically, it is C. Baron Cagniard de Latour who discovered in 1822 the critical point of a substance in his famous cannon barrel experiments. Listening to discontinuities in the sound of a rolling flint ball in a sealed cannon filled with fluids at various temperatures, he observed the critical temperature. At the critical point, the densities of the liquid and gas phases become equal and the distinction between them disappears, resulting in a single supercritical fluid phase.

During an investigation in 1822-1823 on the effects of heat and pressure on certain liquids he discovered that for each there was a certain temperature above which it refused to

remain liquid but passed into the gaseous state, no matter what amount of pressure it was subjected to, and in the case of water he determined, with a remarkable accuracy, this critical temperature to be 362 °C (actually of 374 °C) [227]. This study is considered to be the first publication describing the supercritical phenomenon.

In 1869, T. Andrews established the concepts of critical temperature and critical pressure, showing that a substance passes from vapor to liquid state without any breach of continuity [228], and in 1873, Van der Waals obtained his doctor's degree for a thesis entitled *Over de Continuïteit van den Gas- en Vloeistoftoestand (on the continuity of the gas and liquid state)* [229] in which, by considering the gaseous and liquid states as being continuous with each other although in the liquid state the sizes of the molecules could not be ignored as in the gaseous state, he was especially able to explain the fact that for each gas there is a 'critical temperature' above which the gas cannot be made liquid no matter how high the pressure. Quantifying the weak attractive forces among molecules, Van der Waals was able to correct the ideal gas law to apply to condensed gases and liquids as well (eq. 9):

$$\left(p + \frac{n^2 a}{V^2}\right) \times (V - nb) = nRT \quad (9)$$

now called the Van der Waals equation of state, with p the pressure, V the volume of the container containing the fluid, n the number of moles of the gas, T the temperature, R the universal gas constant ($8.314 \text{ J.K}^{-1}.\text{mol}^{-1}$), a the cohesion pressure (measure of the attraction between the molecules) and b the covolume (volume excluded by a mole of molecules). Thanks to this work Van der Waals not only was awarded the Nobel Prize in physics in 1910 but he also started to explain what supercritical fluids are. He developed the first equation of state that is able to describe vapor, liquid and supercritical domain. Several authors have proposed modifications of this equation and extended them to the representation of sophisticated fluids (pure compounds and mixtures) [230].

I.2.1. Definition and generalities

A pure substance can be found in three different states – solid, liquid or gas – represented by the equation of state $f(p, T, V_m) = 0$ in which the variables are the pressure p , the temperature T and the molar volume V_m [231]. The (p,T) projection of this phase diagram

(Figure I.11) clearly shows the different states in which this substance can be, depending on the combination pressure-temperature. On this diagram, the critical point is located at the maximum of the liquid/gas equilibrium curve.

A fluid is said to be “supercritical” when its pressure and temperature exceed the critical pressure p_c and critical temperature T_c . The critical coordinates of the more commonly used fluids to synthesize nanostructured materials are listed in Table I.5.

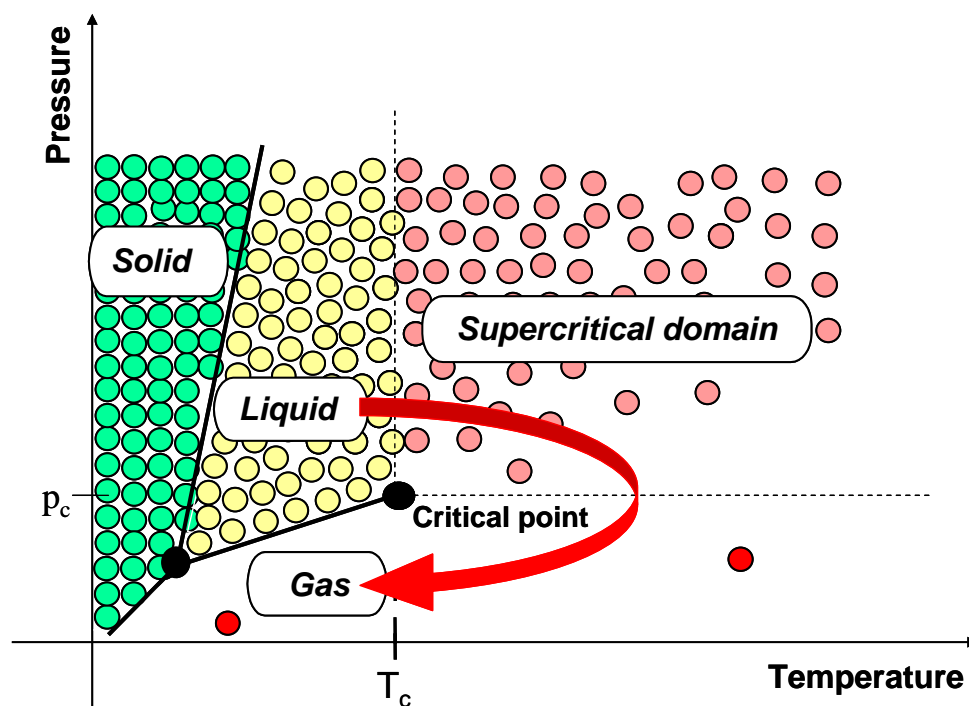


Figure I.11: Schematic representation of microscopic behavior of a pure substance in the (p,T) plane phase diagram [232]

Table I.5: Commonly used supercritical fluids and their characteristics (adapted from [233])

Compounds		T_c (°C)	p_c (MPa)	ρ_c (g.mL ⁻¹)	Molar mass (g.mol ⁻¹)
CO ₂	Carbon Dioxide	31	7.38	0.46	44
H ₂ O	Water	374	22.1	0.32	18
CH ₄ O	Methanol	239.5	8.1	0.27	32
C ₂ H ₆ O	Ethanol	241	6.3	0.28	46
C ₃ H ₈ O	1-Propanol	235.8	4.9	0.28	60
C ₃ H ₈ O	Isopropanol	264.2	5.3	0.27	60

Their viscosity is of the order of magnitude to those of gases while their density (thus their solvency) is closer to that of liquids (Table I.6). Furthermore, surface tension vanishes above the critical point. Thereby, supercritical fluids exhibit this unique property which is the opportunity to manipulate at will the reaction environment through the control of pressure and temperature, continuously from gas to liquid properties.

Supercritical fluids have physicochemical properties which are “hybrids” of those normally associated with liquids and gases.

Table I.6: Characteristic magnitudes of thermophysical properties of fluids [233]

Properties	Liquid	Supercritical fluid	Gas ^a
ρ (kg.m ⁻³)	1000	100 - 800	1
η (Pa.s)	10 ⁻³	10 ⁻⁴ - 10 ⁻⁵	10 ⁻⁵
D^b (m ² .s ⁻¹)	10 ⁻⁹	10 ⁻⁸	10 ⁻⁵

ρ = density; η = dynamic viscosity; D = diffusion coefficient. ^a At ambient conditions. ^b For small-molecule solute

As illustrated in Figure I.12 (a), the local organization includes simultaneously regions of both gas and liquid local densities. This local organization is dynamic (with a lifetime of approximately 100 ps) implying local fluctuations of density which easily explains the increase of the fluid compressibility. Figure I.12 (b) illustrates the behavior of the solvent in the case of an attractive mixture with a solute.

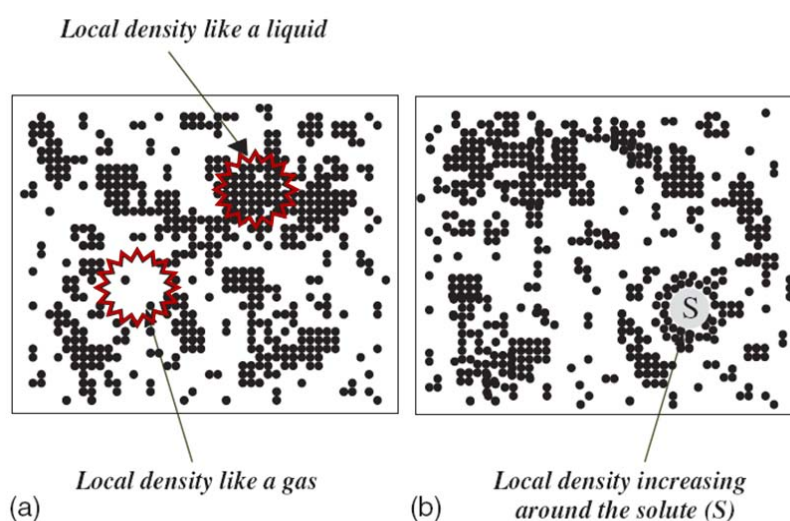


Figure I.12: Simulation of the molecule distribution in (a) a pure supercritical fluid & (b) in a supercritical fluid with a solute molecule [232]

All those specific properties such as low viscosity and high diffusivity (matrix penetration similar to gas) and relatively high density allow easier mass transfer which led to the development of supercritical fluids at an industrial scale for extraction processes [234,235]. Concerning hydrothermal oxidation for waste management, the main interest is connected to the chemical reactivity with a high solubility of organic compounds and oxygen (suppression of interface) and a high reactivity (total organic destruction) [236]. The specific properties of supercritical water are also exploited for biomass conversion and material recycling [237,238].

Concerning this PhD work, we will rather focus on the advantages and possibilities supercritical fluids offer us in materials processing and particularly in the synthesis of nanostructured materials playing with the chemistry and the nucleation/growth phenomena, parameters at the root of the characteristics of the synthesized objects.

I.2.2. Synthesis of nanomaterials in SCFs

Supercritical fluids have been used in the field of materials science since the early 90s with the rise of nanosciences and nanotechnologies. Particle processing is today one of the developments of supercritical fluid applications in fields such as chemistry, pharmacy, cosmetics, agro-food industries, energy or still microelectronics.

As already mentioned, supercritical fluids exhibit unique properties which offer the opportunity to manipulate the reaction environment such as density, viscosity, diffusivity or surface tension, through the accurate control of pressure and temperature, continuously from gas-type to liquid-type properties. These specific properties are then exploited for application in materials processing. For example, the ability to control mass transfer properties of a supercritical fluid is particularly useful for the nucleation and growth of crystals or films [239].

Classically, materials preparation in supercritical fluid can be described in three steps:

- i) solubilization of precursor in dense fluid (close to the liquid phase) since the solute solubility varies generally as a power law with respect to density,

- ii) particle formation, based on either a physical transformation or a chemical reaction,
- iii) nanopowders recovery in the low density fluid domain (close to the gas phase) in order to obtain clean and dry materials (Figure I.13).

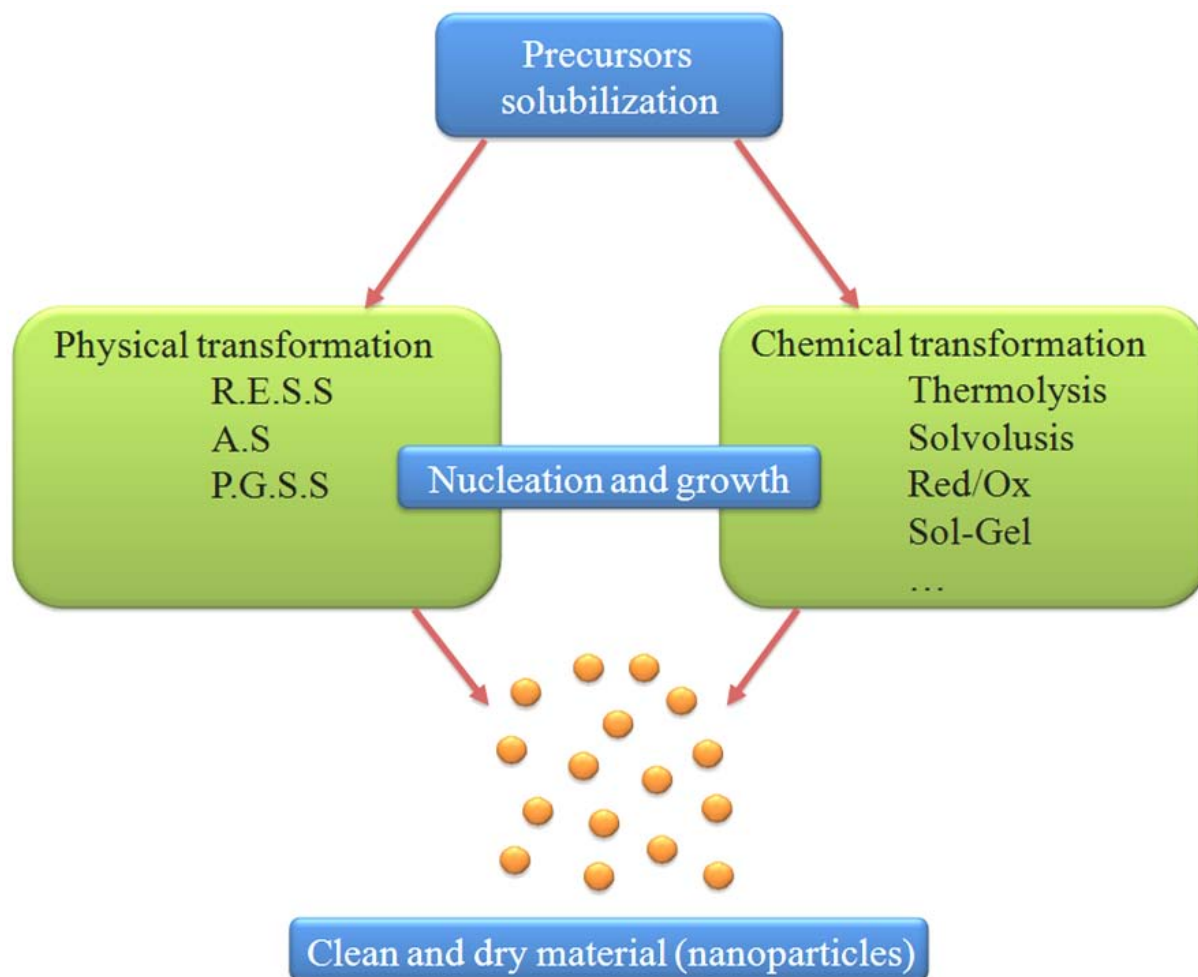


Figure I.13: General principle scheme for material processing using SCFs (adapted from [233]). Acronyms are developed further

Several papers present a good overview of the state of the art concerning processes where the driving force of nanoparticles precipitation is a physical transformation [240-242]. Those techniques are essentially used to process organic particles from nano to micrometer scale. Compared to conventional processes that use large quantities of dangerous solvents, surfactants and additives and often reject toxic wastes, SCFs technologies permit to overcome most of those drawbacks [243]. Here after are presented common techniques:

Rapid expansion of Supercritical Solution (RESS). RESS consists in saturating a supercritical fluid with a solid substrate and then depressurizing the solution through a heated nozzle into a low pressure vessel inducing a rapid nucleation of very small particles which characteristics depend on RESS parameters (temperature, pressure, nozzle geometry, etc) [244-246]. An interesting variation of RESS, the RESOLV method, consists in spraying a supercritical solution (supercritical fluid + solute) into a liquid which can contain reagents or stabilizing agents [247].

Antisolvent (A.S). When the solute is poorly soluble in a supercritical media, this one can act as an antisolvent. Practically, a liquid solution containing the solute is exposed to the supercritical fluid. The supercritical fluid should be completely miscible with the liquid solvent and diminishes its solvation capacity. Therefore, the contact between the liquid solution and the supercritical fluid induces the precipitation of the solute [231,248].

Particles from Gas-Saturated Solution/Suspension (PGSS). This process consists in solubilizing supercritical carbon dioxide in melted, liquid-suspended or solubilized substance(s), leading to a gas-saturated solution/suspension that is further expanded through a nozzle with formation of solid particles, or droplets. Cooling due to volume expansion of the gas makes the substance precipitate and the particles thus obtained are recovered from the reactor after depressurization and the supercritical fluid can be reused.

Table I.7 gathers some examples of compounds obtained from those processes and their applications

Table I.7: Examples of nanomaterials synthesized in supercritical fluids media from a physical transformation

Process	Compounds	Application	References
Polymers (some examples among a large quantity)			
R.E.S.S	Polypropylene/Polystyrene	plastics	[245]
	Polysaccharide	pharmacology	[249]
	Polycaprolactone	pharmacology	[250]
	Poly(heptadecafluorodecylacrylate)	plastics	[251,252]
S.A.S	Polystyrene	plastics	[253]
P.G.S.S	Polymethyl Methacrylate	plastics	[254]
	Pigments	paints	[246]
Hybrid material			
R.E.S.S	KI/poly(vinyl chloride)	chemical precursors	[245]
	Si(Ti)O ₂ @Polymer	model for medical researches	[255]
	Pd/C ₆ F ₁₃ C ₂ H ₄ SH	catalysis, electronics, optics...	[247]
	Cd(Pd)S/(N-Vinyl-2-pyrrolidone)	semiconductors	[256,257]
	Ag/(N-Vinyl-2-pyrrolidone)	catalysis, electronics, optics...	[258]
Inorganic material			
RESOLV	Ni, Co	additive, catalysis	[259]
	Fe	hyperthermia, magnetism	[259]
A.S	Y(Sm) acetate	high temperature superconductors	[260]
	NiCl ₂	chemical precursors	[261]
	AgNO ₃	chemical precursors	[261]
	BaCl ₂	chemical precursors	[262]
	Zn acetate	chemical precursors	[263]
P.G.S.S	Pigments	paints	[263]
Chemicals [264]			
R.E.S.S	Ibuprofen	pharmacology	[265,266]
	Naproxen	pharmacology	[265]
	Digitoxin	pharmacology	[267]
A.S	Amoxicillin	pharmacology	[268]
	Insulin	pharmacology	[269-271]
	Antibiotics	pharmacology	[268]
	Chitosan	pharmacology	[272]

Yet, those methods are not really suited for the controlled formation of inorganic nanomaterials. The second family involving a chemical reaction in supercritical fluids is better adapted for synthesizing inorganic nanostructured materials. Therefore, considering the material we are studying, we will now focus on those methods.

I.2.2.1. Formation of nanostructures in SCFs from a chemical reaction: principle

Synthesis of nanomaterials in supercritical fluids from a chemical reaction has also received considerable attention. Although the most popular material synthesis in SCF researches concern oxides with water as solvent and/or reagent, other media such as alcohol, CO₂, ammonia (or mixtures of them) are increasingly being employed for producing metals, oxides, semi-conductors and nitrides from the micrometer down to the nanometer scale.

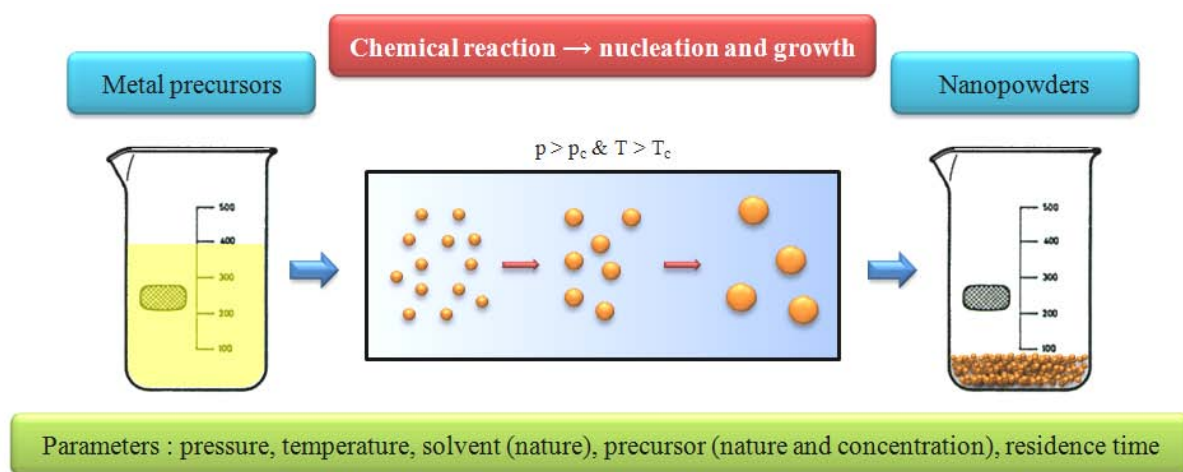


Figure I.14: General principle scheme for nanostructured material synthesis from a chemical transformation in SCFs

Different chemical reactions, which take their inspiration from solution chemistry, can be performed in supercritical fluids for nanomaterials synthesis.

Hydrothermal reactions. A really complete review on hydrothermal technology has recently been proposed [273]. The reaction equilibrium of metal precursor (salt or organic) aqueous solutions changes with temperatures which results in the formation of metal hydroxides or metal oxides. Supercritical water provides with an excellent reaction medium for hydrothermal synthesis, since it allows varying the equilibrium by shifting the dielectric constant and solvent density with pressure and temperature. The expected benefits are higher reaction rates and smaller particles. The reaction products have to be insoluble in sc-water. These reactions are based on a two-step mechanism, first is the production of monomer by hydrolysis followed by a dehydration reaction. When the supersaturation degree becomes high enough, nucleation takes place, followed by the crystal growth [242,274].

When the solvent-reactant is different from water (H_2S , NH_3 , C_6H_6 ...), this reaction is then called a solvothermal reaction and allows applying such chemical reactions for several classes of materials: sulfides, nitrides, carbides...

Thermolysis reactions. The process based on the thermal decomposition of a metal precursor is very interesting to produce fine particle with an accurate control of the size, the size distribution, the morphology and the structure [275-278]. The thermal decomposition of a metal-organic precursor is a classical process used to induce high supersaturation in a fluid phase which leads to the formation of nanoparticles. ICMCB proposed, for instance, the thermal decomposition of metallic precursors, generally from the family of acetates and acetylacetonates [233,278].

Red/Ox reactions. Oxidizing or reducing media are easily obtained by introducing oxidizing (O_2 , etc.) or reducing (H_2 , CO , etc.) gases in the reactor [279]. The degree of oxidation of an oxide can easily be controlled thanks to the enhancement of gas miscibility under supercritical conditions. These gases can also be formed *in situ* when the decomposition of precursors takes place. The reduction of metal salts or metal-organic precursors soluble in a supercritical fluid, generally in the presence of hydrogen, induces, as in the case of thermolysis reaction, high supersaturation in the SCF leading to the formation of metal nanoparticles [280]. This reaction is generally carried out in presence of surfactants to stabilize the so-formed nanoparticles. The surfactants must be soluble in the SCF to have an affinity with the nanoparticles surface to stabilize them. The functionalized nanoparticles are recovered as a dry powder, free from any organic solvents and can then be re-dispersed in an appropriate

solvent. This approach limits the number of steps for the preparation of functional nanoparticles which are ready for use.

It is also possible to use oxygen via the injection of hydrogen peroxide to control the degree of oxidation of the material to be synthesized.

Sol/Gel reactions. These reactions are based on the well known two-step mechanism, namely the hydrolysis and condensation that leads from the sol to the gel [281]. The material is recovered by removing the solvent, sometimes followed by a calcination step. The solubilized precursors form hydrated ionic species $[M(H_2O)_x]^{z+}$ that can react with water to form hydroxides $[M(H_2O)_{x-h}(OH)_h]^{(z-h)+}$. The condensation step allows forming a gel from the sol by ololation and/or oxolation, process by which metal ions form polymeric oxides in aqueous solution.

Classical sol-gel procedure produces amorphous powder which may require further thermal treatment to obtain the wished properties. Moreover, the decomposition of the precursors in the gas phase gives a final material polluted by organic residues. In comparison, the supercritical path allows the obtention of well crystallized dry powders at relatively low temperature, without any trace of solvent or modifiers since they are not needed. Moreover, this technique provides short reaction times, easy composition tuning of the mixed oxides and high surface areas for the material. Sol-Gel reactions can be carried out in pure supercritical solvents (sc-H₂O, sc-CO₂, sc-ROH, etc...) or a mix of them. Because no liquid-solid interface appears during the process, dried powders are directly recovered by removal of the supercritical solution.

The synthesis of nanomaterials in supercritical fluids by a chemical reaction is all governed by the process operating parameters. They play an important role in the design and tailoring of materials. The following part aims at presenting these parameters and their effects on the nanopowders.

I.2.2.2. Process and operation parameters

The general scheme of processes used to synthesize nanomaterials via a chemical reaction in supercritical fluids is represented on [Figure I.15](#). It is constituted of three modules (in green): the injection module, the reaction module and the material recovery module. In red are the parameters related to the components of the system.

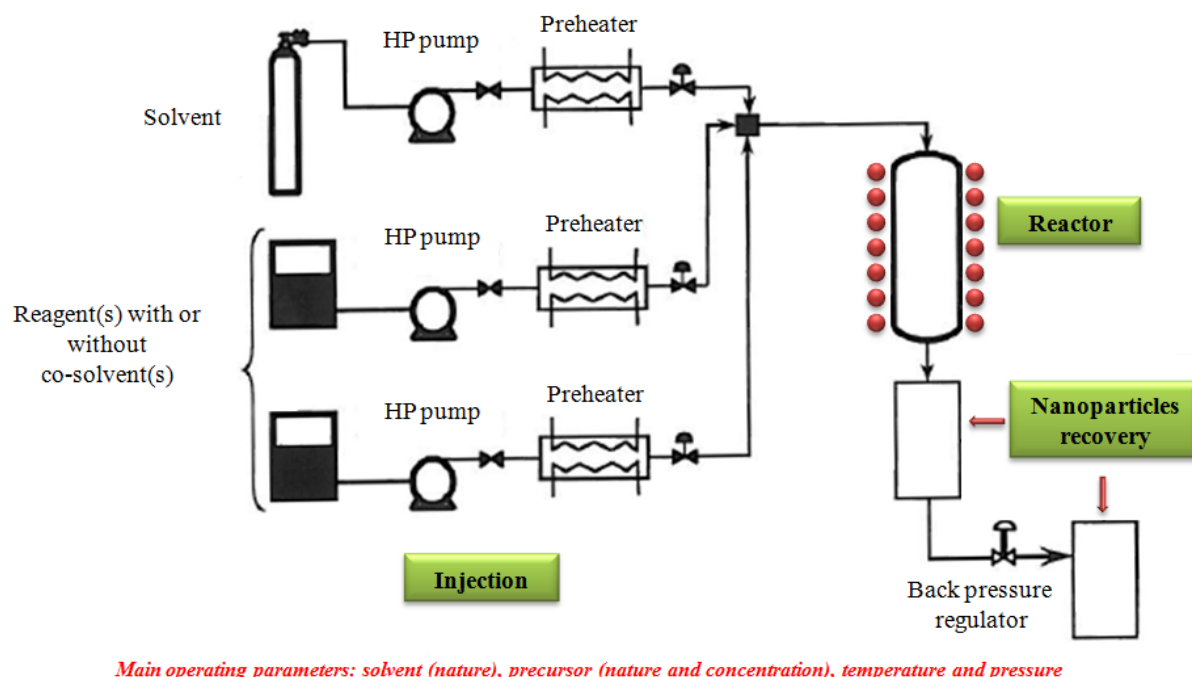


Figure I.15: General scheme of a continuous process involving chemical transformation in SCF (adapted from [\[239\]](#))

Experimental parameters must be well known and understood to use them in the best manner considering the targeted applications. From the above general scheme of our process, we can identify the following parameters we will describe then: solvent, nature and concentration of the metal precursor, residence time, temperature and pressure.

Solvent. Please note that the most commonly used supercritical fluids and their characteristics have been presented in [Table I.5](#) ([chapter I.2.1](#)). As in the case of more classical solution chemical reactions, the solvent plays an important role from various aspects. Depending on how the problem is approached, the choice of the solvent is determined by the preliminary choice of reagents, or, determines the type of reagents to use (solvation consideration). For example, the use of acetate-metal precursors as reagents will favor the choice of water as reaction media since this type of precursors are easily solvated in it.

The nature of the solvent obviously has an impact on the chemical reaction. A good example with copper: spherical metal copper particles were produced by the decomposition of copper precursors in a CO₂/ethanol supercritical mixture [282], whereas in a NH₃/methanol mixture, cubic copper nitride was obtained [278]. This result is due to the fact that supercritical CO₂ acts as an inert solvent, while NH₃ reacts with metal atoms to produce nitrides (NH₃ plays the role of both solvent and reagent).

This way, it is also possible to tune the crystallinity of the powders [283]. Regarding alumina, amorphous or boehmite alumina could be successfully synthesized using respectively CO₂/EtOH or H₂O/EtOH mixtures from Al(C₅H₇O₂)₃ (Figure I.16). The two powders present very different morphologies resulting in a different sintering path for the alumina starting material. It has been established that the alumina formed in CO₂/ethanol exhibits a significant decrease of the γ -Al₂O₃ \rightarrow α -Al₂O₃ transition temperature during sintering. The phase transition of the powder synthesized in H₂O/EtOH actually started at 1150 °C, whereas the transition of the powder obtained from CO₂/EtOH began at 1000 °C. This results in a lower densification temperature (80 °C diminution). This temperature decrease is very interesting regarding the cost reduction of the sintering process.

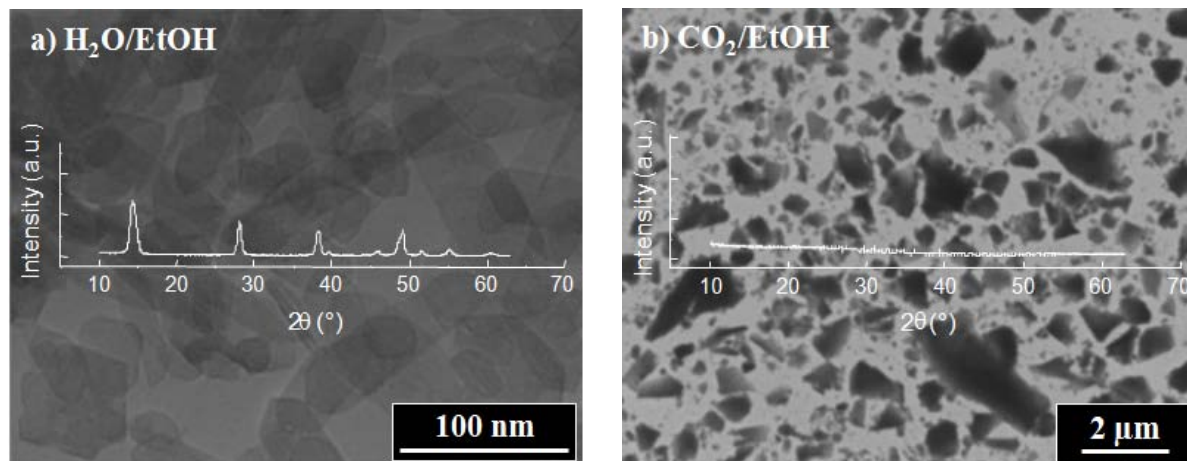


Figure I.16: Tuning of crystallinity rate of alumina powders with the fluid nature: (a) XRD pattern and TEM micrograph of boehmite nanoparticles formed in a H₂O/EtOH mixture, (b) XRD and SEM micrograph of amorphous alumina synthesized in scCO₂/EtOH mixture [223].

When using a mixture of solvents, their ratio also has an influence on the product synthesized as illustrated with BaTiO₃ synthesized under supercritical conditions. The crystallinity of the as-prepared nanoparticles can easily be controlled by changing the water/ethanol ratio, achieving up to 90% when the weight ratio is equal to 1 (Figure I.17).

This is one way to obtain a highly crystallized BaTiO₃ nanopowder that is synthesized through a one-pot process [284].

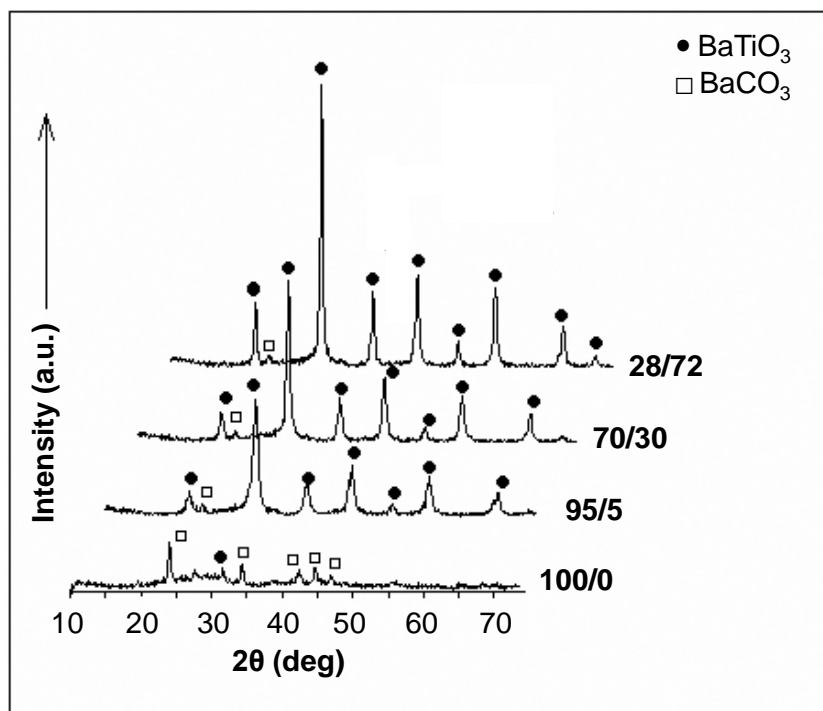


Figure I.17: Powder XRD patterns showing the phase evolution as a function of the water to ethanol weight ratio (• cubic BaTiO₃, □ BaCO₃). The patterns have been shifted gradually along both axes for the sake of clarity [284]

Metal precursor. Once again, the type of metal precursor is closely related to the nature of the solvent. Classical types of precursors used in SCFs are acetates ($M^{n+}[\text{OOC-CH}_3]_n$), acetylacetonates ($M^{n+}[\text{CH}_3\text{COCHCOCH}_3]_n$), alkoxides ($M^{n+}[\text{O-C}_x\text{H}_y]_n$) or even carbonates ($M^{n+}[\text{CO}_3]_n$) and nitrates ($M^{n+}[\text{NO}_3]_n$). An example of the importance of the nature of the precursor comes from the synthesis of ferrous-ferric oxide. Magnetite (Fe₃O₄) spherical nanoparticles (50 nm) prepared from Fe(NH₄)₂H(C₆H₅O₇)₂ solutions in supercritical water. The Fe³⁺ ions are reduced to Fe²⁺ by the CO produced during the thermal decomposition of the ammonium citrate precursor. If one wants to synthesize Fe₂O₃, the reduction of Fe³⁺ must be avoided. Under identical pressure and temperature conditions (35 MPa and 400 °C), the decomposition of Fe(NO₃)₃ results in single step-phase Fe₂O₃ nanoparticles having the same morphology and mean particle size than Fe₃O₄ [279].

Residence time. The residence time depends on the volume of the reactor, the flow rate and temperature and pressure via the density. It usually lasts from a few seconds to two minutes and can be expressed as (eq. 10):

$$t_s = \frac{V_r \cdot \rho_f(T)}{D_m} \quad (10)$$

where t_s is the residence time (s), V_r is the volume of the reactor (cm^3), ρ_f the density of the fluid depending on the temperature T and the pressure p ($\text{g} \cdot \text{cm}^{-3}$) and D_m the mass flow of the solution ($\text{g} \cdot \text{s}^{-1}$). As a general rule, the size and the crystallinity of the particles increase with the residence time since it has an influence on the degree of conversion of the reaction [285].

Temperature and pressure. The range of temperature accessible in SCFs technology is really large, starting from 31 °C (T_C of CO_2) to 500 - 600 °C depending on the studied phase.

The classical effect of the temperature on a chemical reaction is on its reaction kinetic. The Arrhenius law simply describes this temperature dependence of the rate constant.

In our case, the temperature is a parameter of paramount importance to assess whether the chemical reaction occurs under supercritical conditions or not: a too low temperature and pressure could result in a biphasic (liquid + gas) system and the reaction would occur in subcritical conditions instead of supercritical conditions.

Moreover, as illustrated by Adschiri et al., the crystallinity and nature of phases synthesized can also be driven by changing the temperature of the reactor [279,286]. In general, oxide crystallinity is enhanced by raising the reactor temperature. After hydrothermal reaction of ZrOCl_2 or TiCl_4 solutions, the products obtained at different temperatures were: (i) amorphous hydrous oxide gels (400 °C), (ii) anatase nanoparticles (TiO_2 of 20 nm at 450 °C) and (iii) cubic zirconia (ZrO_2 of 20 nm at 490 °C).

By mastering these operating parameters (solvent, precursor, residence time, temperature and pressure), supercritical fluids permit the accurate control of the physicochemical properties of nanopowders, especially the control of their composition, crystallinity rate, size and morphology.

This control over the material characteristics opens the way to numerous materials design and a wide panel of applications. Hereafter are presented some of the possibilities offered by SCFs technology in the synthesis of inorganic and hybrid nanostructured materials.

I.2.2.3. Opportunity

The ability to control the structure, chemical composition, crystallinity permits the development of numerous materials as illustrated on some examples in [Table I.8](#).

Table I.8: Examples of nanomaterials synthesized in supercritical fluids media from a chemical transformation

Material	Chemical reaction	References
Metals		
Cu	thermolysis, reduction	[287-289]
Ge	thermolysis	[290,291]
Ag	reduction	[247,292-294]
Pd	reduction	[247,294]
Ir, Pt	reduction	[295]
Nitrides		
Cu ₃ N, Ni ₃ N, Fe ₄ N, Cr ₂ N, Co ₂ N, <i>etc.</i>	thermolysis	[278]
Others		
C	reduction	[296]
NTC	hydrothermal, reduction	[297-303]
CdS	reduction	[304,305]
ZnS	reduction	[305]
CoS ₂ @C	thermolysis	[306]
Oxides: Table I.9		

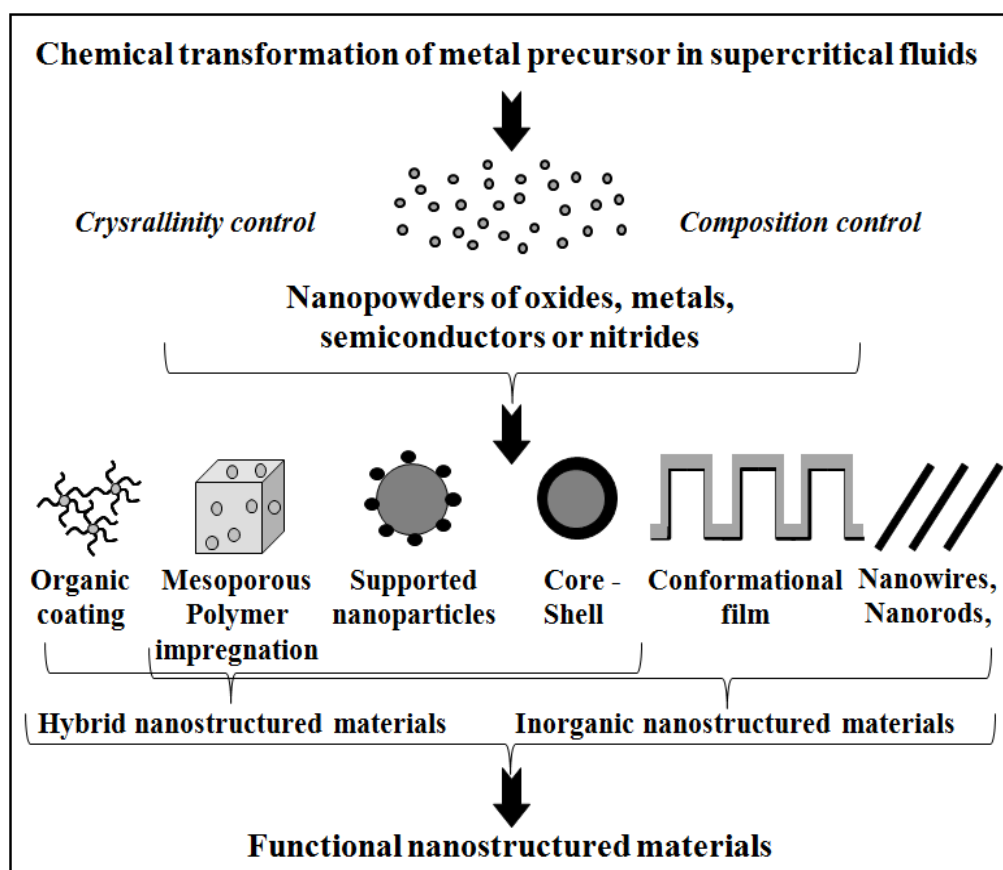


Figure I.18: Functional nanostructured materials starting from a metal precursor [223]

Supercritical fluids have been exploited for synthesizing functional nanostructured materials from the structure formation of “nanobricks” (Figure I.18). This way, we are given access to the design of advanced nanostructured materials with specific properties. This was illustrated with the design of nanorods, nanowires, conformational films, core-shell structures, supported nanoparticles, polymer impregnation with nanoparticles and organic coating of particles. The advanced nanostructured materials exhibit interesting properties for applications in many interesting fields, such as electronics, energy, optics and of course catalysis.

Our project focuses on the synthesis of the oxide NiMoO_4 , the precursor of HDS catalysts. In the following part, we will dwell a little bit more upon oxides synthesis in supercritical fluids.

I.2.3. Focus on oxides

One common use of supercritical fluids as reaction media is for the synthesis of ceramics and closely related oxide materials, in order to improve the physicochemical properties of the powders (chemical homogeneity or structural properties of materials). Metal oxide nanoparticles are of particular interest in a variety of applications including high-density information storage, magnetic resonance imaging, targeted drug delivery, bio-imaging, cancer therapy, hyperthermia, neutron capture therapy, photocatalysis, luminescence, electronic, catalysis, optics, etc... Majority of these applications requires particles of pre-determined size and narrow distribution with a high dispersibility [232,277].

The principal techniques developed for the synthesis of oxides are thermolysis, sol-gel and hydrothermal reaction. Different kinds of fine oxide particles, nanocrystalline or amorphous, simple or composite, were obtained in a range of temperatures between 180 and 260 °C at about 16 MPa for thermolysis [278,282,307] and 40 and 500 °C at 10 to 40 MPa in the case of sol/gel reaction (that can be carried out in supercritical water but also in supercritical CO₂) [274,281,308-317]. The most widely spread method to synthesize fine oxide particles in the supercritical fluid world is definitely hydrothermal synthesis in sc-H₂O and many research teams explored this technique [242,274,279,286,309,318-326]. The syntheses were mainly performed between 400 and 490 °C, using continuous reactors pressurized at 25-40 MPa. The syntheses were carried out in the temperature range of 200 to 400 °C and at 25 MPa. Iversen et al. designed specific *in situ* supercritical fluid devices for SAXS/WAXS or XRD experiments, able to work either in batch or continuous flow mode, what permits to acquire crucial information on the synthesis products and reactions kinetics in supercritical fluids, particularly for hydrothermal synthesis of various oxides (Al₂O₃ [327], Ce_{1-x}Zr_xO₂ [328], TiO₂ [329,330]).

Some examples of oxides and mixed oxides synthesized using supercritical fluids technologies are presented in Table I.9 together with some characteristics and associated applications.

Table I.9: Examples of oxides synthesized in supercritical fluids media from a chemical transformation

Oxides	Characteristics	Applications	References
LiCoO ₂ , LiFePO ₄	40 nm - 2 μm	cathode for Li batteries	[279,331]
MFe ₂ O ₄ , BaFe ₁₂ O ₁₉	30 - 110 nm (M = Fe, Co, Ni, Zn)	pigments, magnetic fluids, magnetic storage	[325]
Ce _{1-x} Zr _x O ₂	3 - 7 nm (0 < x < 1)	catalysis, UV absorbent, fuel cell	[274,286,315, 318,328,332]
SiO ₂	mesoporous	Isolation, catalysis, cosmetic, pharmaceutical...	[308,310,333]
MgO	0.5 - 2 μm	catalysts, refractory ceramics	[307,334]
ZnO	15 - 100 nm, various morphologies (nanowires, nanoparticles...)	catalysis, optics, electronics...	[335,336]
Al ₂ O ₃	100 nm - 1.5 μm, various phases (γ, α) and morphologies (nanowires, slabs, nanoparticles...)	catalysis, electronics, energy storage, medical field...	[278,282,319, 322,327,337]
TiO ₂	20 - 50 nm, various shapes (mesoporous, fibers)	sensors, catalysis, pigments, photoelectrochemical cells, membranes...	[278,282,286,311,315, 318,329,330,338-340]
MgAl ₂ O ₄	20 - 60 nm	ceramics	[341,342]
Cu ₂ O	10 - 350 nm	solar cell, semiconductors	[278,282,287]
BaTiO ₃ , Ba _{0.6} Sr _{0.4} TiO ₃	7 - 100 nm	electronics	[343-347]
Ga ₂ O ₃	1 - 10 nm	lasers, catalysis, sensors, solar cell	[278,282]
La ₂ CuO ₄ , La _{2-x} Sr _x CuO _{4-δ} , La ₂ Cu _{1-x} Pd _x O ₄	19 m ² .g ⁻¹	high-Tc superconductors, catalysis	[309]
Zr _{1-x} In _x O ₂	135 m ² .g ⁻¹	catalysis	[326]
Ce _{0.1} Y _x Zr _{0.9-x} O ₂	115 m ² .g ⁻¹	catalysis	[326]

As far as we know, studies on the synthesis of “NiMo” in supercritical fluids only concern the impregnation of NiMo on Al₂O₃ by supercritical water deposition [22]. The synthesis of bulk NiMoO₄ in SCFs has not been studied so far; this we propose to initiate with this PhD project.

I.2.4. Conclusion on SCFs opportunities

We have seen that in HDS, bulk catalysts usually develop low specific surface area (S_{BET}). Since they present better catalytic activity than supported catalysts, new solutions have to be found in order to address this weakness. We propose to develop a new synthesis method for this material using supercritical fluids as reaction media. Their unique physicochemical properties “hybrids” of those normally associated with liquids and gases offer a completely original media never used so far to synthesize “bulk” NiMoO_4 nanopowders.

This technique appears to be a versatile approach to successfully tune and improve nanoparticles or powders characteristics thanks to the possibility to modify continuously the SCFs properties by little adjustments of pressure and/or temperature. In this PhD project, we will take advantage of the possibilities chemical reactions in SCFs offer us in materials processing, particularly in the synthesis of nanostructured materials, playing with the chemistry and the nucleation/growth phenomena what is at the root of the characteristics of the synthesized objects. Using supercritical fluids renders those processes more flexible and/or simplified often with a reduction of the environmental impact. As a result, contaminant-free nanomaterials with potentially better performances (higher S_{BET} , smaller particles...), have been obtained using those improved systems compared to more classical synthesis ways.

The application to a large variety of nanomaterials has been proposed: not only oxides nanoparticles or metal and nitride nanoparticles, but also nanocomposites, nanostructured films, supported nanoparticles, polymers, core-shell particles and many other options not developed here are offered using supercritical fluids, and we can expect that even more materials will be tested in the future. However, further scientific research is still required on the large majority of the process proposed to evaluate the extent of their applicability and their scalability outside the laboratory. Yet, we expect that the shift to supercritical fluid technology for material processing in industry will be achieved in the near future by combining economical efficiency and sustainable development.

I.3. Conclusion

Through this general overview of the context of our project, we could highlight the importance of hydrodesulfurization (HDS) both from environmental and industrial considerations: sulfur compounds in fuels are partly responsible for acid rains together with NO_x , but also poison noble metal catalysts used to reduce greenhouse gases in catalytic converter and within refinery plants. Therefore, hydrotreatment (thus hydrodesulfurization) intervenes at multiple stages in refinery process what makes it a leading step in crude oil processing.

Huge research efforts have been made to remove them from any oil fractions, but traces remain, principally from dibenzothiophene and its refractive alkylated derivatives, and regarding current and future regulations toward sulfur concentrations fuels, together with the lower quality of the available crude oils, those compounds appears to be the main challenge in hydrodesulfurization for petroleum industries. This situation asks for innovative and efficient solutions for oil desulfurizing. Numerous alternative to HDS are proposed, however, as they imply costly modifications of the existing equipments, solutions that improve hydrotreatment are preferred.

What raises problems is that refractive sulfur compounds such as 4,6-dimethyldibenzothiophen (4,6-DMDBT) ask for more stringent and costly conditions to be converted, higher quantity of hydrogen and even multiple consecutive hydrotreatments to achieve set regulations. Today's objective is to develop a new generation of catalysts to achieve Deep-HDS (HDS of feedstock containing less than 500 wppm of sulfur). The open literature revealed that 4,6-DMDBT is easier to convert after hydrogenation of one of its rings (the HYD pathway) suggesting that a catalyst with good hydrogenation activity is required. Among the well known HDS catalysts, nickel promoted molybdenum catalysts have this specific ability over cobalt promoted ones and are therefore preferred when referring to Deep-HDS.

Classical HDS catalysts are composed of a supported active phase but studies showed that bulk active phase present advantages over supported one in term of catalytic activity and numerous patents already exist proposing various synthesise solutions. However, the principal weakness of bulk catalysts compared to supported ones is that they usually develop low specific surface area (S_{BET}), classically lower than $30 \text{ m}^2.\text{g}^{-1}$, maximum $80 \text{ m}^2.\text{g}^{-1}$ when supported ones present S_{BET} higher than $200 \text{ m}^2.\text{g}^{-1}$. Increasing this S_{BET} appears to be a very

interesting lead in the development of a new generation of catalysts. We have shown that supercritical fluids technology is a versatile approach to successfully tune and improve nanopowders characteristics thanks to the possibility to modify continuously the SCFs properties by little adjustments of pressure and/or temperature. They proved to be efficient in synthesizing contaminant-free oxide nanoparticles of high S_{BET} and controlled size and crystallinity.

Therefore, we propose in this project a new and original solution to achieve the synthesis of a new generation of deep-HDS “bulk” catalysts presenting high S_{BET} . Our objective is to synthesize nickel molybdate oxides NiMoO_4 powders with a targeted S_{BET} of $100 \text{ m}^2.\text{g}^{-1}$. We chose nickel promoted catalysts for their well known propensity for catalyzing the Deep-HDS reaction. They were elaborated and characterized in France within the group “supercritical fluids” of the Institut de Chimie de la Matière Condensée de Bordeaux (ICMCB-CNRS) based at the Université de Bordeaux I (UB1).

We stress that NiMoO_4 is only the precursor of the HDS catalyst, the real active phase being the sulfided form, obtained *in situ* in the reactor we used for the catalytic tests realized in Spain at the Instituto de Tecnología Química (ITQ-CSIC) located at the Universidad Politécnica de Valencia (UPV). We chose to carry out those tests on a model feedstock containing the aforementioned refractive sulfur compounds: dibenzothiophene (DBT) and 4,6-dimethyldibenzothiophene (4,6-DMDBT).

The following chapters present the results obtained in the synthesis of Deep-HDS catalyst precursors and their characteristics as well as their catalytic activity regarding DBT and 4,6 DMDBT.

I.4. References

- [1] Schulz, H., Böhringer, W., Waller, P., and Ousmanov, F. "Gas oil deep hydrodesulfurization: refractory compounds and retarded kinetics." *Catalysis Today* **1999**. vol. 49, no. 1-3, 87
- [2] Steiner, P. "Kinetic and deactivation studies of hydrodesulfurization catalysts." Ph.D. thesis, The Norwegian University of Science and Technology **2002**
- [3] Torrisi, J. S., Remans, T., and Swain, J. "The challenging chemistry of ultra-low-sulfur diesel." *World refining* **2002**. vol. December, not provided
- [4] Girgis, M. J. and Gates, B. C. "Reactivities, reaction networks, and kinetics in high-pressure catalytic hydroprocessing." *Industrial & Engineering Chemistry Research* **1991**. vol. 30, no. 9, 2021
- [5] Mazzini, S. "The big 4." *Hydrocarbon Engineering* **2009**. vol. 14, 47
- [6] Prins, R. 13.2. In: *Hydrotreating*, edited by G. Ertl. Wiley-VCH Verlag GmbH & Co. KGaA Weinheim, Germany, vol. 6 **2008** 2695–2718
- [7] Ancheyta-Juárez, J., Aguilar-Rodríguez, E., Salazar-Sotelo, D., Betancourt-Rivera, G., and Leiva-Nuncio, M. "Hydrotreating of straight run gas oil-light cycle oil blends." *Applied Catalysis A: General* **1999**. vol. 180, no. 1-2, 195
- [8] Marroquín-Sánchez, G. and Ancheyta-Juárez, J. "Catalytic hydrotreating of middle distillates blends in a fixed-bed pilot reactor." *Applied Catalysis A: General* **2001**. vol. 207, no. 1-2, 407
- [9] Ancheyta, J., Betancourt, G., Marroquín, G., G., C., Castañeda, L. C., Alonso, F., Muñoz, J. A., Gómez, M. T., and Rayo, P. "Hydroprocessing of Maya heavy crude oil in two reaction stages." *Applied Catalysis A: General* **2002**. vol. 233, no. 1-2, 159
- [10] Reinhoudt, H. R., Troost, R., Van Langeveld, A. D., Sie, S. T., Van Veen, J. A. R., and Moulijn, J. A. "Catalysts for second-stage deep hydrodesulfurisation of gas oils." *Fuel Processing Technology* **1999**. vol. 61, no. 1-2, 133
- [11] Anderson, J. R. "Kinetics and mechanisms of model compound reactions." In: *Catalysis: science and technology*, edited by H. Topsøe, B. S. Clausen, and F. E. Massoth. Springer-verlag (Berlin) **1996** 114
- [12] Norvell, N. and Levy, R. B. "The organic chemistry of hydrodenitrogenation." *Journal of Catalysis* **1979**. vol. 58, no. 3, 485
- [13] Zdrasil, M. "Comments on "denitrogenation of piperdine on alumina, silica, and silica-aluminas: The effect of surface acidity"." *Journal of Catalysis* **1993**. vol. 141, no. 1, 316
- [14] Rajagopal, S. and Miranda, R. "Reply to comments on "denitrogenation of piperdine on alumina, silica, and silica-aluminas: The effect of surface acidity"." *Journal of Catalysis* **1993**. vol. 141, no. 1, 318
- [15] Todorova, T., Prins, R., and Weber, T. "A density functional theory study of the hydrogenolysis reaction of CH₃SH to CH₄ on the catalytically active (100) edge of 2H-MoS₂." *Journal of Catalysis* **2005**. vol. 236, no. 2, 190
- [16] Kieran, P. and Kemball, C. "Catalytic reactions of ethyl mercaptan on disulfides of molybdenum and tungsten." *Journal of Catalysis* **1965**. vol. 4, no. 3, 380
- [17] Wilson, R. L. and Kemball, C. "Catalytic reactions of methyl mercaptan on disulfides of molybdenum and tungsten." *Journal of Catalysis* **1964**. vol. 3, no. 5, 426

- [18] Schulz, H., Schon, M., and Rahman, N. M. "Chapter 6: hydrogenative denitrogenation of model compounds as related to the refining of liquid fuels." In: *Catalytic Hydrogenation*, edited by L. Cervený, Elsevier, *Studies in Surface Science and Catalysis*, vol. 27, 201 – 255 **1986**
- [19] Brunet, S., Mey, D., Pérot, G., Bouchy, C., and Diehl, F. "On the hydrodesulfurization of FCC gasoline: a review." *Applied Catalysis A: General* **2005**. vol. 278, no. 2, 143
- [20] Sauer, N. N., Markel, E. J., Schrader, G. L., and Angelici, R. J. "Studies of the mechanism of thiophene hydrodesulfurization: Conversion of 2,3- and 2,5-dihydrothiophene and model organometallic compounds." *Journal of Catalysis* **1989**. vol. 117, no. 1, 295
- [21] Xu, H. and Friend, C. M. "Effect of sulfur on desulfurization kinetics and selectivity: 2,5-dihydrothiophene on molybdenum(110)-(4.times.1)-sulfur." *The Journal of Physical Chemistry* **1993**. vol. 97, no. 14, 3584
- [22] Alibouri, M., Ghoreishi, S. M., and Aghabozorg, H. R. "Effect of supercritical deposition synthesis on dibenzothiophene hydrodesulfurization over NiMo/Al₂O₃ nanocatalyst." *AIChE Journal* **2009**. vol. 55, no. 10, 2665
- [23] Vanrysselberghe, V. and Froment, G. F. "Hydrodesulfurization of dibenzothiophene on a CoMo/Al₂O₃ catalyst: Reaction network and kinetics." *Industrial & Engineering Chemistry Research* **1996**. vol. 35, no. 10, 3311
- [24] Vanrysselberghe, V., Le Gall, R., and Froment, G. F. "Hydrodesulfurization of 4-methyldibenzothiophene and 4,6-dimethyldibenzothiophene on a CoMo/Al₂O₃ catalyst: Reaction network and kinetics." *Industrial & Engineering Chemistry Research* **1998**. vol. 37, no. 4, 1235
- [25] Song, C. J., Kwak, C., and Moon, S. H. "Effect of fluorine addition on the formation of active species and hydrotreating activity of NiWS/Al₂O₃ catalysts." *Catalysis Today* **2002**. vol. 74, no. 3-4, 193
- [26] Kwak, C., Lee, J. J., Bae, J. S., Choi, K., and Moon, S. H. "Hydrodesulfurization of DBT, 4-MDBT, and 4,6-DMDBT on fluorinated CoMoS/Al₂O₃ catalysts." *Applied Catalysis A: General* **2000**. vol. 200, no. 1-2, 233
- [27] Oyama, S. T., Gott, T., Zhao, H., and Lee, Y. K. "Transition metal phosphide hydroprocessing catalysts: A review." *Catalysis Today* **2009**. vol. 143, no. 1-2, 94 . International Symposium on Catalysis for Clean Energy and Sustainable Chemistry, on occasion of the 60th birthday of Prof. Jose L.G. Fierro
- [28] Heinemann, H. A.1.3. In: *Handbook of Heterogeneous Catalysis*, edited by G. Ertl, H. Knözinger, and J. Weitkamp. Wiley-VCH, New-York, vol. 1 **1997** 35
- [29] Delmon, B. A.2.2.2. In: *Handbook of Heterogeneous Catalysis*, edited by G. Ertl, H. Knözinger, and J. Weitkamp. Wiley-VCH, New-York, vol. 1 **1997** 264
- [30] Luck, F. "A review of support effects on the activity and selectivity of hydrotreating catalysts." *Bulletin des Sociétés Chimiques Belges* **1991**. vol. 100, 781
- [31] Vít, Z. "Comparison of carbon- and alumina-supported Mo, CoMo and NiMo catalysts in parallel hydrodenitrogenation and hydrodesulphurization." *Fuel* **1993**. vol. 72, no. 1, 105
- [32] Massoth, F. E., Muralidhar, G., and Shabtai, J. "Catalytic functionalities of supported sulfides : II. effect of support on Mo dispersion." *Journal of Catalysis* **1984**. vol. 85, no. 1, 53
- [33] Muralidhar, G., Massoth, F. E., and Shabtai, J. "Catalytic functionalities of supported sulfides : I. effect of support and additives on the CoMo catalyst." *Journal of Catalysis* **1984**. vol. 85, no. 1, 44
- [34] Shimada, H., Sato, T., Yoshimura, Y., Hiraishi, J., and Nishijima, A. "Support effect on the catalytic activity and properties of sulfided molybdenum catalysts." *Journal of Catalysis* **1988**. vol. 110, no. 2, 275

- [35] Ramirez, J., Fuentes, S., Díaz, G., Vrinat, M., Breysse, M., and Lacroix, M. "Hydrodesulphurization activity and characterization of sulphided molybdenum and cobalt-molybdenum catalysts : Comparison of alumina-, silica-alumina- and titania-supported catalysts." *Applied Catalysis* **1989**. vol. 52, no. 1, 211
- [36] Ramirez, J., Ruiz-Ramirez, L., Cedeno, L., Harle, V., Vrinat, M., and Breysse, M. "Titania-alumina mixed oxides as supports for molybdenum hydrotreating catalysts." *Applied Catalysis A: General* **1993**. vol. 93, no. 2, 163
- [37] Ledoux, M. J., Peter, A., Blekkan, E. A., and Luck, F. "The role of the nature and the purity of the alumina support on the hydrodesulfurization activity of CoMo sulfides." *Applied Catalysis A: General* **1995**. vol. 133, no. 2, 321
- [38] Sakashita, Y., Araki, Y., and H., S. "Effects of surface orientation of alumina supports on the catalytic functionality of molybdenum sulfide catalysts." *Applied Catalysis A: General* **2001**. vol. 215, no. 1-2, 101
- [39] Maugé, F., Lamotte, J., Nesterenko, N. S., Manoilova, O., and Tsyganenko, A. A. "FT-IR study of surface properties of unsupported MoS₂." *Catalysis Today* **2001**. vol. 70, no. 1-3, 271
- [40] Schuit, G. C. A. and Gates, B. C. "Chemistry and engineering of catalytic hydrodesulfurization." *AIChE Journal* **1973**. vol. 19, no. 3, 417
- [41] Lipsch, J. M. J. G. and Schuit, G. C. A. "The CoO-MoO₃/Al₂O₃ catalyst : I. cobalt molybdate and the cobalt oxide molybdenum oxide system." *Journal of Catalysis* **1969**. vol. 15, no. 2, 163
- [42] Lipsch, J. M. J. G. and Schuit, G. C. A. "The CoO-MoO₃/Al₂O₃ catalyst : Ii. the structure of the catalyst." *Journal of Catalysis* **1969**. vol. 15, no. 2, 174
- [43] Lipsch, J. M. J. G. and Schuit, G. C. A. "The CoO-MoO₃/Al₂O₃ catalyst : Iii. catalytic properties." *Journal of Catalysis* **1969**. vol. 15, no. 2, 179
- [44] De Beer, V. H. J., Van Sint Fiet, T. H. M., Engelen, J. F., Van Haandel, A. C., Wolfs, M. W. J., Amberg, C. H., and Schuit, G. C. A. "The CoO-MoO₃/Al₂O₃ catalyst. iv. pulse and continuous flow experiments and catalyst promotion by cobalt, nickel, zinc, and manganese." *Journal of Catalysis* **1972**. vol. 27, no. 3, 357
- [45] Voorhoeve, R. J. H. and Stuiver, J. C. M. "Kinetics of hydrogenation on supported and bulk nickel-tungsten sulfide catalysts." *Journal of Catalysis* **1971**. vol. 23, no. 2, 228
- [46] Voorhoeve, R. J. H. "Electron spin resonance study of active centers in nickel-tungsten sulfide hydrogenation catalysts." *Journal of Catalysis* **1971**. vol. 23, no. 2, 236
- [47] Huisman, R., de Jonge, R., Haas, C., and Jellinek, F. "Trigonal-prismatic coordination in solid compounds of transition metals." *Journal of Solid State Chemistry* **1971**. vol. 3, no. 1, 56
- [48] Grange, P. "Catalytic hydrodesulfurization." *Catalysis Reviews: Science and Engineering* **1980**. vol. 21, no. 1, 135
- [49] Delmon, B. "A new hypothesis explaining synergy between two phases in heterogeneous catalysis. the case of hydrodesulfurization catalysts." *Bulletin des Sociétés Chimiques Belges* **1979**. vol. 88, 979
- [50] Pirote, D., Zabala, J. M., Grange, P., and Delmon, B. "The remote control of the active sites of hydrodesulfurization catalysts: comparison of experimental results with the model." *Bulletin des Sociétés Chimiques Belges* **1981**. vol. 90, 1239
- [51] Clausen, B. S., Topsøe, H., Candia, R., Villadsen, J., Lengeler, B., Als-Nielsen, J., and Christensen, F. "Extended X-ray absorption fine structure study of the cobalt-molybdenum hydrodesulfurization catalysts." *The Journal of Physical Chemistry* **1981**. vol. 85, no. 25, 3868

- [52] Topsøe, H., Clausen, B. S., Candia, R., Wivel, C., and Mørup, S. "In situ Mössbauer emission spectroscopy studies of unsupported and supported sulfided Co-Mo hydrodesulfurization catalysts: Evidence for and nature of a Co-Mo-S phase." *Journal of Catalysis* **1981**. vol. 68, no. 2, 433
- [53] Wivel, C., Candia, R., Clausen, B. S., Mørup, S., and Topsøe, H. "On the catalytic significance of a Co-Mo-S phase in Co-Mo/Al₂O₃ hydrodesulfurization catalysts: Combined in situ Mössbauer emission spectroscopy and activity studies." *Journal of Catalysis* **1981**. vol. 68, no. 2, 453
- [54] Clausen, B. S., Lengeler, B., Candia, R., Als-Nielsen, J., and Topsøe, H. "EXAFS studies of calcined and sulfided cobalt-molybdenum HDS catalysts." *Bulletin des Sociétés Chimiques Belges* **1981**. vol. 90, 1249
- [55] Topsøe, H., Clausen, B. S., Candia, R., Wivel, C., and Moerup, S. "Applications of Mössbauer spectroscopy to the study of HDS catalysts." *Bulletin des Sociétés Chimiques Belges* **1981**. vol. 90, 1189
- [56] Topsøe, H., Candia, R., Topsøe, N. Y., and Clausen, B. S. "On the state of the cobalt-molybdenum-sulfur model." *Bulletin des Sociétés Chimiques Belges* **1984**. vol. 93, 783
- [57] Topsøe, N. Y. and Topsøe, H. "Characterization of the structures and active sites in sulfided Co-Mo/Al₂O₃ and Ni-Mo/Al₂O₃ catalysts by NO chemisorption." *Journal of Catalysis* **1983**. vol. 84, no. 2, 386
- [58] Byskov, L. S., Nørskov, J., Clausen, B. S., and Topsøe, H. "Edge termination of MoS₂ and CoMoS₂ catalyst particles." *Catalysis Letters* **2000**. vol. 64, no. 2, 95
- [59] Topsøe, H. and Clausen, B. S. "Importance of Co-Mo-S type structures in hydrodesulfurization." *Catalysis Reviews: Science and Engineering* **1984**. vol. 26, no. 3, 395
- [60] Byskov, L. S., Nørskov, J. K., Clausen, B. S., and Topsøe, H. "DFT calculations of unpromoted and promoted MoS₂-based hydrodesulfurization catalysts." *Journal of Catalysis* **1999**. vol. 187, no. 1, 109
- [61] Raybaud, P., Hafner, J., Kresse, G., Kasztelan, S., and Toulhoat, H. "Structure, energetics, and electronic properties of the surface of a promoted MoS₂ catalyst: An *ab initio* local density functional study." *Journal of Catalysis* **2000**. vol. 190, no. 1, 128
- [62] Raybaud, P., Hafner, J., Kresse, G., Kasztelan, S., and Toulhoat, H. "*Ab initio* study of the H₂-H/MoS₂ gas-solid interface: The nature of the catalytically active sites." *Journal of Catalysis* **2000**. vol. 189, no. 1, 129
- [63] Cristol, S., Paul, J. F., Payen, E., Bougeard, D., Clemendot, S., and Hutschka, F. "Theoretical study of the MoS₂ (100) surface: A chemical potential analysis of sulfur and hydrogen coverage." *The Journal of Physical Chemistry B* **2000**. vol. 104, no. 47, 11220
- [64] Sun, M., Nelson, A. E., and Adjaye, J. "On the incorporation of nickel and cobalt into MoS₂-edge structures." *Journal of Catalysis* **2004**. vol. 226, no. 1, 32
- [65] Schweiger, H., Raybaud, P., Kresse, G., and Toulhoat, H. "Shape and edge sites modifications of MoS₂ catalytic nanoparticles induced by working conditions: A theoretical study." *Journal of Catalysis* **2002**. vol. 207, no. 1, 76
- [66] Schweiger, H., Raybaud, P., and Toulhoat, H. "Promoter sensitive shapes of Co(Ni)MoS nanocatalysts in sulfo-reductive conditions." *Journal of Catalysis* **2002**. vol. 212, no. 1, 33
- [67] Ho, T. C. "Hydrodenitrogenation catalysis." *Catalysis Reviews: Science and Engineering* **1988**. vol. 30, no. 1, 117
- [68] Prins, R., De Beer, V. H. J., and Somorjai, G. A. "Structure and function of the catalyst and the promoter in CoMo hydrodesulfurization catalysts." *Catalysis Reviews: Science and Engineering* **1989**. vol. 31, no. 1, 1

- [69] Farias, M. H., Gellman, A. J., Somorjai, G. A., Chianelli, R. R., and Liang, K. S. "The Co coadsorption and reactions of sulfur, hydrogen and oxygen on clean and sulfided Mo(100) and on MoS₂(0001) crystal faces." *Surface Science* **1984**. vol. 140, no. 1, 181
- [70] Nørskov, J. K., Clausen, B. S., and Topsøe, H. "Understanding the trends in the hydrodesulfurization activity of the transition metal sulfides." *Catalysis Letters* **1992**. vol. 13, no. 1, 1
- [71] Schulz, H., Böhringer, W., Ousmanov, F., and Waller, P. "Refractory sulfur compounds in gas oils." *Fuel Processing Technology* **1999**. vol. 61, no. 1-2, 5
- [72] Rabarihoela-Rakotovo, V., Diehl, F., and Brunet, S. "Deep HDS of diesel fuel: Inhibiting effect of nitrogen compounds on the transformation of the refractory 4,6-dimethyldibenzothiophene over a NiMoP/Al₂O₃ catalyst." *Catalysis Letters* **2009**. vol. 129, no. 1, 50
- [73] Adam, F., Bertoncini, F., Dartiguelongue, C., Marchand, K., Thiébaud, D., and Hennion, M. C. "Comprehensive two-dimensional gas chromatography for basic and neutral nitrogen speciation in middle distillates." *Fuel* **2009**. vol. 88, no. 5, 938
- [74] Zhang, Q., Ishihara, A., Yashima, H., Qian, W., Tsutsui, H., and Kabe, T. "Deep desulfurization of light oil (part 5) hydrodesulfurization of methyl-substituted benzothiophenes and dibenzothiophenes in light gas oil catalyzed by various sulfided Co-Mo/Al₂O₃ and Ni-Mo/Al₂O₃." *Journal of The Japan Petroleum Institute* **1997**. vol. 40, 29
- [75] Kabe, T., Ishihara, A., and Zhang, Q. "Deep desulfurization of light oil. part 2: hydrodesulfurization of dibenzothiophene, 4-methyldibenzothiophene and 4,6-dimethyldibenzothiophene." *Applied Catalysis A: General* **1993**. vol. 97, no. 1, L1
- [76] Ma, X., Sakanishi, K., Isoda, T., and Mochida, I. "Comparison of sulfided Co-Mo/Al₂O₃ and Ni-Mo/Al₂O₃ catalysts in deep hydrodesulfurization of gas oil fractions." *Preprints - American Chemical Society, Division of Petroleum Chemistry* **1994**. vol. 39, 622
- [77] Farag, H., Whitehurst, D. D., Sakanishi, K., and Mochida, I. "Improving kinetic analysis of sequential and parallel reactions of hydrodesulfurization of dibenzothiophenes by establishing reasonable boundaries for reaction rate constants." *Catalysis Today* **1999**. vol. 50, no. 1, 49
- [78] Chianelli, R. R., Siadati, M. H., De la Rosa, M. P., Berhault, G., Wilcoxon, J. P., Bearden, R., and Abrams, B. L. "Catalytic properties of single layers of transition metal sulfide catalytic materials." *Catalysis Reviews: Science and Engineering* **2006**. vol. 48, no. 1, 1
- [79] Kim, H., Lee, J. J., Koh, J. H., and Moon, S. H. "Performance of fluorine-added, sonochemically prepared MoS₂/Al₂O₃ catalysts in the hydrodesulfurization of dibenzothiophene compounds." *Applied Catalysis B: Environmental* **2004**. vol. 54, no. 1, 33
- [80] Lee, J. J., Kim, H., Koh, J. H., Jo, A., and Moon, S. H. "Performance of fluorine-added CoMoS/Al₂O₃ prepared by sonochemical and chemical vapor deposition methods in the hydrodesulfurization of dibenzothiophene and 4,6-dimethyldibenzothiophene." *Applied Catalysis B: Environmental* **2005**. vol. 61, no. 3-4, 274
- [81] Usman, Yamamoto, T., Kubota, T., and Okamoto, Y. "Effect of phosphorus addition on the active sites of a Co-Mo/aAl₂O₃ catalyst for the hydrodesulfurization of thiophene." *Applied Catalysis A: General* **2007**. vol. 328, no. 2, 219

- [82] Okamoto, Y. "A novel preparation-characterization technique of hydrodesulfurization catalysts for cleaner fuels." *Catalysis Today* **2008**. vol. 132, no. 1-4, 9 . 11th Korea-Japan Symposium on Catalysis, 21-23 May 2007, Seoul, Korea
- [83] Ramos, R. R., Bolívar, C., Castillo, J., Hung, J., and Scott, C. E. "Ultrasound assisted synthesis of nanometric Ni, Co, NiMo and CoMo HDS catalysts." *Catalysis Today* **2008**. vol. 133-135, 277 . Selected Contributions of the XX Ibero-American Symposium of Catalysis
- [84] Skrabalak, S. E. and Suslick, K. S. "Porous MoS₂ synthesized by ultrasonic spray pyrolysis." *Journal of the American Chemical Society* **2005**. vol. 127, no. 28, 9990
- [85] Liu, B., Xha, X., Sheng, S., Yang, W., and G. -. *Cuihua Xuebao* **2004**. vol. 25, 770
- [86] Liu, B., Zha, X., Meng, Q., Hou, H., Gao, S., Zhang, J., Sheng, S., and Yang, W. -. *Cuihua Xuebao* **2005**. vol. 26, 458
- [87] Liu, X., Zhang, L., Shi, Y., Nie, H., and Long, X. -. *Cuihua Xuebao* **2004**. vol. 25, 748
- [88] Toba, M., Miki, Y., Kanda, Y., Matsui, T., Harada, M., and Yoshimura, Y. "Selective hydrodesulfurization of FCC gasoline over CoMo/Al₂O₃ sulfide catalyst." *Catalysis Today* **2005**. vol. 104, no. 1, 64 . Catalysis in Ultra-clean Fuels Production
- [89] Fujikawa, T., Kato, M., Ebihara, T., Hagiwara, K., Kubota, T., and Okamoto, Y. "Development of highly active Co-Mo catalysts with phosphorus and citric acid for ultra-deep desulfurization of diesel fractions (part 2) characterization of active sites." *Journal of the Japan Petroleum Institute* **2005**. vol. 48, no. 2, 114
- [90] Escobar, J., Barrera, M., de los Reyes, J., Toledo, J., Santes, V., and Colín, J. "Effect of chelating ligands on Ni-Mo impregnation over wide-pore ZrO₂-TiO₂." *Journal of Molecular Catalysis A: Chemical* **2008**. vol. 287, no. 1-2, 33
- [91] Costa, V., Marchand, K., Digne, M., and Geantet, C. "New insights into the role of glycol-based additives in the improvement of hydrotreatment catalyst performances." *Catalysis Today* **2008**. vol. 130, no. 1, 69 . New developments in sulfide catalysis: Linking industrial needs to fundamental challenges - Proceedings of the 4th International Symposium on Molecular Aspects of Catalysis by Sulfides (MACS-IV)
- [92] Lélías, M., van Gestel, J., Maugé, F., and van Veen, J. "Effect of NTA addition on the formation, structure and activity of the active phase of cobalt-molybdenum sulfide hydrotreating catalysts." *Catalysis Today* **2008**. vol. 130, no. 1, 109 . New developments in sulfide catalysis: Linking industrial needs to fundamental challenges - Proceedings of the 4th International Symposium on Molecular Aspects of Catalysis by Sulfides (MACS-IV)
- [93] Rana, M. S., Capitaine, E. M. R., Leyva, C., and Ancheyta, J. "Effect of catalyst preparation and support composition on hydrodesulfurization of dibenzothiophene and Maya crude oil." *Fuel* **2007**. vol. 86, no. 9, 1254 . Special Issue: Mexican Congress on Chemical Reaction Engineering 2006
- [94] Rana, M. S., Ramírez, J., Gutiérrez-Alejandre, A., Ancheyta, J., Cedeño, L., and Maity, S. K. "Support effects in CoMo hydrodesulfurization catalysts prepared with EDTA as a chelating agent." *Journal of Catalysis* **2007**. vol. 246, no. 1, 100
- [95] Texier, S., Berhault, G., Pérot, G., and Diehl, F. "Activation of alumina-supported hydrotreating catalysts by organosulfides or H₂S: Effect of the H₂S partial pressure used during the activation process." *Applied Catalysis A: General* **2005**. vol. 293, 105

- [96] Frizi, N., Blanchard, P., Payen, E., Baranek, P., Lancelot, C., Rebeilleau, M., Dupuy, C., and Dath, J. P. "Genesis of new gas oil HDS catalysts: Study of their liquid phase sulfidation." *Catalysis Today* **2008**. vol. 130, no. 1, 32. New developments in sulfide catalysis: Linking industrial needs to fundamental challenges - Proceedings of the 4th International Symposium on Molecular Aspects of Catalysis by Sulfides (MACS-IV)
- [97] Ojeda, J., Escalona, N., Fierro, J. L. G., López Agudo, A., and Gil-Llambías, F. J. "Effect of the preparation of Re/ γ -Al₂O₃ catalysts on the HDS and HDN of gas oil." *Applied Catalysis A: General* **2005**. vol. 281, no. 1-2, 25
- [98] Hubaut, R. "Vanadium-based sulfides as hydrotreating catalysts." *Applied Catalysis A: General* **2007**. vol. 322, 121. Active Phases for Hydrotreating Catalysis
- [99] Vít, Z. "Iridium sulfide and Ir promoted mo based catalysts." *Applied Catalysis A: General* **2007**. vol. 322, 142. Active Phases for Hydrotreating Catalysis
- [100] Escalona, N., Vrinat, M., Laurenti, D., and Gil-Llambías, F. J. "Rhenium sulfide in hydrotreating." *Applied Catalysis A: General* **2007**. vol. 322, 113. Active Phases for Hydrotreating Catalysis
- [101] Escalona, N., Ojeda, J., Baeza, P., García, R., Palacios, J. M., Fierro, J. L. G., López Agudo, A., and Gil-Llambías, F. J. "Synergism between unsupported Re and Co or Ni sulfide catalysts in the HDS and HDN of gas oil." *Applied Catalysis A: General* **2005**. vol. 287, no. 1, 47
- [102] De Los Reyes, J. A. "Ruthenium sulfide supported on alumina as hydrotreating catalyst." *Applied Catalysis A: General* **2007**. vol. 322, 106. Active Phases for Hydrotreating Catalysis
- [103] Giraldo, S. A., Pinzón, M. H., and Centeno, A. "Behavior of catalysts with rhodium in simultaneous hydrodesulfurization and hydrogenation reactions." *Catalysis Today* **2008**. vol. 133-135, 239. Selected Contributions of the XX Ibero-American Symposium of Catalysis
- [104] Baldovino-Medrano, V., Giraldo, S. A., and Centeno, A. "The functionalities of Pt/ γ -Al₂O₃ catalysts in simultaneous HDS and HDA reactions." *Fuel* **2008**. vol. 87, no. 10-11, 1917
- [105] Ishihara, A., Mochizuki, H., Lee, J., Qian, E. W., Kabe, T., Tatsumi, Y., and Umehara, K. "Development of hydrodesulfurization catalysts using molybdenum complex with molybdenum-sulfur bonds (part 1) effect of activation method on catalytic activity." *Journal of the Japan Petroleum Institute* **2005**. vol. 48, no. 3, 137
- [106] Ho, T. C. "Hydroprocessing catalysis on metal sulfides prepared from molecular complexes." *Catalysis Today* **2008**. vol. 130, no. 1, 206. "New developments in sulfide catalysis: Linking industrial needs to fundamental challenges" - Proceedings of the 4th International Symposium on Molecular Aspects of Catalysis by Sulfides (MACS-IV)
- [107] Poisot, M., Bensch, W., Fuentes, S., and Alonso, G. "Decomposition of tetra-alkylammonium thiomolybdates characterised by thermoanalysis and mass spectrometry." *Thermochimica Acta* **2006**. vol. 444, no. 1, 35
- [108] Poisot, M. and Bensch, W. "Decomposition of tetraalkylammonium thiotungstates characterized by thermoanalysis, mass spectrometry, X-ray diffractometry and scanning electron microscopy." *Thermochimica Acta* **2007**. vol. 453, no. 1, 42
- [109] Romero-Rivera, R., Del Valle, M., Alonso, G., Flores, E., Castellón, F., Fuentes, S., and Cruz-Reyes, J. "Cyclohexene hydrogenation with molybdenum disulfide catalysts prepared by *ex situ* decomposition of ammonium thiomolybdate-cetyltrimethylammonium thiomolybdate mixtures." *Catalysis Today* **2008**. vol. 130, no. 2-4, 354. International Symposium on Advances in Hydroprocessing of Oils Fractions (ISAHOF 2007)

- [110] González-Cortés, S. L., Xiao, T. C., Costa, P. M. F. J., Fontal, B., and Green, M. L. H. "Urea-organic matrix method: an alternative approach to prepare Co-MoS₂/γ-Al₂O₃ HDS catalyst." *Applied Catalysis A: General* **2004**. vol. 270, no. 1-2, 209
- [111] González-Cortés, S. L., Xiao, T. C., Rodulfo-Baechler, S. M. A., and Green, M. L. "Impact of the urea-matrix combustion method on the HDS performance of Ni-MoS₂/γ-Al₂O₃ catalysts." *Journal of Molecular Catalysis A: Chemical* **2005**. vol. 240, no. 1-2, 214
- [112] González-Cortés, S. L., Xiao, T. C., Lin, T. W., and Green, M. L. "Influence of double promotion on HDS catalysts prepared by urea-matrix combustion synthesis." *Applied Catalysis A: General* **2006**. vol. 302, no. 2, 264
- [113] González-Cortés, S. L., Rodulfo-Baechler, S. M. A., Xiao, T. C., and Green, M. L. H. "Rationalizing the catalytic performance of γ-alumina-supported Co(Ni)-Mo(W) HDS catalysts prepared by urea-matrix combustion synthesis." *Catalysis Letters* **2006**. vol. 111, no. 1, 57
- [114] Olivas, A., Verduzco, R., Alonso, G., and Fuentes, S. "Trimetallic NiMoW unsupported catalysts for HDS." *American Chemical Society, Division of Petroleum Chemistry, Preprints* **2005**. vol. 50, no. 4, 372
- [115] Nava, H., Pedraza, F., and Alonso, G. "Nickel-molybdenum-tungsten sulfide catalysts prepared by *in situ* activation of tri-metallic (Ni-Mo-W) alkylthiomolybdotungstates." *Catalysis Letters* **2005**. vol. 99, no. 1, 65
- [116] Huirache-Acuña, R., Albiter, M. A., Ornelas, C., Paraguay-Delgado, F., Martínez-Sánchez, R., and Alonso-Núñez, G. "Ni(Co)-Mo-W sulphide unsupported HDS catalysts by *ex situ* decomposition of alkylthiomolybdotungstates." *Applied Catalysis A: General* **2006**. vol. 308, 134
- [117] Huirache-Acuña, R., Albiter, M. A., Espino, J., Ornelas, C., Alonso-Núñez, G., Paraguay-Delgado, F., Rico, J. L., and Martínez-Sánchez, R. "Synthesis of Ni-Mo-W sulphide catalysts by *ex situ* decomposition of trimetallic precursors." *Applied Catalysis A: General* **2006**. vol. 304, 124
- [118] Nava, H., Espino, J., Berhault, G., and Alonso-Núñez, G. "Effect of phosphorus addition on unsupported Ni-Mo-W sulfide catalysts prepared by the *in situ* activation of nickel/tetramethylammonium thiomolybdotungstate." *Applied Catalysis A: General* **2006**. vol. 302, no. 2, 177
- [119] Segawa, K., Funamoto, T., and Watanabe, M. "Development of a new type of NiMo/TiO₂-Al₂O₃ catalysts for ultra deep HDS of gas oil." *American Chemical Society, Division of Petroleum Chemistry, Preprints* **2005**. vol. 50, no. 4, 454
- [120] Saih, Y., Nagata, M., Funamoto, T., Masuyama, Y., and Segawa, K. "Ultra deep hydrodesulfurization of dibenzothiophene derivatives over NiMo/TiO₂-Al₂O₃ catalysts." *Applied Catalysis A: General* **2005**. vol. 295, no. 1, 11
- [121] Rayo, P., Ancheyta, J., Ramírez, J., and Gutiérrez-Alejandre, A. "Hydrotreating of diluted Maya crude with NiMo/Al₂O₃-TiO₂ catalysts: effect of diluent composition." *Catalysis Today* **2004**. vol. 98, no. 1-2, 171. International Symposium on Advances in Hydroprocessing of Oil Fractions (ISAHOF 2004)
- [122] Ramírez, J., Macías, G., Cedeño, L., Gutiérrez-Alejandre, A., Cuevas, R., and Castillo, P. "The role of titania in supported Mo, CoMo, NiMo, and NiW hydrodesulfurization catalysts: Analysis of past and new evidences." *Catalysis Today* **2004**. vol. 98, no. 1-2 SPEC. ISS., 19
- [123] Altamirano, E., De los Reyes, J. A., Murrieta, F., and Vrinat, M. "Hydrodesulfurization of dibenzothiophene and 4,6-dimethyl-dibenzothiophene: Gallium effect over NiMo/Al₂O₃ sulfided catalysts." *Journal of Catalysis* **2005**. vol. 235, no. 2, 403

- [124] Altamirano, E., De los Reyes, J. A., Murrieta, F., and Vrinat, M. "Hydrodesulfurization of 4,6-dimethyldibenzothiophene over Co(Ni)MoS₂ catalysts supported on alumina: Effect of gallium as an additive." *Catalysis Today* **2008**. vol. 133-135, 292 . Selected Contributions of the XX Ibero-American Symposium of Catalysis
- [125] Huang, W., Duan, A., Zhao, Z., Wan, G., Jiang, G., Dou, T., Chung, K. H., and Liu, J. "Ti-modified alumina supports prepared by sol-gel method used for deep HDS catalysts." *Catalysis Today* **2008**. vol. 131, no. 1-4, 314 . Recent advances in catalysis - selected papers from APCAT 4 (Singapore, 6-8 December 2006)
- [126] Usman, U., Kubota, T., Araki, Y., Ishida, K., and Okamoto, Y. "The effect of boron addition on the hydrodesulfurization activity of MoS₂/Al₂O₃ and Co-MoS₂/Al₂O₃ catalysts." *Journal of Catalysis* **2004**. vol. 227, no. 2, 523
- [127] Usman, U., Takaki, M., Kubota, T., and Okamoto, Y. "Effect of boron addition on a MoO₃/Al₂O₃ catalyst: Physicochemical characterization." *Applied Catalysis A: General* **2005**. vol. 286, no. 1, 148
- [128] Usman, U., Kubota, T., Hiromitsu, I., and Okamoto, Y. "Effect of boron addition on the surface structure of Co-Mo/Al₂O₃ catalysts." *Journal of Catalysis* **2007**. vol. 247, no. 1, 78
- [129] Dumeignil, F., Sato, K., Imamura, M., Matsubayashi, N., Payen, E., and Shimada, H. "Characterization and hydrodesulfurization activity of CoMo catalysts supported on boron-doped sol-gel alumina." *Applied Catalysis A: General* **2006**. vol. 315, 18
- [130] Giraldo, S. A. and Centeno, A. "Isomerization and cracking under HDS conditions using γ -alumina modified with boron as catalysts support." *Catalysis Today* **2008**. vol. 133-135, 255 . Selected Contributions of the XX Ibero-American Symposium of Catalysis
- [131] Ferdous, D., Dalai, A. K., Adjaye, J., and Kotlyar, L. "Surface morphology of NiMo/Al₂O₃ catalysts incorporated with boron and phosphorus: Experimental and simulation." *Applied Catalysis A: General* **2005**. vol. 294, no. 1, 80
- [132] Sun, M., Nicosia, D., and Prins, R. "The effects of fluorine, phosphate and chelating agents on hydrotreating catalysts and catalysis." *Catalysis Today* **2003**. vol. 86, no. 1-4, 173 . Effects of Support in Hydrotreating Catalysis for Ultra-clean Fuels
- [133] Maity, S. K., Flores, G. A., Ancheyta, J., and Rana, M. S. "Effect of preparation methods and content of phosphorus on hydrotreating activity." *Catalysis Today* **2008**. vol. 130, no. 2-4, 374 . International Symposium on Advances in Hydroprocessing of Oils Fractions (ISAHOF 2007)
- [134] Ding, L., Zhang, Z., Zheng, Y., Ring, Z., and Chen, J. "Effect of fluorine and boron modification on the HDS, HDN and HDA activity of hydrotreating catalysts." *Applied Catalysis A: General* **2006**. vol. 301, no. 2, 241
- [135] Kim, H., Lee, J. J., and Moon, S. H. "Hydrodesulfurization of dibenzothiophene compounds using fluorinated NiMo/Al₂O₃ catalysts." *Applied Catalysis B: Environmental* **2003**. vol. 44, no. 4, 287
- [136] Mey, D., Brunet, S., Canaff, C., Maugé, F., Bouchy, C., and Diehl, F. "HDS of a model FCC gasoline over a sulfided CoMo/Al₂O₃ catalyst: Effect of the addition of potassium." *Journal of Catalysis* **2004**. vol. 227, no. 2, 436
- [137] Fan, Y., Lu, J., Shi, G., Liu, H., and Bao, X. "Effect of synergism between potassium and phosphorus on selective hydrodesulfurization performance of Co-Mo/Al₂O₃ FCC gasoline hydro-upgrading catalyst." *Catalysis Today* **2007**. vol. 125, no. 3-4, 220 . Catalysts and Processes for Heavy Oil Upgrading

- [138] Mizutani, H., Godo, H., Ohsaki, T., Kato, Y., Fujikawa, T., Saih, Y., Funamoto, T., and Segawa, K. "Inhibition effect of nitrogen compounds on CoMoP/Al₂O₃ catalysts with alkali or zeolite added in hydrodesulfurization of dibenzothiophene and 4,6-dimethyldibenzothiophene." *Applied Catalysis A: General* **2005**. vol. 295, no. 2, 193
- [139] Van der Meer, Y., Hensen, E. J. M., Van Veen, J. A. R., and Van der Kraan, A. M. "Characterization and thiophene hydrodesulfurization activity of amorphous-silica-alumina-supported NiW catalysts." *Journal of Catalysis* **2004**. vol. 228, no. 2, 433
- [140] Kunisada, N., Choi, K. H., Korai, Y., Mochida, I., and Nakano, K. "Contrast activities of four alumina and alumina-silica-supported nickel-molybdenum sulfide catalysts for deep desulfurization of gas oils." *Applied Catalysis A: General* **2005**. vol. 279, no. 1-2, 235
- [141] Kunisada, N., Choi, K. H., Korai, Y., Mochida, I., and Nakano, K. "Optimization of silica content in alumina-silica support for NiMo sulfide to achieve deep desulfurization of gas oil." *Applied Catalysis A: General* **2004**. vol. 273, no. 1-2, 287
- [142] Leyva, C., Rana, M. S., and Ancheyta, J. "Surface characterization of Al₂O₃-SiO₂ supported NiMo catalysts: An effect of support composition." *Catalysis Today* **2008**. vol. 130, no. 2-4, 345 . International Symposium on Advances in Hydroprocessing of Oils Fractions (ISAHOF 2007)
- [143] Zhou, Y. H. and Chen, G. D. "Heat transfer model and numerical simulation for terminally guided projectile in heated tube." *Bingong Xuebao/Acta Armamentarii* **2005**. vol. 26, no. 4, 449
- [144] Li, G., Li, W., Zhang, M., and Tao, K. "Morphology and hydrodesulfurization activity of CoMo sulfide supported on amorphous ZrO₂ nanoparticles combined with Al₂O₃." *Applied Catalysis A: General* **2004**. vol. 273, no. 1-2, 233
- [145] Kraveva, E., Paneva, D., Spojakina, A., Mitov, I., and Petrov, L. "Study of iron state in titania-supported FeMo catalysts of hydrodesulfurization." *Reaction Kinetics and Catalysis Letters* **2005**. vol. 85, no. 2, 283
- [146] El Azarifi, N., Aït Chaoui, M., El Ouassouli, A., Ezzamarty, A., Travert, A., Leglise, J., De Ménorval, L. C., and Moreau, C. "Hydroprocessing of dibenzothiophene, 1-methylnaphthalene and quinoline over sulfided NiMo-hydroxyapatite-supported catalysts." *Catalysis Today* **2004**. vol. 98, no. 1-2, 161 . International Symposium on Advances in Hydroprocessing of Oil Fractions (ISAHOF 2004)
- [147] Chen, H., Gao, J., Ruan, M., Shi, J., and Yan, D. "A facile grafting method to synthesize novel monodispersive core-shell structure of spherical mesoporous silica @ nanocrystalline zirconia." *Microporous and Mesoporous Materials* **2004**. vol. 76, no. 1-3, 209
- [148] Eswaramoorthi, I., Sundaramurthy, V., Das, N., Dalai, A. K., and Adjaye, J. "Application of multi-walled carbon nanotubes as efficient support to NiMo hydrotreating catalyst." *Applied Catalysis A: General* **2008**. vol. 339, no. 2, 187
- [149] Shang, H., Liu, C., Xu, Y., Qiu, J., and Wei, F. "States of carbon nanotube supported Mo-based HDS catalysts." *Fuel Processing Technology* **2007**. vol. 88, no. 2, 117
- [150] Carrado, K. A., Song, C., Kim, J. H., Castagnola, N., Fernandez-Saavedra, R., Marshall, C. L., and Schwartz, M. M. "HDS & deep HDS activity of Co/Mo/S-mesostructured synthetic clays." In: *ACS Division of Fuel Chemistry, Preprints*. Chemical Engineering Division, Argonne National Laboratory, Argonne, IL, United States, vol. 50 **2005** 344–347

- [151] Carrado, K. A., Kim, J. H., Song, C. S., Castagnola, N., Marshall, C. L., and Schwartz, M. M. "HDS and deep HDS activity of CoMoS-mesostructured clay catalysts." *Catalysis Today* **2006**. vol. 116, no. 4, 478 . Sulfur Removal to Produce Ultra Clean Fuel
- [152] Herrera, J. M., Reyes, J., Roquero, P., and Klimova, T. "New hydrotreating NiMo catalysts supported on MCM-41 modified with phosphorus." *Microporous and Mesoporous Materials* **2005**. vol. 83, no. 1-3, 283
- [153] Gutiérrez, O. Y., Valencia, D., Fuentes, G. A., and Klimova, T. "Mo and NiMo catalysts supported on SBA-15 modified by grafted ZrO₂ species: Synthesis, characterization and evaluation in 4,6-dimethyldibenzothiophene hydrodesulfurization." *Journal of Catalysis* **2007**. vol. 249, no. 2, 140
- [154] Klimova, T., Reyes, J., Gutiérrez, O. Y., and Lizama, L. "Novel bifunctional NiMo/Al-SBA-15 catalysts for deep hydrodesulfurization: Effect of support Si/Al ratio." *Applied Catalysis A: General* **2008**. vol. 335, no. 2, 159
- [155] Dhar, G. M., Kumaran, G. M., Kumar, M., Rawat, K. S., Sharma, L. D., Raju, B. D., and Rao, K. S. R. "Physico-chemical characterization and catalysis on SBA-15 supported molybdenum hydrotreating catalysts." *Catalysis Today* **2005**. vol. 99, no. 3-4, 309 . Recent Advances in Fuel Processing for Fuel Cell Applications
- [156] Garg, S., Soni, K., Kumaran, G. M., Kumar, M., Gupta, J. K., Sharma, L. D., and Dhar, G. M. "Effect of Zr-SBA-15 support on catalytic functionalities of Mo, CoMo, NiMo hydrotreating catalysts." *Catalysis Today* **2008**. vol. 130, no. 2-4, 302 . International Symposium on Advances in Hydroprocessing of Oils Fractions (ISAHOF 2007)
- [157] Li, X., Wang, A., Zhang, S., Chen, Y., and Hu, Y. "Effect of surface Na⁺ or K⁺ ion exchange on hydrodesulfurization performance of MCM-41-supported Ni-W catalysts." *Applied Catalysis A: General* **2007**. vol. 316, no. 2, 134
- [158] Montesinos-Castellanos, A. and Zepeda, T. A. "High hydrogenation performance of the mesoporous NiMo/Al(Ti, Zr)-HMS catalysts." *Microporous and Mesoporous Materials* **2008**. vol. 113, no. 1-3, 146
- [159] Zepeda, T. A., Fierro, J. L. G., Pawelec, B., Nava, R., Klimova, T., Fuentes, G. A., and Halachev, T. "Synthesis and characterization of Ti-HMS and CoMo/Ti-HMS oxide materials with varying Ti content." *Chemistry of Materials* **2005**. vol. 17, no. 16, 4062
- [160] Zepeda, T., Pawelec, B., Fierro, J., and Halachev, T. "Removal of refractory S-containing compounds from liquid fuels on novel bifunctional CoMo/HMS catalysts modified with Ti." *Applied Catalysis B: Environmental* **2007**. vol. 71, no. 3-4, 223
- [161] Zepeda, T., Pawelec, B., Fierro, J., Olivas, A., Fuentes, S., and Halachev, T. "Effect of Al and Ti content in HMS material on the catalytic activity of NiMo and CoMo hydrotreating catalysts in the HDS of DBT." *Microporous and Mesoporous Materials* **2008**. vol. 111, no. 1-3, 157
- [162] Nava, R., Ortega, R. A., Alonso, G., Ornelas, C., Pawelec, B., and Fierro, J. L. G. "CoMo/Ti-SBA-15 catalysts for dibenzothiophene desulfurization." *Catalysis Today* **2007**. vol. 127, no. 1-4, 70 . I.A. Vasalos Festschrift
- [163] Rodríguez-Castellón, E., Jiménez-López, A., and Eliche-Quesada, D. "Nickel and cobalt promoted tungsten and molybdenum sulfide mesoporous catalysts for hydrodesulfurization." *Fuel* **2008**. vol. 87, no. 7, 1195

- [164] Silva-Rodrigo, R., Calderón-Salas, C., Melo-Banda, J. A., Domínguez, J. M., and Vázquez-Rodríguez, A. "Synthesis, characterization and comparison of catalytic properties of NiMo- and NiW/Ti-MCM-41 catalysts for HDS of thiophene and HVGO." *Catalysis Today* **2004**. vol. 98, no. 1-2, 123 . International Symposium on Advances in Hydroprocessing of Oil Fractions (ISAHOF 2004)
- [165] Zeng, S., Blanchard, J., Breyse, M., Shi, Y., Su, X., Nie, H., and Li, D. "Mesoporous materials from zeolite seeds as supports for nickel-tungsten sulfide active phases: Part 2. catalytic properties for deep hydrodesulfurization reactions." *Applied Catalysis A: General* **2006**. vol. 298, 88
- [166] Ho, T. "Deep HDS of diesel fuel: chemistry and catalysis." *Catalysis Today* **2004**. vol. 98, no. 1-2, 3. International Symposium on Advances in Hydroprocessing of Oil Fractions (ISAHOF 2004)
- [167] Chianelli, R. R., Berhault, G., and Torres, B. "Unsupported transition metal sulfide catalysts: 100 years of science and application." *Catalysis Today* **2009**. vol. 147, no. 3-4, 275 . Special Issue dedicated to Marc Jacques Ledoux on the occasion of his 60th birthday
- [168] Eijsbouts, S., Mayo, S., and Fujita, K. "Unsupported transition metal sulfide catalysts: From fundamentals to industrial application." *Applied Catalysis A: General* **2007**. vol. 322, 58 . Active Phases for Hydrotreating Catalysis
- [169] Hermann, N., Brorson, M., and Topsøe, H. "Activities of unsupported second transition series metal sulfides for hydrodesulfurization of sterically hindered 4,6-dimethyldibenzothiophene and of unsubstituted dibenzothiophene." *Catalysis Letters* **2000**. vol. 65, no. 4, 169
- [170] Ho, T. C., Jacobson, A. J., Chianelli, R. R., and Lund, C. R. F. "Hydrodenitrogenation-selective catalysts i. Fe promoted Mo/W sulfides." *Journal of Catalysis* **1992**. vol. 138, no. 1, 351
- [171] Ho, T. C. "Hydrogenation of aromatics over hydrodenitrogenation-selective and hydrodesulfurization-selective catalysts." *Industrial & Engineering Chemistry Research* **1993**. vol. 32, no. 8, 1568
- [172] Ho, T., Chianelli, R., and Jacobson, A. "Promotion effects in bulk metal sulfide catalysts." *Applied Catalysis A: General* **1994**. vol. 114, no. 1, 127
- [173] Harris, S. and Chianelli, R. R. "Catalysis by transition metal sulfides: A theoretical and experimental study of the relation between the synergic systems and the binary transition metal sulfides." *Journal of Catalysis* **1986**. vol. 98, no. 1, 17
- [174] Lacroix, M., Boutarfa, N., Guillard, C., Vrinat, M., and Breyse, M. "Hydrogenating properties of unsupported transition metal sulphides." *Journal of Catalysis* **1989**. vol. 120, no. 2, 473
- [175] Raje, A. P., Liaw, S. J., Srinivasan, R., and Davis, B. H. "Second row transition metal sulfides for the hydrotreatment of coal-derived naphtha i. catalyst preparation, characterization and comparison of rate of simultaneous removal of total sulfur, nitrogen and oxygen." *Applied Catalysis A: General* **1997**. vol. 150, no. 2, 297
- [176] Toulhoat, H. A., Raybaud, P. A., Kasztelan, S. A., Kresse, G. B., and Hafner, J. B. "Transition metals to sulfur binding energies relationship to catalytic activities in HDS: Back to Sabatier with first principle calculations." *ACS Division of Petroleum Chemistry, Inc. Preprints* **1997**. vol. 42, 114
- [177] Mironov, O. and Kuperman, A. E. "Hydroprocessing bulk catalyst and uses thereof" **2009** US 2009054225 (A1)

- [178] Bai, C., Beeckman, J., McCarthy, S. J., Hou, Z., and Wu, J. "Preparation of bulk metallic group VIII/group VIB metal catalysts" **2009** WO 2009061295 (A1)
- [179] Soled, S. L., Miseo, S., Eijsbouts, S., and Plantaga, F. L. "Bulk bimetallic catalysts, method of making bulk bimetallic catalysts and hydroprocessing using bulk bimetallic catalysts" **2007** US 2007084754 (A1)
- [180] Ho, T. C. and McCandlish, L. E. "Method of making self-promoted hydrotreating catalysts" **1986** US 4595672 (A)
- [181] Paraguay-Delgado, F., García-Alamilla, R., Lumbreras, J. A., Cizniega, E., and Alonso-Núñez, G. "Synthesis of Ni-Mo-W sulfide nanorods as catalyst for hydrodesulfurization of dibenzothiophene." *Journal of Nanoscience and Nanotechnology* **2008**. vol. 8, 6406
- [182] Peng, Y., Meng, Z., Zhong, C., Lu, J., Yu, W., Yang, Z., and Qian, Y. "Hydrothermal synthesis of MoS₂ and its pressure-related crystallization." *Journal of Solid State Chemistry* **2001**. vol. 159, no. 1, 170
- [183] Maione, A. and Devillers, M. "Solid solutions of Ni and Co molybdates in silica-dispersed and bulk catalysts prepared by sol-gel and citrate methods." *Journal of Solid State Chemistry* **2004**. vol. 177, no. 7, 2339
- [184] Vie, D., Martinez, E., Sapina, F., Folgado, J. V., Beltran, A., Valenzuela, R. X., and Cortes-Corberan, V. "Freeze-dried precursor-based synthesis of nanostructured cobalt-nickel molybdates Co_{1-x}Ni_xMoO₄." *Chemistry of Materials* **2004**. vol. 16, no. 9, 1697
- [185] Bej, S. K., Maity, S. K., and Turaga, U. T. "Search for an efficient 4,6-DMDBT hydrodesulfurization catalyst: A review of recent studies." *Energy & Fuels* **2004**. vol. 18, no. 5, 1227
- [186] Olivas, A., Galván, D., Alonso, G., and Fuentes, S. "Trimetallic NiMoW unsupported catalysts for HDS." *Applied Catalysis A: General* **2009**. vol. 352, no. 1-2, 10
- [187] Malandra, J. L., Sughrue, E. L., Johnson, M. J., Dodwell, G. W., Reed, L. E., Bares, J. E., Gislason, J. J., and Morton, R. W. "Desulfurization and sorbents for same" **2004** US 2004048743 (A1)
- [188] Gislason, J. J., Schmidt, R., Welch, M. B., Simon, D. E., and Morton, R. W. "Desulfurization and novel compositions for same" **2004** US 20040007130
- [189] Khare, G. P., Cass, B. W., Engelbert, D. R., Sughrue, E. L., Kidd, D. R., and Thompson, M. W. "Improved desulfurization process" **2003** WO 03087269 (A1)
- [190] Salem, A. B. S. H. "Naphtha desulfurization by adsorption." *Industrial & Engineering Chemistry Research* **1994**. vol. 33, no. 2, 336
- [191] Irvin, L. R. "Process for desulfurizing gasoline and hydrocarbon feedstocks" **1997** WO 9707054 (A1)
- [192] Huff, G. A. J. and Owen, O. S. "Sulfur removal by catalytic distillation" **1999** WO 9909117 (A1)
- [193] Alexander, B. D., Huff, G. A., Pradhan, V. R., Reagan, W. J., and Cayton, R. H. "Sulfur removal process" **2000**. WO0014182 (A2)
- [194] Bourbigou, O. H., Uzio, D., Diehl, F., and Magna, L. "Process for the elimination of sulfur and nitrogen compounds from hydrocarbon cuts by contacting with a non-aqueous ionic liquid containing an alkylating agent, useful for obtaining low sulfur petrols" **2003** FR 2840916 (A1)
- [195] Zhao, X., Krishnaiah, G., and Cartwright, T. "S-brane™ technology brings flexibility to refiners' clean fuel solutions." *NPRA paper* **2004**. vol. AM-04-17,
- [196] Kumar, S. and Gentry, J. "Remove sulfur, retain octane." *Hydrocarbon Engineering* **2003**. vol. 8, no. 12, 27.

- [197] Shiraishi, Y., Tachibana, K., Taki, Y., Hirai, T., and Komasaawa, I. "A novel desulfurization process for fuel oils based on the formation and subsequent precipitation of s-alkylsulfonium salts. 2. catalytic-cracked gasoline." *Industrial & Engineering Chemistry Research* **2001**. vol. 40, no. 4, 1225
- [198] Schucker, R. C. and Baird, J. W. C. "Electrochemical oxidation of sulfur compounds in naphtha using ionic liquids" **2001** US 6274026 (B1)
- [199] Ito, E. and Van Veen, R. J. A. "On novel processes for removing sulphur from refinery streams." *Catalysis Today* **2006**. vol. 116, no. 4, 446 . Sulfur Removal to Produce Ultra Clean Fuel
- [200] Babich, I. V. and Moulijn, J. A. "Science and technology of novel processes for deep desulfurization of oil refinery streams: a review" *Fuel* **2003**. vol. 82, no. 6, 607
- [201] Shan, G., Zhang, H., Xing, J., Chen, G., Li, W., and Liu, H. "Biodesulfurization of hydrodesulfurized diesel oil with pseudomonas delafieldii R-8 from high density culture." *Biochemical Engineering Journal* **2006**. vol. 27, no. 3, 305
- [202] Rashtchi, M., Mohebbali, G. H., Akbarnejad, M. M., Towfighi, J., Rasekh, B., and Keytash, A. "Analysis of biodesulfurization of model oil system by the bacterium, strain RIPI-22." *Biochemical Engineering Journal* **2006**. vol. 29, no. 3, 169
- [203] Hou, Y., Kong, Y., Yang, J., Zhang, J., Shi, D., and Xin, W. "Biodesulfurization of dibenzothiophene by immobilized cells of pseudomonas Stutzeri UP-1." *Fuel* **2005**. vol. 84, no. 14-15, 1975
- [204] Li, F., Zhang, Z., Feng, J., Cai, X., and Xu, P. "Biodesulfurization of DBT in tetradecane and crude oil by a facultative thermophilic bacterium mycobacterium goodii X7B." *Journal of Biotechnology* **2007**. vol. 127, no. 2, 222
- [205] Mohebbali, G., Ball, A. S., Rasekh, B., and Kaytash, A. Biodesulfurization potential of a newly isolated bacterium, gordonia alkanivorans RIPI90A." *Enzyme and Microbial Technology* **2007**. vol. 40, no. 4, 578
- [206] Soleimani, M., Bassi, A., and Margaritis, A. "Biodesulfurization of refractory organic sulfur compounds in fossil fuels." *Biotechnology Advances* **2007**. vol. 25, no. 6, 570
- [207] Chen, H., Zhang, W. J., Cai, Y. B., Zhang, Y., and Li, W. "Elucidation of 2-hydroxybiphenyl effect on dibenzothiophene desulfurization by microbacterium sp. strain ZD-M2." *Bioresource Technology* **2008**. vol. 99, no. 15, 6928
- [208] Chen, H., Zhang, W. J., Chen, J. M., Cai, Y. B., and Li, W. "Desulfurization of various organic sulfur compounds and the mixture of DBT + 4,6-DMDBT by mycobacterium sp. ZD-19." *Bioresource Technology* **2008**. vol. 99, no. 9, 3630
- [209] Liu, S., Wang, B., Cui, B., and Sun, L. "Deep desulfurization of diesel oil oxidized by Fe(VI) systems." *Fuel* **2008**. vol. 87, no. 3, 422
- [210] Ma, X., Zhou, A., and Song, C. "A novel method for oxidative desulfurization of liquid hydrocarbon fuels based on catalytic oxidation using molecular oxygen coupled with selective adsorption." *Catalysis Today* **2007**. vol. 123, no. 1-4, 276 . M. Albert Vannice Festschrift
- [211] Sampanthar, J. T., Xiao, H., Dou, J., Nah, T. Y., Rong, X., and Kwan, W. P. "A novel oxidative desulfurization process to remove refractory sulfur compounds from diesel fuel." *Applied Catalysis B: Environmental* **2006**. vol. 63, no. 1-2, 85
- [212] Chica, A., Corma, A., and Dómine, M. E. "Catalytic oxidative desulfurization (ODS) of diesel fuel on a continuous fixed-bed reactor." *Journal of Catalysis* **2006**. vol. 242, no. 2, 299

- [213] Yu, G., Lu, S., Chen, H., and Zhu, Z. "Diesel fuel desulfurization with hydrogen peroxide promoted by formic acid and catalyzed by activated carbon." *Carbon* **2005**. vol. 43, no. 11, 2285
- [214] Al-Shahrani, F., Xiao, T., Llewellyn, S. A., Barri, S., Jiang, Z., Shi, H., Martinie, G., and Green, M. L. H. "Desulfurization of diesel via the H_2O_2 oxidation of aromatic sulfides to sulfones using a tungstate catalyst." *Applied Catalysis B: Environmental* **2007**. vol. 73, no. 3-4, 311
- [215] Mondal, S., Hangan-Balkir, Y., Alexandrova, L., Link, D., Howard, B., Zandhuis, P., Cugini, A., Horwitz, C. P., and Collins, T. J. "Oxidation of sulfur components in diesel fuel using Fe-TAML® catalysts and hydrogen peroxide." *Catalysis Today* **2006**. vol. 116, no. 4, 554 . Sulfur Removal to Produce Ultra Clean Fuel
- [216] García-Gutiérrez, J. M., Fuentes, G. A., Hernández-Terán, M. E., Murrieta, F., Navarrete, J., and Jiménez-Cruz, F. "Ultra-deep oxidative desulfurization of diesel fuel with H_2O_2 catalyzed under mild conditions by polymolybdates supported on Al_2O_3 ." *Applied Catalysis A: General* **2006**. vol. 305, no. 1, 15
- [217] García-Gutiérrez, J. L., Fuentes, G. A., Hernández-Terán, M. E., García, P., Murrieta-Guevara, F., and Jiménez-Cruz, F. "Ultra-deep oxidative desulfurization of diesel fuel by the $\text{Mo}/\text{Al}_2\text{O}_3\text{-H}_2\text{O}_2$ system: The effect of system parameters on catalytic activity." *Applied Catalysis A: General* **2008**. vol. 334, no. 1-2, 366
- [218] Thompson, L. H. and Doraiswamy, L. K. "Sonochemistry: Science and engineering." *Industrial & Engineering Chemistry Research* **1999**. vol. 38, no. 4, 1215
- [219] Mei, H., Mei, B. W., and Yen, T. F. "A new method for obtaining ultra-low sulfur diesel fuel via ultrasound assisted oxidative desulfurization." *Fuel* **2003**. vol. 82, no. 4, 405
- [220] Etemadi, O. and Yen, T. F. "Selective adsorption in ultrasound-assisted oxidative desulfurization process for fuel cell reformer applications." *Energy & Fuels* **2007**. vol. 21, no. 4, 2250
- [221] Wan, M. W. and Yen, T. F. "Enhance efficiency of tetraoctylammonium fluoride applied to ultrasound-assisted oxidative desulfurization (UAOD) process." *Applied Catalysis A: General* **2007**. vol. 319, 237
- [222] Zhao, D., Ren, H., Wang, J., Yang, Y., and Zhao, Y. "Kinetics and mechanism of quaternary ammonium salts as phase-transfer catalysts in the liquid/liquid phase for oxidation of thiophene." *Energy & Fuels* **2007**. vol. 21, no. 5, 2543
- [223] Cansell, F. and Aymonier, C. "Design of functional nanostructured materials using supercritical fluids." *The Journal of Supercritical Fluids* **2009**. vol. 47, no. 3, 508 . 20th Year Anniversary Issue of the Journal of Supercritical Fluids
- [224] Aymonier, C. and Cansell, F. "Supercritical fluid techniques." *Annales de Chimie - Science des Matériaux* **2006**. vol. 31, 317
- [225] United-Nations. Stockholm. declaration of the united nations conference on the human environment **1972**
- [226] Brundtland, G. "Our Common Future : World Commission on Environment and Development." Oxford University Press (Oxford) **1987**, 461
- [227] Cagniard de Latour, C. "Exposé de quelques résultats obtenus par l'action combinée de la chaleur et de la compression sur certains liquides, tels que l'eau, l'alcool, l'éther sulfurique et l'essence de pétrole rectifiée." *Annales de Chimie et de Physique* **1822**. vol. 21, 127
- [228] Andrews, T. "On the continuity of the gaseous and liquid states of matter." *Philosophical Transactions of the Royal Society* **1869**. vol. 159, 575

- [229] Van der Waals, J. D. “Over de Continuïteit van den Gas- en Vloeistofoestand” (“On the continuity of the gas and liquid state”). Ph.D. thesis, University of Leiden **1873**
- [230] Coquelet, C. and Richon, D. “State of the art of equations of state.” INPL (Nancy) **2007** 75–101
- [231] Marre, S. “Ingénierie de surface des matériaux en milieux fluides supercritiques.” Ph.D. thesis, Université de bordeaux 1 **2006**
- [232] Cansell, F., Aymonier, C., and Loppinet-Serani, A. “Review on materials science and supercritical fluids.” *Current Opinion in Solid State and Materials Science* **2003**. vol. 7, no. 4-5, 331
- [233] Cansell, F., Chevalier, B., Demourgues, A., Etourneau, J., Even, C., Pessey, V., Petit, S., Tressaud, A., and Weill, F. “Supercritical fluid processing: a new route for materials synthesis.” *journal of materials chemistry* **1999**. vol. 9, 61
- [234] Rosa, P. T. V., Parajo, J. C., Dominguez, H., Moure, A., Diaz-Reinoso, B., Smith, R. L. J., Toyomizu, M., Florusse, L. J., Peters, C. J., Goto, M., Lucas, S., and Meireles, M. A. A. “Supercritical and pressurized fluid extraction applied to the food industry.” In: *Extracting Bioactive Compounds for Food Products*, edited by M. A. A. Meireles. CRC Press (Boca Raton, Fla) **2009** 269–288
- [235] King, J. W. “Sub- and supercritical fluid processing of agrimaterials: extraction, fractionation and reaction modes.” *NATO Science Series, Series E: Applied Sciences* **2000**. vol. 366, 451
- [236] Bottreau, M. and Cansell, F. “Hydrothermal oxidation: a new concept for treatment of industrial and urban liquid wastes.” In: *Supercritical fluids and materials*. INPL (Nancy) **2002** 703–706
- [237] Loppinet-Serani, A., Aymonier, C., and Cansell, F. “Current and foreseeable applications of supercritical water for energy and the environment.” *ChemSusChem* **2008**. vol. 1, no. 6, 486
- [238] Loppinet-Serani, A., Aymonier, C., and Cansell, F. “Supercritical water for environmental technologies.” *Journal of Chemical Technology & Biotechnology* **2010**. vol. 85, no. 5, 583
- [239] Aymonier, C., Loppinet-Serani, A., Reverón, H., Garrabos, Y., and Cansell, F. “Review of supercritical fluids in inorganic materials science.” *The Journal of Supercritical Fluids* **2006**. vol. 38, no. 2, 242 . A collection of papers dedicated to the memory of Prof. Aydin Akgerman - Akgerman S.I.
- [240] Reverchon, E. and Adami, R. “Nanomaterials and supercritical fluids.” *The Journal of Supercritical Fluids* **2006**. vol. 37, no. 1, 1
- [241] Fages, J. “Powder processing using supercritical fluids.” *Supercritical Fluids and Materials* **2003**. vol. 1, 33
- [242] Hakuta, Y., Hayashi, H., and Arai, K. “Fine particle formation using supercritical fluids.” *Current Opinion in Solid State and Materials Science* **2003**. vol. 7, no. 4-5, 341
- [243] Fages, J., Lochard, H., Rodier, E., Letourneau, J. J., and Sauceau, M. “Formation of finely divided solids by supercritical fluids.” *the Canadian Journal of Chemical Engineering* **2003**. vol. 81, 161
- [244] Petersen, R. C., Matson, D. W., and Smith, R. D. “Rapid precipitation of low vapor pressure solids from supercritical fluid solutions: the formation of thin films and powders.” *Journal of the American Chemical Society* **1986**. vol. 108, no. 8, 2100
- [245] Matson, D. W., Fulton, J. L., Petersen, R. C., and Smith, R. D. “Rapid expansion of supercritical fluid solutions: solute formation of powders, thin films, and fibers.” *Industrial & Engineering Chemistry Research* **1987**. vol. 26, no. 11, 2298

- [246] Jung, J. and Perrut, M. "Particle design using supercritical fluids: Literature and patent survey." *The Journal of Supercritical Fluids* **2001**. vol. 20, no. 3, 179
- [247] McLeod, M. C., Gale, W. F., and Roberts, C. B. "Metallic nanoparticle production utilizing a supercritical carbon dioxide flow process." *Langmuir* **2004**. vol. 20, no. 17, 7078
- [248] Reverchon, E. "Supercritical antisolvent precipitation of micro- and nano-particles." *Journal of Supercritical Fluids* **1999**. vol. 15, no. 1, 1
- [249] Benedetti, L., Bertucco, A., and Pallado, P. "Production of micronic particles of biocompatible polymer using supercritical carbon dioxide." *Biotechnology & Bioengineering* **1997**. vol. 53, 232
- [250] Lele, A. K. and Shine, A. D. "Morphology of polymers precipitated from a supercritical solvent." *AIChE Journal* **1992**. vol. 38, no. 5, 742
- [251] Meziani, M. J., Pathak, P., Hurezeanu, R., Thies, M. C., Enick, R. M., and Sun, Y. P. "Supercritical-fluid processing technique for nanoscale polymer particles." *Angewandte Chemie International Edition* **2004**. vol. 43, no. 6, 704
- [252] Sun, Y. P., Meziani, M. J., Pathak, P., and Qu, L. "Polymeric nanoparticles from rapid expansion of supercritical fluid solution." *Chemistry - A European Journal* **2005**. vol. 11, no. 5, 1366
- [253] Lin, I. H., Liang, P. F., and Tan, C. S. "Preparation of polystyrene/poly(methyl methacrylate) blends by compressed fluid antisolvent technique." *The Journal of Supercritical Fluids* **2010**. vol. 51, no. 3, 384
- [254] Reverchon, E. and Spada, A. "Crystalline microparticles of controlled size produced by supercritical-assisted atomization." *Industrial & Engineering Chemistry Research* **2004**. vol. 43, no. 6, 1460
- [255] Kongsombut, B., Tsutsumi, A., Suankaew, N., and Charinpanitkul, T. "Encapsulation of SiO₂ and TiO₂ fine powders with poly(dl-lactic-co-glycolic acid) by rapid expansion of supercritical CO₂ incorporated with ethanol cosolvent." *Industrial & Engineering Chemistry Research* **2009**. vol. 48, no. 24, 11230
- [256] Sun, Y. P. and Rollins, H. R. "Preparation of polymer-protected semiconductor nanoparticles through the rapid expansion of supercritical fluid solution." *Chemical Physics Letters* **1998**. vol. 288, no. 2-4, 585
- [257] Sun, Y. P., Guduru, R., Lin, F., and Whiteside, T. "Preparation of nanoscale semiconductors through the rapid expansion of supercritical solution (RESS) into liquid solution." *Industrial & Engineering Chemistry Research* **2000**. vol. 39, no. 12, 4663
- [258] Sun, Y. P., Atornigijawat, P., and Meziani, M. J. "Preparation of silver nanoparticles via rapid expansion of water in carbon dioxide microemulsion into reductant solution." *Langmuir* **2001**. vol. 17, no. 19, 5707
- [259] Sun, Y. P., Rollins, H. W., and Guduru, R. "Preparations of nickel, cobalt, and iron nanoparticles through the rapid expansion of supercritical fluid solutions (RESS) and chemical reduction." *Chemistry of Materials* **1999**. vol. 11, no. 1, 7
- [260] Reverchon, E., Della Porta, G., Di Trollo, A., and Pace, S. "Supercritical antisolvent precipitation of nanoparticles of superconductor precursors." *Industrial & Engineering Chemistry Research* **1998**. vol. 37, no. 3, 952
- [261] Hanna, M. and York, P. "Method and apparatus for the formation of particles" **1995** WO 9501221 A1
- [262] Yeo, S. D., Choi, J. H., and Lee, T. J. "Crystal formation of BaCl₂ and NH₄Cl using a supercritical fluid antisolvent." *The Journal of Supercritical Fluids* **2000**. vol. 16, no. 3, 235
- [263] Reverchon, E., Della Porta, G., Sannino, D., and Ciambelli, P. "Supercritical antisolvent precipitation of nanoparticles of a zinc oxide precursor." *Powder Technology* **1999**. vol. 102, no. 2, 127

- [264] Jain, T., Jain, V., Pandey, R., Daharwal, S. J., Shukla, S. S., and Vyas, A. "Supercritical fluid technology in pharmaceuticals: an overview." *the journal of Pharmacy Technology* **2009**. vol. 2, 65
- [265] Pathak, P., Meziani, M. J., Desai, T., and Sun, Y. P. "Nanosizing drug particles in supercritical fluid processing." *Journal of the American Chemical Society* **2004**. vol. 126, no. 35, 10842
- [266] Hezave, A. Z. and Esmaeilzadeh, F. "Micronization of drug particles via RESS process." *The Journal of Supercritical Fluids* **2010**. vol. 52, no. 1, 84
- [267] Atila, C., N., Y., and Çalimli, A. "Particle size design of digitoxin in supercritical fluids." *The Journal of Supercritical Fluids* **2010**. vol. 51, no. 3, 404
- [268] Reverchon, E. and Della Porta, G. "Production of antibiotic micro- and nano-particles by supercritical antisolvent precipitation." *Powder Technology* **1999**. vol. 106, no. 1-2, 23
- [269] Thiering, R., Dehghani, A., Dillow, A., and Foster, N. "Micronization of model proteins using compressed carbon dioxide." In: *Proceedings of the 5th international symposium on supercritical fluids* **2000** 8-12. Atlanta
- [270] Snavely, W. K., Subramaniam, B., Rajewski, R. A., and Defelippis, M. R. "Micronization of insulin from halogenated alcohol solution using supercritical carbon dioxide as an antisolvent." *Journal of Pharmaceutical Sciences* **2002**. vol. 91, no. 9, 2026
- [271] Pyo, D. "Two different shapes of insulin microparticles produced by solution enhanced dispersion supercritical fluid (SEDS) process." *Bulletin of the Korean Chemical Society* **2009**. vol. 30, 1215
- [272] Lan, H. Q., Zhang, L., Zhuang, W. Y., Wu, Z. J., Su, Y. Z., and Li, J. "Preparation of chitosan microparticles by SAS-A." *Xiamen Daxue Xuebao, Ziran Kexueban* **2010**. vol. 49, 139
- [273] Byrappa, K. and Adschiri, T. "Hydrothermal technology for nanotechnology." *Progress in Crystal Growth and Characterization of Materials* **2007**. vol. 53, no. 2, 117
- [274] Cabañas, A., Darr, J. A., Poliakoff, M., and Lester, E. "A continuous and clean one-step synthesis of nano-particulate $Ce_{1-x}Zr_xO_2$ solid solutions in near-critical water." *Chemical Communications* **2000**. vol. 11, no. 11, 901
- [275] Garriga, R., Pessey, V., Weill, F., Chevalier, B., Etourneau, J., and Cansell, F. "Kinetic study of chemical transformation in supercritical media of bis(hexafluoroacetylacetonate)copper(II) hydrate." *The Journal of Supercritical Fluids* **2001**. vol. 20, no. 1, 55
- [276] Bobet, J. L., Desmoulins-Krawiec, S., Grigorova, E., Cansell, F., and Chevalier, B. "Addition of nanosized Cr_2O_3 to magnesium for improvement of the hydrogen sorption properties." *Journal of Alloys and Compounds* **2003**. vol. 351, no. 1-2, 217
- [277] Loppinet-Serani, A., Aymonier, C., Desmoulins-Krawiec, S., Etourneau, J., and Cansell, F. "Material synthesis using supercritical fluids as reactive media." In: *Supercritical fluids and materials*, edited by F. O. Bonnaud N, Cansell F **2003** 1-32
- [278] Desmoulins-Krawiec, S., Aymonier, C., Loppinet-Serani, A., Weill, F., Gorsse, S., Etourneau, J., and Cansell, F. "Synthesis of nanostructured materials in supercritical ammonia: nitrides, metals and oxides." *Journal of materials chemistry* **2004**. vol. 14, 228
- [279] Adschiri, T., Hakuta, Y., and Arai, K. "Hydrothermal synthesis of metal oxide fine particles at supercritical conditions." *Industrial & Engineering Chemistry Research* **2000**. vol. 39, no. 12, 4901

- [280] Moisan, S., Martinez, V., Weisbecker, P., Cansell, F., Mecking, S., and Aymonier, C. "General approach for the synthesis of organic-inorganic hybrid nanoparticles mediated by supercritical CO₂." *Journal of the American Chemical Society* **2007**. vol. 129, no. 34, 10602
- [281] Moner-Girona, M., Roig, A., Benito, M., and Molins, E. "Aerogel thin film synthesis by supercritical fluid-assisted sol-gel route in a single processing unit." *Journal of Materials Chemistry* **2003**. vol. 13, 2066
- [282] Pessey, V., Garriga, R., Weill, F., Chevalier, B., Etourneau, J., and Cansell, F. "Control of particle growth by chemical transformation in supercritical CO₂/ethanol mixtures." *Journal of materials chemistry* **2002**. vol. 12, 958
- [283] Bousquet, C., Elissalde, C., Aymonier, C., Maglione, M., Cansell, F., and Heintz, J. "Tuning Al₂O₃ crystallinity under supercritical fluid conditions: Effect on sintering." *Journal of the European Ceramic Society* **2008**. vol. 28, no. 1, 223
- [284] Reverón, H., Aymonier, C., Loppinet-Serani, A., Elissalde, C., Maglione, M., and Cansell, F. "Single-step synthesis of well-crystallized and pure barium titanate nanoparticles in supercritical fluids." *Nanotechnology* **2005**. vol. 16, no. 8, 1137
- [285] Erriguible, A., Marias, F., Cansell, F., and Aymonier, C. "Monodisperse model to predict the growth of inorganic nanostructured particles in supercritical fluids through a coalescence and aggregation mechanism." *The Journal of Supercritical Fluids* **2009**. vol. 48, no. 1, 79
- [286] Adschiri, T., Hakuta, Y., Sue, K., and Arai, K. "Hydrothermal synthesis of metal oxide nanoparticles at supercritical conditions." *Journal of Nanoparticle Research* **2001**. vol. 3, no. 2, 227
- [287] Pessey, V., Garriga, R., Weill, F., Chevalier, B., Etourneau, J., and Cansell, F. "Submicronic particles synthesis by a supercritical way." *High Pressure Research: An International Journal* **2001**. vol. 20, no. 1, 289
- [288] Shah, P. S., Holmes, J. D., Doty, R. C., Johnston, K. P., and Korgel, B. A. "Steric stabilization of nanocrystals in supercritical CO₂ using fluorinated ligands." *Journal of the American Chemical Society* **2000**. vol. 122, no. 17, 4245
- [289] Kitchens, C. L. and Roberts, C. B. "Copper nanoparticle synthesis in compressed liquid and supercritical fluid reverse micelle systems." *Industrial & Engineering Chemistry Research* **2004**. vol. 43, no. 19, 6070
- [290] Lu, X., Korgel, B. A., and Johnston, K. P. "Synthesis of germanium nanocrystals in high temperature supercritical CO₂." *Nanotechnology* **2005**. vol. 16, 389
- [291] Yoo, B., Dodabalapur, A., Lee, D. C., Hanrath, T., and Korgel, B. A. "Germanium nanowire transistors with ethylene glycol treated poly(3,4-ethylenedioxythiophene): poly(styrene sulfonate) contacts." *Applied Physics Letters* **2007**. vol. 90, 072106/1
- [292] Ohde, H., Hunt, F., and Wai, C. M. "Synthesis of silver and copper nanoparticles in a water-in-supercritical-carbon dioxide microemulsion." *Chemistry of Materials* **2001**. vol. 13, 4130
- [293] Martin, R. B., Meziani, M. J., Pathak, P., Riggs, J. E., Cook, D. E., Perera, S., and Sun, Y. P. "Optical limiting of silver-containing nanoparticles." *Optical Materials* **2007**. vol. 29, 788
- [294] Kameo, A., Tomokazu, Y., and Kunio, E. "Preparation of noble metal nanoparticles in supercritical carbon dioxide." *Colloids and Surfaces A: Physicochemical and Engineering Aspects* **2003**. vol. 215, no. 1-3, 181
- [295] Shah, P. S., Husain, S., Johnston, K. P., and Korgel, B. A. "Nanocrystal arrested precipitation in supercritical carbon dioxide." *The Journal of Physical Chemistry B* **2001**. vol. 105, no. 39, 9433

- [296] Lou, Z., Chen, C., Zhao, D., Luo, S., and Li, Z. "Large-scale synthesis of carbon spheres by reduction of supercritical CO₂ with metallic calcium." *Chemical Physics Letters* **2006**. vol. 421, no. 4-6, 584
- [297] Gogotsi, Y., Libera, J. A., and Yoshimura, M. "Hydrothermal synthesis of multiwall carbon nanotubes." *Journal of Materials Research* **2000**. vol. 15, 2591
- [298] Calderon Moreno, J. M. and Yoshimura, M. "Hydrothermal processing of high-quality multiwall nanotubes from amorphous carbon." *Journal of the American Chemical Society* **2001**. vol. 123, no. 4, 741
- [299] Motiei, M., Rosenfeld Hachon, Y., Calderon-Moreno, J. M., and Gedanken, A. "Preparing carbon nanotubes and nested fullerenes from supercritical CO₂ by a chemical reaction." *Journal of the American Chemical Society* **2001**. vol. 123, no. 35, 8624
- [300] Lee, D. C., Mikulec, F. V., and Korgel, B. A. "Carbon nanotube synthesis in supercritical toluene." *Journal of the American Chemical Society* **2004**. vol. 126, no. 15, 4951
- [301] Liu, Z. "Nanocomposites synthesized using supercritical fluids." *Journal of Physics: Conference Series* **2009**. vol. 165, No pp. given
- [302] Taylor, A. D., DiLeo, G. J., and Sun, K. "Hydrogen production and performance of nickel based catalysts synthesized using supercritical fluids for the gasification of biomass." *Applied Catalysis, B: Environmental* **2009**. vol. 93, 126
- [303] Ye, S., Wu, F., Ye, X. R., and Lin, Y. "Supercritical fluid assisted synthesis and processing of carbon nanotubes." *Journal of Nanoscience and Nanotechnology* **2009**. vol. 9, 2781
- [304] Holmes, J. D., Bhargava, P. A., Korgel, B. A., and Johnston, K. P. "Synthesis of cadmium sulfide Q particles in water-in-CO₂ microemulsions." *Langmuir* **1999**. vol. 15, no. 20, 6613
- [305] Ohde, H., Ohde, M., Bailey, F., Kim, H., and Wai, C. M. "Water-in-CO₂ microemulsions as nanoreactors for synthesizing CdS and ZnS nanoparticles in supercritical CO₂." *Nano Letters* **2002**. vol. 2, no. 7, 721
- [306] Luo, W., Xie, Y., Wu, C., and Zheng, F. "Spherical CoS₂ @ carbon core-shell nanoparticles: one-pot synthesis and Li storage property." *Nanotechnology* **2008**. vol. 19, no. 7, 075602
- [307] Chhor, K., Bocquet, J. F., and Pommier, C. "Syntheses of submicron magnesium oxide powders." *Materials Chemistry and Physics* **1995**. vol. 40, no. 1, 63
- [308] Loy, D. A., Russick, E. M., Yamanaka, S. A., Baugher, B. M., and Shea, K. J. "Direct formation of aerogels by sol-gel polymerizations of alkoxysilanes in supercritical carbon dioxide." *Chemistry of Materials* **1997**. vol. 9, no. 11, 2264
- [309] Galkin, A. A., Kostyuk, B. G., Lunin, V. V., and Poliakoff, M. "Continuous reactions in supercritical water: A new route to La₂CuO₄ with a high surface area and enhanced oxygen mobility." *Angewandte Chemie International Edition* **2000**. vol. 39, no. 15, 2738
- [310] Moner-Girona, M., Roig, A., Molins, E., and Llibre, J. "Sol-gel route to direct formation of silica aerogel microparticles using supercritical solvents." *Journal of Sol-Gel Science and Technology* **2003**. vol. 26, no. 1, 645
- [311] Sui, R., Rizkalla, A. S., and Charpentier, P. A. "Formation of titania nanofibers: A direct sol-gel route in supercritical CO₂." *Langmuir* **2005**. vol. 21, no. 14, 6150
- [312] Hald, P., Becker, J., Bremholm, M., Pedersen, J. N., Chevallier, J., Iversen, S. B., and Iversen, B. B. "Supercritical propanol-water synthesis and comprehensive size characterisation of highly crystalline anatase TiO₂ nanoparticles." *Journal of Solid State Chemistry* **2006**. vol. 179, no. 8, 2674 . Von Schnering 75th Birthday

- [313] Sui, R., Rizkalla, A. S., and Charpentier, P. A. "FTIR study on the formation of TiO₂ nanostructures in supercritical CO₂." *The Journal of Physical Chemistry B* **2006**. vol. 110, no. 33, 16212
- [314] Sui, R., Rizkalla, A. S., and Charpentier, P. A. "Direct synthesis of zirconia aerogel nanoarchitecture in supercritical CO₂." *Langmuir* **2006**. vol. 22, no. 9, 4390
- [315] Sui, R., Rizkalla, A. S., and Charpentier, P. A. "Kinetics study on the sol-gel reactions in supercritical CO₂ by using in situ ATR-FTIR spectrometry." *Crystal Growth & Design* **2008**. vol. 8, no. 8, 3024
- [316] Becker, J., Hald, P., Bremholm, M., Pedersen, J. S., Chevallier, J., Iversen, S. B., and Iversen, B. B. "Critical size of crystalline ZrO₂ nanoparticles synthesized in near- and supercritical water and supercritical isopropyl alcohol." *ACS Nano* **2008**. vol. 2, no. 5, 1058
- [317] Taboada, E., Solanas, R., Rodríguez, E., Weissleder, R., and Roig, A. "Supercritical-fluid-assisted one-pot synthesis of biocompatible core γ -Fe₂O₃/shell(SiO₂) nanoparticles as high relaxivity T₂-contrast agents for magnetic resonance imaging." *Advanced Functional Materials* **2009**. vol. 19, no. 14, 2319
- [318] Adschiri, T., Kanazawa, K., and Arai, K. "Rapid and continuous hydrothermal crystallization of metal oxide particles in supercritical water." *Journal of the American Ceramic Society* **1992**. vol. 75, no. 4, 1019
- [319] Adschiri, T., Kanazawa, K., and Arai, K. "Rapid and continuous hydrothermal synthesis of boehmite particles in subcritical and supercritical water." *Journal of the American Ceramic Society* **1992**. vol. 75, no. 9, 2615
- [320] Hakuta, Y., Onai, S., Terayama, H., Adschiri, T., and Arai, K. "Production of ultra-fine ceria particles by hydrothermal synthesis under supercritical conditions." *Journal of Materials Science Letters* **1998**. vol. 17, no. 14, 1211
- [321] Hakuta, Y., Seino, K., Ura, H., Adschiri, T., Takizawa, H., and Arai, K. "Production of phosphor (YAG: Tb) fine particles by hydrothermal synthesis in supercritical water." *Journal of materials chemistry* **1999**. vol. 9, 2671
- [322] Li, G., Smith, R. L., Inomata, H., and Arai, K. "Synthesis and thermal decomposition of nitrate-free boehmite nanocrystals by supercritical hydrothermal conditions." *Materials Letters* **2002**. vol. 53, no. 3, 175
- [323] Sue, K., Murata, K., Kimura, K., and Arai, K. "Continuous synthesis of zinc oxide nanoparticles in supercritical water." *Green Chemistry* **2003**. vol. 5, 659
- [324] Hakuta, Y., Hayashi, H., and Arai, K. "Hydrothermal synthesis of photocatalyst potassium hexatitanate nanowires under supercritical conditions." *Journal of Materials Science* **2004**. vol. 39, no. 15, 4977
- [325] Cabañas, A. and Poliakov, M. "The continuous hydrothermal synthesis of nano-particulate ferrites in near critical and supercritical water." *Journal of Materials Chemistry* **2001**. vol. 11, 1408
- [326] Galkin, A. A., Kostyuk, B. G., Kuznetsova, N. N., Turakulova, A. O., Lunin, V. V., and Polyakov, M. "Unusual approaches to the preparation of heterogeneous catalysts and supports using water in subcritical and supercritical states." *Kinetics and Catalysis* **2001**. vol. 42, no. 2, 154
- [327] Lock, N., Bremholm, M., Christensen, M., Almer, J., Chen, Y. S., and Iversen, B. "In situ high-energy synchrotron radiation study of boehmite formation, growth, and phase transformation to alumina in sub- and supercritical water." *Chemistry - A European Journal* **2009**. vol. 15, no. 48, 13381
- [328] Tyrsted, C., Becker, J., Hald, P., Bremholm, M., Pedersen, J. S., Chevallier, J., Cerenius, Y., Iversen, S. B., and Iversen, B. B. "In-situ synchrotron radiation study of formation and growth of crystalline Ce_xZr_{1-x}O₂ nanoparticles synthesized in supercritical water." *Chemistry of Materials* **2010**. vol. 22, no. 5, 1814

- [329] Bremholm, M., Jensen, H., Iversen, S. B., and Iversen, B. B. "Reactor design for in situ X-ray scattering studies of nanoparticle formation in supercritical water syntheses." *The Journal of Supercritical Fluids* **2008**. vol. 44, no. 3, 385 . 8th International Symposium on Supercritical Fluids, 5-8 November, 2006, Kyoto, Japan
- [330] Toft, L. L., Aarup, D. F., Bremholm, M., Hald, P., and Iversen, B. B. "Comparison of T-piece and concentric mixing systems for continuous flow synthesis of anatase nanoparticles in supercritical isopropanol/water." *Journal of Solid State Chemistry* **2009**. vol. 182, no. 3, 491
- [331] Lee, J. and Teja, A. S. "Characteristics of lithium iron phosphate (LiFePO₄) particles synthesized in subcritical and supercritical water." *The Journal of Supercritical Fluids* **2005**. vol. 35, no. 1, 83
- [332] Cabañas, A., Darr, J. A., Lester, E., and Poliakoff, M. "Continuous hydrothermal synthesis of inorganic materials in a near-critical water flow reactor; the one-step synthesis of nano-particulate Ce_{1-x}Zr_xO₂ (x = 0 - 1) solid solutions." *Journal of Materials Chemistry* **2001**. vol. 11, 561
- [333] Hanrahan, J. P., Copley, M. P., Ziegler, K. J., Spalding, T. R., Morris, M. A., Steytler, D. C., Heenan, R. K., Schweins, R., and Holmes, J. D. "Pore size engineering in mesoporous silicas using supercritical CO₂." *Langmuir* **2005**. vol. 21, no. 9, 4163
- [334] Znaidi, L., Chhor, K., and Pommier, C. "Batch and semi-continuous synthesis of magnesium oxide powders from hydrolysis and supercritical treatment of Mg(OCH₃)₂." *Materials Research Bulletin* **1996**. vol. 31, no. 12, 1527
- [335] Ohara, S., Mousavand, T., Umetsu, M., Takami, S., Adschiri, Y., Kuroki, Y., and Takata, M. "Hydrothermal synthesis of fine zinc oxide particles under supercritical conditions." *Solid State Ionics* **2004**. vol. 172, no. 1-4, 261 . Proceedings of the Fifteenth International Symposium on the Reactivity of Solids
- [336] Sue, K., Kimura, K., Yamamoto, M., and Arai, K. "Rapid hydrothermal synthesis of ZnO nanorods without organics." *Materials Letters* **2004**. vol. 58, no. 26, 3350
- [337] Panasyuk, G. P., Danchevskaya, M. N., Belan, V. N., Voroshilov, I. L., and Ivakin, Y. D. "Phenomenology of corundum crystal formation in supercritical water fluid." *Journal of Physics: Condensed Matter* **2004**. vol. 16, no. 14, S1215
- [338] Reverchon, E., Caputo, G., Correra, S., and Cesti, P. "Synthesis of titanium hydroxide nanoparticles in supercritical carbon dioxide on the pilot scale." *The Journal of Supercritical Fluids* **2003**. vol. 26, no. 3, 253
- [339] Lim, K. T., Hwang, H. S., Lee, M. S., Lee, G. D., Hong, S. S., and Johnston, K. P. "Formation of TiO₂ nanoparticles in water-in-CO₂ microemulsions." *Chemical communication* **2002**. vol. 14, 1528
- [340] Alonso, E., Montequi, I., Lucas, S., and Cocero, M. "Synthesis of titanium oxide particles in supercritical CO₂: Effect of operational variables in the characteristics of the final product." *The Journal of Supercritical Fluids* **2007**. vol. 39, no. 3, 453
- [341] Barj, M., Bocquet, J. F., Chhor, K., and Pommier, C. "Submicronic MgAl₂O₄ powder synthesis in supercritical ethanol." *Journal of Materials Science* **1992**. vol. 27, no. 8, 2187
- [342] Pommier, C., Chhor, K., and Bocquet, J. F. "The use of supercritical fluids as reaction medium for ceramic powder synthesis." *Silicates Industriels* **1994**. vol. 59, 141
- [343] Hakuta, Y., Ura, H., Hayashi, H., and Arai, K. "Effect of water density on polymorph of BaTiO₃ nanoparticles synthesized under sub and supercritical water conditions." *Materials Letters* **2005**. vol. 59, no. 11, 1387

- [344] Bocquet, J. F., Chhor, K., and Pommier, C. "Barium titanate powders synthesis from solvothermal reaction and supercritical treatment." *Materials Chemistry and Physics* **1999**. vol. 57, no. 3, 273
- [345] Hakuta, Y., Ura, H., Hayashi, H., and Arai, K. "Continuous production of BaTiO₃ nanoparticles by hydrothermal synthesis." *Industrial & Engineering Chemistry Research* **2005**. vol. 44, no. 4, 840
- [346] Atashfaraz, M., Shariaty-Niassar, M., Ohara, S., Minami, K., Umetsu, M., Naka, T., and Adschiri, T. "Effect of titanium dioxide solubility on the formation of BaTiO₃ nanoparticles in supercritical water." *Fluid Phase Equilibria* **2007**. vol. 257, no. 2, 233 . 4th MTMS, 4th International Symposium on Molecular Thermodynamics and Molecular Simulation
- [347] Reveròn, H., Elissalde, C., Aymonier, C., Bidault, O., Maglione, M., and Cansell, F. "Supercritical fluid route for synthesizing crystalline barium strontium titanate nanoparticles." *Journal of Nanoscience and Nanotechnology* **2005**. vol. 5, 1741

Chapter II

Synthesis of HDS catalyst precursors in SCFs

II. Synthesis of HDS catalyst precursors in SCFs	103
II.1. Experimental section.....	107
II.1.1. Setup and general strategy	107
II.1.1.1. Experimental setup	108
II.1.1.2. Reagents	110
II.1.1.3. Protocol	112
II.1.1.4. Powder Characterizations	113
II.2. Results.....	114
II.2.1. Ni-Mo based oxides	115
II.2.2. Determination of the first synthesis operation parameters.....	119
II.2.2.1. Synthesis of NiMoO ₄ in supercritical H ₂ O/EtOH mixture.....	120
<i>II.2.2.1.1. Ni-Mo based oxide at the outlet of the supercritical reactor.....</i>	<i>121</i>
<i>II.2.2.1.2. Structural evolution of material with temperature</i>	<i>126</i>
II.2.2.2. Conclusion.....	137
II.2.3. Influence of some operating parameters.....	138
II.2.3.1. Influence of the alcohol nature in H ₂ O/ROH systems.....	139
II.2.3.2. Influence of the Ni/Mo ratio.....	149
<i>II.2.3.2.1. Ni/Mo = 0: synthesis of MoO_x</i>	<i>149</i>
<i>II.2.3.2.2. Ni/Mo ≠ 0: influence of the cations ratio on the characteristics of the powders</i>	<i>152</i>
II.2.3.3. Synthesis of CoMoO ₄	157
II.3. Conclusion	161
II.4. References.....	163

As stated in chapter I, the primary objective of this PhD work is to explore a new way of synthesizing bulk precursors of the HDS catalysts with the declared aim of obtaining a bulk material with high specific surface area. Bulk catalysts precursors synthesized via more classical ways usually present S_{BET} ranging from 10 to 50 $\text{m}^2.\text{g}^{-1}$. In this work, our objective primarily was the production of a material with a specific surface area of 100 $\text{m}^2.\text{g}^{-1}$.

In a first part we will describe the experimental setup specially developed at the ICMCB (Bordeaux) for the synthesis of material in a continuous process, together with the reagents and the protocol of our process. We then expose our characterization strategy and the results obtained with this synthesis method will finally be exposed and discussed.

II.1. Experimental section

For the preparation of our materials, we used a reactor that operates in a continuous mode. The use of a continuous process allows having a good control of the experimental conditions like pressure, temperature and residence time, but also to obtain sufficient materials to carry out characterizations and catalytic tests in a comfortable manner.

II.1.1. Setup and general strategy

In this first part will be described the setup and the general protocol developed in order to study the synthesis of the $\text{Ni}_x\text{Co}_{1-x}\text{MoO}_4$ phase ($0 \leq x \leq 1$) and produce enough nanopowders for the catalytic runs.

II.1.1.1. Experimental setup

The experimental setup developed for this PhD work is based on a former one incremented at the ICMCB, in the “supercritical fluids” group [1-4]. It has been already successfully operated for synthesizing various nanostructured materials (metals, oxides or nitrides) recovered as powders. We have improved this setup for the particular synthesis of different oxides precursors of the HDS catalysts named after their general label “NiMo” and “CoMo” referring to powders of nickel molybdenum oxides and cobalt molybdenum oxides in catalytic jargon (relative abundance of the metallic elements can vary). The versatility of this system makes it handy to transform, remove or add elements at will.

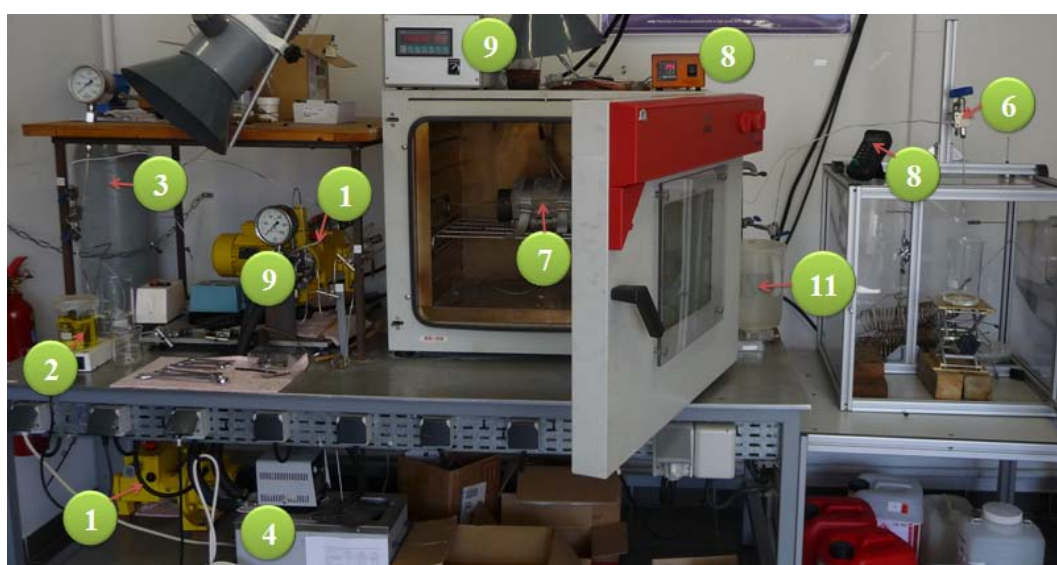
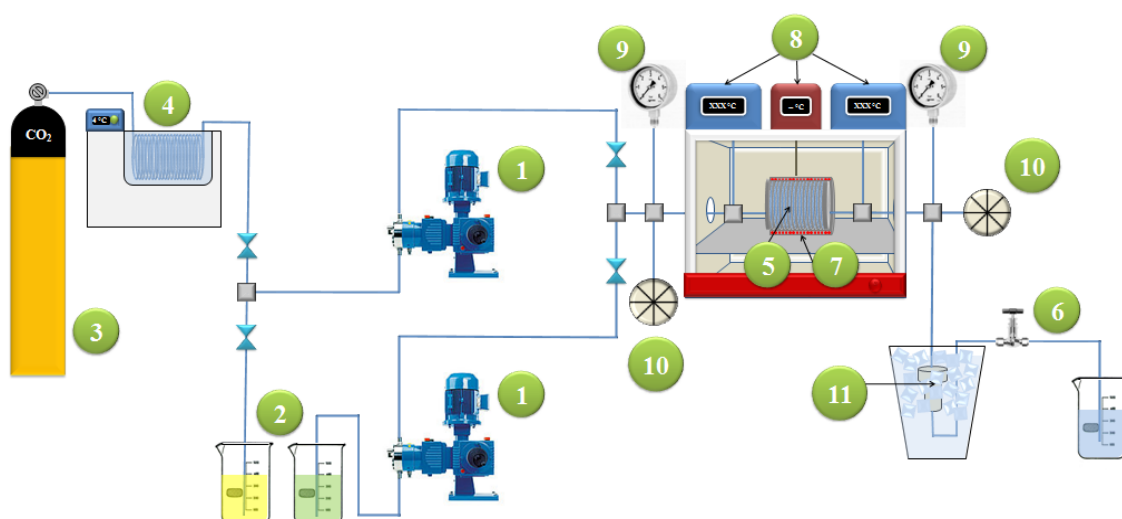


Figure II.1: Experimental setup operated for the synthesis of the catalyst precursors

The experimental setup consists of two high pressure pumps (50 mL.h^{-1} to 1 L.h^{-1}) (1), one dedicated to the injection of a metallic precursor solubilized in a solvent (2), the other one for the injection of either another solvent (with or without metallic precursor) or for the injection of CO_2 (3). CO_2 can be used as a solvent as already described in previous works from our research group. In this particular study, the CO_2 is used to check whether the system is leak free. After having been liquefied flowing through a cooler (4), CO_2 is injected in the circuit and brought to a pressure slightly above the experimental operating pressure to ensure the system sustains the pressure before carrying out any experiment. Depending on the synthesis, this pump could then be isolated from the system or used for the injection of a second solution of precursors.

The tubular reactor (6 m long, 8.2 mL) (5) in which the chemical reaction and the nucleation and growth of the nanoparticles take place, is maintained under pressure thanks to a back pressure regulator ($\pm 0.5 \text{ MPa}$) (6) and at constant temperature with the use of a heater band (maximum 600°C) (7). The reactor is rolled around a threaded piece of bronze to ensure a good heat transfer between it and the heating device. An insulation layer minimizes the heat radiation of the reactor and the whole system is put into an oven for a better protection.

Since type 316 stainless steel permanently loses more than two thirds of its mechanical properties when heated at a temperature above 427°C , Inconel® 625, a heat-resistant alloy, is preferred as reactor material when operating temperatures are above 400°C . K-type thermocouples (8) are positioned before, after and against the reactor to control the temperature of the whole system and manometers (9) permit the pressure control. Rupture discs (10) adjusted at 40 MPa are located at both sides of the reactor thus avoiding excessive pressures in the system and protecting the experimenter.

A filter (11) blocks the nanoparticles on the streamline before they pollute the back pressure regulator. It is immersed in iced water to prevent the back pressure regulator from being overheated and damaged by the hot fluid going through it.

The different elements are connected to each other via high pressure tubes made of stainless steel (type 316) with an inner diameter of 1.32 mm.

The residence time corresponds to the time during which the reaction media stays in the reactor. In continuous mode, it depends on the volume of the reactor, the flow and the density of the fluid (which depends on the pressure and the temperature). It can be calculated with the following equation (eq. 1):

$$t_s = \frac{V \cdot \rho(T)}{D} \quad (1)$$

with t_s the residence time (s), V the volume of the reactor (cm^3), ρ the density of the fluid ($\text{g} \cdot \text{cm}^{-3}$) and D the mass flow of the precursor solution ($\text{g} \cdot \text{s}^{-1}$). We estimate the residence time at about 55 seconds in our case. In all our experiments, we approximate the Reynolds number and we obtained $\text{Re} < 2300$ meaning that our flow regime is laminar (viscous forces are dominant) and is characterized by smooth and constant fluid motion.

With this setup, we can reach a maximal pressure of 40 MPa and a maximal temperature of 600 °C. In the following sections we will expose our choice concerning the metallic precursors, the solvents and the protocol we worked with.

II.1.1.2. Reagents

The choice of solvent and metallic precursors is of critical importance. Among the metallic precursors classically used in SCFs are acetates ($\text{M}^{n+}[\text{OOC-CH}_3]_n$) and acetylacetonates ($\text{M}^{n+}[\text{CH}_3\text{COCHCOCH}_3]_n$). The choice is based on commercial availability, cost and atom saving considerations (sustainable development). Molybdenum, nickel and cobalt acetates are all three commercially available. Therefore, we selected nickel(II) acetate ($\text{Ni}^{2+}[\text{OOC-CH}_3]_2$), cobalt(II) acetate ($\text{Co}^{2+}[\text{OOC-CH}_3]_2$) as metallic precursors for the catalyst “promoters”. However, Molybdenum acetate is particularly expensive, thirty times more than Molybdenum dioxide acetylacetonate ($\text{MoO}_2^{2+}[\text{CH}_3\text{COCHCOCH}_3]_2$). For this reason we choose this precursor also called molybdenum (VI) bis(2,4-pentanedionate) for the catalyst “active phase”.

From those metallic precursors depends the choice of solvent. Acetates have a good solubility in water, classically used as solvent for the synthesis of oxides in supercritical fluids. However, the precursor of molybdenum is not well soluble in water. Adding an alcohol appreciably increases its solubility, what makes us choose to work with the binary mixture water/alcohol. Moreover, the adjunction of alcohol to water permits to lower the critical coordinates of the fluid: for pure water: $[\text{p}_c (\text{MPa}); \text{T}_c (^\circ\text{C})] = [22.1; 374]$, for molar ratio $\text{H}_2\text{O}/\text{EtOH} = 1:1$: $\sim [8.2; 272]$. Water/ethanol system had already been studied at the ICMCB on the synthesis of $\text{Ba}_{1-x}\text{Sr}_x\text{TiO}_3$ (BST, $0 \leq x \leq 1$) [5,6] what oriented our choice for ethanol as the first alcohol to consider in our studies. Miscibility in water is a prevailing argument in the

II. Synthesis of HDS catalyst precursors in supercritical fluids

choice of the alcohol to test. Methanol and isopropanol are miscible in water, a reason why we chose to test them (butanol is not what excludes it from our list).

The different precursors and solvents we used in this work are listed and shortly described respectively in Table II.1 and Table II.2.

Table II.1: Metallic precursors used in this PhD work

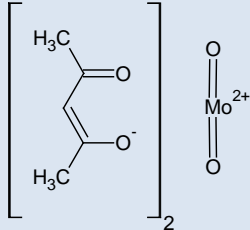
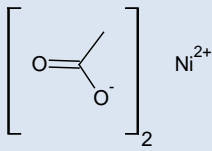
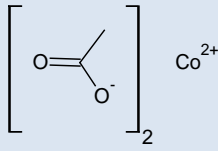
Precursors		
Molybdenum(VI) oxide bis(2,4-pentanedionate)	Nickel(II) acetate	Cobalt(II) acetate
- Good solubility in alcohol, not in water; - Chemical formula:	- Good solubility in water, not in alcohol; - Chemical formula:	- Good solubility in water, not in alcohol; - Chemical formula:
		

Table II.2: Solvents used in this PhD work

Reaction media, main characteristics and properties					
Water			Alcohol (methanol, ethanol, isopropanol)		
- Principal solvent used to synthesize oxides; - Low cost; - Innocuousness.			- Good solvent of the molybdenum precursor; - Relative low cost; - Lower T_c and p_c compared to pure water.		
Compounds		T_c (°C)	p_c (MPa)	ρ_c (g.mL ⁻¹)	Molar mass (g.mol ⁻¹)
H ₂ O	Water	374	22.1	0.32	18
CH ₄ O	Methanol	239.5	8.1	0.27	32
C ₂ H ₆ O	Ethanol	241	6.3	0.28	46
C ₃ H ₈ O	Isopropanol	264.2	5.3	0.27	60

The general protocol followed in our experiments to synthesize the mixed oxides from the transformation of Mo, Ni and Co precursors is detailed hereafter.

II.1.1.3. Protocol

The process to synthesize inorganic nanoparticles is based on a chemical transformation of metallic precursors (Table II.1). The process falls into different steps:

- The first step consists in solubilizing a determined amount of the precursors in the solvent. The solvent we consider is a mixture water/alcohol (adaptable ratio) as already mentioned, that permits both to solubilize molybdenum and promoters metallic precursors. Mo is directly solubilized in the mixture whereas the acetates are first put into distillate water before adding the proper quantity of alcohol, avoiding thus any risk of precipitation due to alcohol-aversion of the acetate. The solutions are put into an ultrasonic bath to improve and quicken this step. The two solutions are then put together for a one-line injection or kept separate for a two-line injection process. Practically, we fixed the molybdenum concentration to $[\text{Mo}] = 7.2 \cdot 10^{-3} \text{ mol.L}^{-1}$ (limiting reactor plugging) and based our promoters concentration on this value. In the mean time, the reactor is heated and the reaction media (water/alcohol), without precursor, is injected in the semi-continuous system to reach the steady state (stable temperature and pressure, both above the critical coordinates).
- The second step consists in injecting the solutions of precursors. The fluid containing the precursors will reach its supercritical condition in the reactor, and the chemical reaction will take place leading to the nucleation and growth of the nanoparticles. The nanoparticles thus formed in the reactor follow their way to the filter deepened in the ice bath to quench the growth of nanoparticles.
- The third step consists in bringing the system back to room temperature and atmospheric pressure by injecting water in the reactor to help cooling down and to wash the product.
- Finally, once the experiment is over, the filter is cleaned with distilled water and the product is recovered by vacuum filtration of the resulting slurry, washed with distilled water, and the product is dried at room temperature and crushed in a mortar to condition it as a powder before further treatment (particularly calcinations), analysis, transportation and tests.

Following this protocol, we have a powder production comprised between 400 mg and 1 g per experiment. This powder is used on one hand for different characterization mentioned in the following paragraph and on the other hand for catalytic tests.

II.1.1.4. Powder Characterizations

Once the nanoparticles are synthesized, crossing information from different characterization techniques is necessary to describe the powders and improve the understanding of reactions and mechanisms occurring in the SCFs reactor. Many characterization techniques are available at the ICMCB and [Figure II.2](#) exposes the strategy we followed and the techniques we used, associated with the type of information they provide. These techniques and machines used are presented in the [appendix IV.1-7](#).

These characterizations aim at both understanding the nucleation and growth mechanisms in supercritical fluids and making a selection of the materials to test in catalysis.

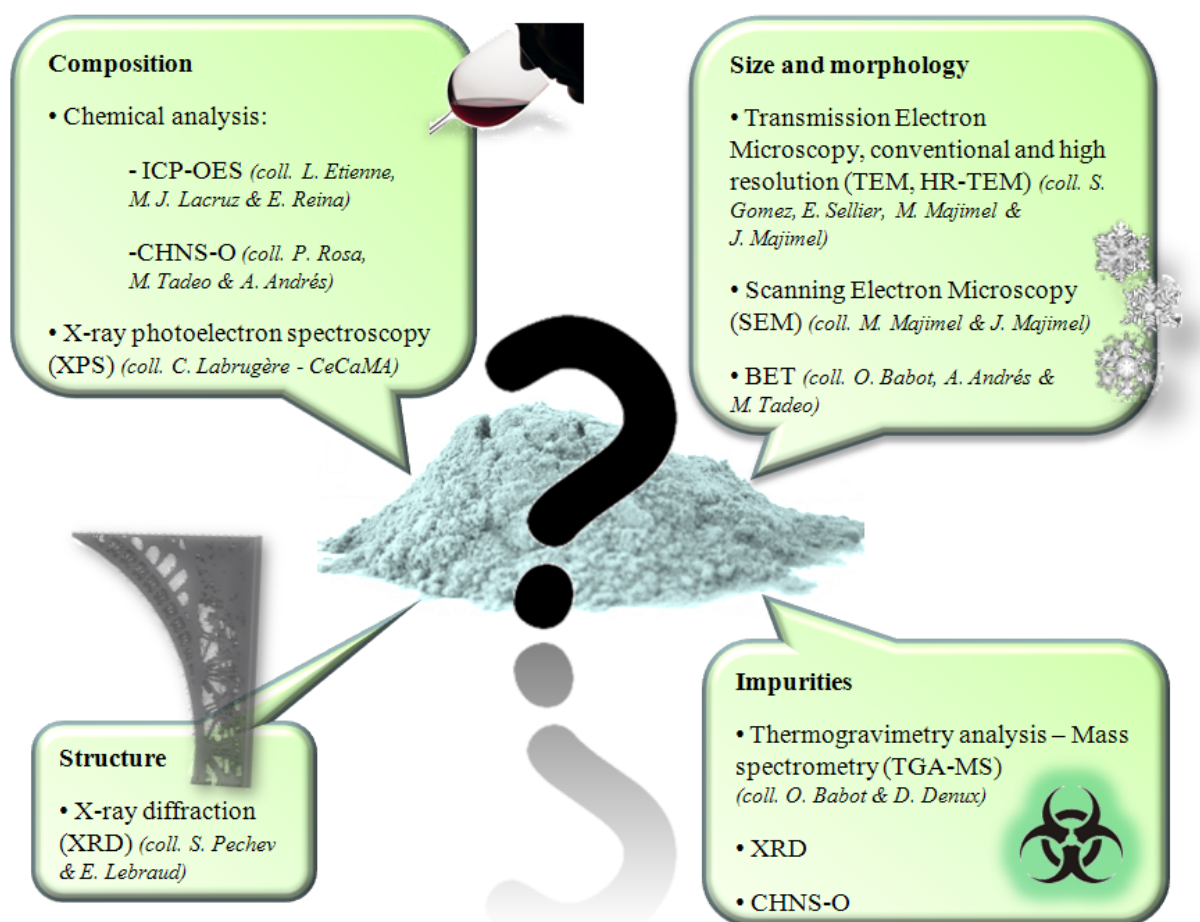


Figure II.2: Characterization strategy of our nanoparticles

The results and their interpretations obtained with these techniques concerning the synthesis of NiMoO_4 and CoMoO_4 obtained during this PhD project are presented in the next section.

II.2. Results

This chapter falls into two main parts consisting of the presentation of the initial parameters chosen for the synthesis of Ni-Mo based oxides like the solvent, the operating temperature and pressure, and the preliminary results obtained under those conditions. We then present the study of the influence of the variation of some of the operating parameters on the characteristics of our HDS catalyst precursors.

We propose first a complementary literature work concerning NiMoO_4 as an introduction to the first part before going through our own results.

II.2.1. Ni-Mo based oxides

Ni-Mo based oxides are our reference material in this PhD project. The following section goes even deeper in its description before presenting the studies performed in this project.

According to the ternary diagram of the system Ni-Mo-O (Figure II.3), NiMoO_4 is a stoichiometric compound which implies that neither Ni nor Mo are soluble in solid NiMoO_4 and different Ni/Mo ratios should result in powders containing a mixture of NiMoO_4 with other compounds based on the majority element. Mo, MoO_3 , Ni and NiO were used as starting materials to realize this diagram. The mixtures of metals and oxides were pelletized, placed in small alumina crucibles sealed inside evacuated silica capsules, and heated at 1100°C for 168 h. Phases were identified by metallography and XRD. The alloy compositions were determined by EDAX using pure metals as standards. On this diagram, α represents a solid solution based on metallic Ni and β represents a solid solution based on metallic Mo [7].

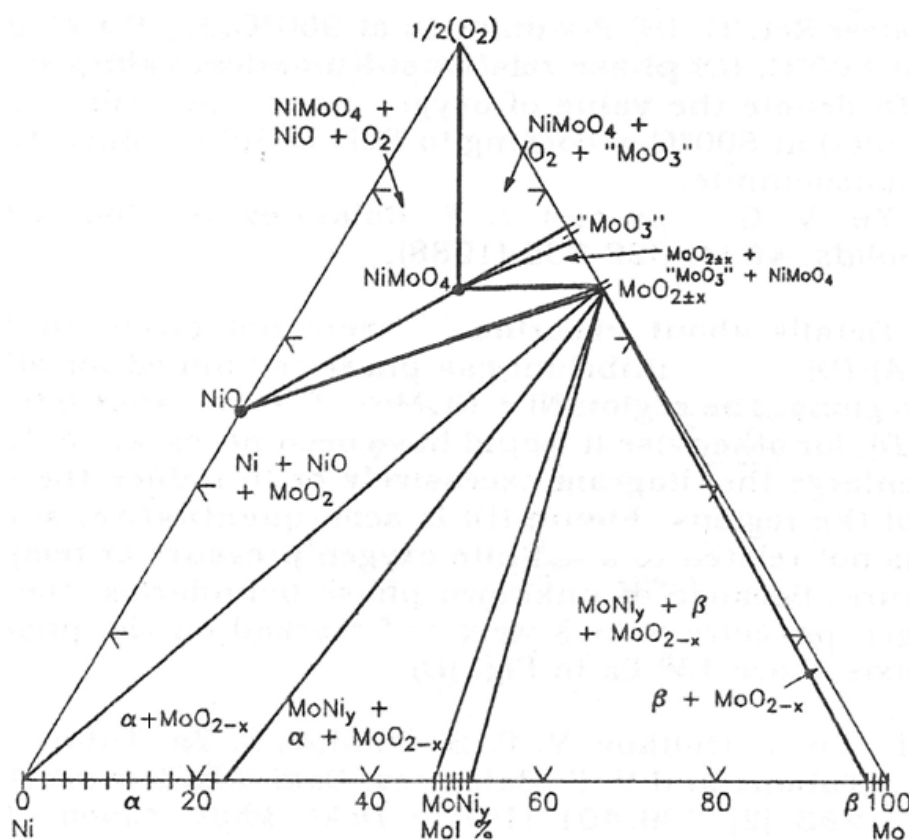


Figure II.3: Ternary diagram of the system Ni-Mo-O [8]

NiMoO_4 may exist in several polymorphs at atmospheric pressure: the low temperature α -phase [9,10], the high temperature β -isomorph [11,12], and the hydrate $\text{NiMoO}_4 \cdot n\text{H}_2\text{O}$ ($n = 0.75, 1$) [13-16]. Yet, according to literature, the pure β -phase is generated by heating the α - NiMoO_4 at temperatures above 690 °C and is stable only if kept over 180 °C [17,18].

Both phases (α and β) are monoclinic with space group $C2/m$ [19]. The structural building units of α - NiMoO_4 (isotypic with α - CoMoO_4 [9]) are NiO_6 and MoO_6 distorted octahedra, which share edges and form chains parallel to the “c” direction (Figure II.4 a). Each chain is surrounded by four other chains and joined to them by corner sharing of oxygen atoms. Between the filled chains occur chains of “holes” of unfilled octahedra (Figure II.4 b). It also presents alternative layers of NiO_6 and MoO_6 parallel to the “b” direction as represented on Figure II.4 c.

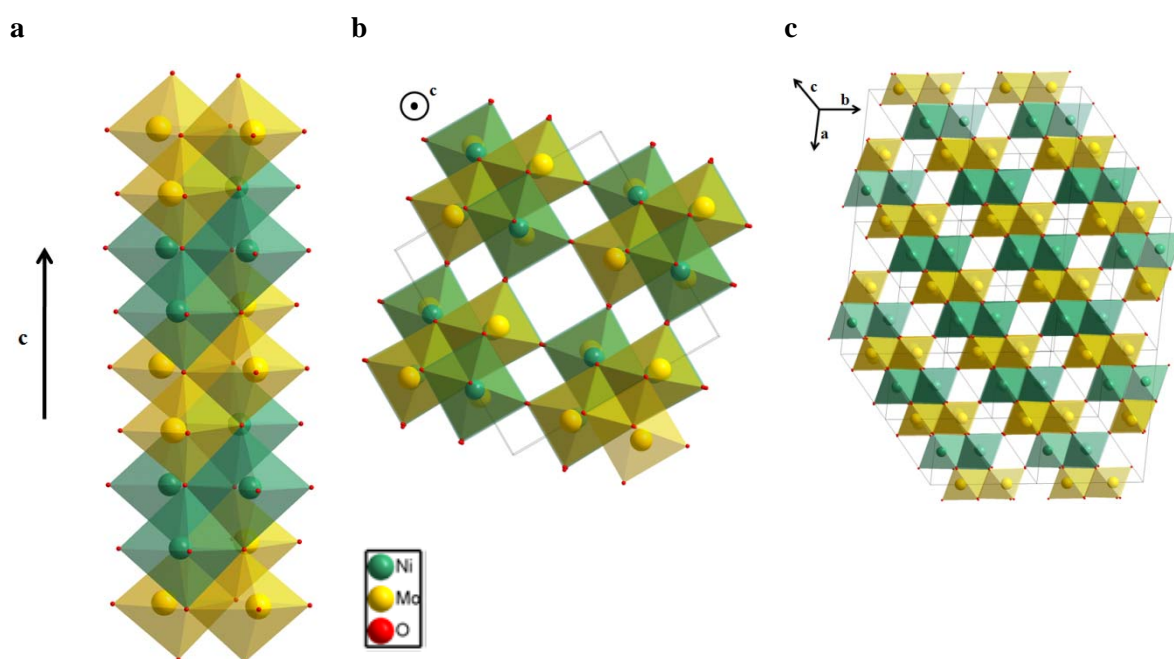


Figure II.4: Structure of α - NiMoO_4 (ICSD #81059)

The structure of β - NiMoO_4 is isotypic with α - MnMoO_4 (ICSD #78328). To the best of our knowledge, no ICSD cards exist for its structure and we don't have atomic position at this point of the study. Yet, we proposed the one of α - MnMoO_4 (Figure II.5). By analogy, it consists of molybdate distorted tetrahedra, which share corners with four different manganese octahedra. The general description is similar to the α -phase with chains joined by corner

sharing of oxygen atoms and with chains of unfilled octahedra between them. The displacement of the molybdenum atoms is obvious by comparison.

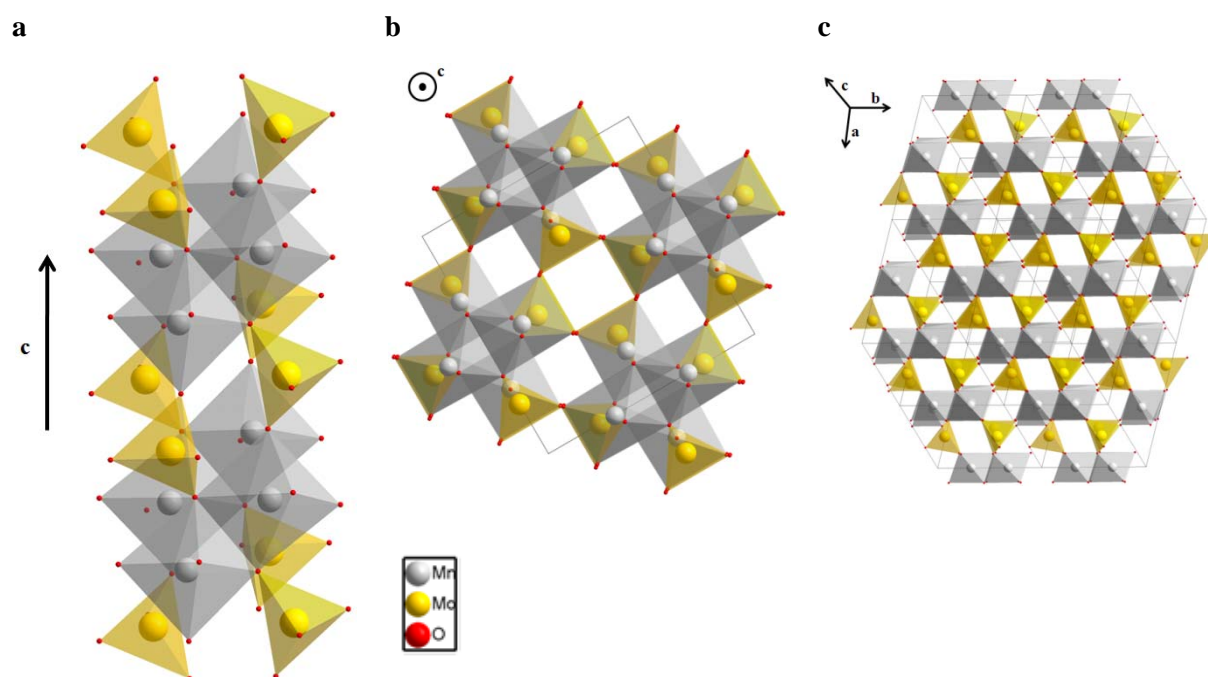


Figure II.5: Structure of α -MnMoO₄ (ICSD #78328)

Figure II.6 details the difference between the two phases and one can see from α to β , we have a contraction in the “c” axis and an expansion in the “a” and “b” axes of the cell. The formal oxidation state of Ni is +II, whereas that of Mo is +VI as in MoO₃ [13,20].

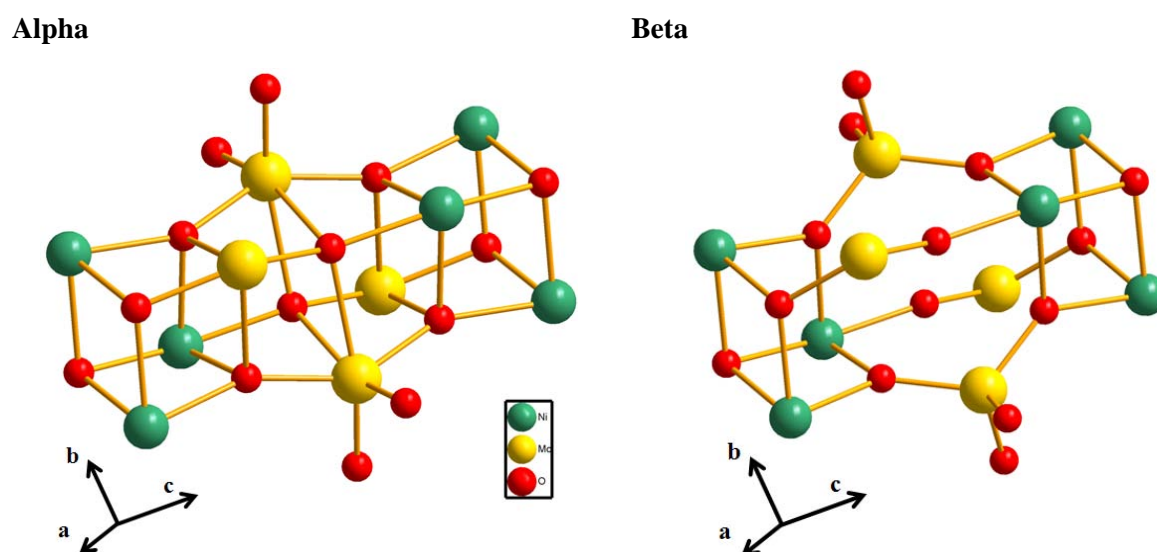


Figure II.6: Partial view of the crystal structures of the α and β polymorphs of NiMoO₄ (adapted from [20])

Recent studies give a description of the hydrated phase $\text{NiMoO}_4 \cdot n\text{H}_2\text{O}$ with $n = 1$ or 0.75 [15,16]. Measurements of differential thermal analysis (DTA) suggest that in these systems the metal cations have coordination similar to that seen in $\beta\text{-NiMoO}_4$ [18,21]. Only the $\text{NiMoO}_4 \cdot 0.75\text{H}_2\text{O}$ structure has been recently described as a triclinic system (space group $P-1$) tetrameric z-shaped unit of Ni octahedra, two NiO_6 and two $\text{NiO}_5(\text{OH}_2)$, that share edges. These units are interconnected by MoO_4 tetrahedra to form a network structure having open channels. The coordination water (O1w) of $\text{NiO}_5(\text{OH}_2)$ projects into the channel, and additional lattice water (O2w) is included in it (Figure II.7). $\text{NiMoO}_4 \cdot \text{H}_2\text{O}$ might present a similar structure with lattice and coordination water.

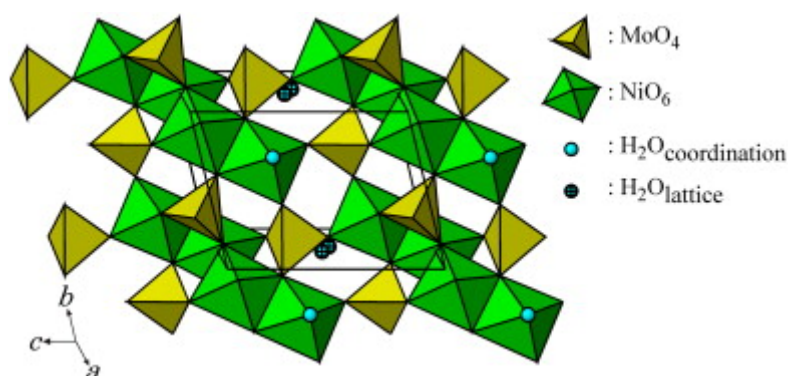


Figure II.7: Crystal structure of the $\text{NiMoO}_4 \cdot 0.75\text{H}_2\text{O}$ [16]

The catalytic properties of the nickel molybdates are closely related to their structures: it is generally assumed that the $\beta\text{-NiMoO}_4$ shows a better active and selective catalysis compared to the α -phase for various reactions, better activity attributed to the tetrahedral environment of Mo in the β -phase: in the tetrahedral environment of the β -phase, a Mo^{6+} ion is unsaturated and in overall its empty 4d orbitals are less destabilized than in an octahedral field. This favors bonding interactions between the $\text{Mo}(4d)$ orbitals and the sulfur lone pairs of H_2S . Therefore, under the HDS conditions, $\beta\text{-NiMoO}_4$ (sulfided) produces a greater number of active sites [22,23]. In a serial of studies [17,21], the sulfided $\text{NiMoO}_4 \cdot \text{H}_2\text{O}$ compounds is found to be much better catalysts for the HDS of thiophene than the corresponding sulfided α - and β -isomorphs. The HDS activity of these systems increased in the following order: $\alpha < \beta < \text{hydrate}$. Researches are still carried out to better stabilize the β -phase at lower temperatures and several leads have been explored like testing new synthesis [24], improving the thermal treatment [18], modifying the support [25,26], adding excess of nickel [27,28] or even by further processing of the material like by γ -irradiations [29].

II.2.2. Determination of the first synthesis operation parameters

Most of the researches on the synthesis of oxides in supercritical fluids consider water as the reaction media. Hydrothermal reaction, hydrolysis of the metallic precursors and dehydration of the so-formed hydroxides lead to the desired oxides. In our specific case, we chose to work with Molybdenum (VI) oxide bis(2,4-pentanedionate) for the reasons described in II.1.1.2, and it is only slightly soluble in water on the contrary to Ni and Co acetates. The first objective was thus to determine a suitable media in which both precursors are soluble.

Different solubilization tests of our molybdenum precursor in pure water, pure ethanol, pure isopropanol, pure acetone and pure acetylacetone (also called 2,4-pentanedione) rapidly lead to the conclusion that alcohols are good solvents at room temperature for our precursor and are relatively affordable. Yet, acetate precursors are not soluble at all in alcohol which brought us to consider a mixture water/alcohol as the reaction media. Few researches have been working on the synthesis of oxides in supercritical water/alcohol mixtures, nevertheless we can mention researches done at the ICMCB on the synthesis of $\text{Ba}_{1-x}\text{Sr}_x\text{TiO}_3$ (BST, $0 \leq x \leq 1$) in supercritical water/ethanol media [5,6,30]. The precursors were solubilized in pure ethanol before being mixed with distilled water at the reactor entrance. From barium, titanium and strontium isopropoxides, BaCO_3 was first obtained in pure ethanol and adding water progressively leads to the crystallization of the $\text{Ba}_{1-x}\text{Sr}_x\text{TiO}_3$ phase ($0 \leq x \leq 1$). In our case, the difference comes from the fact that the precursor can be directly injected in presence of water since Ni and Co acetates are stable in water at room temperature and atmospheric pressure.

Ethanol was retained as the alcohol for the first investigations. Different molar ratios have been tested to solubilize the precursors of molybdenum and nickel. This study brings us to consider that the $\text{H}_2\text{O}/\text{EtOH}$ molar ratio 1:1 best suits our objective. Bazaev et al. reported a pretty complete and useful work on the thermodynamic properties of water/ethanol mixture in near-critical and supercritical regions [31]. According to Figure II.8 dragged out this work, the critical coordinates of a water/ethanol mixture of molar ratio 1:1 are $T_c \approx 274^\circ\text{C}$ (a), p_c would be between 9 and 14 MPa (b).

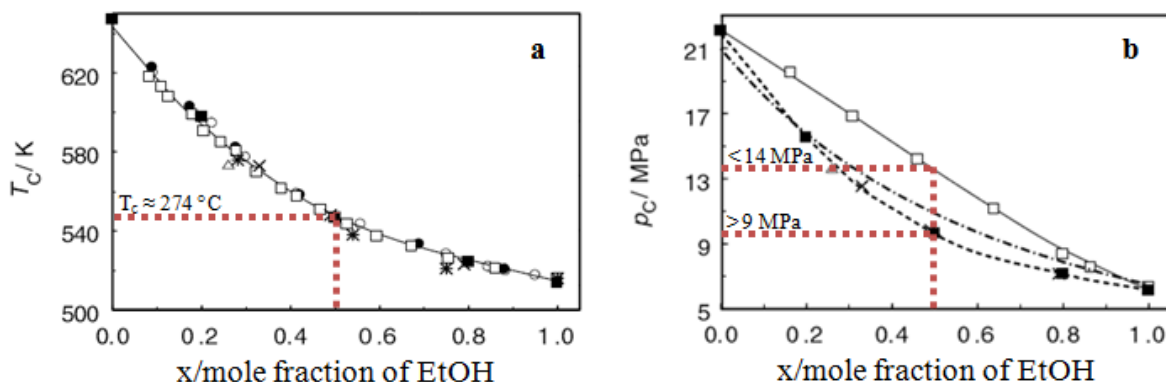


Figure II.8: Plot of critical temperature T_c (a) and critical pressure p_c (b) versus mole fraction of EtOH for ($\text{H}_2\text{O} + \text{EtOH}$) mixtures (■, □, x and * reported by various authors [31] and references therein)

Working at a fix molar ratio of 1:1, we decided to work at a temperature of 290°C and a pressure of 23 MPa to be sure we are in supercritical conditions. The system $\text{H}_2\text{O}/\text{EtOH}$ was our benchmark system for the synthesis of Ni-Mo based oxides in this work since it is the best known and described system in literature and in our research group.

We study the decomposition of the selected precursors of molybdenum and nickel in a water/ethanol solution of molar ratio 1:1 at $T = 290^\circ\text{C}$ and $p = 23 \text{ MPa}$ for a t_s of about 55 s. For this mixture, $\rho_c = 332 \text{ kg.m}^{-3}$ and $\eta_c = 7.7 \cdot 10^{-5} \text{ Pa.s}$ what gives us a $Re \approx 650$: we are in a laminar flow regime.

Now that our operating conditions are fixed, we expose the results obtained for the synthesis of NiMoO_4 .

II.2.2.1. Synthesis of NiMoO_4 in supercritical $\text{H}_2\text{O}/\text{EtOH}$ mixture

In a first attempt to synthesize NiMoO_4 , we worked with a method we call “one way injection” which consists in injecting our precursors from one unique solution via one high-pressure pump. In this purpose, two solutions, one for each precursor, are prepared separately to ensure a good primary solubilization. The two solutions are then mixed together before being injected in the reactor.

The Inductively Coupled Plasma – Optical Emission Spectroscopy (ICP-OES) results revealed that our powders contain $50 \pm 2 \%$ of nickel. This slight difference to stoichiometry

could be due to the use of a continuous process what implies we may have variations over time of the parameters, mainly of pumps efficiency. An optimization would be the use of high pressure pumps with a better control over the flow rate.

II.2.2.1.1. Ni-Mo based oxide at the outlet of the supercritical reactor

From now on, we will call fresh powders the powders obtained directly after synthesis in supercritical fluids (no further processing). As pointed out in [chapter I, 1.2.3](#) supercritical fluids technology provides with contaminant-free powders. This was confirmed in our case since CHNS-O analysis revealed that a mean of 0.43 ± 0.13 wt% carbons is present in our fresh powders. As we already mentioned in [chapter I, 1.1.3.1.3](#) carbon inhibits the active sites of HDS catalysts. During the sulfidation of the catalyst precursors and the HDS reaction by itself, carbon and sulfur react to form coking on the surface of the catalyst and inhibit the catalyst activity. Those same data revealed that our powders are free from nitrogen, another poison of HDS catalysts. Hydrogen is present at 0.99 ± 0.26 wt% we relate to traces of carbon and water detected by TGA-MS described further.

Cleanness of catalyst precursors was an important deliverable for refinery industries we successfully achieve with the supercritical fluid technology.

The TGA-MS showed in [Figure II.9](#) displays four loss of mass for a total mass loss of 8 %. A first loss of 2.79 %, between room temperature and 243 °C, is attributed to adsorbed water as the line shape of mass 18 suggests in the mass spectroscopy results associated. A second loss of 4.20 % occurs from 243 °C to 468 °C attributed this time to the departure of carbon and structural water according to line shape of mass 18 and mass 44. The third loss of 0.50 % between 468 °C and 538 °C can also be attributed to both water and carbon regarding the MS results, and the last loss of 0.51 % between 538 °C and 800 °C seems to be exclusively due to carbon departure. Those departures of water seem to be in good agreement with results obtained by Rodriguez et al. [\[13\]](#) or Eda et al. [\[16\]](#) on their study of $\text{NiMoO}_4 \cdot n\text{H}_2\text{O}$ ($n = 0.75$ or 1). Upon heating $\text{NiMoO}_4 \cdot n\text{H}_2\text{O}$ to high temperature in TGA-MS experiments, they observed that water desorbs in three peaks. The first one appears at 100–200 °C and is associated with water molecules reversibly bounded to the hydrate. The second peak appears from 200 to 400 °C and corresponds to desorption of water molecules

that form part of the crystal structure of the hydrate and they assess that at the onset of this peak, the formation of β -NiMoO₄ starts. They pointed out an additional small desorption peak between 490 °C and 520 °C they also attributed to water according to their MS results. Eda considers that the ideal hydrate is NiMoO₄.0.75H₂O. Considering the mass losses obtained with our TGA, we approximate a close value for our material.

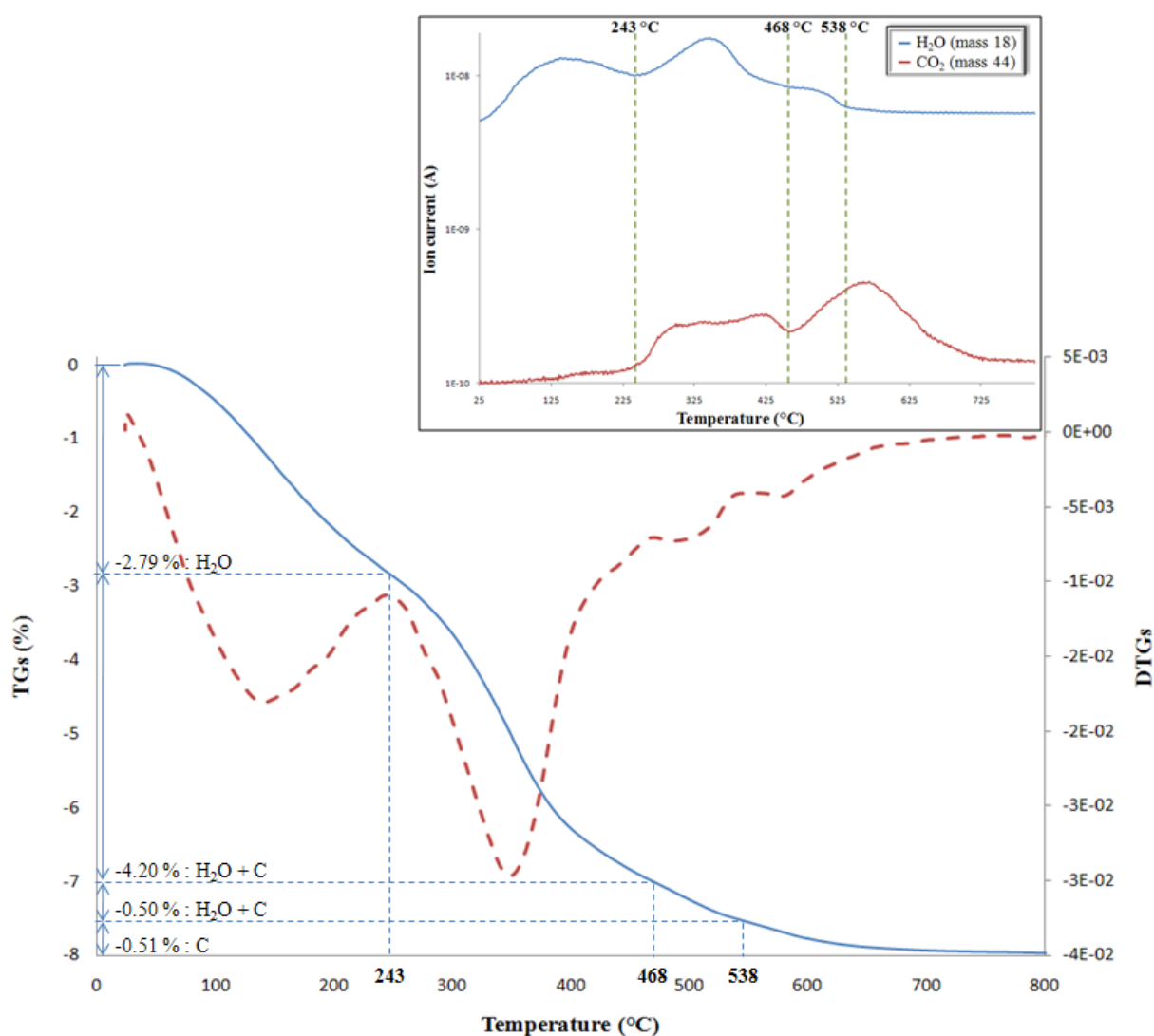


Figure II.9: TGA-MS of the stoichiometric NiMo based powder synthesized in supercritical H₂O/EtOH mixture, from room temperature to 800 °C under Ar atmosphere, ramp = 1 °C.min⁻¹

Most of the peaks of the XRD pattern can be assigned with the help of JCPDS cards of low quality (indexed as Questionable - Q) (Figure II.10). Among those cards, we find the JCPDS 13-0128 corresponding to hydrated nickel molybdate NiMoO₄.xH₂O (no value given for x). The presence of this isomorph in our powder is consistent with the strong similarities we observe between our TGA and those performed by Rodriguez and Eda what comfort us in

the hypothesis that we partly obtain this isomorph. Moreover, a similar XRD pattern (better peaks definition) has been obtained by Eda et al. [16] on material synthesized by hydrothermal approach (rods of diameter of 130 nm, $S_{\text{BET}} = 31 \text{ m}^2 \cdot \text{g}^{-1}$). As already mentioned they consider having $\text{NiMoO}_4 \cdot 0.75\text{H}_2\text{O}$ what fits with our work.

We can also detect $\text{MoO}_3 \cdot \text{H}_2\text{O}$ (JCPDS 01-125) and MoO_2 (JCPDS 32-0671). Our hypothesis to explain the presence of these phases comes from the stoichiometry of the powder used to perform this XRD: according to the ICP results, we have an excess of Mo ($\text{Ni}/\text{Mo} = 0.93$) and since NiMoO_4 is a stoichiometric compound, excess Mo appears as its own oxides. More surprisingly, we also seem to have $\beta\text{-NiMoO}_4$ (JCPDS 45-0142) normally not stable at room temperature but we express a stronger reservation on this one.

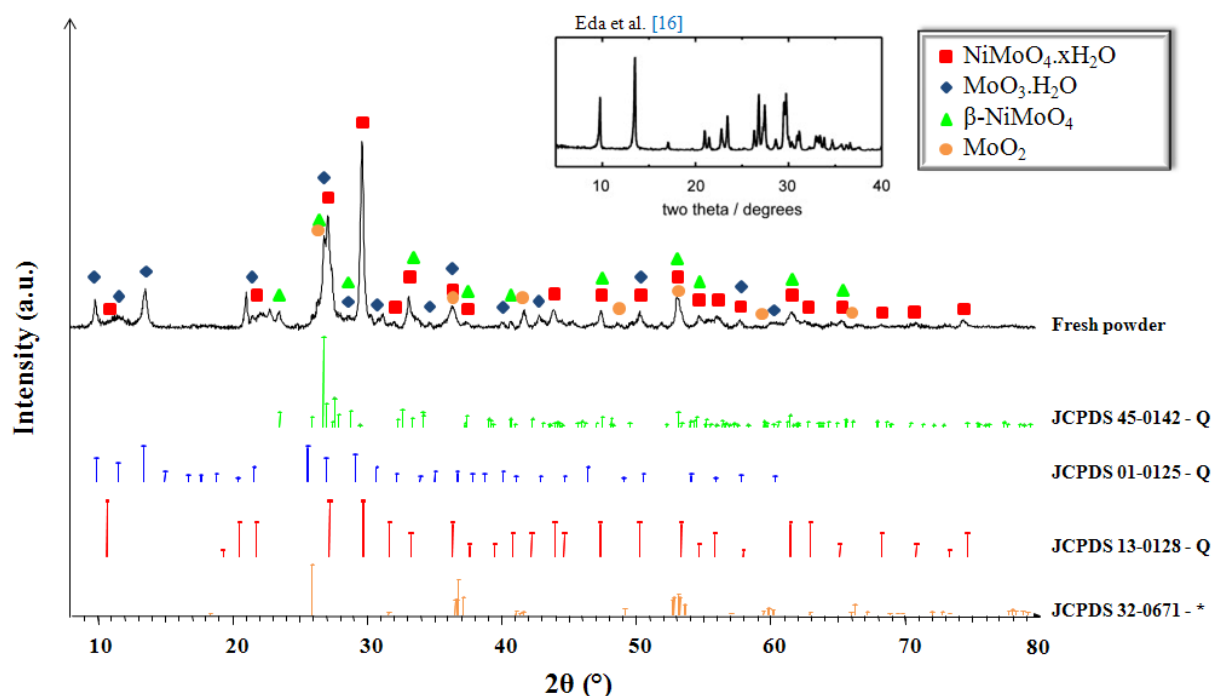


Figure II.10: XRD pattern of the stoichiometric NiMo based powder directly after synthesis in supercritical $\text{H}_2\text{O}/\text{EtOH}$ mixture & pattern obtained by Eda et al. [16]

Powders obtained directly after synthesis in supercritical $\text{H}_2\text{O}/\text{EtOH}$ mixture do not contain $\alpha\text{-NiMoO}_4$, the isomorph stable at room temperature, usually obtained with classical synthesis way, but mainly $\text{NiMoO}_4 \cdot 0.75\text{H}_2\text{O}$, one of the most active material for Deep-HDS.

SEM micrographs of our fresh powders (Figure II.11) show rod-like particles of dispersed sizes. The bigger rods can reach approximately 10 to 15 μm length for 500 nm large

and 250 nm high. Besides, in addition to rods, smaller aggregated particles ($50 \text{ nm} < \varnothing < 200 \text{ nm}$, red circles). Those rods have already been mentioned by Ding et al. [15] and Eda et al. [16], but none of them mentioned the presence of smaller particles in their powders.

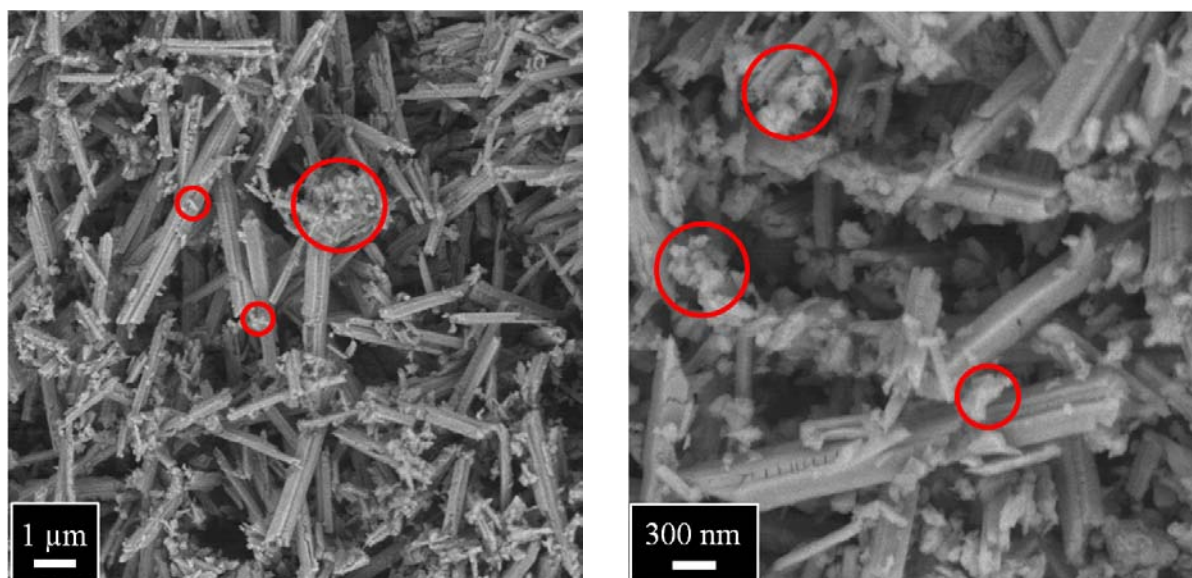


Figure II.11: SEM micrographs of the stoichiometric NiMo based powder directly after synthesis in supercritical $\text{H}_2\text{O}/\text{EtOH}$ mixture

According to the STEM-EDX chemical mapping (Figure II.12) the rod-like particles are homogeneously composed of nickel and molybdenum ($\text{NiMoO}_4 \cdot 0.75\text{H}_2\text{O}$) whereas the smaller particles can be composed of only molybdenum (red circles, $\text{MoO}_3 \cdot \text{H}_2\text{O}$ and MoO_2), or of an homogeneous mixture of Mo and Ni we can attribute to the secondary phase mentioned previously.

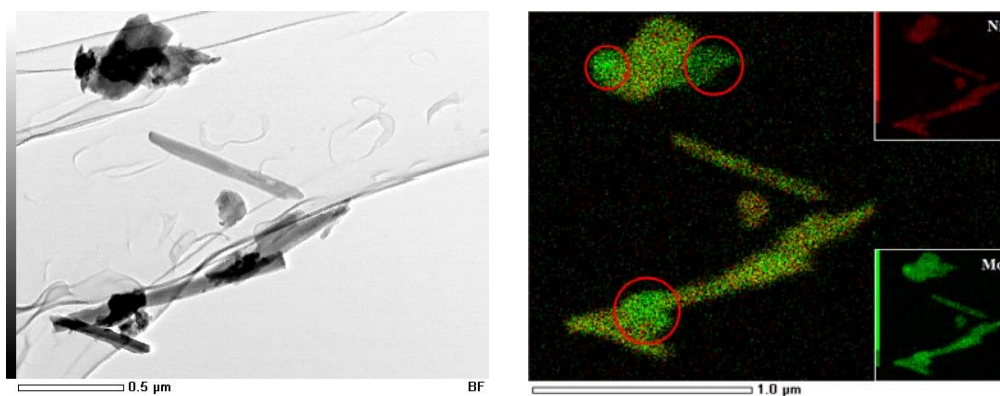


Figure 0.12: STEM-EDX chemical mapping of the stoichiometric NiMo based powder directly after synthesis in supercritical $\text{H}_2\text{O}/\text{EtOH}$ mixture

II. Synthesis of HDS catalyst precursors in supercritical fluids

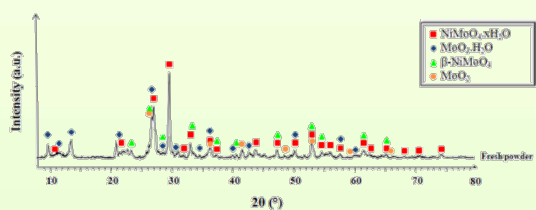
The mean S_{BET} measured with the BET method on the freshly prepared powders is of $134 \pm 14 \text{ m}^2.\text{g}^{-1}$. We remind that bulk catalysts precursors synthesized via more classical ways usually present S_{BET} around $30\text{-}50 \text{ m}^2.\text{g}^{-1}$, maximum $80 \text{ m}^2.\text{g}^{-1}$, and our objective in this work was the synthesis of a material with a specific surface area above $100 \text{ m}^2.\text{g}^{-1}$.

The size of our objects is too important regarding the S_{BET} they developed. A hypothesis to explain this fact could be the porosity of the rods: Eda presented them as network structures having open channels in which molecules of water can be inserted [16]. S_{BET} is measured from the adsorption of nitrogen at the surface of the material what has us think that these open channels contribute to the total S_{BET} .

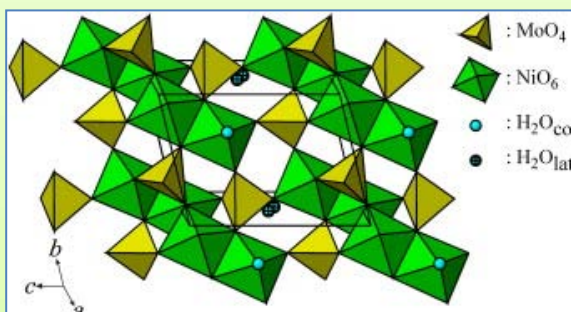
We manage to synthesize powders of bulk catalyst precursors of higher S_{BET} than expected.

An “identity card” of the stoichiometric NiMo based powder directly after synthesis in supercritical $\text{H}_2\text{O}/\text{EtOH}$ mixture is proposed below, summary of its characteristics:

Main characteristics of Ni-Mo oxides after synthesis in sc- $\text{H}_2\text{O}/\text{EtOH}$ (1:1 molar)



Mainly $\text{NiMoO}_4 \cdot 0.75\text{H}_2\text{O}$



$\text{NiMoO}_4 \cdot 0.75\text{H}_2\text{O}$

Triclinic system (space group $P-1$)

$S_{\text{BET}}: 134 \pm 14 \text{ m}^2.\text{g}^{-1}$

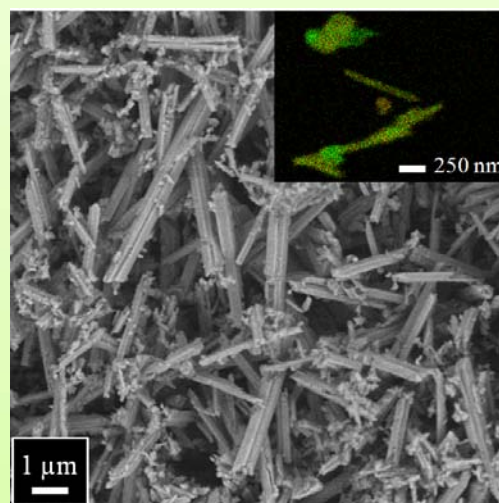
CHNS: $0.43 \pm 0.13 \text{ wt\% C}$

$0.99 \pm 0.26 \text{ wt\% H}$

0 wt\% N

0 wt\% S

ICP: $\text{Ni}/\text{Mo} = 1 \pm 0.08$



Mixture of $\text{NiMoO}_4 \cdot 0.75\text{H}_2\text{O}$,
 $\text{MoO}_3 \cdot \text{H}_2\text{O}$ and MoO_2

The objective of obtaining a new generation of bulk precursors for HDS catalysts based on nickel and molybdenum oxide, clean from active sites inhibitors and developing a high surface area have been reached. Moreover, the previous target of $S_{\text{BET}} = 100 \text{ m}^2.\text{g}^{-1}$ have been outperformed and the main phase obtained is particularly interesting in HDS catalysis.

A calcination step is included in most of the NiMoO_4 synthesis realized for catalytic applications. These calcinations are generally carried out between 350 °C and 550 °C from 2 to 8 hours. We thus decided to also consider calcined material for i) a better understanding of the characteristics of the powder and ii) our catalytic tests. Moreover, as a precursor of HDS catalysts, our material will be sulfided at 400 °C for 5 hours. The effects of those further processing on our material have been investigated and are presented in the following part.

II.2.2.1.2. Structural evolution of material with temperature

We performed XRD on a sample while heating it which allows studying any structural modification with temperature. [Figure II.13](#) represents the evolution of the XRD patterns of our material with temperature (selected patterns). We heated our sample up to 900 °C (ramp = 1 to 2 °C.min⁻¹ with a 30 min stabilization plateau before each acquisition, and shorter ΔT between the acquisitions around 400 °C – temperature classically used for the activation of the catalyst – and 700 °C – temperature where the $\alpha \rightarrow \beta$ transition is said to occur). From those data, we can point out that our powder undergoes a structural evolution that starts around 325 °C with the progressive vanishing of some peaks (marked in blue), the arising of new peaks (marked in red) and some peaks that slightly switch of few degrees or change in intensity (marked in green). This evolution seems complete at 400 °C and surprisingly unique in the studied temperature range. Indeed, we expected to observe a change in the pattern that would correspond to the $\alpha \rightarrow \beta$ transition around 700 °C which is not the case.

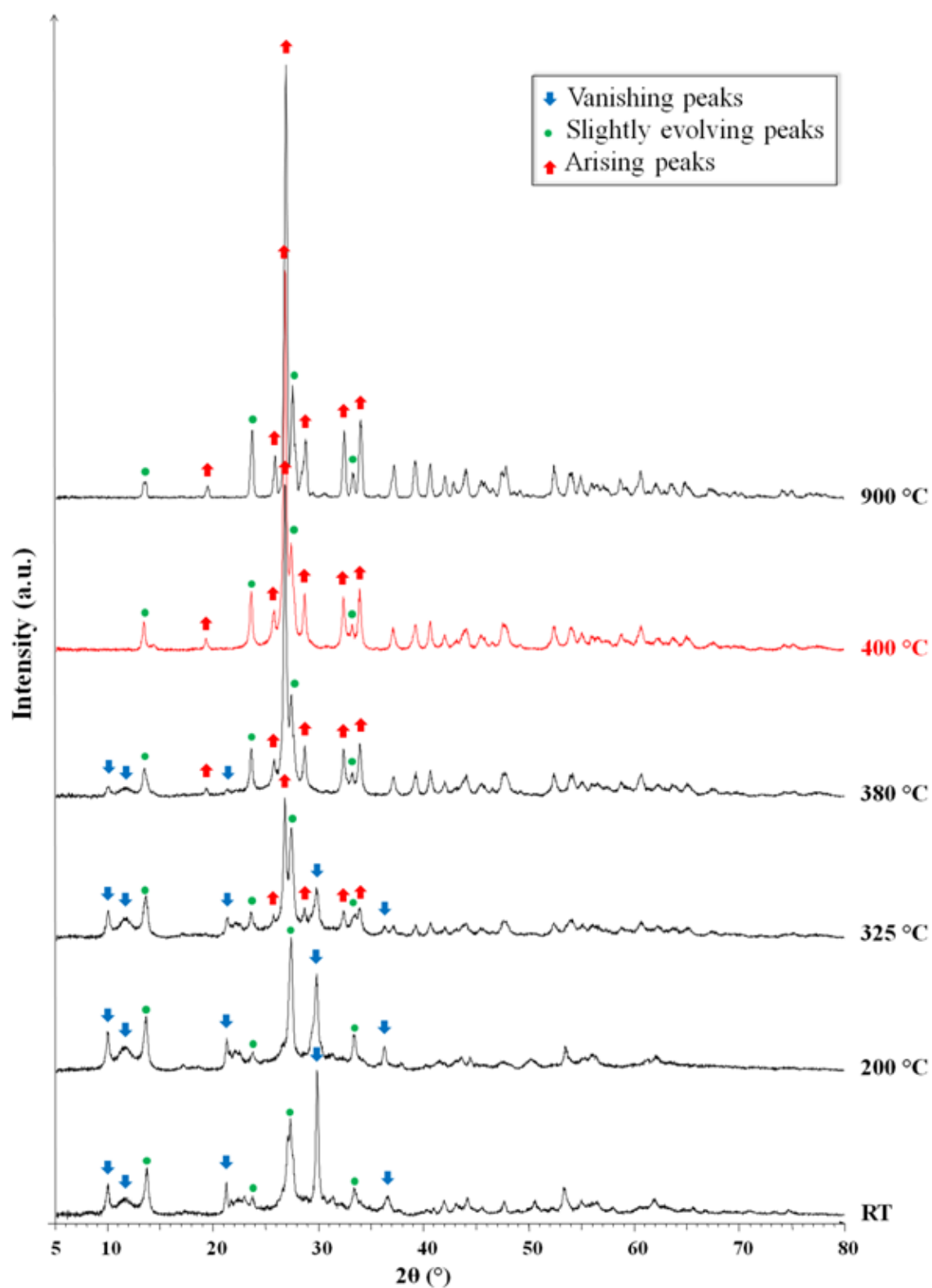


Figure II.13: XRD in temperature of the stoichiometric NiMo based powder synthesized in supercritical $\text{H}_2\text{O}/\text{EtOH}$ mixture

The phase obtained above 400 °C and presented by the XRD pattern on [Figure II.14](#) fits pretty well with the nickel molybdate- β (or β -NiMoO₄) by comparison with JCPDS 12-0348 ($13^\circ < 2\theta < 80^\circ$) and JCPDS 45-0142 ($23^\circ < 2\theta < 133^\circ$). The presence of the β -NiMoO₄ phase already at 400 °C explains why we could not see any evolution of the diffractogram of our powder at higher temperatures.

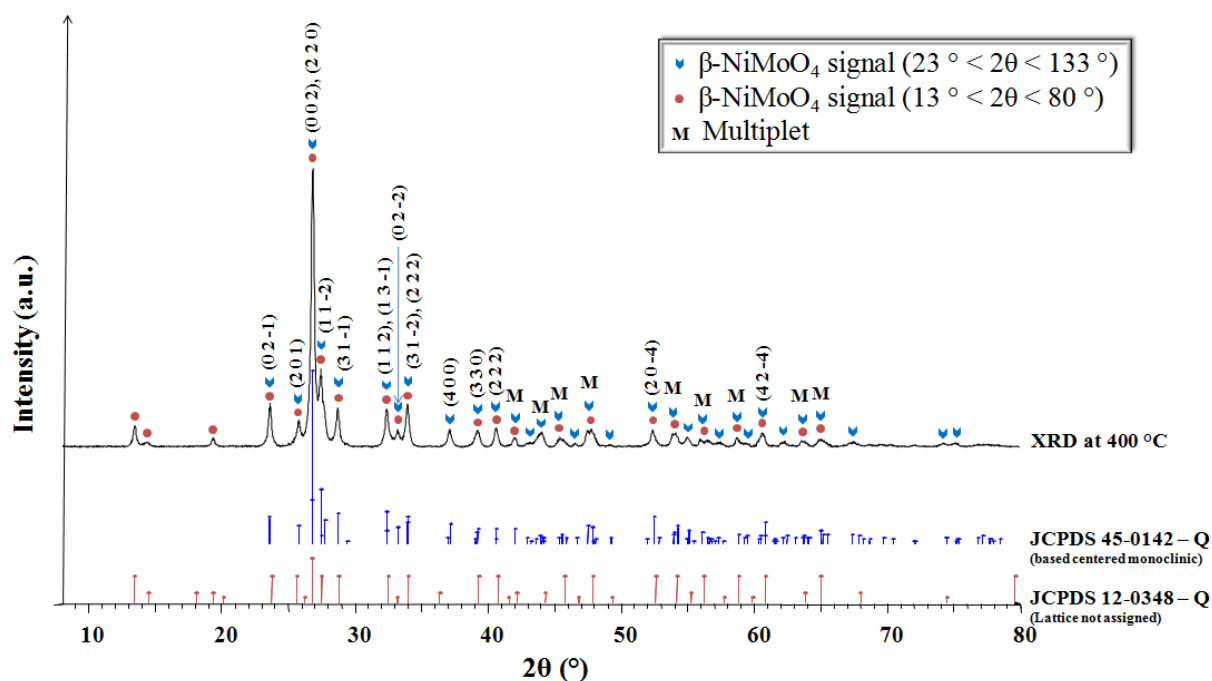


Figure II.14: XRD pattern of the stoichiometric NiMo based powder synthesized in supercritical H₂O/EtOH mixture annealed at 400 °C

A profile matching permits to accurately determine the peaks profile parameters when we have an idea of the lattice cell, space group. We performed a profile matching on this XRD pattern using the Fullprof software ([Figure II.15](#)) to confirm the good agreement between our material structural characteristics and β -NiMoO₄ (refining parameters: $\chi^2 = 2.38$, $cR_{wp} = 14.3$). The cell parameters obtained are in good agreement with the values given by the JCPDS 45-0142 ([Table II.3](#)). Even if the pattern were acquired at high temperature (400 °C) and we don't have information at high θ , we thought it could be interesting to also carry out a Rietveld refinement on this XRD pattern using the isotypy of β -NiMoO₄ with α -MnMoO₄. We obtained fairly good refinement parameters (Bragg R-factor = 4.96, $\chi^2 = 3.05$, $cR_{wp} = 12.8$), and the atomic positions obtained are given in [Table II.4](#).

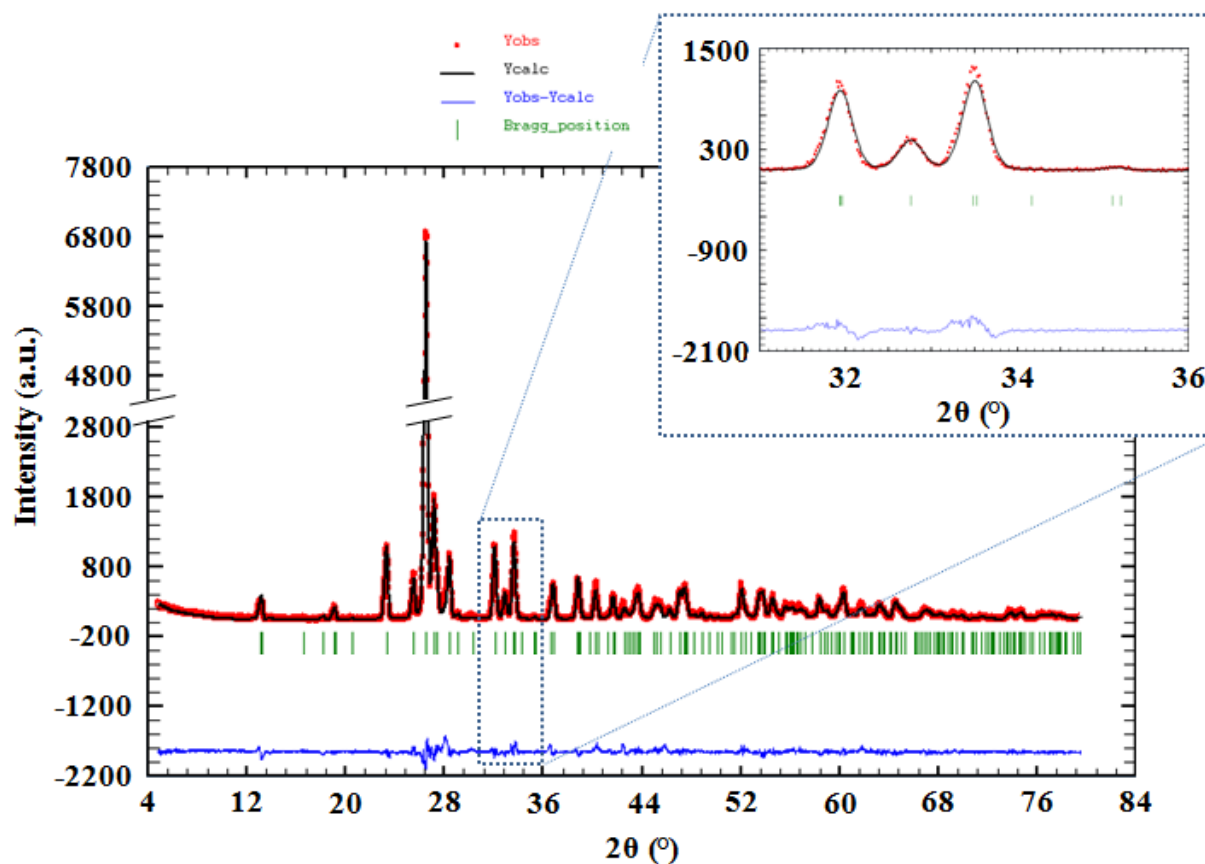


Figure II.15: Rietveld refinement of the XRD pattern of the stoichiometric NiMo based powder synthesized in supercritical H₂O/EtOH mixture annealed at 400 °C

(Bragg R-factor = 4.96, $\chi^2 = 3.05$, cR_{wp} = 12.8)

Table II.3: Cell parameters obtained for the stoichiometric NiMo based powder synthesized in supercritical H₂O/EtOH mixture annealed at 400 °C, on the heating ramp

Space group	a (Å)	b (Å)	c (Å)	β (°)
C 2/m	10.187(5)	9.246(5)	7.020(2)	107.09(3)
JCPDS 45-0142	10.184	9.241	7.0189	107.09

II. Synthesis of HDS catalyst precursors in supercritical fluids

Table II.4: Atomic parameters obtained for the stoichiometric NiMo based powder synthesized in supercritical H₂O/EtOH mixture annealed at 400 °C, on the heating ramp (*comparison with ICSD #78328 for atomic positions)

Atom	Position	x	y	Z
Ni1 Mn1*	4h 4h	0 0	0.182(2) 0.194(2)	0 0
Ni2 Mn2*	4i 4i	0.802(2) 0.795(2)	0 0	0.145(4) 0.135(3)
Mo1 Mo1*	4g 4g	0 0	0.254(1) 0.249	0 0
Mo2 Mo2*	4i 4i	0.272(1) 0.269(1)	0 0	0.398(2) 0.400(2)
O1 O1*	4i 4i	0.360(6) 0.355(1)	0.5 0.5	0.452(9) 0.463(2)
O2 O2*	4i 4i	0.210(9) 0.201(1)	0 0	0.15(4) 0.154(3)
O3 O3*	8j 8j	0.149(5) 0.129(1)	0.363(6) 0.360(1)	0.104(9) 0.101(2)
O4 O4*	8j 8j	0.458(5) 0.461(1)	0.336(5) 0.355(1)	0.20(2) 0.193(1)
O5 O5*	8j 8j	0.361(4) 0.367(1)	0.148(4) 0.149(1)	0.496(9) 0.472(1)

The fairly good agreement between the atomic positions obtained by Rietveld refinement and those given for α -MnMoO₄ suggest the structure of our β -NiMoO₄ is closely similar to the one described in [Figure II.5](#).

Acquisitions were also carried out while cooling down the sample from 900 °C to room temperature (ramp = 1 to 2 °C.min⁻¹ and with a 30 min stabilization plateau before each acquisition, and shorter ΔT between the acquisitions around 180 °C – temperature where the $\beta \rightarrow \alpha$ transition is said to occur). A sharp and unique transition occurs between 210 °C and 200 °C, leading to a radically different phase as illustrated on [Figure II.16](#). We can easily assume that this phase is the α -isomorph of NiMoO₄, the low temperature phase. Indeed, the diffractogram fits well with the α -NiMoO₄ phase as shown on [Figure II.17](#) (diffractogram realized at room temperature after calcination at 400 °C). We reported the (h k l) index for the best defined peaks.

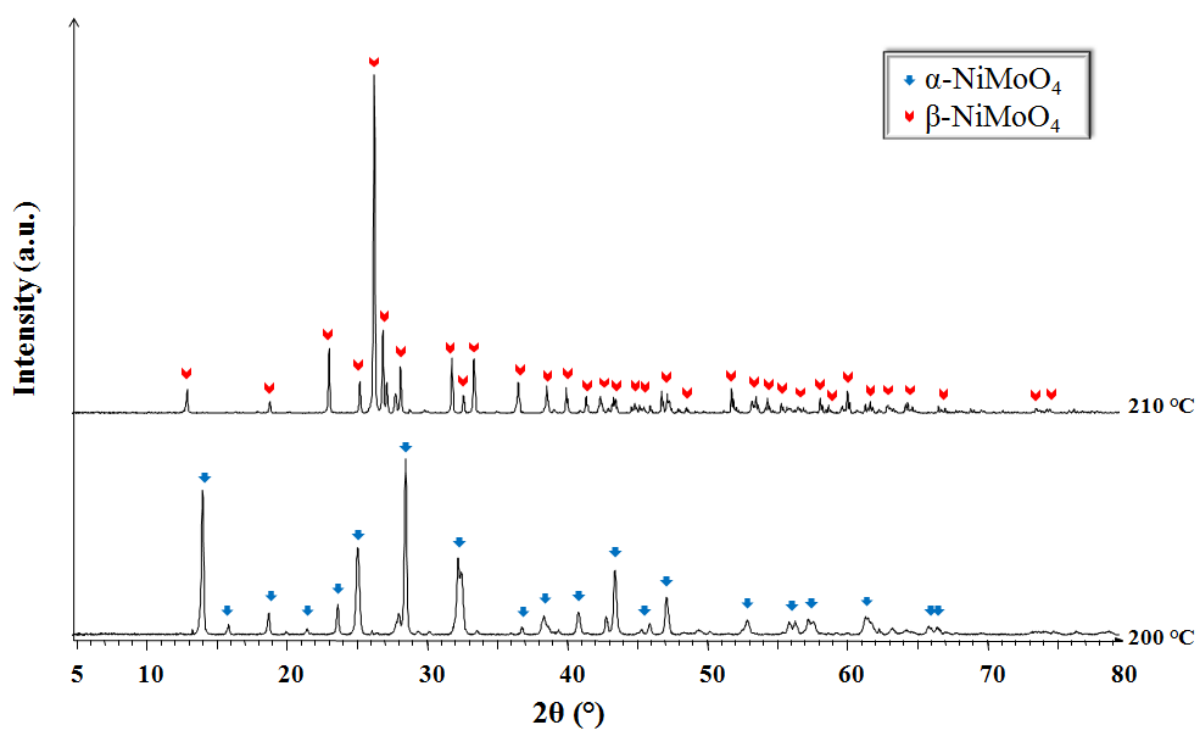


Figure II.16: Evolution of the structure of the stoichiometric NiMo based powder synthesized in supercritical H₂O/EtOH mixture when cooling down after study in temperature

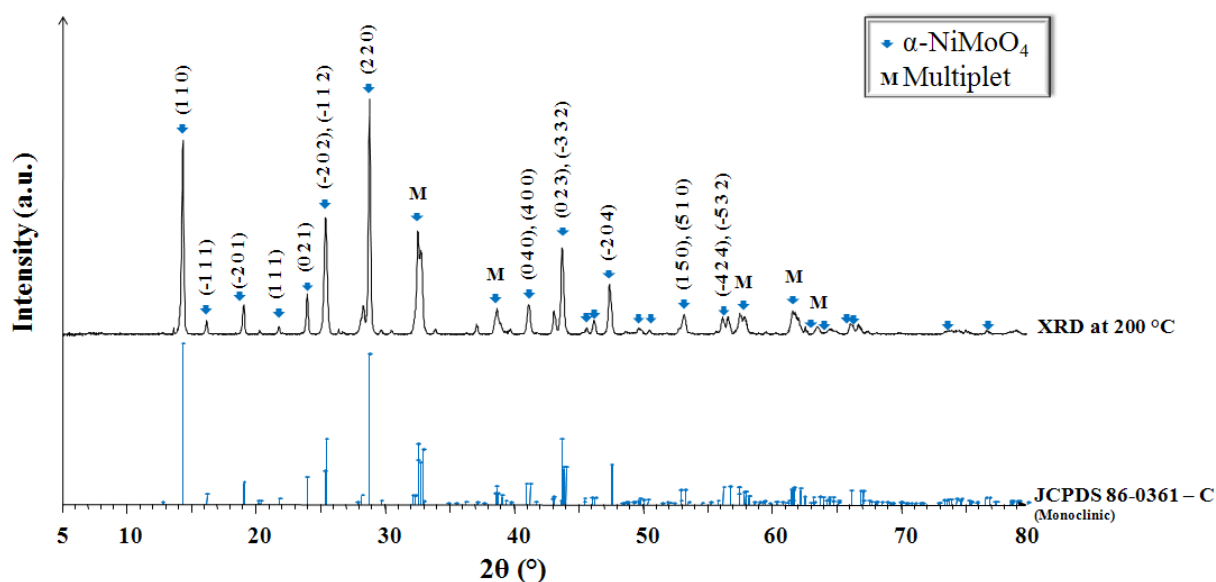


Figure II.17: XRD pattern at 200 °C of the stoichiometric NiMo based powder synthesized in supercritical H₂O/EtOH mixture, when cooling down after study in temperature

Here again we realized a profile matching on the diffractogram at 200 °C (Figure II.18). In this case, we had to consider the presence of a secondary phase we found out to be molybdenum oxide hydrate $\text{MoO}_3 \cdot 2\text{H}_2\text{O}$ (JCPDS 39-0363, monoclinic, P 21/n). We assume that we could not detect any secondary phase at 400 °C because its peaks were hidden by the peaks of the $\beta\text{-NiMoO}_4$ phase which is not the case here.

We could verify the good agreement of our pattern with the values given by the JCPDS 86-0361 (refining parameters: $\chi^2 = 1.05$, $\text{cR}_{\text{wp}} = 7.91$) and approximate the cell parameters of our majority phase Table II.5. We also carried out a Rietveld refinement on this diffractogram ($\chi^2 = 4.11$, $\text{cR}_{\text{wp}} = 14.2$, Bragg R-factor = 7.35), and the atomic positions obtained (Table II.6) are in good agreement with those given in the literature (ICSD card #81059, [32]).

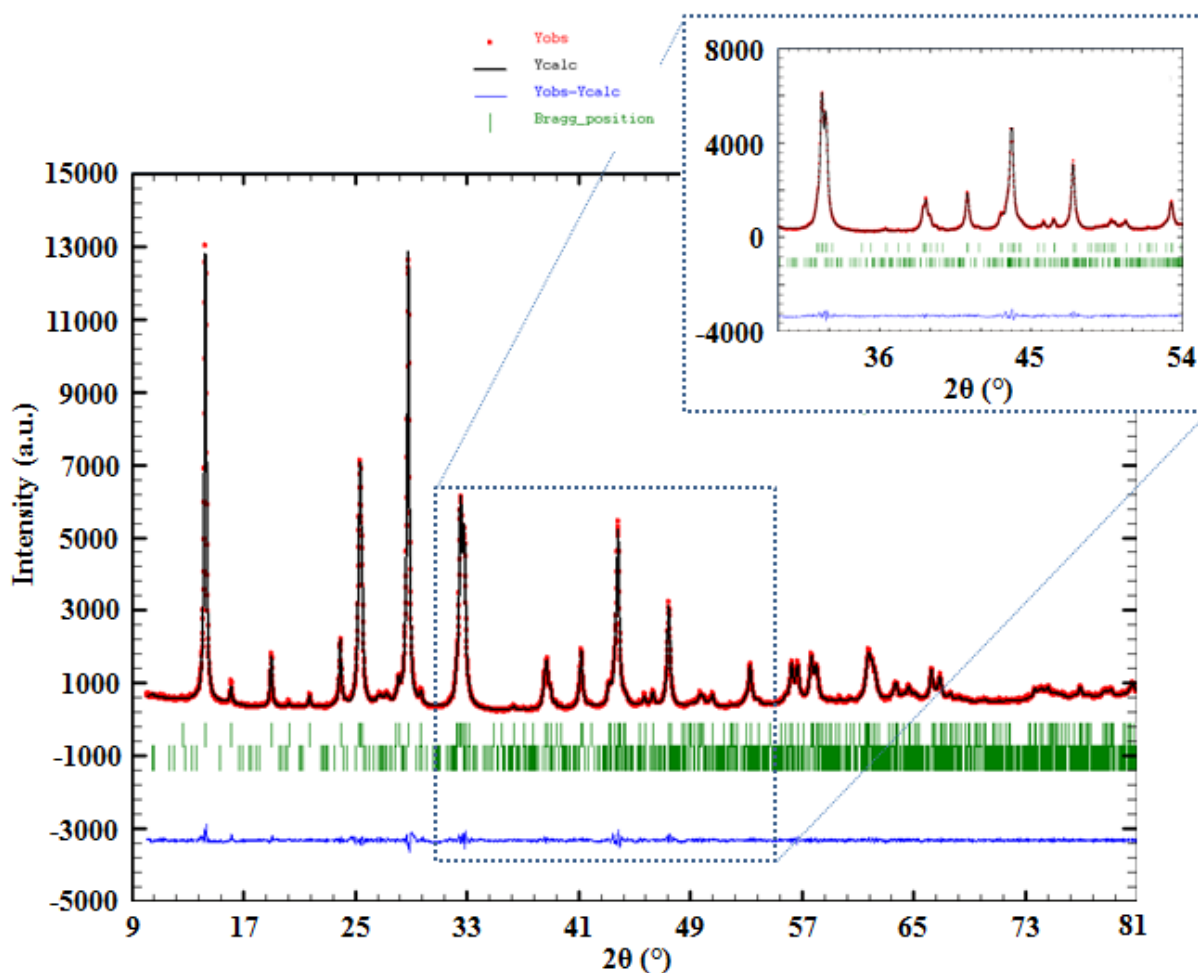


Figure II.18: Profile matching (zoom on 9 - 81 °) on the XRD pattern at 200 °C of the stoichiometric NiMo based powder synthesized in supercritical $\text{H}_2\text{O}/\text{EtOH}$ mixture, when cooling down after study in temperature

$$(\chi^2 = 1.05, \text{cR}_{\text{wp}} = 7.91)$$

II. Synthesis of HDS catalyst precursors in supercritical fluids

Table II.5: Cell parameters obtained at 200 °C for the stoichiometric NiMo based powder synthesized in supercritical H₂O/EtOH, when cooling down after study in temperature

Space group	a (Å)	b (Å)	c (Å)	β (°)
C 2/m	9.589(6)	8.760(6)	7.654(5)	114.16(4)
JCPDS 86-0361	9.566	8.734	7.649	114.22

Table II.6: Atomic parameters obtained at 200 °C for the stoichiometric NiMo based powder synthesized in supercritical H₂O/EtOH, when cooling down after study in temperature (*comparison with ICSD #81059 for atomic positions)

Atom	Position	x	y	z
Ni1	4i	0.312(8)	0	0.152(9)
Ni1*	4i	0.315(1)	0	0.157(1)
Ni2	4h	0	0.315(7)	0.5
Ni2*	4h	0	0.314(1)	0.5
Mo1	4i	0.279(5)	0	0.637(6)
Mo1*	4i	0.282(1)	0	0.638(1)
Mo2	4g	0	0.285(4)	0
Mo2*	4g	0	0.283(1)	0
O1	8j	0.494(19)	0.146(25)	0.260(27)
O1*	8j	0.502(3)	0.152(4)	0.239(3)
O2	8j	0.150(18)	0.156(17)	0.083(24)
O2*	8j	0.155(3)	0.163(3)	0.077(4)
O3	8j	0.161(16)	0.156(15)	0.571(27)
O3*	8j	0.162(3)	0.155(3)	0.579(4)
O4	4i	0.339(20)	0	0.427(23)
O4*	4i	0.348(4)	0	0.436(5)
O5	4i	0.337(30)	0	0.913(37)
O5*	4i	0.349(5)	0	0.913(6)

From this study we show that heating our fresh powder leads to the complete formation of the β -NiMoO₄ phase at 400 °C. Correlated with the literature [13], this confirms the presence of the hydrated phase in the fresh powder. When cooling down to 200 °C, we obtain the α -NiMoO₄, which means we have two options regarding the catalytic application:

- the sulfidation is carried out at 400 °C, if performed on our fresh powder, it is the β -phase that undergoes the sulfidation (the most active phase toward HDS);
- if the powder is calcined previous to sulfidation as conventionally done, we sulfide the α -phase.

Pre-calcination is the convention in HDS catalysis but since our nanopowders are very reactive, a phenomenon of sintering occurs during this step, reducing this specific surface area as illustrated in Figure II.19 which displays the S_{BET} measured for different calcination temperatures (3 hours treatment).

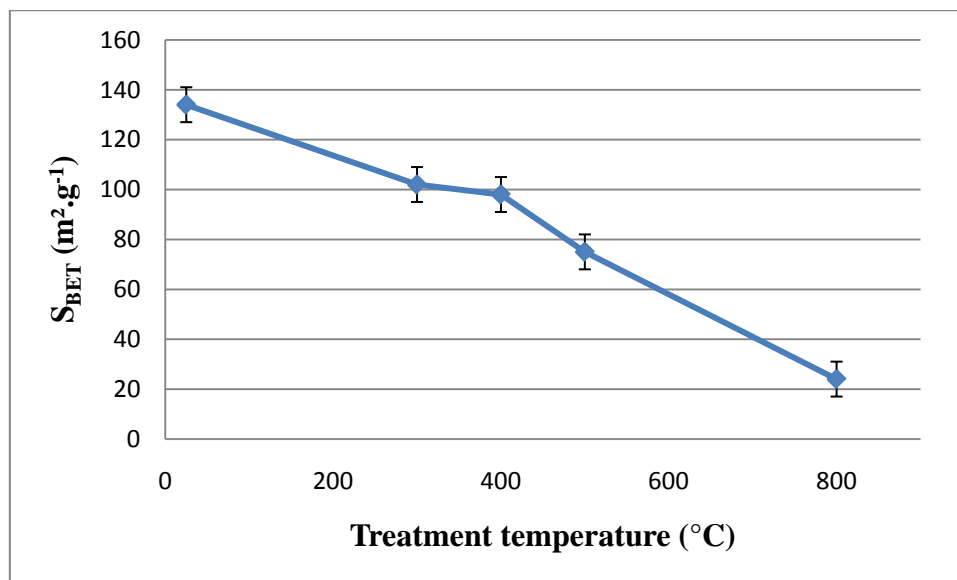


Figure II.19: Evolution of the S_{BET} with calcination temperature (S_{BET} values obtained for the stoichiometric NiMo based powder synthesized in supercritical $\text{H}_2\text{O}/\text{EtOH}$ mixture, calcined at various temperatures for 3 h)

Therefore, we had to optimize this calcination. Figure II.13 shows that we have a complete transformation of our powder at 400°C (what also correspond to the sulfidation temperature). For this reason, we decided to choose 400°C as the temperature of calcination of our material. Other tests realized on our powders for different calcination times at 400°C made us choose 3 hours for the treatment since it is the minimum time necessary to obtain materials of similar diffractograms than $\alpha\text{-NiMoO}_4$ at room temperature (Figure II.20). We also note that the S_{BET} is not particularly affected by the duration of the calcination. With this treatment, the mean resulting S_{BET} is of $98 \pm 11 \text{ m}^2 \cdot \text{g}^{-1}$ which is lower than the S_{BET} of fresh powders but still fits perfectly with our objective of a S_{BET} of $100 \text{ m}^2 \cdot \text{g}^{-1}$.

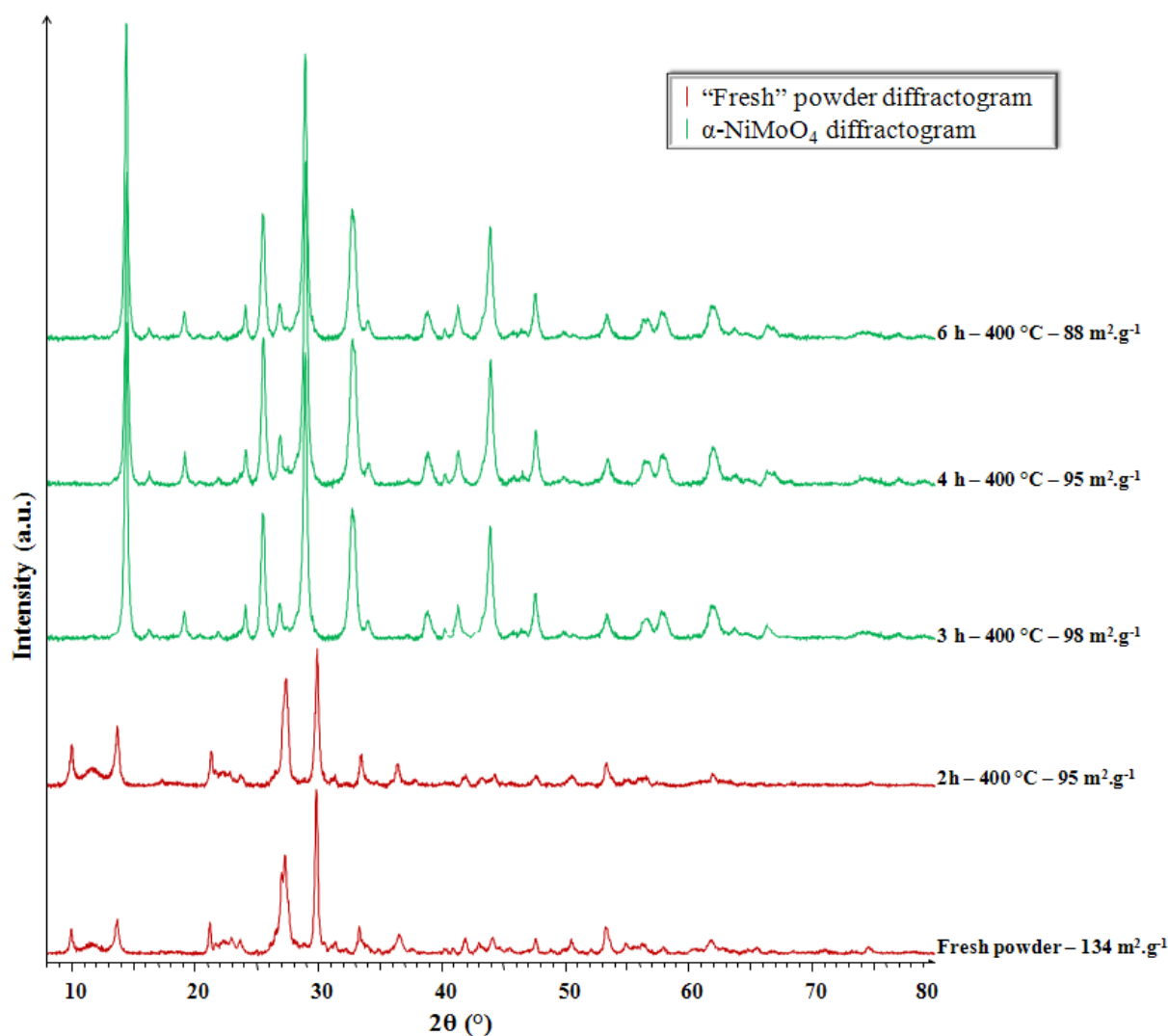


Figure II.20: Importance of calcination duration (XRD patterns acquired on the stoichiometric NiMo based powder synthesized in supercritical H₂O/EtOH mixture for various calcinations durations)

The optimum calcination treatment of our powders is 400 °C for 3 hours. With this treatment we obtain powders of α -NiMoO₄ with a mean S_{BET} of $98 \pm 11 \text{ m}^2.\text{g}^{-1}$ what fits with our objective of $100 \text{ m}^2.\text{g}^{-1}$.

After calcination, the rods are still present but look broken. Moreover, aggregates of particles and slabs appear (Figure II.21). The fact that the rods break should mean an increase of S_{BET} . However, we believe this breaking does not compensate the sintering of the particles and we also believe that the channels of the rods shrink after calcination and are less accessible to nitrogen when measuring the S_{BET} . STEM-EDX chemical mapping confirms that we have particles exclusively composed of molybdenum like in the fresh powder whereas other particles are homogeneously composed of nickel and molybdenum (Figure II.22).

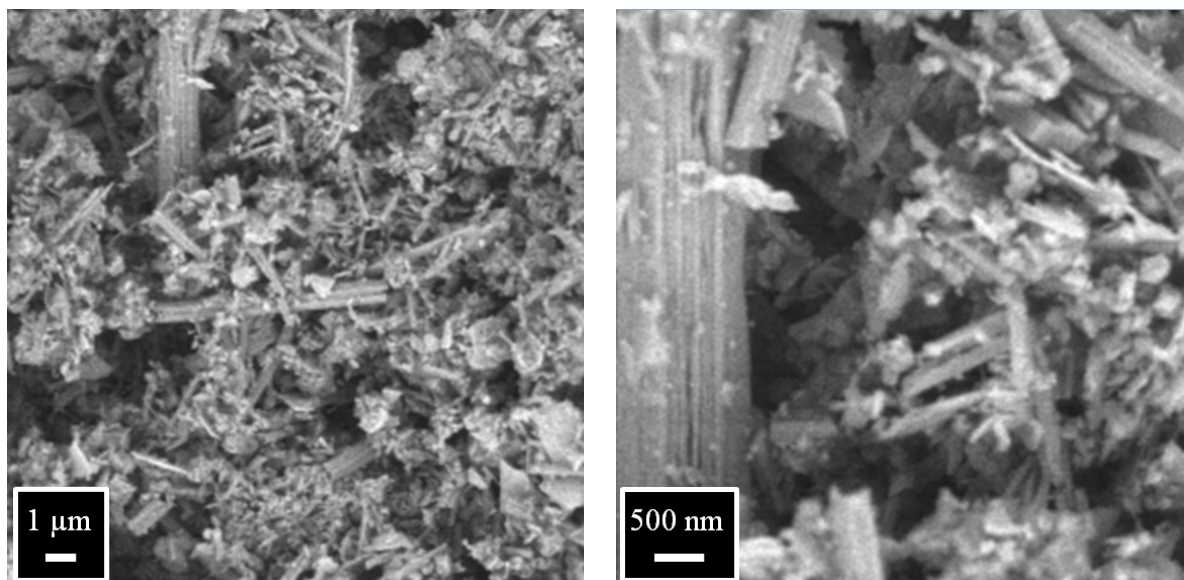


Figure II.21: SEM micrographs of the stoichiometric NiMo based powder synthesized in supercritical $\text{H}_2\text{O}/\text{EtOH}$ mixture, calcined 3 h at 400 $^{\circ}\text{C}$

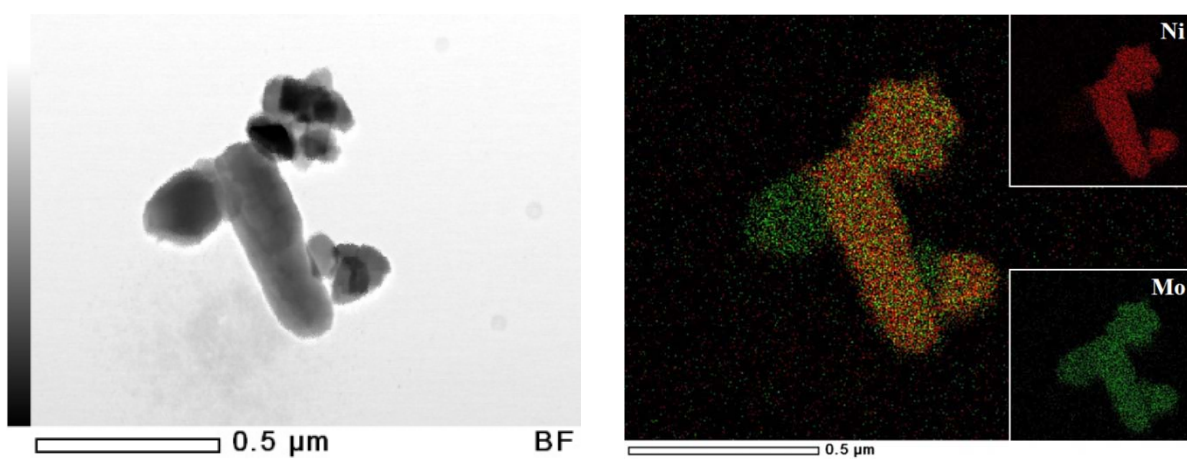
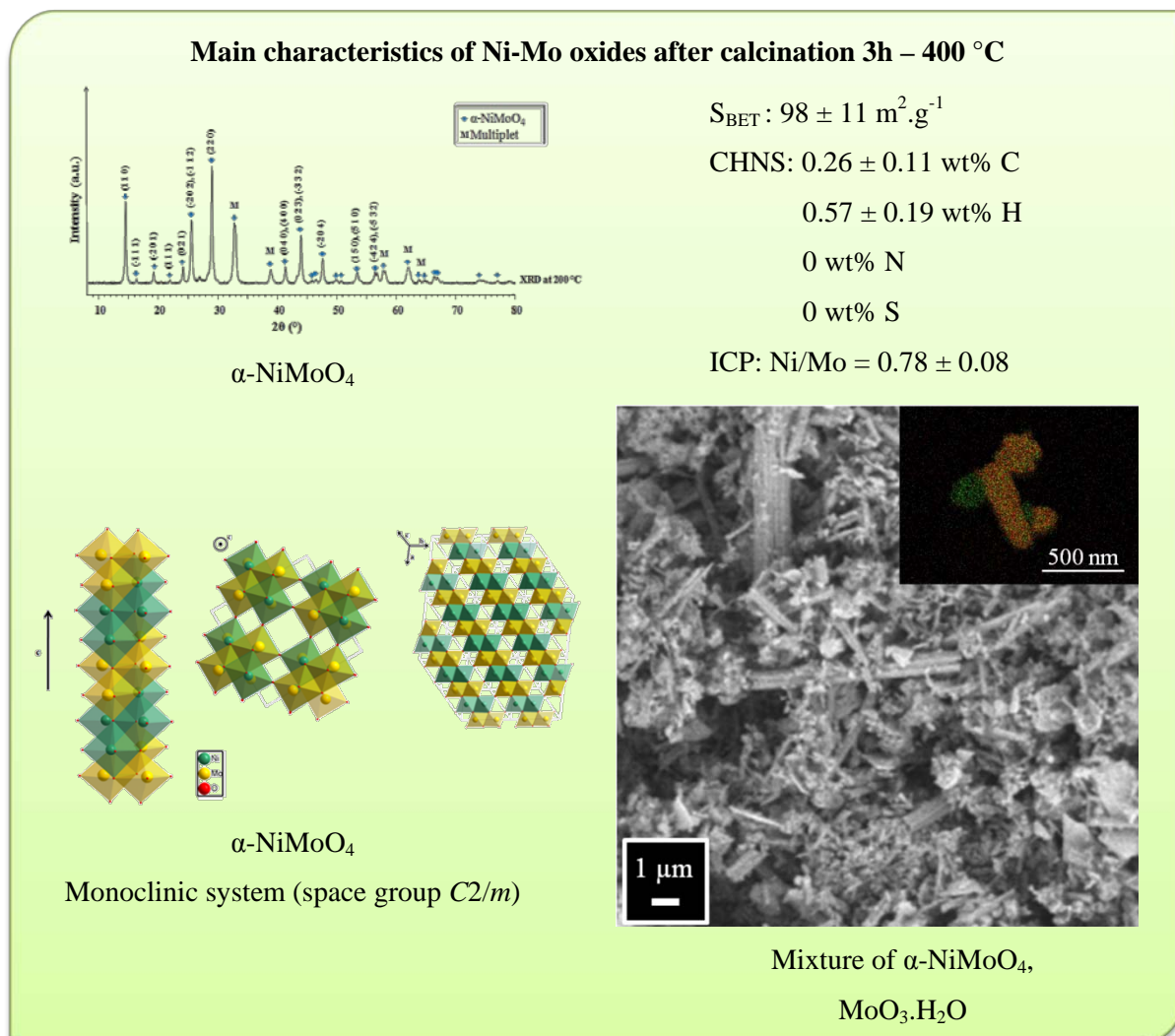


Figure II.22: STEM-EDX chemical mapping of the stoichiometric NiMo based powder synthesized in supercritical $\text{H}_2\text{O}/\text{EtOH}$ mixture, calcined 3 h at 400 $^{\circ}\text{C}$

II. Synthesis of HDS catalyst precursors in supercritical fluids

Below is the I.D card of the stoichiometric NiMo based powder synthesized in supercritical H₂O/EtOH mixture after 3h calcinations at 400 °C:



II.2.2.2. Conclusion

This study showed that supercritical fluids technology is worth being considered for the synthesis of HDS catalyst precursors. From the decomposition of nickel(II) acetate and molybdenum(VI) oxide bis(acetylacetonate) at 290 °C and 23 MPa for a t_s of about 55 s, we synthesized contaminant-free powders composed of mainly NiMoO₄·0.75H₂O. Those powders present higher specific surface areas than encountered in the literature: whereas bulk catalysts classically develop S_{BET} around $30\text{-}50 \text{ m}^2 \cdot \text{g}^{-1}$ maximum $80 \text{ m}^2 \cdot \text{g}^{-1}$, we obtained powders of S_{BET} of $134 \pm 14 \text{ m}^2 \cdot \text{g}^{-1}$, more than our objective of $100 \text{ m}^2 \cdot \text{g}^{-1}$.

We can choose calcining the powder previous to sulfidation with a treatment at 400 °C for 3 hours, and in this case we obtain α -NiMoO₄ as HDS catalyst precursor with a mean S_{BET} of $98 \pm 11 \text{ m}^2 \cdot \text{g}^{-1}$, still in agreement with our set objectives. We can also choose to use the powder as obtained and in this case the formation of β -NiMoO₄ occurs during the heating step of the sulfidation reactor and it is this phase that is the HDS catalyst precursor. We have no S_{BET} value for it but we assume it is at least the same than of the powder after calcination.

We thus have the possibility to work with two different phases of NiMoO₄ as HDS catalysts precursors for our catalytic tests. We effectively compared their relative activity during those tests; however, we worked in majority with pre-calcined powders by conformism with established protocols in the catalytic field.

At this point of the study, our target of obtaining Ni-Mo based oxides powders, free from inhibiting elements and of high specific surface area is fully achieved.

We now explore some variations of parameters in order to optimize our material characteristics. The results obtained are presented in the next section.

II.2.3. Influence of some operating parameters

Considering NiMoO₄ synthesized in the H₂O/EtOH system as our reference, we played with some of the parameters that are easy to change in order to explore the possibilities supercritical fluids offer in the particular synthesis of HDS catalyst precursors. Our guiding thread keeps being the improvement of the catalyst, be it by an increase of its S_{BET} or the obtaining of a more active phase toward HDS and deep-HDS. Therefore, we studied the effect a change of alcohol, of stoichiometry or of cation (Co substituted to Ni) have on the synthesized powders and there characteristics. [Table II.7](#) summarizes the different parameters we worked with in this exploration work.

Table II.7: Studied parameters

Sample	Solvent	Molar ratio	Temperature Pressure	Promoter	At% (ICP) of promoter $\pm 2\%$
MT016	H ₂ O/MeOH	1:1	290 °C 23 MPa	Ni	50
MT011	H ₂ O/EtOH	1:1	290 °C 23 MPa	Ni	50
MT032	H ₂ O/iPrOH	1:1	290 °C 23 MPa	-	0
MT072			290 °C 23 MPa	Ni	36
MT045					50
MT052					57
MT071					60
MT022					66
MT081			290 °C 23 MPa	Co	50

II.2.3.1. Influence of the alcohol nature in H₂O/ROH systems

We wanted to study the influence of different alcohols. Since the previous experiments with ethanol gave us an optimum H₂O/EtOH molar ratio of 1:1, we decided to keep this proportion in the following tests. We carried out experiments with methanol and isopropanol in the same conditions of pressure and temperature than with the system H₂O/EtOH (temperature of 290 °C and a pressure of 23 MPa).

It is difficult to find data in the literature concerning critical coordinates of H₂O/ROH systems for alcohols other than ethanol. Therefore, we realized an experiment with the use of a high pressure and high temperature microfluidic device developed within the MIT-ICMCB collaboration [33] in order to determine whether we actually are in supercritical conditions or not when the reactor is at 290 °C and 23 MPa when using H₂O/MeOH or H₂O/iPrOH systems of molar ratio 1:1. The equipment is schematized in Figure II.23. The fluid is injected through an ISCO pump 260D (1) in a microreactor (2) made of microchannels patterned in a wafer of silicon and further bonded to a Pyrex wafer for a total volume of 4.6 μ L. The system is contacted with an aluminum block equipped with heating cartridges (3) through a graphite layer (4). This leads to a homogeneous temperature in the microreactor. A compression device (5) plays both the roles of maintaining the system leak-free and cooling down the

outing fluid. The pressure is controlled with a back pressure regulator JASCO BP-2080 (6). Optical access through the Pyrex side allows visualizing the behavior of the fluid with a high speed CCD camera (Phantom video camera) (7).

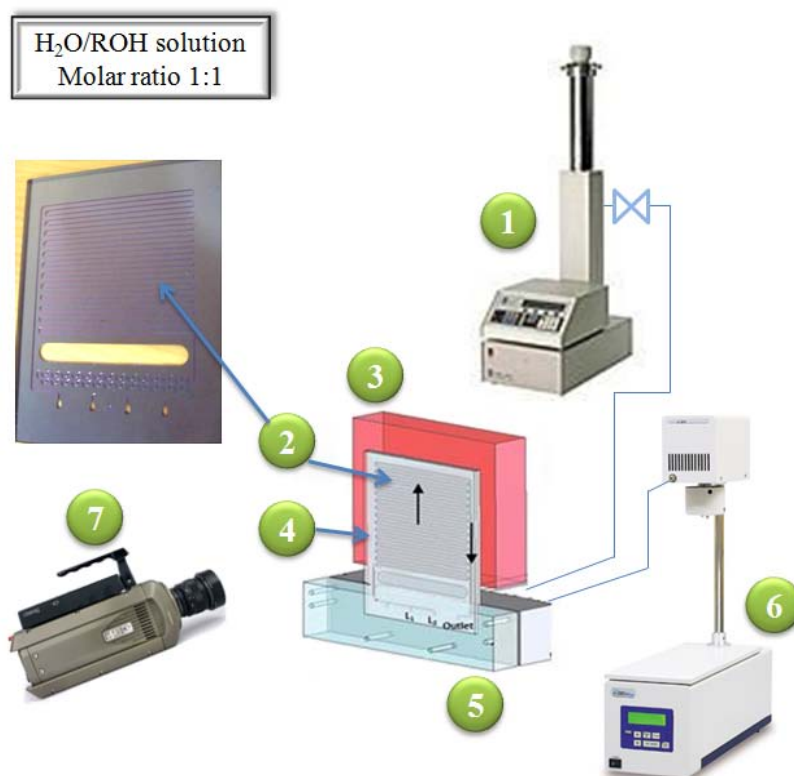


Figure II.23: Equipment used to determine the critical coordinates of $\text{H}_2\text{O}/\text{MeOH}$ and $\text{H}_2\text{O}/i\text{PrOH}$ systems of molar ratio 1:1

As illustrated on Figure II.24, we estimate the critical coordinates of the system by having it evolved from liquid to gas by increasing the temperature at fixed pressure (1). We can this way observe bubbles in the microchannels. We then go back to liquid state by increasing the pressure at fixed temperature (2) and droplets appears (we illustrate these transitions with pictures but films are more convenient to observe and determine them). Repeating these two actions around the liquid-gas equilibrium and refining the increasing steps can give pretty reliable values of the critical coordinates of our system. This method can be applied to a large variety of fluids and promises to be a particularly useful tool in the description of the systems studied in the group. Table II.8 summarizes the estimations we found and remind the critical coordinates of the pure compounds.

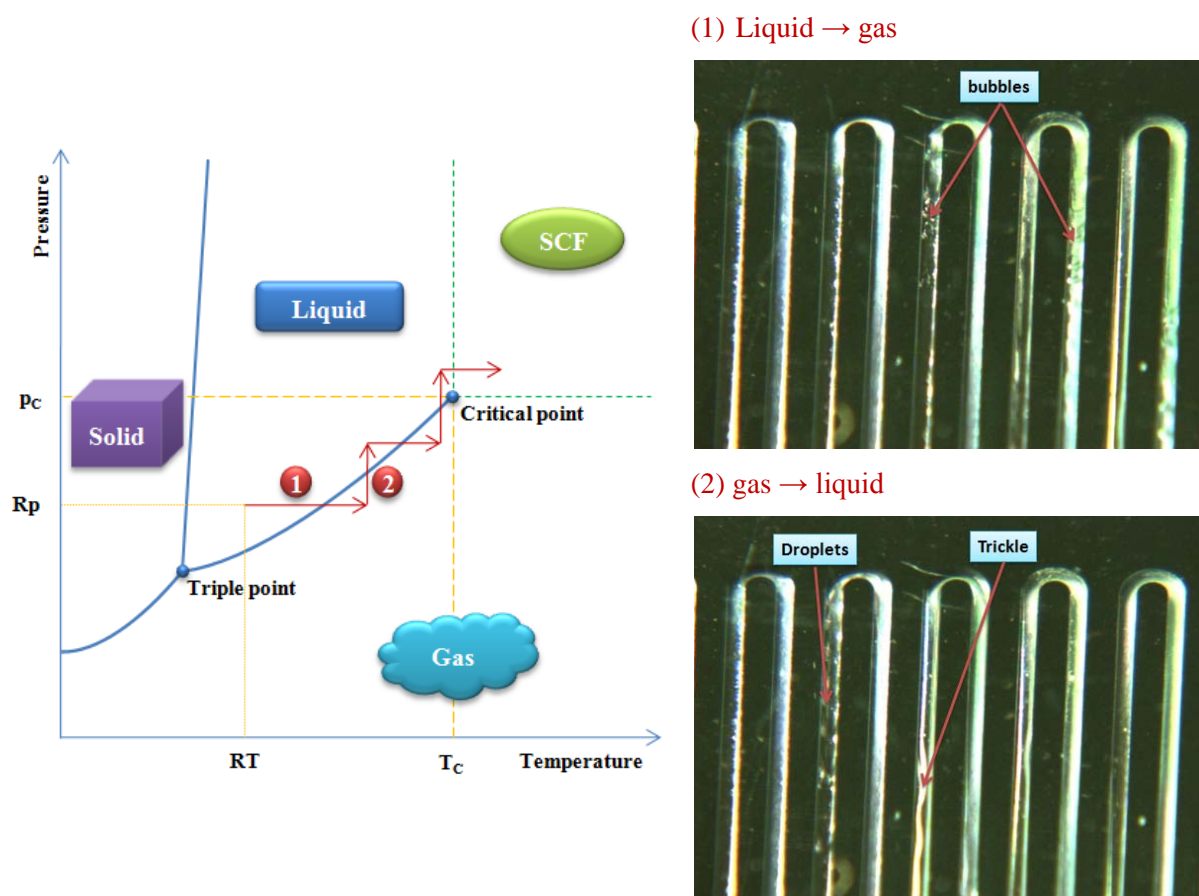


Figure II.24: Method followed to determine the critical coordinates of $\text{H}_2\text{O}/\text{MeOH}$ and $\text{H}_2\text{O}/\text{iPrOH}$ systems of molar ratio 1:1 (RT: room temperature, Rp: room pressure, T_c : critical temperature, p_c : critical pressure)

Table II.8: Estimated critical coordinates of $\text{H}_2\text{O}/\text{MeOH}$ and $\text{H}_2\text{O}/\text{iPrOH}$ systems of molar ratio 1:1 and reminder for pure compounds

System		T_c ($^{\circ}\text{C}$)	p_c (MPa)
H_2O	Water	374	22.1
MeOH	Methanol	239.5	8.1
EtOH	Ethanol	241	6.3
iPrOH	Isopropanol	264.2	5.3
$\text{H}_2\text{O}/\text{MeOH}$, 1:1	Water/Methanol	$280 \leq T_c \leq 283$	~ 11
$\text{H}_2\text{O}/\text{EtOH}$, 1:1	Water/Ethanol	~ 274	$9 \leq p_c \leq 14$
$\text{H}_2\text{O}/\text{iPrOH}$, 1:1	Water/Isopropanol	$270 \leq T_c \leq 273$	~ 8.2

According to those values, we can claim being in supercritical conditions when working at 290°C and 23 MPa. Our attention has particularly been attracted by the results we obtained on the S_{BET} of the as prepared powders. As shown on Figure II.25, isopropanol gave us particularly good results with a mean S_{BET} of $179 \text{ m}^2.\text{g}^{-1}$ for fresh powders and a mean one of $120 \text{ m}^2.\text{g}^{-1}$ after a 3 hours thermal treatment at 400°C .

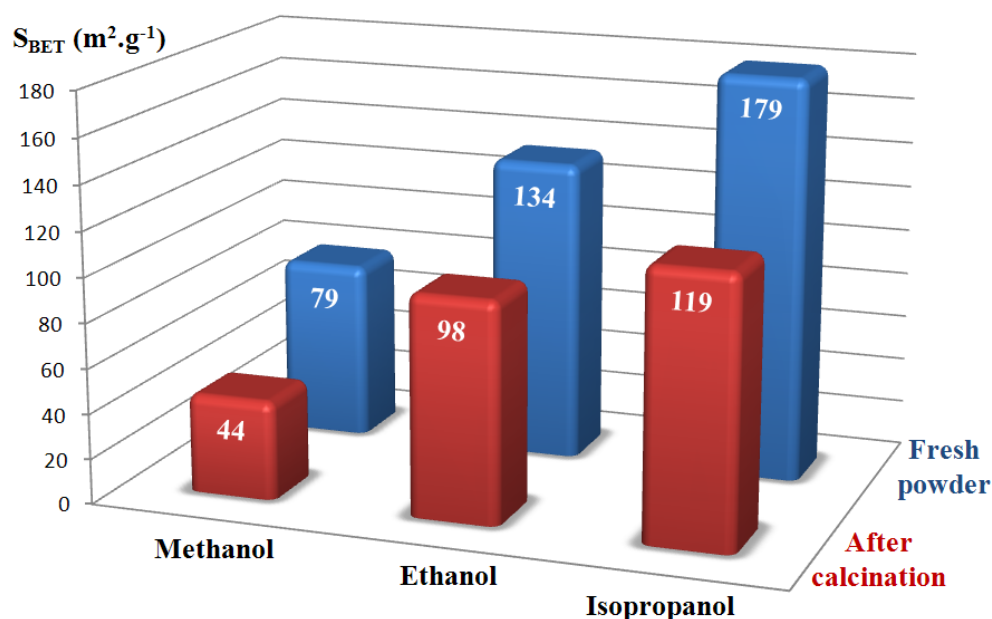
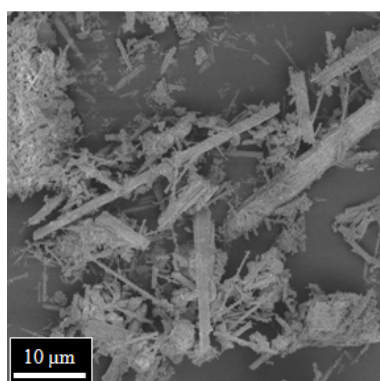


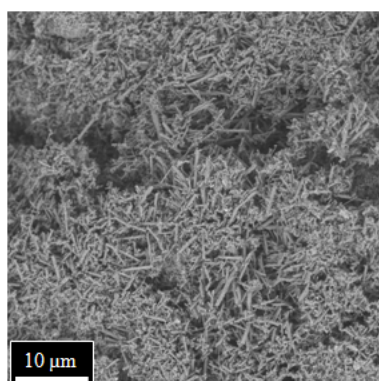
Figure II.25: Evolution of the S_{BET} with the nature of the alcohol

When we compare the critical coordinates of these three systems, the mixture $H_2O/iPrOH$ presents the lowest T_c and p_c . We then assume that under identical temperature and pressure conditions, we have a higher supersaturation in the system $H_2O/iPrOH$ than in the two others what leads to smaller particles and therefore higher S_{BET} of the powders thus synthesized. The size of the objects observed by SEM seems to corroborate this hypothesis (Figure II.26): the rods obtained with methanol can reach 40 μm long when they are of 15 μm with ethanol and 6 μm with isopropanol.

Water/Methanol



Water/Ethanol



Water/Isopropanol

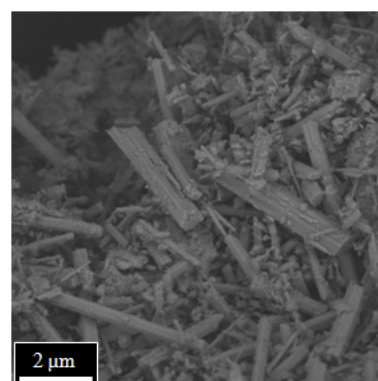


Figure II.26: SEM micrographs of the stoichiometric NiMo based powders directly after synthesis in supercritical H_2O/ROH mixtures (ROH = methanol, ethanol, isopropanol)

We then focus our attention on the water/Isopropanol system for further synthesis of our catalyst precursors.

We study the decomposition of the selected precursors of molybdenum and nickel in a $\text{H}_2\text{O}/\text{iPrOH}$ solution of molar ratio 1:1 at $T = 290\text{ }^\circ\text{C}$ and $p = 23\text{ MPa}$ for a t_s of about 55 s. For this mixture, $\rho_c = 318\text{ kg.m}^{-3}$ and $\eta_c = 6.7.10^{-5}\text{ Pa.s}$ what gives us a $Re \approx 690$: we are in a laminar flow regime.

CHNS-O analysis gave us a mean of $0.37 \pm 0.11\text{ wt\%}$ carbons, $1.12 \pm 0.19\text{ wt\%}$ hydrogen and 0 wt\% for Nitrogen and Sulfur. The change of alcohol does not affect the cleanness of our powders. The powder presented here contains a slight excess of Mo ($\text{Ni}/\text{Mo} = 0.98$).

The TGA-MS showed in [Figure II.27](#) is similar to the one in [Figure II.9](#). It displays three loss of mass for a total mass loss of 9 % (against 8% previously). A first loss of 3.73 %, between room temperature and $262\text{ }^\circ\text{C}$, is attributed to adsorbed water as the line shape of mass 18 suggests in the M.S. results associated. It is 1 % more than for the previous system presented and on a wider range of temperature ($+ 19\text{ }^\circ\text{C}$). The higher surface of the powder may explain this increase of mass loss as more water can adsorb on this powder. A second loss of 4.99 % occurs from $262\text{ }^\circ\text{C}$ to $540\text{ }^\circ\text{C}$ attributed to the departure of carbon and structural water according to line shape of mass 18 and mass 44. This corresponds to the second and third loss detected in [Figure II.9](#) between $243\text{ }^\circ\text{C}$ and $538\text{ }^\circ\text{C}$ with a mass loss of 4.7 %. The third loss of 0.33 % between $540\text{ }^\circ\text{C}$ and $800\text{ }^\circ\text{C}$ is attributed to carbon only and correspond to the last loss of 0.51 % between $538\text{ }^\circ\text{C}$ and $800\text{ }^\circ\text{C}$ of NiMoO_4 synthesized in $\text{H}_2\text{O}/\text{EtOH}$.

The mass spectroscopy results display similarities with the previous one, the third peak of water being less marked but present, suggesting that here again and according to results obtained by Eda et al. [\[16\]](#) the powder synthesized contains $\text{NiMoO}_4.0.75\text{H}_2\text{O}$.

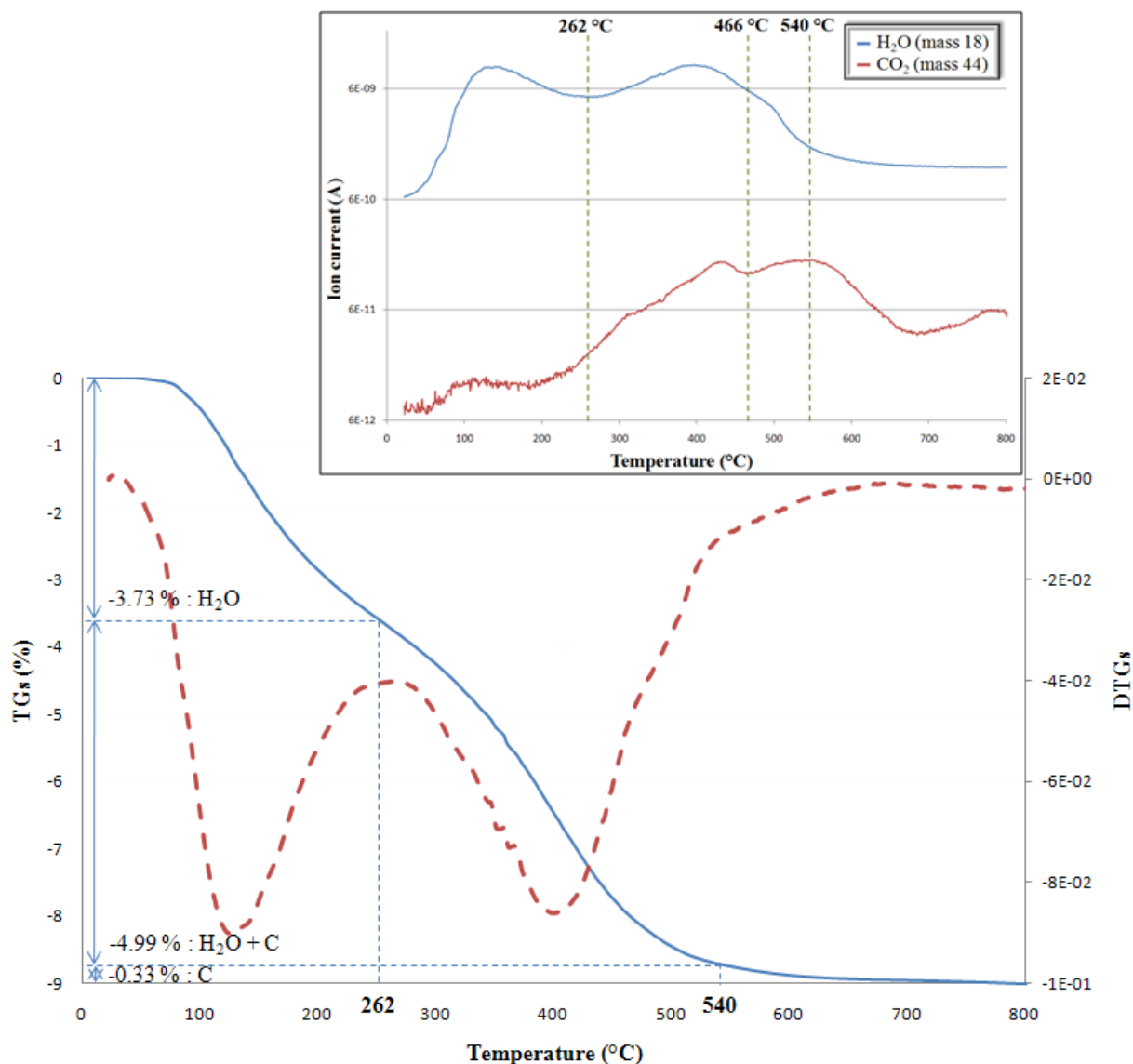


Figure II.27: TGA-MS of the stoichiometric NiMo based powder synthesized in supercritical H₂O/iPrOH mixture, from room temperature to 800 °C under Ar atmosphere, ramp = 1 °C.min⁻¹

The XRD pattern of a fresh powder is not as well-defined as one obtained from a powder synthesized in H₂O/EtOH (Figure II.28) probably due to smaller crystallites. However, it presents close similarities and correlation with the TGA-MS results and SEM micrograph (Figure II.29) - showing rods and small particles aggregates as previously described with H₂O/EtOH system - has us think that we obtain the same phases, namely NiMoO₄.0.75H₂O, MoO₃.H₂O, MoO₂ and possibly β-NiMoO₄.

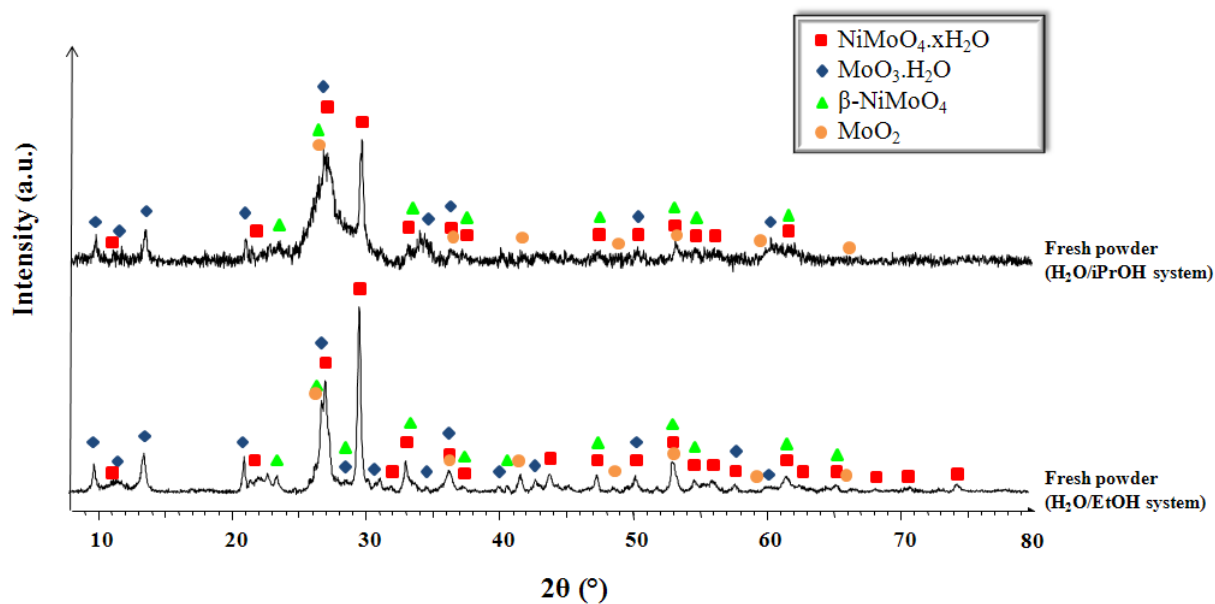


Figure II.28: Comparison of the stoichiometric NiMo based powder directly after synthesis in supercritical $\text{H}_2\text{O}/\text{EtOH}$ mixture and in supercritical $\text{H}_2\text{O}/i\text{PrOH}$ mixture

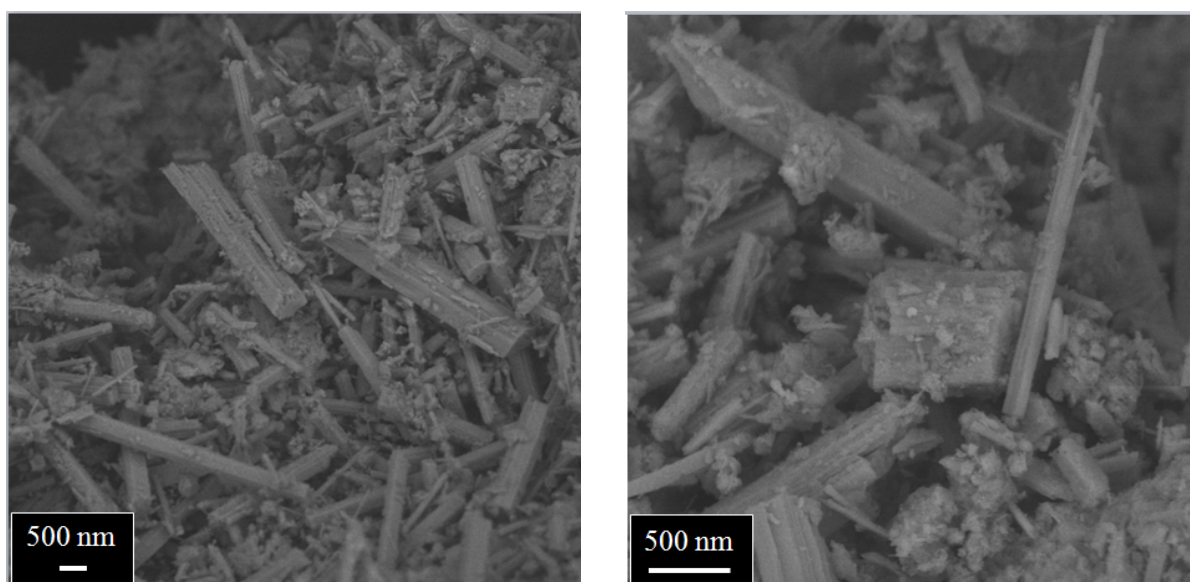
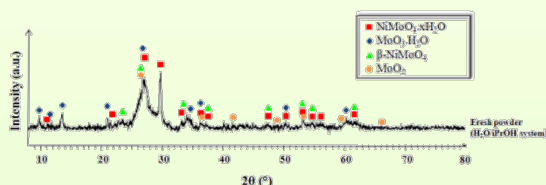


Figure II.29: SEM micrographs of the stoichiometric NiMo based powder directly after synthesis in supercritical $\text{H}_2\text{O}/i\text{PrOH}$ mixture

II. Synthesis of HDS catalyst precursors in supercritical fluids

We can estimate that we produce a similar material with isopropanol than with ethanol with similar but better characteristics summarized below:

Main characteristics of Ni-Mo oxides after synthesis in sc-H₂O/iPrOH (1:1 molar)



Mainly NiMoO₄·0.75H₂O

$$S_{\text{BET}} : 179 \pm 12 \text{ m}^2 \cdot \text{g}^{-1}$$

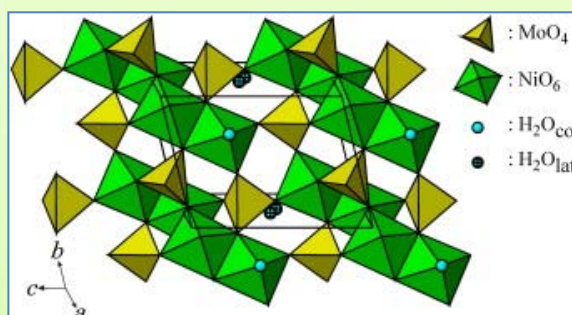
$$\text{CHNS} : 0.37 \pm 0.11 \text{ wt\% C}$$

$$1.24 \pm 0.21 \text{ wt\% H}$$

$$0 \text{ wt\% N}$$

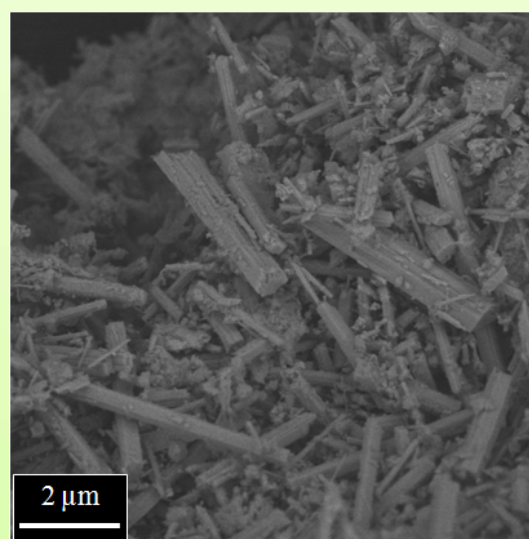
$$0 \text{ wt\% S}$$

$$\text{ICP} : \text{Ni/Mo} = 1 \pm 0.14$$



NiMoO₄·0.75H₂O

Triclinic system (space group *P* -1)



Mixture of NiMoO₄·0.75H₂O,
MoO₃·H₂O and MoO₂

We greatly improved our results using H₂O/iPrOH: we synthesized a bulk precursor for HDS catalysts developing a higher S_{BET} of $179 \text{ m}^2 \cdot \text{g}^{-1}$ against $134 \text{ m}^2 \cdot \text{g}^{-1}$ previously obtained with the system H₂O/EtOH. The phases are identical and the powder is still contaminant-free.

The XRD pattern of the calcined powder (3h, 400 °C) (Figure II.30) corresponds to the α -isomorph of NiMoO₄ (JCPDS 86-0361) plus peaks corresponding to the MoO₃·2H₂O due to the excess of molybdenum detected by ICP and previously mentioned.

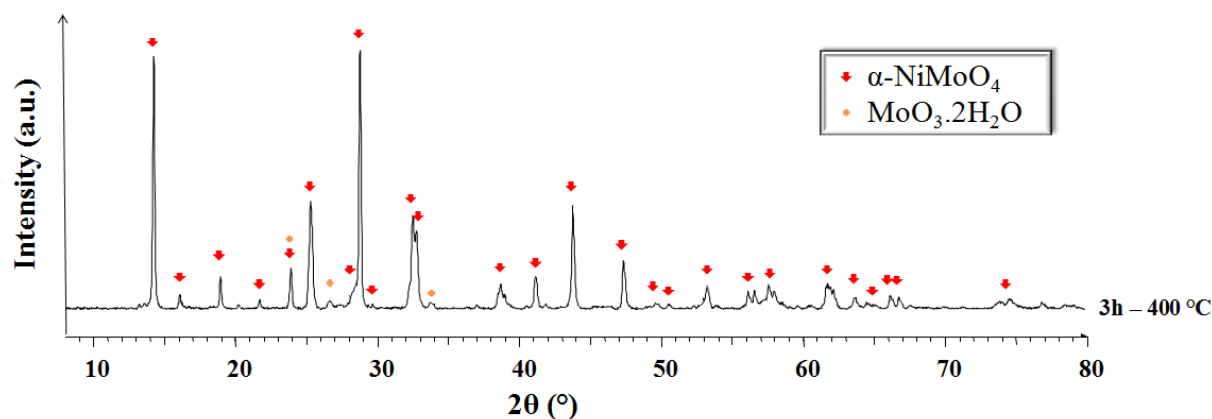


Figure II.30: XRD pattern of the stoichiometric NiMo based powder synthesized in supercritical $\text{H}_2\text{O}/\text{iPrOH}$ mixture, after a thermal treatment of 3h at $400\text{ }^\circ\text{C}$

No more rods can be seen on the SEM micrographs but aggregates of nanoparticles (Figure II.31). The important decrease of the S_{BET} after calcination (179 to $119\text{ m}^2\cdot\text{g}^{-1}$) suggests these aggregates of nanoparticles are closely packed due to sintering. STEM-EDX chemical mapping could not confirm that we have particles exclusively composed of molybdenum this time but it shows aggregates of nanoparticles that are homogeneously composed of nickel and molybdenum (Figure II.32).

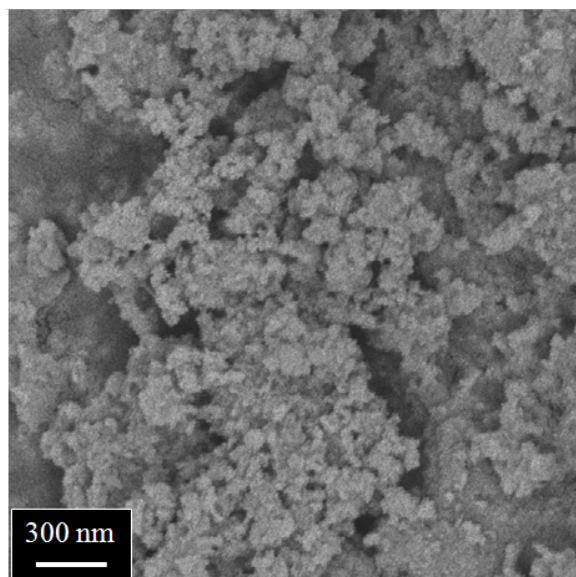


Figure II.31: SEM micrographs of the stoichiometric NiMo based powder synthesized in supercritical $\text{H}_2\text{O}/\text{iPrOH}$ mixture and calcined 3 h at $400\text{ }^\circ\text{C}$

II. Synthesis of HDS catalyst precursors in supercritical fluids

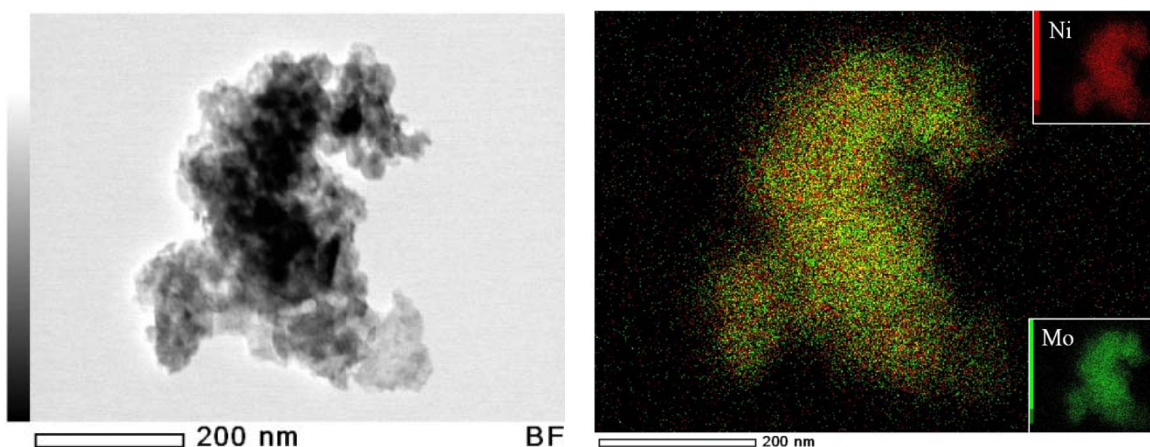
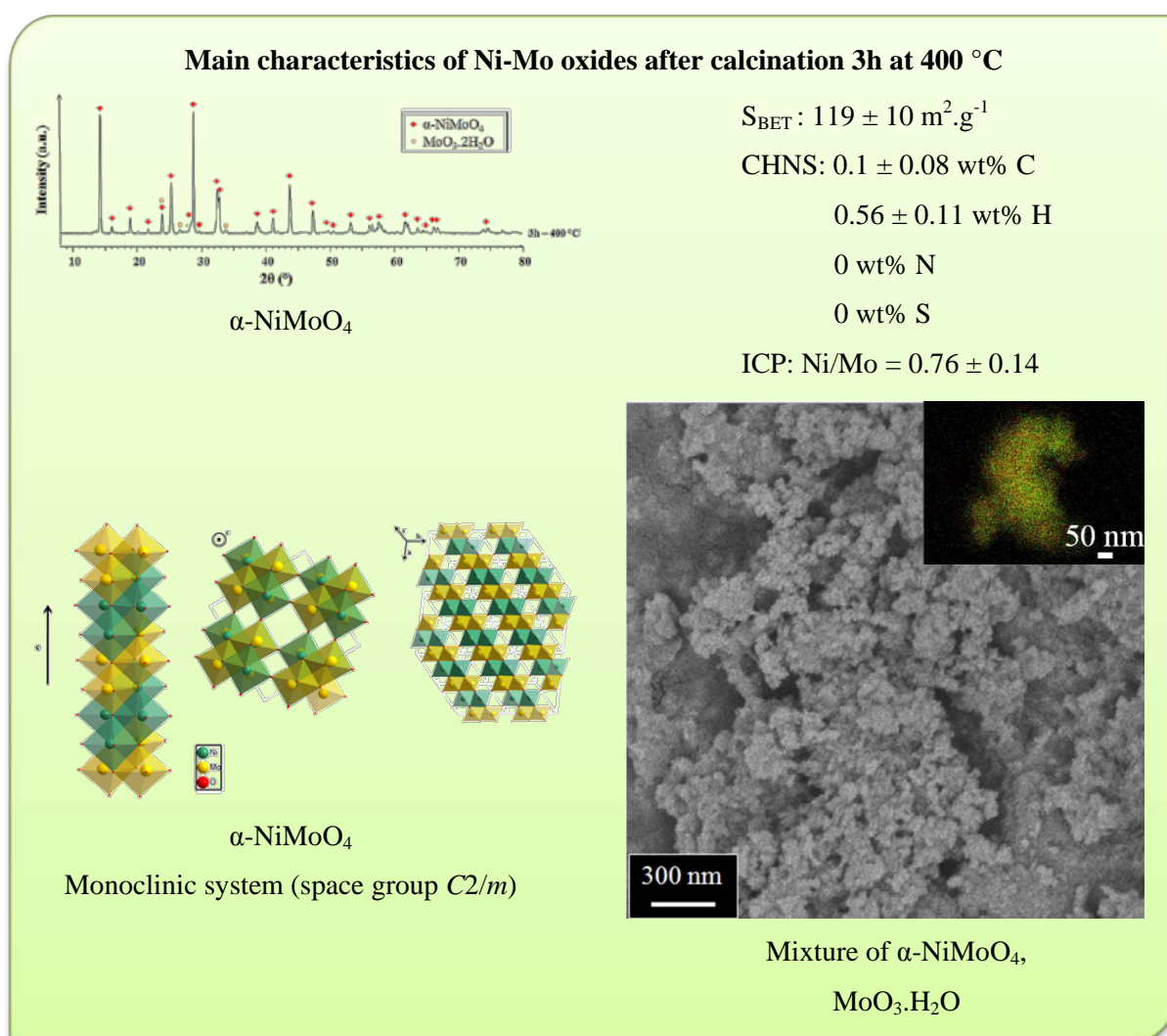


Figure II.32: STEM-EDX chemical mapping of the stoichiometric NiMo based powder synthesized in supercritical $\text{H}_2\text{O}/i\text{PrOH}$ mixture and calcined 3 h at 400°C

As for the other powders, we hereafter propose an identity card for this material synthesized in $\text{H}_2\text{O}/i\text{PrOH}$ system and calcined 3 h at 400°C :



We improved the S_{BET} of our material using isopropanol instead of ethanol as solvent of the synthesis reaction. This HDS catalyst precursor based on nickel and molybdenum oxide is clean from active sites inhibitors.

II.2.3.2. Influence of the Ni/Mo ratio

As we mentioned earlier, having excess of nickel when synthesizing NiMoO_4 may help in stabilizing the β -phase at room temperature [27,28]. From the examples of powders presented so far, the ICP gave a slight excess of Mo, and even if we might have the β -phase in the fresh powder, this is clearly not the case in the calcined powder where only the α -phase is detected. In the following part, we decided to study - in our original synthesis method - the effect of an excess of Ni. The experiments are summed up in Table II.7 (p. 127).

II.2.3.2.1. Ni/Mo = 0: synthesis of MoO_x

MoS_2 historically is the first HDS catalyst, dating from right after World War One [34], and is considered as the active phase in a Mo-based HDS catalyst. It is obtained by the sulfidation of MoO_2 or MoO_3 (MoO_3 being easier to reduce into MoS_2 than MoO_2 [14]).

Again, the cleanness of our fresh powders toward organics is demonstrated via CHNS-O analysis which gives 0.7 ± 0.12 wt% carbon, 0.1 ± 0.05 wt% nitrogen and 0.5 ± 0.10 wt% hydrogen.

The XRD pattern of our fresh powders corresponds to the Tugarinovite (JCPDS 32-0671) which is MoO_2 with a monoclinic lattice (Figure II.33). The S_{BET} measured on this powder ($56 \pm 8 \text{ m}^2 \cdot \text{g}^{-1}$) is low in comparison to the one reached for NiMoO_4 under the same conditions of synthesis.

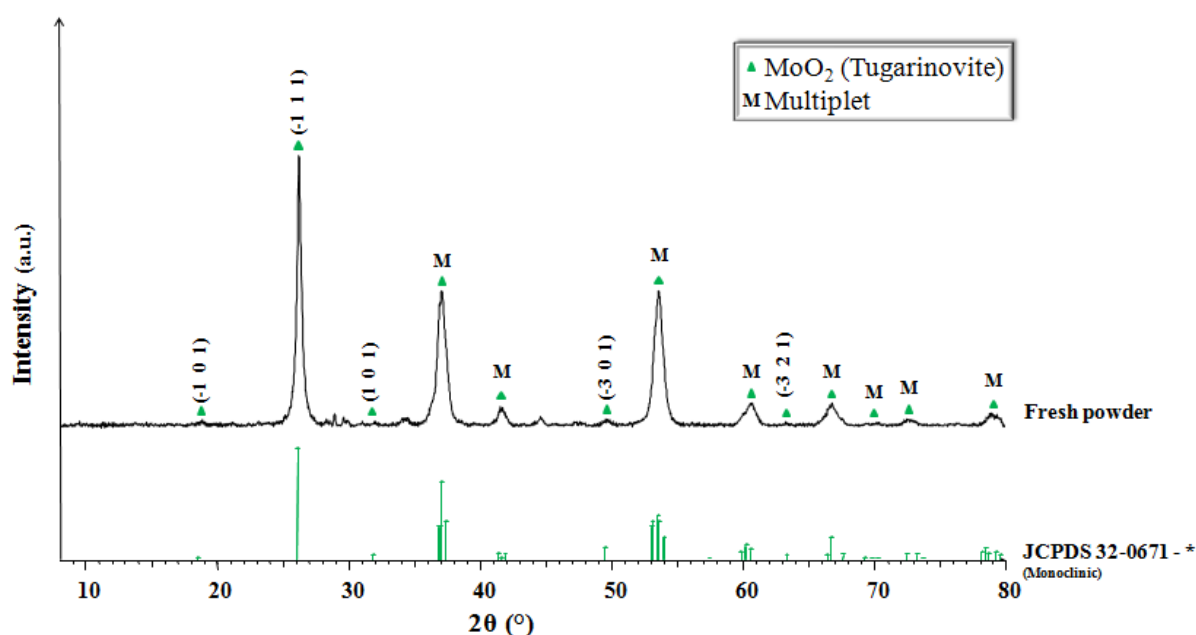


Figure II.33: XRD pattern of Mo based powder directly after synthesis in supercritical $\text{H}_2\text{O}/\text{iPrOH}$ mixture

We applied the same thermal treatment to those powders than we did for NiMoO_4 , 3 h at 400°C under air atmosphere. The XRD patterns of the obtained phase fit with the JCPDS 35-0609 corresponding to Molybdate (MoO_3) of orthorhombic lattice (Figure II.34). The S_{BET} is of course lower than for the “fresh” powder ($30 \pm 3 \text{ m}^2.\text{g}^{-1}$) because of the sintering resulting from the calcination.

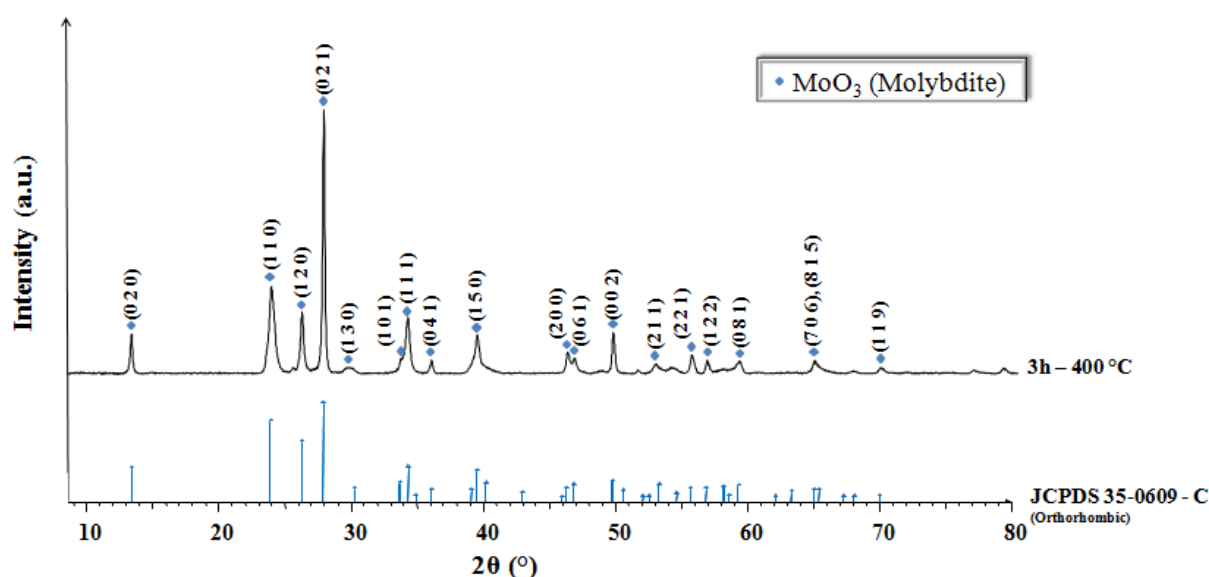
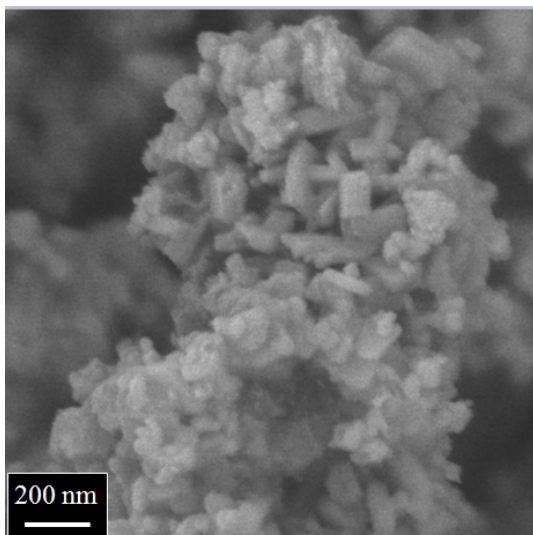


Figure II.34: XRD pattern of Mo based powder synthesized in supercritical $\text{H}_2\text{O}/\text{iPrOH}$ mixture and calcined 3 h at 400°C

II. Synthesis of HDS catalyst precursors in supercritical fluids

The SEM micrographs show aggregates of nanoslabs and nanoparticles with sizes ≤ 100 nm for MoO_2 powders whereas MoO_3 presents nanoslabs and particles that looks like nanocubes (Figure II.35). We also present two “I.D.” cards, one for MoO_2 and one for MoO_3 .

MoO_2



MoO_3

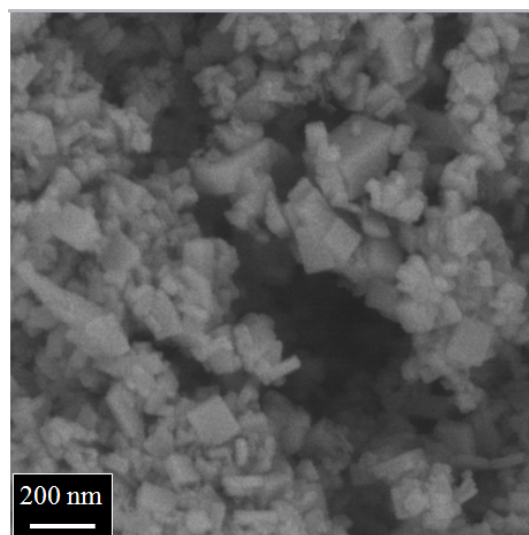
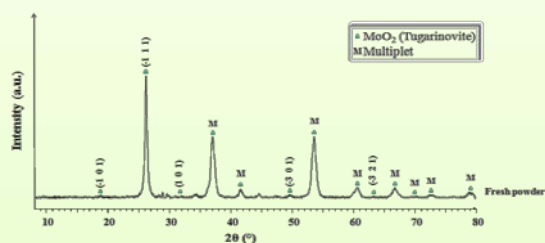


Figure II.35: SEM micrographs of MoO_2 and MoO_3 synthesized in $\text{sc-H}_2\text{O}/i\text{PrOH}$ mixture

Main characteristics of MoO_2 synthesized in $\text{sc-H}_2\text{O}/i\text{PrOH}$ (1:1 molar)



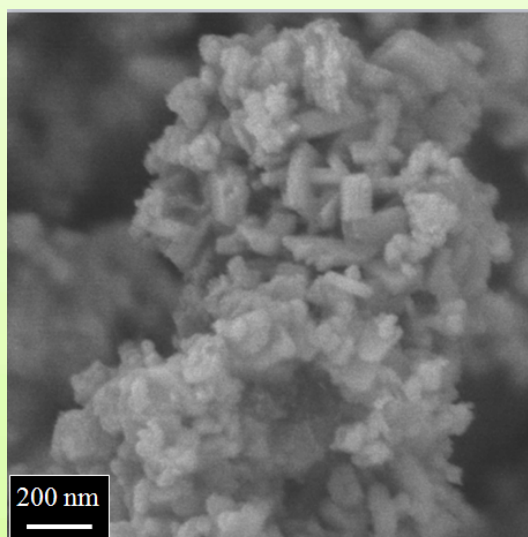
$$S_{\text{BET}} : 56 \pm 8 \text{ m}^2 \cdot \text{g}^{-1}$$

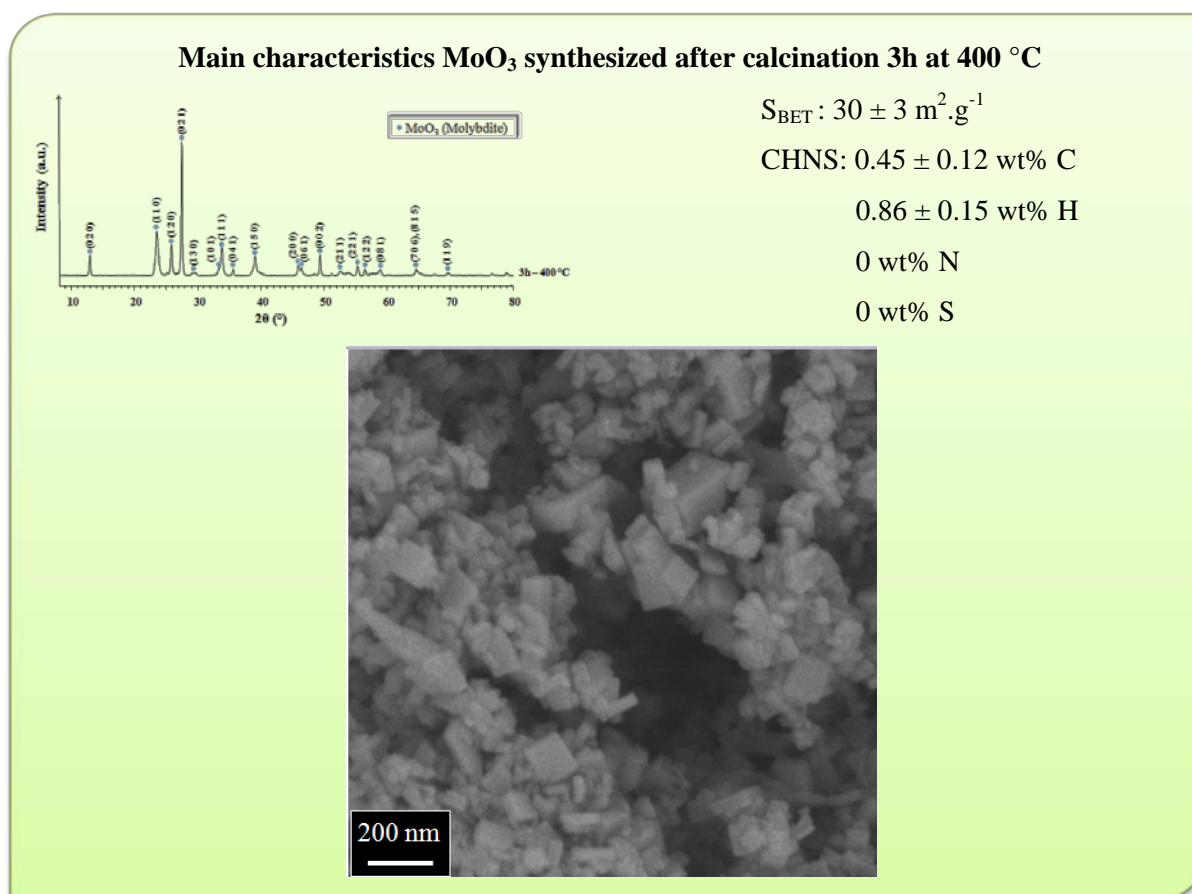
$$\text{CHNS} : 0.7 \pm 0.12 \text{ wt\% C}$$

$$0.5 \pm 0.10 \text{ wt\% H}$$

$$0.1 \pm 0.05 \text{ wt\% N}$$

$$0 \text{ wt\% S}$$





II.2.3.2.2. Ni/Mo \neq 0: influence of the cations ratio on the characteristics of the powders

We change the Ni/Mo ratios at the inlet of the supercritical reactor from in order to prepare different compositions of high specific surface area HDS catalyst precursors. The compositions of the materials are analyzed by ICP-OES ([Table II.7, p. 127](#)).

When we take a look at the fresh powders, their XRD patterns ([Figure II.36](#)) give peaks indexation of a powders mixture (MoO₃·H₂O: JCPDS 01-125, MoO₂ JCPDS 32-0671, NiMoO₄·0.75H₂O: JCPDS 13-0128, β-NiMoO₄: JCPDS 45-0142). The fresh powder with the more Mo at% presents higher peak intensity for MoO₂ phase. New molybdenum species appear with the increase of Ni concentration: MoO₃·2H₂O (JCPDS 39-0363). No peaks corresponding to nickel species are detectable on these patterns. [Pereñíguez et al. \[35 and references therein\]](#) encountered this phenomenon with LaNiO₃: although not evidenced by XRD data, results from EXAFS and TPR measurements showed the presence of an amorphous NiO in the sample. [Lavrenov et al. \[36\]](#) suggest that a minimum wt% of NiO is necessary to detect the presence of cubic nickel oxide phase. By analogy, we believe we have amorphous NiO in the fresh powder.

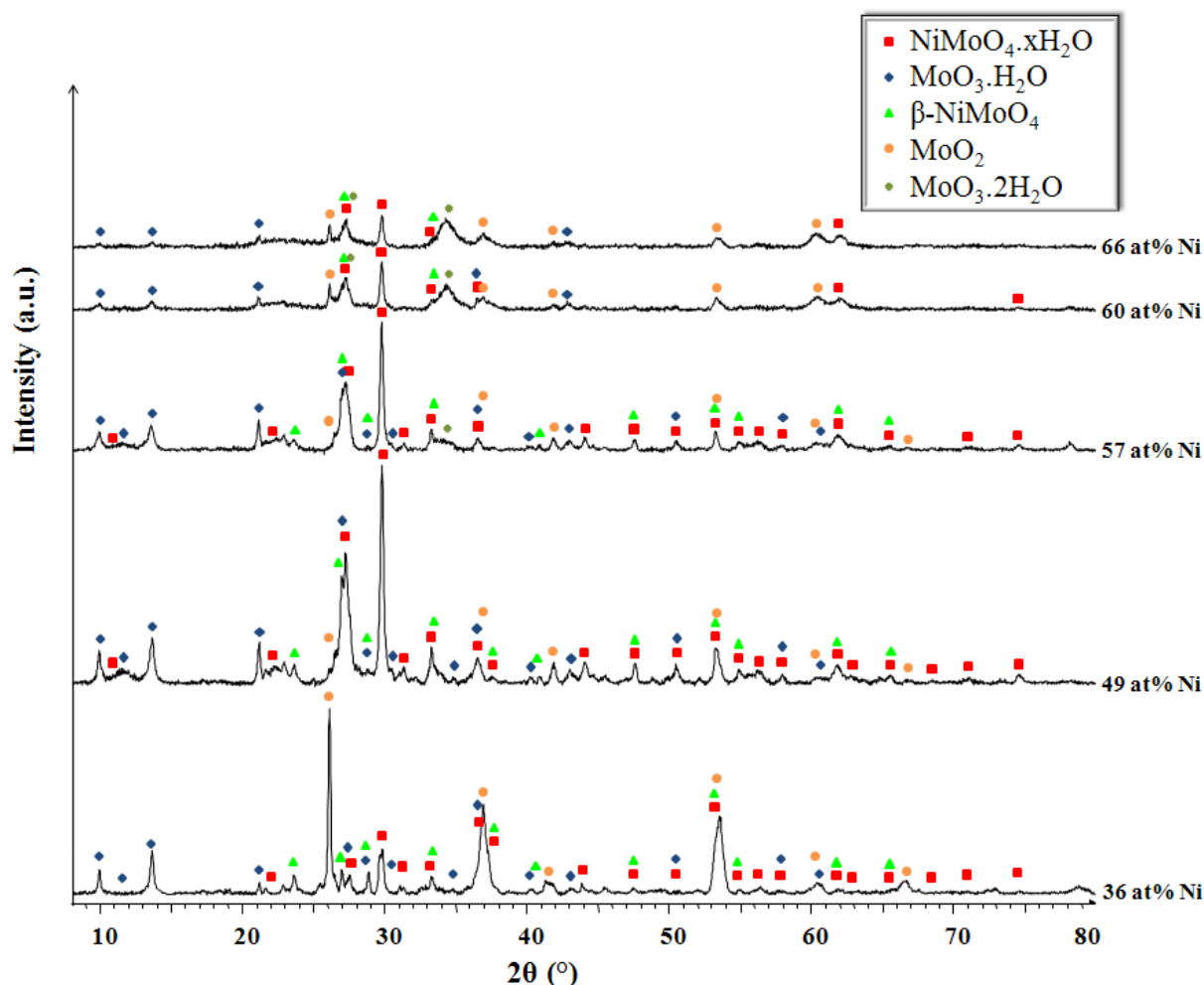


Figure II.36: Evolution of XRD patterns with at% of Nickel of NiMo based powder synthesized in supercritical $\text{H}_2\text{O}/i\text{PrOH}$ mixture

XRD patterns of calcined powders (Figure II.37) reveal two trends:

- when $\text{Ni}/\text{Mo} \leq 1$, we obtain the α - NiMoO_4 , alone when $\text{Ni}/\text{Mo} = 1$ and together with $\text{MoO}_3 \cdot \text{H}_2\text{O}$ when $\text{Ni}/\text{Mo} < 1$ (the pattern displayed correspond to 64 % molar of molybdenum to nickel, ICP results)
- the coexistence of both α - and β -phases of NiMoO_4 when the molar ratio $\text{Ni}/\text{Mo} > 1$ plus NiO crystallized by the thermal treatment, what is in favor of our assumption of having amorphous NiO in the fresh powders (the pattern displayed correspond to 66 % molar of nickel to molybdenum, ICP results)

The fact that there are no Mo simple oxides in the Ni-rich powder after calcination has us think that the calcination is a necessary step to complete the synthesis of NiMoO_4 .

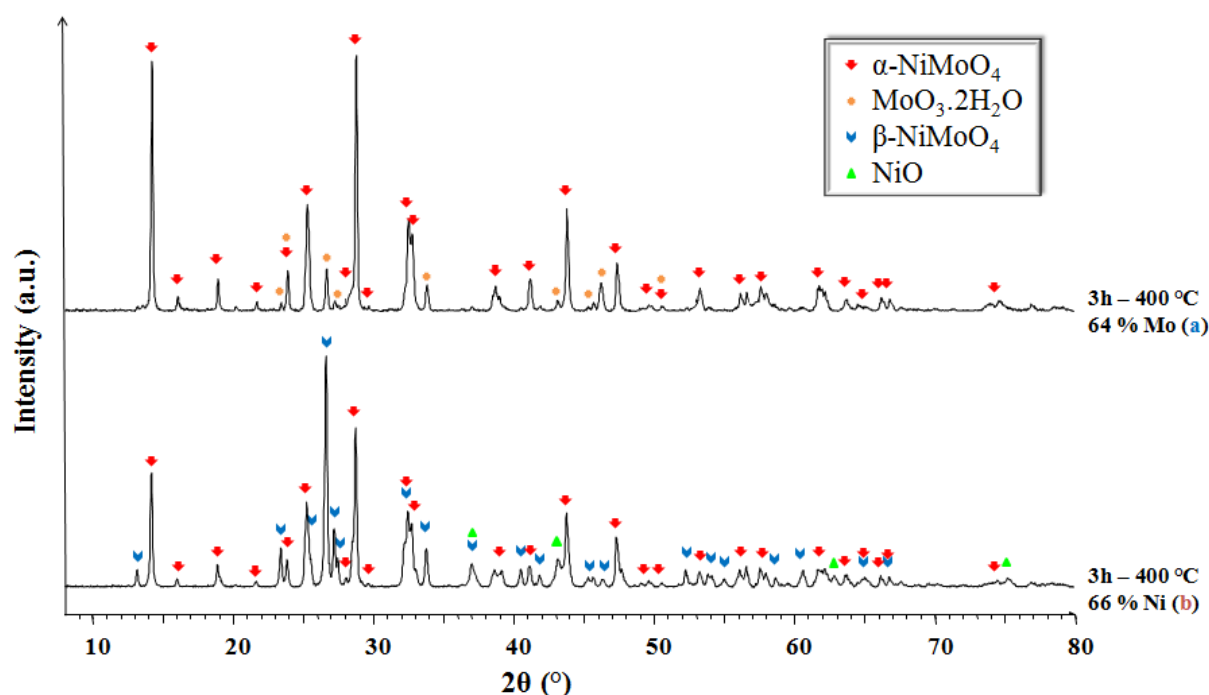


Figure II.37: Examples of XRD patterns of NiMo based powder synthesized in supercritical $\text{H}_2\text{O}/\text{iPrOH}$ mixture with different Ni/Mo ratios

We reported the compositions of those two powders on the ternary diagram of the system Ni-Mo-O (Figure II.38). The two points (**a** for Mo excess and **b** for Ni excess) correspond to powder compositions where the oxygen comes exclusively from the oxides. The real positions of the powders on the diagram are somewhere on the segments $[\text{a};\text{O}]$ or $[\text{b};\text{O}]$. Even though this ternary diagram was realized at 1100 °C and we calcined our powders at only 400 °C, we effectively obtain $\text{NiMoO}_4 + \text{“MoO}_3\text{”}$ when Mo is in excess (MoO_3 being hydrated in our case) and $\text{NiMoO}_4 + \text{NiO}$ when Ni is in excess. The STEM-EDX chemical mappings associated to these two compositions illustrates this fact showing the presence of particles containing only Mo for **a** and particularly rich in Ni for **b** (Figure II.39).

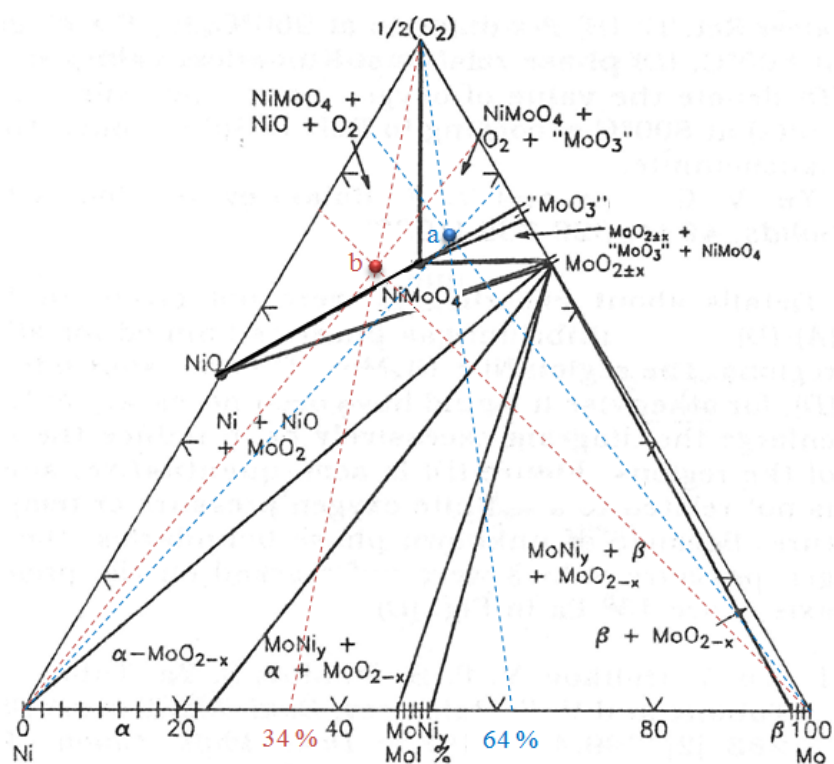
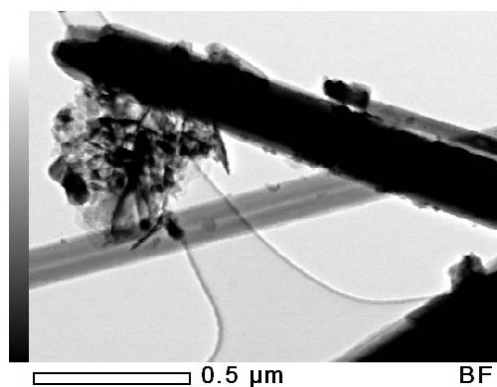
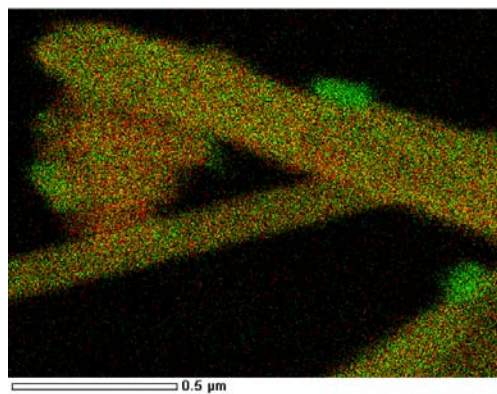


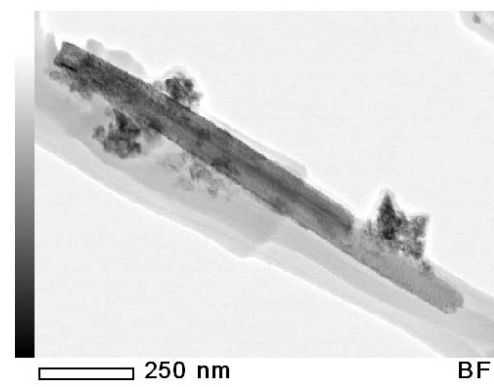
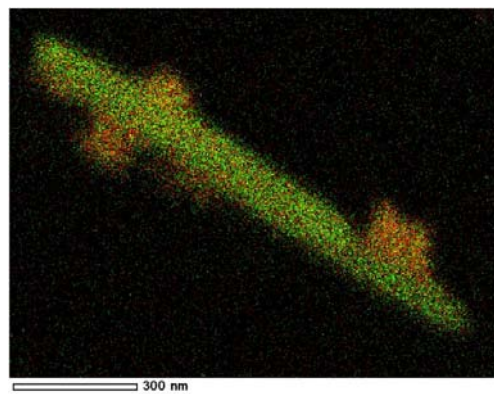
Figure II.38: Ternary diagram of the system Ni-Mo-O [8]

a) 64 at% Mo



BF

b) 34 at% Mo



BF

Figure II.39: STEM-EDX chemical mapping of NiMo based powders a) (excess of Mo in green), and b) (excess of Ni in red) synthesized in supercritical H₂O/iPrOH mixture

Those results remind us the studies carried out by Di Renzo et al. [27,28] concerning the stabilization of β -NiMoO₄ at room temperature with an excess of nickel. According to their work, only the α -phase can be considered as a stoichiometric compound whereas the β -phase can form solid solution with Ni by insertion in localized vacant sites in the network of β -NiMoO₄, thus stabilizing the structure of the phase. This effect is not observed with Mo assumingly due to an obvious matter of steric hindrance.

X-ray Photoelectron Spectroscopy (XPS) gives us supporting information to this hypothesis. Measurements of surface Ni/Mo molar ratios for different compositions (Table II.9) show that when we have an excess of Mo, the Ni/Mo surface ratio is lower than the bulk ratio what can easily be explained by the presence of Mo-rich particles in the powder. When the ratio is equal to one, both ratios are equivalent and when we have an excess of Ni, by analogy with Mo-rich samples, the surface ratio should be higher than the bulk one. However, this is not the case and we explain this by considering that part of the Ni in excess is inside the NiMoO₄ network and therefore is not detected by XPS.

Table II.9: Comparison of bulk and surface Ni/Mo molar ratio

Sample	Type of powder	Ni/Mo molar ratio (ICP)	Ni/Mo molar ratio (XPS)	Ni at% (ICP)
MT014	calcined	1.99	1.76	66
MT055	calcined	1.56	1.42	61
MT053	calcined	1.5	1.35	60
MT052	calcined	1.33	1.26	57
MT045	calcined	0.99	0.96	50
MT084	calcined	0.58	0.39	36

We could partly stabilize β -NiMoO₄ among α -NiMoO₄ at room temperature by adding an excess of nickel in the reaction system. This phase being more active toward hydrogenation, we believe this material to be an efficient catalyst of the deep-HDS reaction once sulfided.

II.2.3.3. Synthesis of CoMoO_4

When synthesizing CoMoO_4 , we encountered a major issue with the “one way” synthesis method. Once the two preliminary solutions are put together, an immediate precipitation occurs, and injecting this resulting solution is not possible. To get round of this situation, we decided to inject the two precursor solutions separately in such a way that they mix in a T connection right before entering the reactor (see [Figure II.1](#)).

Again, the cleanness of our fresh powders toward organics is proved: 0.34 ± 0.01 wt% carbon, 0.7 ± 0.05 wt% hydrogen and free from nitrogen.

The XRD pattern acquired directly after reaction ([Figure II.40](#)) fits with a mixture of two different structures of CoMoO_4 : α - CoMoO_4 (monoclinic, JCPDS 73-1331) and β - CoMoO_4 (base-centered monoclinic, JCPDS 21-0868). The β -isomorph, which is the high temperature isomorph of CoMoO_4 , is clearly the majority phase. Nothing surprising since it has already been proved that on the contrary of β - NiMoO_4 unstable below 180°C , CoMoO_4 β -isomorph can easily be stabilized at room temperature [37]. As the XRD patterns show, the α -phase almost disappears after thermal treatment at 400°C for 3 h. Since it seems of negligible quantity, calcination appears useless in this case, all the more since it decreases the S_{BET} (from $52\text{ m}^2\cdot\text{g}^{-1}$ down to $38\text{ m}^2\cdot\text{g}^{-1}$).

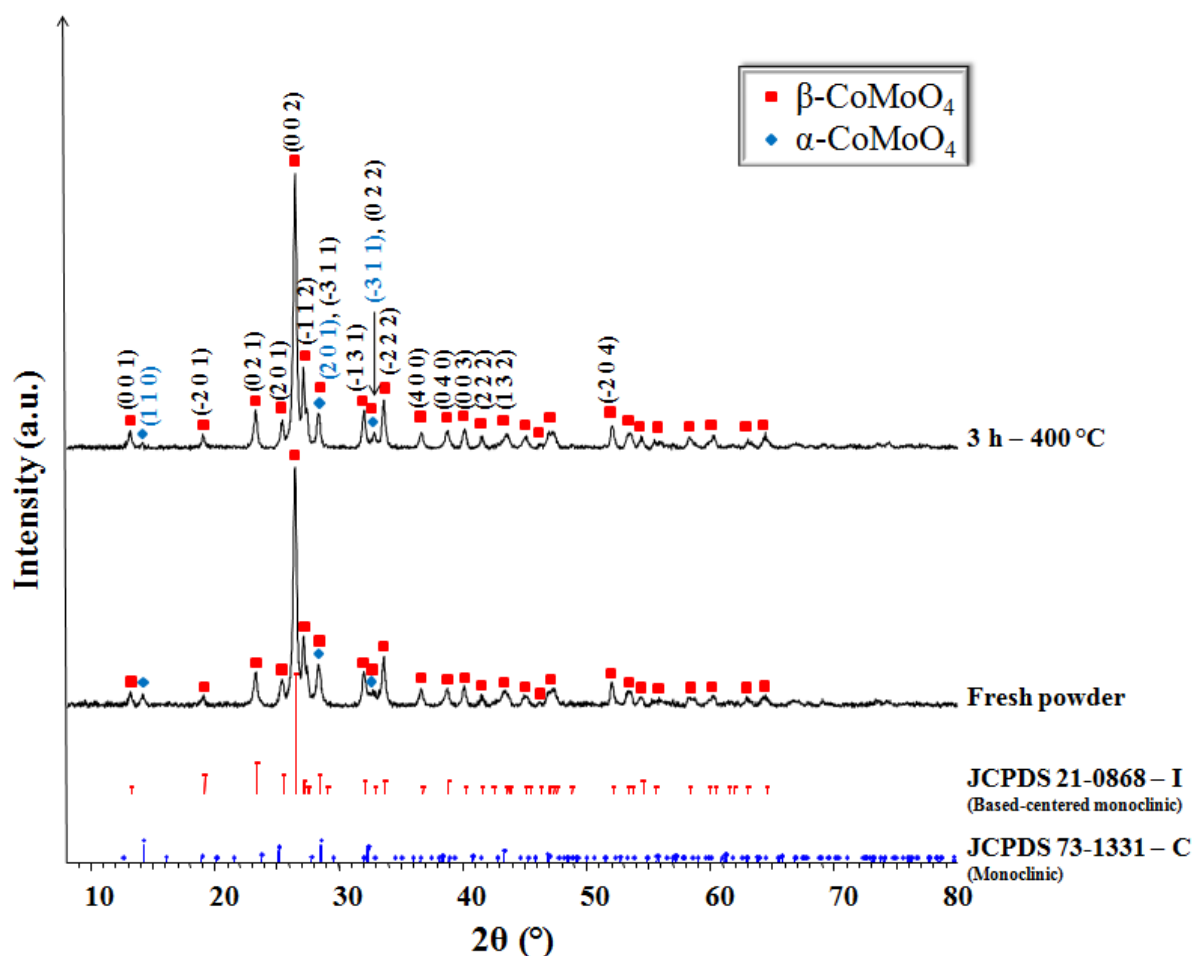


Figure II.40: XRD patterns of stoichiometric CoMo based powders synthesized in supercritical $\text{H}_2\text{O}/i\text{PrOH}$ mixture, directly after synthesis (below) and after a 3 h calination at 400 °C (above)

Profile matching on the XRD pattern of the calcined powder (Figure II.41) gave us refining parameters of $\chi^2 = 0.801$ and $\text{cR}_{\text{wp}} = 13.8$. The cell parameters found for the two phases are in good agreement with the values given by the JCPDS cards (Table II.10, Table II.11).

Table II.10: Cell parameters obtained for the stoichiometric CoMo based powders synthesized in supercritical $\text{H}_2\text{O}/i\text{PrOH}$ mixture after a 3 h calination at 400 °C for $\beta\text{-CoMoO}_4$

Space group	a (Å)	b (Å)	c (Å)	β (°)
C 2/m	10.234(2)	9.279(2)	7.029(1)	106.937(8)
JCPDS 21-0868	10.210	9.268	7.022	106.90

Table II.11: Cell parameters obtained for the stoichiometric CoMo based powders synthesized in supercritical $\text{H}_2\text{O}/i\text{PrOH}$ mixture after a 3 h calination at 400 °C for $\alpha\text{-CoMoO}_4$

Space group	a (Å)	b (Å)	c (Å)	β (°)
C 2/m	9.668(1)	8.857(1)	7.757(1)	113.826(7)
JCPDS 73-1331	9.666	8.854	7.755	113.82

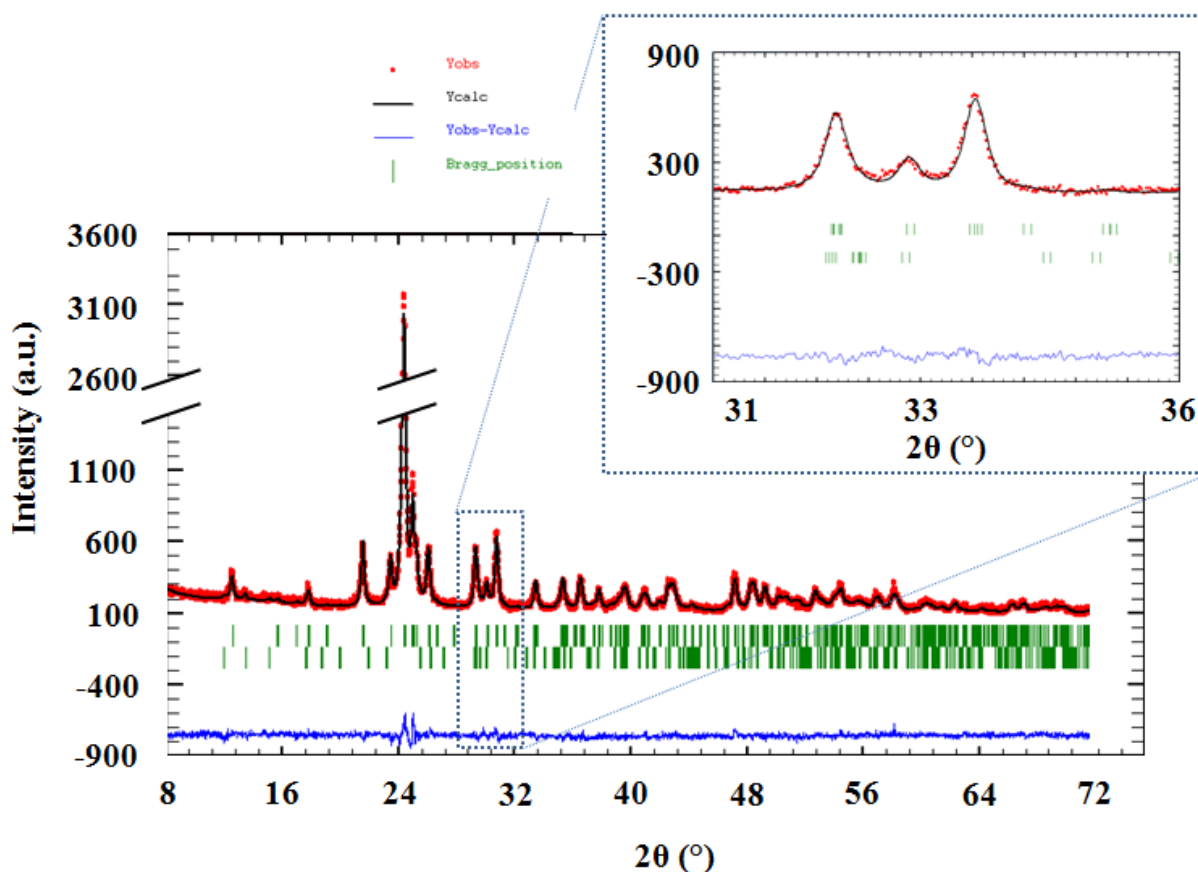


Figure II.41: Profile matching of the XRD patterns of the stoichiometric CoMo based powder synthesized in supercritical $\text{H}_2\text{O}/i\text{PrOH}$ mixture, calcinated 3 h at 400 °C

We also carried out a Rietveld refinement on this XRD pattern. We have the atomic positions and anisotropic coefficient for $\alpha\text{-CoMoO}_4$ from the ICSD card #23808 [38]. We included them in the simulation but since the phase is hardly detectable, we fixed those values for the refinement. As for $\beta\text{-NiMoO}_4$, $\beta\text{-CoMoO}_4$ also is isotypic with $\alpha\text{-MnMoO}_4$. We thus used the ICSD card #78328 corresponding to $\alpha\text{-MnMoO}_4$ to make a first approximation of the atomic positions. The refinement parameters obtained are $\chi^2 = 1.04$, $cR_{wp} = 15.7$, Bragg R-factor = 5.52 for the $\beta\text{-CoMoO}_4$. The refined atomic positions are presented in Table II.12 and the structural representation associated is given in Figure II.42. As one can see, it is very similar to the one already described in Figure II.5.

II. Synthesis of HDS catalyst precursors in supercritical fluids

Table II.12: Atomic parameters obtained for the stoichiometric CoMo based powders synthesized in supercritical H₂O/iPrOH mixture after a 3 h calination at 400 °C for β -CoMoO₄ (*comparison with ICSD #78328 for atomic positions)

Atom	position	x	y	Z
Co1	4h	0	0.175(2)	0
Mn1*	4h	0	0.194(2)	0
Co2	4i	0.808(2)	0	0.137(3)
Mn2*	4i	0.795(2)	0	0.135(3)
Mo1	4g	0	0.250(1)	0
Mo1*	4g	0	0.249	0
Mo2	4i	0.271(1)	0	0.401(1)
Mo2*	4i	0.269(1)	0	0.400(2)
O1	4i	0.323(6)	0.5	0.467(9)
O1*	4i	0.355(1)	0.5	0.463(2)
O2	4i	0.220(6)	0	0.140(6)
O2*	4i	0.201(1)	0	0.154(3)
O3	8j	0.118(3)	0.345(3)	0.095(5)
O3*	8j	0.129(1)	0.360(1)	0.101(2)
O4	8j	0.461(5)	0.357(5)	0.189(6)
O4*	8j	0.461(1)	0.355(1)	0.193(1)
O5	8j	0.375(2)	0.153(3)	0.451(4)
O5*	8j	0.367(1)	0.149(1)	0.472(1)

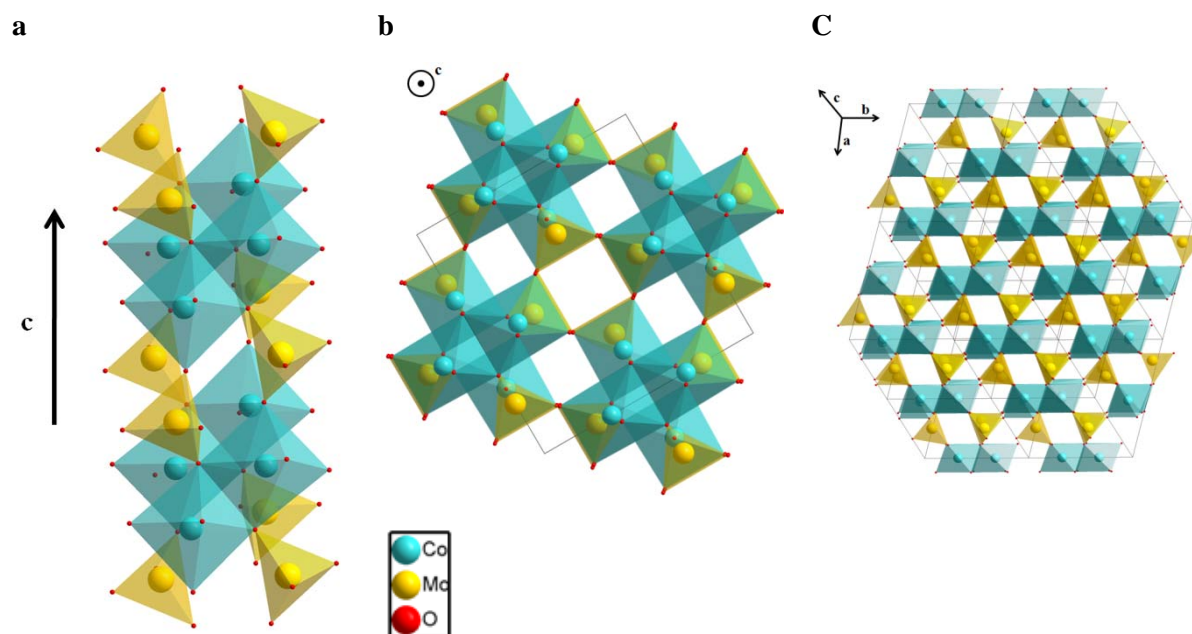
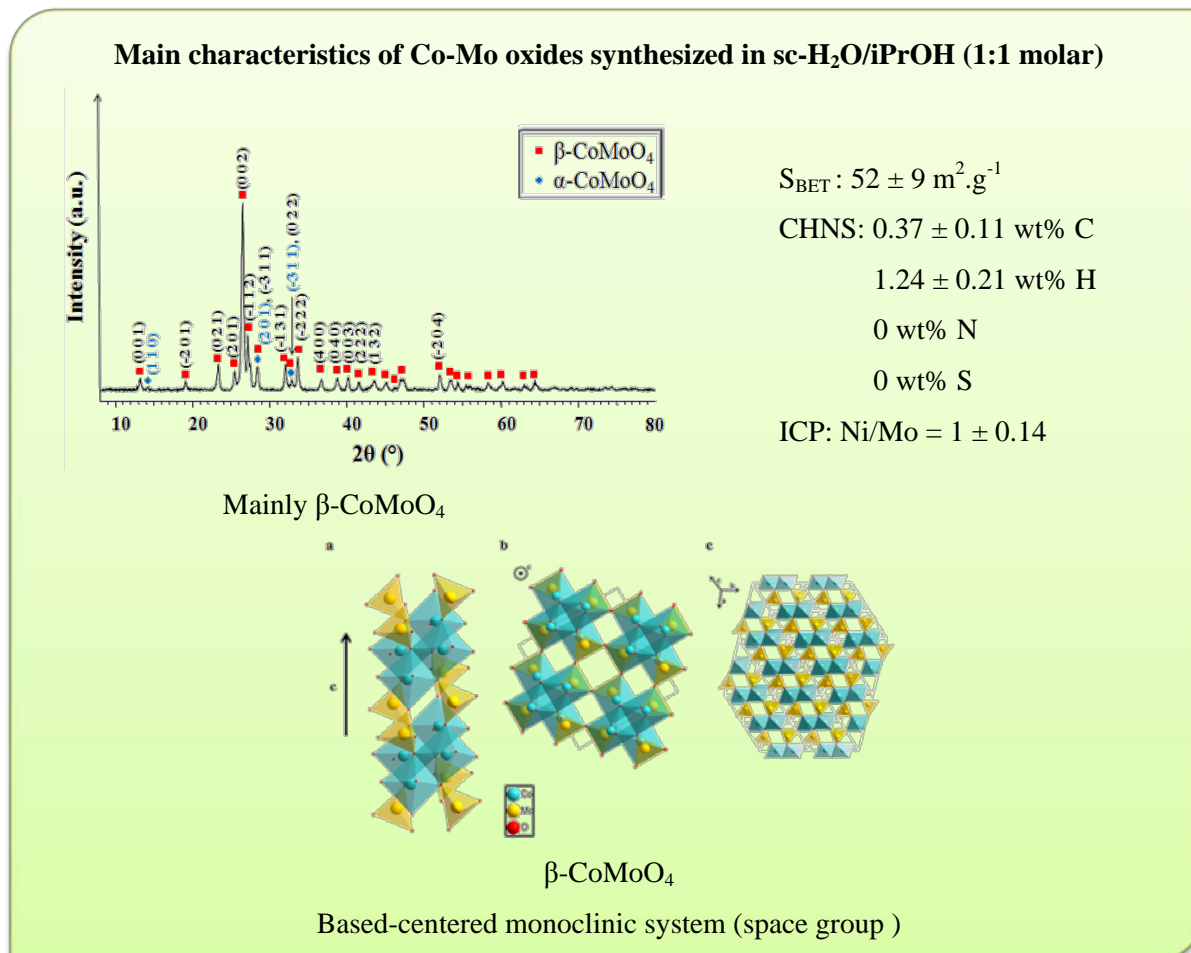


Figure II.42: Structure of β -CoMoO₄

The study of this material has not been as complete as for the others; however, we also propose a short summary of the main characteristics of this powder:



II.3. Conclusion

With the use of supercritical water/alcohol systems as reaction media for the synthesis of NiMoO₄ in a continuous process, we successfully manage to obtain with short reaction time a contaminant-free material of high specific surface area: we reach $179 \pm 12 \text{ m}^2 \cdot \text{g}^{-1}$, almost twice the objective we set at the beginning of this project. The best S_{BET} results were obtained with the use of isopropanol as alcohol of the solvent mixture. We assume that these better S_{BET} are due to higher supersaturation of the media for similar conditions of temperature and pressure (290 °C and 23 MPa) and therefore formation of smaller nanoparticles (rod-like nanoparticles). Indeed, with the use of isopropanol, the critical coordinates of the system are lower than with methanol or ethanol and we proved that the lengths L of the nanorods decrease depending on the alcohol: $L_{\text{methanol}} > L_{\text{ethanol}} > L_{\text{isopropanol}}$.

With this study, we showed that we obtained a mix of different phases directly after the synthesis depending on the Ni/Mo ratio and with $\text{NiMoO}_4 \cdot 0.75\text{H}_2\text{O}$ being the main phase for Ni/Mo close to 1. When optimizing our calcination program (3 h at 400 °C) we proved that by heating our material, we form $\beta\text{-NiMoO}_4$ (the high temperature phase), catalytically more active toward HDS reaction than $\alpha\text{-NiMoO}_4$. At room temperature, we showed that the powder becomes a mixture of $\alpha\text{-NiMoO}_4$ and $\text{MoO}_3 \cdot \text{H}_2\text{O}$ when it is prepared with an excess of molybdenum, and a mixture of $\alpha\text{-NiMoO}_4$, $\beta\text{-NiMoO}_4$ and NiO when prepared with an excess of nickel. Regarding the application of our project, a Ni-rich powder must present better results toward deep-HDS since it contains the most active phase toward HDS reaction catalysis and also Ni species well known for their hydrogenation capacity, properties highly appreciable in Deep-HDS since it occurs via hydrogenation of the aromatic rings of the most refractory sulfided compounds, particularly 4,6-DMDBT.

We manage to fulfill and even outperform our objectives from the French part of this project: we synthesize a new generation of bulk HDS catalysts precursors presenting higher S_{BET} than commercially available products.

The second important objective of this project was of course to prove the efficiency of our catalysts in the reaction of deep-HDS. This whole work was therefore performed in parallel with catalytic tests at the Instituto de Tecnología Química (ITQ - Valencia) in Spain. Since the high S_{BET} materials were not obtained at first time, the results presented in the next chapter include some materials of lower S_{BET} . As we also proved that we could synthesize CoMoO_4 directly as its high temperature phase, we included this material in our tests to go further in our general study and make comparisons with NiMoO_4 .

II.4. References

- [1] Cansell, F., Chevalier, B., Demourgues, A., Etourneau, J., Even, C., Pessey, V., Petit, S., Tressaud, A., and Weill, F. "Supercritical fluid processing: a new route for materials synthesis." *journal of materials chemistry* **1999**. vol. 9, 61
- [2] Cansell, F., Aymonier, C., and Loppinet-Serani, A. "Review on materials science and supercritical fluids." *Current Opinion in Solid State and Materials Science* **2003**. vol. 7, no. 4-5, 331
- [3] Aymonier, C., Loppinet-Serani, A., Reverón, H., Garrabos, Y., and Cansell, F. "Review of supercritical fluids in inorganic materials science." *The Journal of Supercritical Fluids* **2006**. vol. 38, no. 2, 242 . A collection of papers dedicated to the memory of Prof. Aydin Akgerman - Akgerman S.I.
- [4] Cansell, F. and Aymonier, C. "Design of functional nanostructured materials using supercritical fluids." *The Journal of Supercritical Fluids* **2009**. vol. 47, no. 3, 508 . 20th Year Anniversary Issue of the Journal of Supercritical Fluids
- [5] Reverón, H., Aymonier, C., Loppinet-Serani, A., Elissalde, C., Maglione, M., and Cansell, F. "Single-step synthesis of well-crystallized and pure barium titanate nanoparticles in supercritical fluids." *Nanotechnology* **2005**. vol. 16, no. 8, 1137
- [6] Reverón, H., Elissalde, C., Aymonier, C., Bidault, O., Maglione, M., and Cansell, F. "Supercritical fluid route for synthesizing crystalline barium strontium titanate nanoparticles." *Journal of Nanoscience and Nanotechnology* **2005**. vol. 5, 1741
- [7] Jacob, K. T., Kale, G. M., and Iyengar, G. N. K. "Phase equilibria and thermodynamic properties in the system Ni-Mo-O." *Journal of Materials Science* **1987**. vol. 22, no. 12, 4274
- [8] Rath, R. S. "O-Mo-Ni: Phase diagrams." In: *Phase diagrams for ceramists*. vol. 11: Oxides, edited by W. O. the American Ceramic Society. Westerville (Ohio): the American Ceramic Society **1995** 12
- [9] Smith, G. W. "The crystal structure of cobalt molybdate, CoMoO_4 and nickel molybdate NiMoO_4 ." *Acta Crystallographica* **1962**. vol. 15, 1054
- [10] Smith, G. W. and Ibers, J. A. "The crystal structure of cobalt molybdate, CoMoO_4 ." *Acta Crystallographica* **1969**. vol. 19, 269
- [11] Abrahams, S. C. and Reddy, J. M. "Crystal structure of the transition-metal molybdates. i. paramagnetic $\alpha\text{-MnMoO}_4$." *The Journal of Chemical Physics* **1965**. vol. 43, no. 7, 2533
- [12] Sleight, A. W. and Chamberland, B. L. "Transition metal molybdates of the type AMoO_4 ." *Inorganic Chemistry* **1968**. vol. 7, no. 8, 1672
- [13] Rodriguez, J. A., Chaturvedi, S., Hanson, J. C., Albornoz, A., and Brito, J. L. "Electronic properties and phase transformations in CoMoO_4 and NiMoO_4 : XANES and time-resolved synchrotron XRD studies." *The Journal of Physical Chemistry B* **1998**. vol. 102, no. 8, 1347
- [14] Rodriguez, J. A., Chaturvedi, S., Hanson, J. C., and Brito, J. L. "Reaction of H_2 and H_2S with CoMoO_4 and NiMoO_4 : TPR, XANES, time-resolved XRD, and molecular-orbital studies." *The Journal of Physical Chemistry B* **1999**. vol. 103, no. 5, 770

- [15] Ding, Y., Wan, Y., Min, Y. L., Zhang, W., and Yu, S. H. "General synthesis and phase control of metal molybdate hydrates $\text{MMoO}_4 \cdot n\text{H}_2\text{O}$ ($\text{M} = \text{Co}, \text{Ni}, \text{Mn}$, $n = 0, 3/4, 1$) nano/microcrystals by a hydrothermal approach: Magnetic, photocatalytic, and electrochemical properties." *Inorganic Chemistry* **2008**. vol. 47, no. 17, 7813
- [16] Eda, K., Kato, Y., Ohshiro, Y., Sugitani, T., and Whittingham, M. S. "Synthesis, crystal structure, and structural conversion of Ni molybdate hydrate $\text{NiMoO}_4 \cdot n\text{H}_2\text{O}$." *Journal of Solid State Chemistry* **2010**. vol. 183, no. 6, 1334
- [17] Brito, J. L., Barbosa, A. L., Alborno, A., Severino, F., and Laine, J. "Nickel molybdate as precursor of HDS catalysts: Effect of phase composition." *Catalysis Letters* **1994**. vol. 26, no. 3, 329
- [18] Di Renzo, F. and Mazzocchia, C. "How thermal treatment influences the phase transition of NiMoO_4 ." *Thermochimica Acta* **1985**. vol. 85, 139
- [19] Klissurski, D., Mancheva, M., Iordanova, R., Tyuliev, G., and Kunev, B. "Mechanochemical synthesis of nanocrystalline nickel molybdates." *Journal of Alloys and Compounds* **2006**. vol. 422, no. 1-2, 53
- [20] Rodriguez, J. A., Hanson, J. C., Chaturvedi, S., Maiti, A., and Brito, J. L. "Phase transformations and electronic properties in mixed-metal oxides: Experimental and theoretical studies on the behavior of NiMoO_4 and MgMoO_4 ." *Journal of Chemical Physics* **2000**. vol. 112, 935
- [21] Brito, J. L. and Barbosa, A. L. "Effect of phase composition of the oxidic precursor on the HDS activity of the sulfided molybdates of Fe(II), Co(II), and Ni(II)." *Journal of Catalysis* **1997**. vol. 171, no. 2, 467
- [22] Mazzocchia, C., Aboumradi, C., Diagne, C., Tempesti, E., Herrmann, J. M., and Thomas, G. "On the NiMoO_4 oxidative dehydrogenation of propane to propene: some physical correlations with the catalytic activity." *Catalysis Letters* **1991**. vol. 10, no. 3, 181
- [23] Chaturvedi, S., Rodriguez, J., and Brito, J. "Characterization of pure and sulfided NiMoO_4 catalysts using synchrotron-based X-ray absorption spectroscopy (XAS) and temperature-programmed reduction (TPR)." *Catalysis Letters* **1998**. vol. 51, no. 1, 85
- [24] Moreno, B., Chinarro, E., Colomer, M. T., and Jurado, J. R. "Combustion synthesis and electrical behavior of nanometric $\beta\text{-NiMoO}_4$." *The Journal of Physical Chemistry C* **2010**. vol. 114, no. 10, 4251
- [25] Kaddouri, A., Tempesti, E., and Mazzocchia, C. "Comparative study of beta-nickel molybdate phase obtained by conventional precipitation and the sol-gel method." *Materials Research Bulletin* **2004**. vol. 39, no. 4-5, 695
- [26] Zăvoianu, R., Dias, C. R., and Portela, M. F. "Stabilisation of $\beta\text{-NiMoO}_4$ in TiO_2 -supported catalysts." *Catalysis Communications* **2001**. vol. 2, no. 1, 37
- [27] Di Renzo, F., Mazzocchia, C., Thomas, G., and Vernay, A. "Formation and properties of the solid solution of NiO in NiMoO_4 ." *Reactivity of Solids* **1988**. vol. 6, no. 2-3, 145
- [28] Mazzocchia, C., Di Renzo, F., Aboumradi, C., and Thomas, G. "Stability of β -nickel molybdate." *Solid State Ionics* **1989**. vol. 32-33, no. Part 1, 228
- [29] Dayem, H. M. A. and Sadek, S. A. "How does γ -irradiation influence the phase transition of $\alpha\text{-NiMoO}_4$?" *Thermochimica Acta* **2008**. vol. 473, no. 1-2, 96
- [30] Bousquet, C. "Chimie en milieux fluides supercritiques pour l'élaboration de céramiques ferroélectriques nanostructurées." Ph.D. thesis, Université de bordeaux 1 **2008**

- [31] Bazaev, A. R., Abdulagatov, I. M., Bazaev, E. A., and Abdurashidova, A. “(p, v, T, x) measurements of $(1 - x)\text{H}_2\text{O} + x\text{C}_2\text{H}_5\text{OH}$ mixtures in the near-critical and supercritical regions.” *The Journal of Chemical Thermodynamics* **2007**. vol. 39, no. 3, 385
- [32] Ehrenberg, H., Svoboda, I., Wltschek, G., Wiesmann, M., Trouw, F., Weitzel, H., and Fuess, V. “Crystal and magnetic structure of $\alpha\text{-NiMoO}_4$.” *Journal of Magnetism and Magnetic Materials* **1995**. vol. 150, no. 3, 371
- [33] Marre, S., Park, J., Rempel, J., Guan, J., Bawendi, M. G., and Jensen, K. F. “Supercritical continuous-microflow synthesis of narrow size distribution quantum dots.” *Advanced Materials* **2008**. vol. 20, no. 24, 4830
- [34] Heinemann, H. A.1.3. In: *Handbook of Heterogeneous Catalysis*, edited by G. Ertl, H. Knözinger, and J. Weitkamp. Wiley-VCH, New-York, vol. 1 **1997** 35
- [35] Pereñíguez, R., González-DelaCruz, V. M., Holgado, J. P., and Caballero, A. “Synthesis and characterization of a LaNiO_3 perovskite as precursor for methane reforming reactions catalysts.” *Applied Catalysis B: Environmental* **2010**. vol. 93, no. 3-4, 346
- [36] Lavrenov, A., Buluchevskii, E., Moiseenko, M., Drozdov, V., Arbuzov, A., Gulyaeva, T., Likholobov, V., and Duplyakin, V. “Chemical composition optimization and characterization of the $\text{NiO/B}_2\text{O}_3\text{-Al}_2\text{O}_3$ system as a catalyst for ethylene oligomerization.” *Kinetics and Catalysis* **2010**. vol. 51, no. 3, 404
- [37] Ponceblanc, H., Millet, J. M. M., Coudurier, G., Legendre, O., and Védrine, J. C. “Solid-solid phase equilibria in the binary system cobalt molybdate (CoMoO_4)-iron molybdate (FeMoO_4) and effect of iron on the phase equilibria.” *The Journal of Physical Chemistry* **1992**. vol. 96, no. 23, 9462
- [38] Smith, G. W. and Ibers., J. A. “The crystal structure of cobalt molybdate, CoMoO_4 .” *Acta Crystallographica* **1965**. vol. 19, 269

Chapter III

Catalytic tests

III. Catalytic tests	167
III.1. HDS: experimental setup and parameters	171
III.1.1. HDS reactor description	171
III.1.2. HDS products characterized by Gas chromatography	174
III.1.2.1. Gas chromatograph characteristics	174
III.1.2.2. Pulsed Flame Photometric Detector (PFPD).....	175
III.1.3. Feedstock	178
III.1.4. Experimental procedure	180
III.1.4.1. Preparation of the catalytic bed.....	180
<i>III.1.4.1.1. Liquid Hourly Space Velocity (LHSV).....</i>	<i>180</i>
<i>III.1.4.1.2. Activation of the catalyst precursors: sulfidation.....</i>	<i>181</i>
III.1.4.2. Reaction conditions.....	182
III.1.4.3. Product analysis by gas chromatography	183
III.2. Catalytic activity checking	185
III.2.1. Spider Reactor	185
III.2.2. Tests preparation.....	186
III.2.3. Results.....	187
III.3. Experiments with HDS-specific reactor	188
III.3.1. First tests: materials and experimental conditions.....	189
III.3.1.1. Influence of the M_G/M_L ratio	190
III.3.1.2. Influence of the composition.....	191
III.3.2. Higher LHSV	192
III.3.2.1. Tested materials	193
III.3.2.2. Influence of the composition.....	194
III.3.2.3. Influence of the calcination.....	199
III.3.2.4. Influence of the promoter nature.....	201
III.3.2.5. Conclusion	203

III.4. Tests on real feed.....	203
III.4.1. Description of the Light Cycle Oil	204
III.4.2. HDS test.....	206
III.4.2.1. Cut points	206
III.4.2.2. Sulfur compounds conversion.....	207
III.5. Conclusion.....	209
III.6. References	210

Selected catalyst precursors prepared in supercritical fluids (ICMCB – France) have been tested for the reaction of hydrodesulfurization (ITQ – Spain). They have been chosen by mean of S_{BET} , cations ratio and type of promoter.

The following chapter first describes the equipment and protocol followed to achieve this work and then the results obtained with our materials comparatively to commercial catalysts used as references.

III.1. HDS: experimental setup and parameters

In this part we describe the experimentation by itself, from the setup to the general procedure followed to prepare the catalytic bed and perform the catalytic tests.

III.1.1. HDS reactor description

The equipment used for the HDS reaction is a down flow fixed bed stainless steel tubular reactor, fully automatized and schematically represented in [Figure III.1](#). The software used for control and programming of the different process steps is Factory Floor developed by Opto22. Pressure, temperatures, flows (liquid and gas) and valves can be all set and controlled manually via this scheme (settings are in blue, real values in red, regulators values in green) and their values can also be scheduled in a program, offering thus a large flexibility of action while operating. Comparatively to an industrial hydrotreatment process, our reactor is simplified and focuses on the reaction by itself.

The different parts of the equipment can be bring to the wanted temperature thanks to heat-resistances placed all along the circuit, ensuring thus a better flowing of the feedstock, particularly useful when working with highly viscous ones. The real temperature is controlled via the computer through K-type thermocouples located at various points of the setup. As shown in [Figure III.2](#), the circuit is confined in boxes during the reaction and a ventilator (1) has the hot air circulated in the whole system and this to better homogenize the overall heating by convection.

The setup comprises a 150 ml tank (2) filled with the studied feedstock and pressurized with nitrogen (about 0.3 MPa) to ensure a correct sucking up by the injection

pump (3). The feedstock is vaporized in a pre-heater (4) before entering the HDS reactor itself (5). Two valves (6) turn the general flow either to the bypass (7) or to the reactor and a third one (8) directs the reactor outlet to the vent or to a possible online chromatograph (9). Four flow-meters (10), each one dedicated to a specific gas, deliver an accurate flow of the desired gas in the system. Since we did not need any argon, only the flow-meters of hydrogen, hydrogen sulfide and nitrogen were used. The pressure in the whole system is controlled and adjusted by an automatic badger meter pressure control valve (11). A final tank (12) permits to recover the treated feedstock for further analysis.

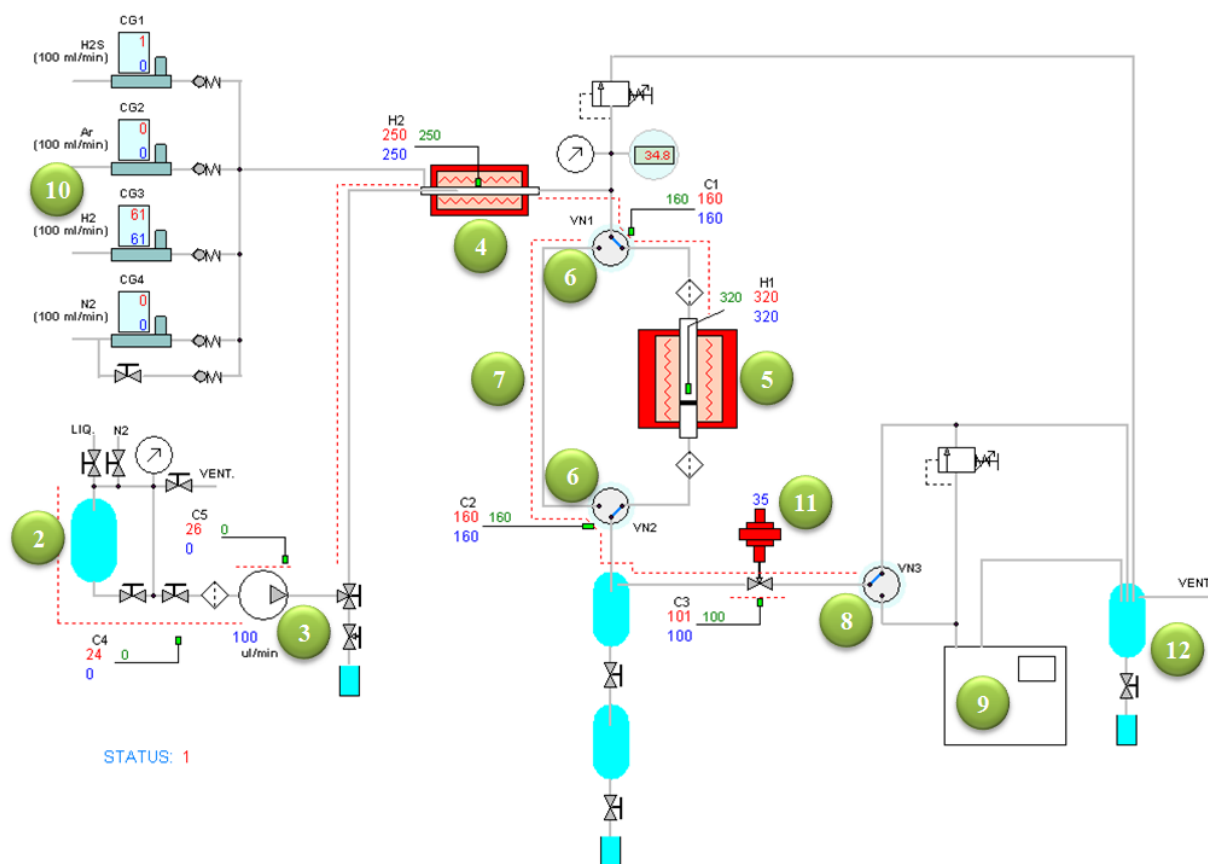


Figure III.1: Scheme of the HDS reactor



Figure III.2 : Equipment used for the HDS reaction

II.1.2. HDS products characterized by Gas chromatography

The use of gas chromatography has been reported for a long time as a technique of choice for the analysis of gas oils and their hydrotreating products [1]. Substances are identified by the order in which they emerge (elute) from the column, in other words, by the retention time of the analyte in the column, and their concentration can be determined thanks to the use of response factors. In our study, two detectors are used to monitor the outlet stream from the column: a pulsed flame photometric detector (PFPD) specific for sulfur compounds, and a flame ionization detector (FID) that detects all hydrocarbons. They give the time at which each component reaches the outlet and their amount.

II.1.2.1. Gas chromatograph characteristics

The gas chromatograph we used is an automatic GC 3400 supplied by Varian, schematically represented on Figure III.3.

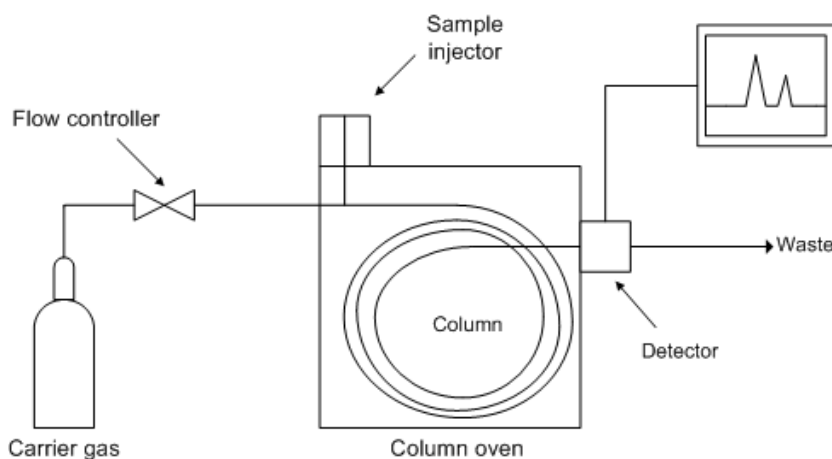


Figure III.3 : Schematic representation of a gas chromatograph

The feedstock components and reaction products were separated in a 30 m long FactorFour™ column by Varian (VF 5ms CP8944), a column with an inner diameter of 0.25 mm and a bonded stationary phase made of a 0.25 μm thick film, equivalent to a (5 % phenyl 95 % dimethyl) polysiloxane, a slightly polar phase well suited for hydrocarbons, aromatic hydrocarbons and sulfur compounds analysis (among others). At the end of the column, a quartz Y tube splits the flow and directs the eluent toward two detectors installed in

parallel. We explain in more details what the PFPD is in the next section since it specifically detects sulfur compounds what is of particular interest in this project work. The FID is described in the [appendix IV.8](#).

The GC is equipped with a Varian-8200-CX autosampler permitting up to 40 consecutive automatic injections. This procedure provides better reproducibility and time-optimization as compared to manual injection. The amount of sample injected was in all cases 0.5 μl .

II.1.2.2. Pulsed Flame Photometric Detector (PFPD)

For the selective analysis of sulfur compounds by gas chromatography, the Pulsed Flame Photometric Detector (PFPD) ([Figure III.5](#)) [2,3] manufactured and commercialized by Varian Chromatography Systems since the 90's, is proved to be particularly efficient and to give a good sensitivity toward sulfur compounds [4].

Hydrogen-rich flames containing sulfur compounds show a broad chemoluminescence band emission around 400 nm which is ascribed to excited S_2 molecules (S_2^*) as the predominant source. The flame emitted light is measured with a photomultiplier/electrometer device. At least two mechanisms are suggested in the literature for the origin of the S_2^* chemoluminescence [2,5]: the direct recombination reaction of two sulfur atoms ($\text{S} + \text{S} \rightarrow \text{S}_2^*$) and the recombination reaction of hydrogen atoms, thereby exciting S_2 molecules which have been formed from sulfur species in a preceding step (e.g., $2\text{H}_2\text{S} + 2\text{H} \rightarrow \text{S}_2 + 3\text{H}_2$ and $\text{H} + \text{H} + \text{S}_2 \rightarrow \text{H}_2 + \text{S}_2^*$). Since the pseudo steady state concentration of S_2 molecules is very small at high temperature and since the lifetime of both hydrogen atoms and sulfur atoms in hydrogen-rich flames is very long, S_2 formation mainly proceeds under colder conditions in the flame border zone, near the wall of the combustion chamber, or in the after flame media. With both the mechanisms the S_2^* concentration (and thereby the detected chemoluminescent emission intensity) is a square-law function of sulfur concentration in the flame ($I \sim a.[\text{S}]^2$).

In the Pulsed Flame concept, a single hydrogen-rich premixed flame is applied. Relatively low flows of hydrogen and air, together with the column effluent are fed to the combustion chamber continuously, thereby mixing. The mixture is ignited at the off site whereupon the flame immediately propagates through the whole combustion chamber. After

having burnt completely in a bright emission flash, the flame self-terminates. This cycle is repeated automatically several times a second. The almost autothermal rapid combustion in the premixed flame causes very high combustion temperature and therefore very rapid and complete degradation and oxidation of all sulfur analytes and matrix constituents. The response is independent of the sulfur compound type and other matrix effects are drastically reduced. The PFPD response is indeed a purely square-law one: an exponential constant of 2.00 ± 0.03 was reported from tetrahydrothiophene dilution series [2]. Time dependences of sulfur emission (S_2^* , gated at 5-16 ms) and hydrocarbon emission (such as CH^* or C_2^* , gated at 1-3 ms) after ignition are much different (Figure III.4).

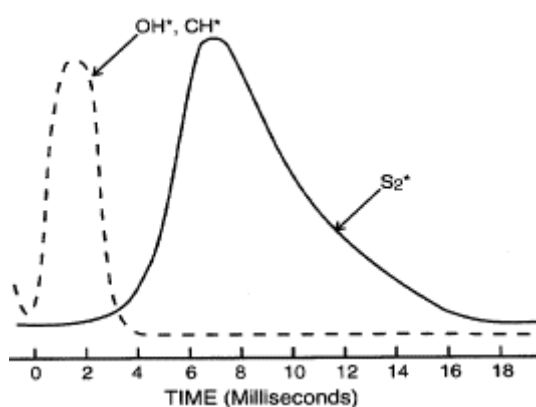


Figure III.4 : Light emission from background (OH^* , CH^*) and sulfur (S_2^*)

With the pulse mode of detector operation, signals can be separated completely in time. Because the emission from sulfur is delayed as against the emission from hydrocarbons but lasts much longer, signal separation can be performed by restricting emission recording to a well defined “delayed” time gate after ignition. That way, C/S-selectivity is improved and the photomultiplier noise is reduced. Additionally, as it emanates from a highly concentrated reaction mixture and almost autothermal high temperature combustion, flash emission is very bright. Much higher sensitivity is obtained than with continuously operated flames.

With the current status of prominent sulfur selective detectors, the PFPD appears to be the first choice for petroleum sulfur compounds determination.

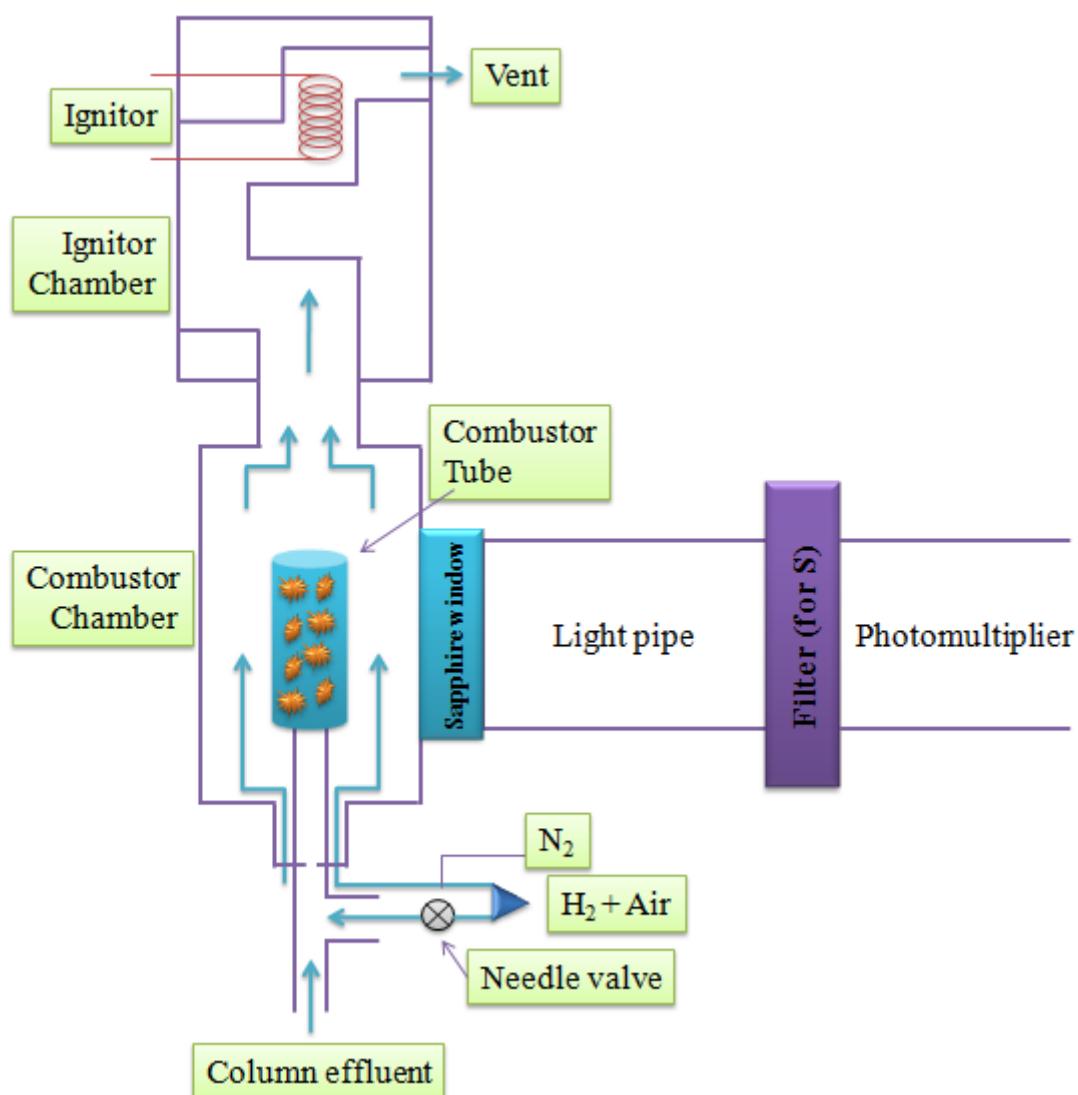


Figure III.5 : Scheme of a PFPD

A continuous flow of air and hydrogen mixed with the products coming from the column results in a flammable gas that ignites when in contact with a heat resistance. The resulting flame propagates in the detector in few milliseconds and burns the compounds coming from the column. The emitted photons of this combustion are then transformed in electrons, themselves amplified in a photomultiplier to finally be represented as a peak on a chromatogram.

II.1.3. Feedstock

Most of the studies found in the literature test the catalytic activity on specific compounds using feedstocks as simple as possible, neglecting thus the “matrix effect” [4,6]. However, catalyst life and efficiency depends on the feedstock properties and composition. As mentioned in the first chapter, industrial feedstocks are complex mixtures of different molecules, some of which act as inhibitors and directly affect the real activity of the catalyst and therefore the HDS efficiency.

In this work, to take the “matrix effect” into account in a more relevant way, we decided to work with a model feedstock enclosing the most representative compounds of a feedstock for deep-HDS. However, we did not add nitrogen compounds in this feedstock, which means that competition with HDN is not taken into account. The composition of our model feedstock is described in Table III.1 with the compounds characteristics.

Table III.1 : Characteristics of our model feedstock

Compounds		Formula	Boiling point (°C)	Concentration
Type	Name			
Paraffins	Heptane	C ₇ H ₁₆	99	30 wt%
	Dodecane	C ₁₂ H ₂₆	216	30 wt%
Olefins	Hexene	C ₆ H ₁₂	63	15 wt%
	Octene	C ₈ H ₁₆	123	15 wt%
Aromatics	Naphthalene	C ₁₀ H ₈	218	5 wt%
	Benzene	C ₆ H ₆	80	3 wt%
	Toluene	C ₇ H ₈	110	2 wt%
Sulfur compounds	Thiophene	C ₄ H ₄ S	84	100 wppm (S)
	Methylthiophene (<i>M-Thiophene</i>)	C ₅ H ₆ S	113	100 wppm (S)
	Tetrahydrothiophene (<i>THT</i>)	C ₄ H ₈ S	119	50 wppm (S)
	Benzothiophene (<i>BT</i>)	C ₈ H ₆ S	222	50 wppm (S)
	Dibenzothiophene (<i>DBT</i>)	C ₁₂ H ₈ S	333	100 wppm (S)
	4,6-dimethyldibenzothiophene (<i>4,6-DMDBT</i>)	C ₁₄ H ₁₂ S	340	100 wppm (S)

This model feedstock has a density of 671 g.L⁻¹ and a mean molar mass of 123 g.mol⁻¹. It is composed of 60 wt% of paraffins (saturated hydrocarbons – namely heptanes and dodecane), 30 wt% of olefins (unsaturated hydrocarbon – namely hexene and octene), and 10 wt% of aromatics hydrocarbons (naphthalene, benzene and toluene).

Concerning the sulfur content, the total concentration used is 500 wppm and as 4,6-DMDBT is the most difficult sulfur compound to convert under HDS conditions, it has an important contribution in this amount (100 wppm in sulfur as 4,6-DMDBT).

Sulfur concentration in our model feedstock is such that our experiments correspond to Deep-HDS and as in real feedstock, this concentration is mainly due to refractory molecules. It was thought to take at best the “matrix effect” into account.

Figure III.6 represents the conversion of DBT and 4,6-DMDBT in our model feedstock and in a feedstock composed of only paraffins over NM, a commercial catalyst precursor that will serve as reference from now (4 wt% NiO, 14 wt% MoO₃/γ-Al₂O₃, similar to catalysts classically described in the literature). It clearly illustrates how overestimating the conversion of those compounds is easy when not considering other compounds that can compete with them over the catalyst (cf. III.1.4.3 for the method used).

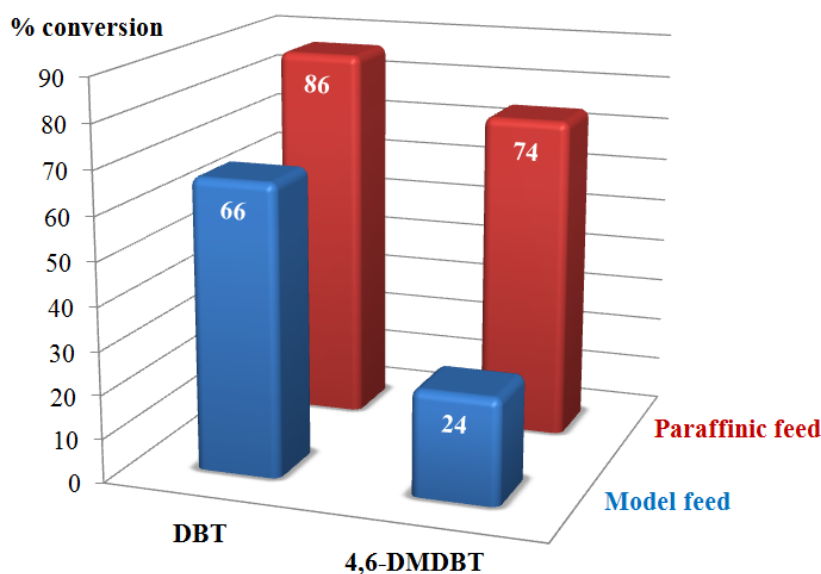


Figure III.6: Conversion of refractive sulfur compounds in different feedstocks – $p_{H_2} = 3.5$ MPa, 400 °C, $M_G/M_L = 5$, LHSV = 150 h⁻¹, catalyst: NM

The boiling range of this model feedstock goes from 63 °C to 218 °C. We do not include the sulfur compounds in this consideration since their concentrations are very low compared to the general composition. Having the pre-heater set at 250 °C thus ensures that the feedstock will enter the reactor in the gas phase.

III.1.4. Experimental procedure

This part concerns the preliminary work that has to be done before starting the catalyst tests, from the preparation of the catalytic bed to the experimental parameters considered for in our experimental plan.

III.1.4.1. Preparation of the catalytic bed

The HDS reactions will be carried out in a down-flow fixed bed tubular reactor. An accurate measurement of the catalytic activity of the materials studied will only be possible if the catalysts are conformed in an adequate manner. If used as powders, preferential paths can be formed for the reactants flow and not all the catalyst will participate in the process. Moreover, pressure drops can have an important effect. If particle size is too large, external diffusion problems can affect the activity results observed. Therefore, the powder of the catalyst precursor must be pelletized, crushed and sieved to particles of an optimum size. The pellets are prepared using a pelleting-press at 3.5 t for 1 min, conditions that do not affect significantly the specific surface area. The pellets are then crushed and sieved to obtain particles with size comprised between 0.250 μm and 0.425 μm .

The desired quantity of catalyst precursor is mixed with silicon carbide (Carborundum SiC) up to 2 mL to form the catalytic bed. SiC is inert toward the reaction of HDS and thus will not interfere with the conversion results. The reactor is filled up with some glass wool before introducing the catalytic bed so that the particles of catalyst are retained and stay in the reactor.

III.1.4.1.1. Liquid Hourly Space Velocity (LHSV)

The volume of catalyst to test depends on the Liquid Hourly Space Velocity (LHSV). LHSV is the ratio of the hourly volume of oil processed referred to the volume of catalyst. It is generally expressed as $\text{v.v}^{-1}.\text{h}^{-1}$ or h^{-1} . As such it controls the residence time of the liquid reactants in typically cylindrical reactors. LHSV is simply an approximate way of estimating the amount of catalyst one would need to purchase for a given feed capacity and product yield. The LHSV is calculated following the equation (1):

$$\frac{L_F}{C_V} = y \quad (1)$$

where L_F is the liquid flow, the direct value expressed in $\mu\text{L.h}^{-1}$ set on the injection pump, C_V the volume of catalyst used for the reaction in μl and y the LHSV in h^{-1} . The higher the LHSV the less time the feedstock is in contact with the catalysts and thus the lower the conversion. We calculated a set of LHSV (Table III.2) for different volumes of catalysts and liquid flows, based on our commercial reference NM whose density is estimated to be 646 g.L^{-1} .

Table III.2: Values of LHSV depending on L_F and C_V

LHSV (h^{-1})							
Mass of catalyst (g)	Volume of Catalyst (mL)	Liquid flow ($\mu\text{L.min}^{-1}$)					
		50	100	200	300	400	500
1	1.548	2	4	8	12	16	19
0.8	1.238	2	5	10	15	19	24
0.6	0.929	3	6	13	19	26	32
0.4	0.619	5	10	19	29	39	48
0.3	0.464	6	13	26	39	52	65
0.2	0.310	10	19	39	58	78	97
0.1	0.155	19	39	78	116	155	194

III.1.4.1.2. Activation of the catalyst precursors: sulfidation

A sulfidation step converts the metal oxides into the metal sulfides, which are the active catalysts for HDS. Our equipment is designed to realize this step *in situ*, which appears to be the best solution to avoid any re-oxidation by possible contact with air. Once the system is checked to be leak free, the catalytic bed is subjected to a gas flow of 10 % in volume of H_2S in H_2 for 5 h at 400°C . This sulfidation protocol has been optimized in previous researches [7]. The catalytic test is realized afterwards.

III.1.4.2. Reaction conditions

One important parameter to consider while doing catalytic tests on the HDS is the ratio of gas to liquid. (eq. 2) and (eq. 3) give their values respectively:

$$M_G = \frac{x}{24.4} \quad (2)$$

where M_G is the molar flow of gas in $\text{mol} \cdot \text{min}^{-1}$, x the gas flow in $\text{L} \cdot \text{min}^{-1}$ and $24.4 \text{ L} \cdot \text{mol}^{-1}$ is the molar volume of gas at 25°C and atmospheric pressure.

$$M_L = \frac{x \times y}{z} \quad (3)$$

where M_L is the molar flow of the feedstock in $\text{mol} \cdot \text{min}^{-1}$, x is the flow in $\text{L} \cdot \text{min}^{-1}$, y is the density of the feedstock in $\text{g} \cdot \text{L}^{-1}$ and z the molar weight in $\text{g} \cdot \text{mol}^{-1}$.

HDS reactions are carried under H_2 atmosphere. The higher the M_G/M_L is, the more hydrogenation we have compared to direct desulfurization. Industrially, this ratio is set around 4. Regarding our own technical limitations – minimum and maximum flows for a proper work of both the injection pump and the flow-meter dedicated to H_2 – we chose to work at a ratio close to 5 to keep closer to Industrial processes but we also carried out some experiments at a ratio of 9 (classical in lab catalytic tests).

In order to vary conversion, experiments were performed at three different temperatures for most of the catalysts. Starting at 320°C , we then switch to 360°C to finish at 400°C . Finally the experiment at 320°C is repeated, and this will give clue concerning the deactivation of the catalyst. The steady state in our system is reached after 3 hours time on stream (TOS), we thus opted for experiments of minimum 4 hours TOS. We recovered liquid samples at the reactor outlet every 40 minutes the first two hours then every hour till the end and analyzed by gas chromatography. Between each experiment, we regenerate the catalyst by subjecting it again to a gas flow of 10 % in volume of H_2S in H_2 for 1 h at 400°C . Among the different experiments we carried out, we verified that the regeneration time was enough. Figure III.7 shows that regenerating the catalyst 5 hours renders the same activity to the catalyst than 1 hour regeneration which validates our choice (cf. III.1.4.3 for the method used).

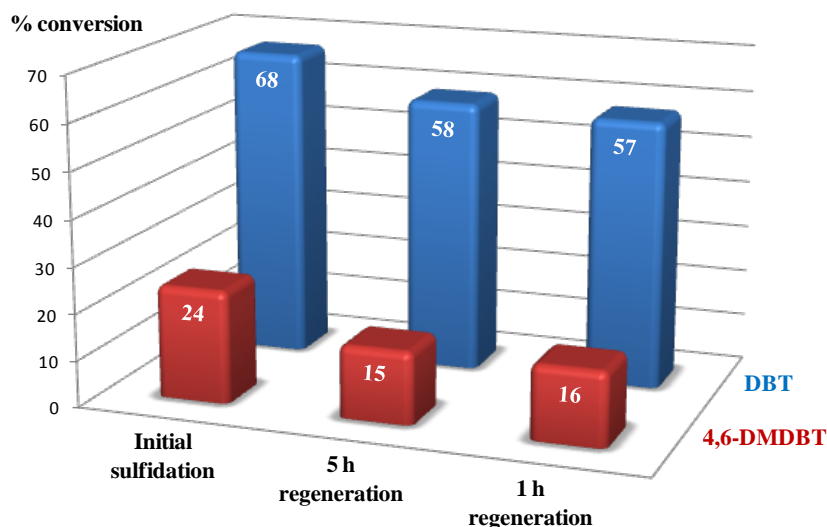


Figure III.7: Effect of regeneration time on the conversion – $p_{H_2} = 3.5$ MPa, 400 °C, $M_G/M_L = 5$, $LHSV = 150$ h⁻¹, catalyst: NM

III.1.4.3. Product analysis by gas chromatography

In the chromatogram, the area under a peak is proportional to the amount of an analyte. By mathematically integrating its area, the concentration of an analyte in the original sample can be determined. With the FID, the concentration in weight of the detected compounds is directly obtained. With the PFPD, we don't have an immediate evaluation of the concentration, yet they can be calculated by using external standards: therefore a calibration curve is created by finding the response for a series of patterns with known concentrations of analyte and by determining the relative response factor of an analyte.

Classically, the relative response factor is the expected ratio of an analyte to an internal standard and is calculated by finding the response of a known amount of analyte and a constant amount of internal standard (a chemical added to the sample at a constant concentration, with a distinct retention time to the analyte). Yet, in our case we normalize the response of the specific PFPD detector to the amount of sample injected, which will be proportional to the total response obtained in the FID.

Since our model feedstock presents many species with various boiling points comprised in a large range of temperature (Table III.1), we have optimized a temperature program for analyzing our reaction mixture in order to have maximum sensitivity and peak resolution at a minimum analysis time (Figure III.8).

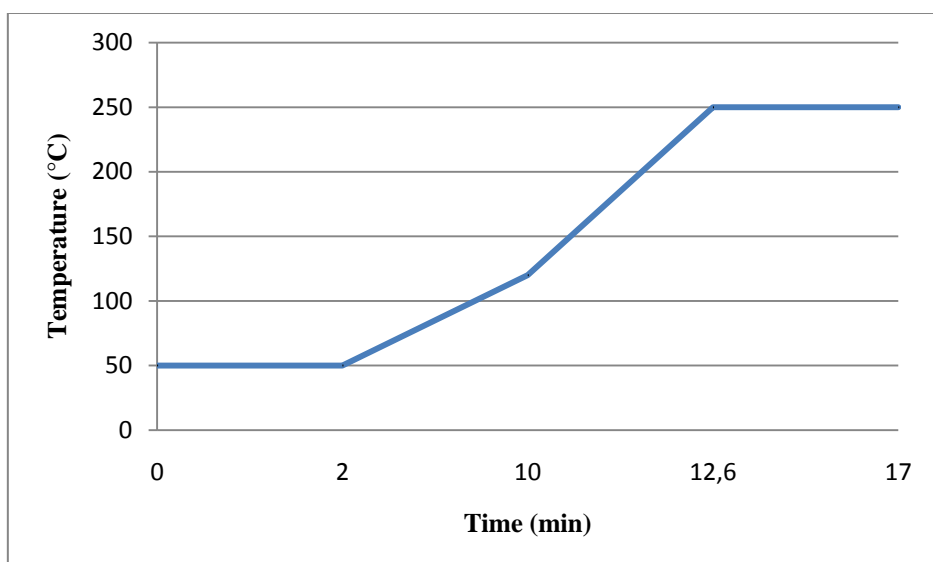


Figure III.8 : Temperature program of our GC

Temperature of the injector and of the detectors is 300°C. The column pressure has been set at 30 psi, in order to have a carrier gas flow through the column of 2.7 mL.min⁻¹. Table III.3 summarizes the retention times of the different analytes we meet when analyzing our samples in these conditions.

Table III.3: Retention times for our analytes (*: present after catalytic test)

Hydrocarbons	Retention time (min)	Sulfur compounds	Retention time (min)
Hexene	1.234	Carbon disulfide	1.157
Hexane*	1.258	Thiophene	1.607
Benzene	1.535	THT	3.062
Heptane	1.776	BT	11.454
Toluene	2.447	DBT	15.647
M-Thiophene	2.536	4,6-DMDBT	16.507
Octene	2.792		
Octane*	2.986		
Tetralin*	10.946		
Naphthalene	11.379		
Dodecane	11.791		

Traces of carbon disulfide may appear on the chromatograms as it is used to clean the micro-syringe between two injections and traces remain in the analysis. Yet, it does not affect the results since it appears at a short retention time (1.157 min) and does not interfere with other signals.

Now we ensure that our model feedstock takes the “matrix effect” into account, that our regenerating program of the catalyst have been proved to be efficient and that we optimized a temperature program in the chromatogram specific to the detection of the compounds present in our model feedstock, the next part dedicates to our study of the catalytic activity of our bulk catalysts.

III.2. Catalytic activity checking

Before setting up the HDS reactor, we carried out some preliminary tests on our material to make sure that it presents activity toward the HDS reaction. Those tests were carried out in a high throughput reactor developed and patented at the ITQ: the Spider Reactor.

III.2.1. Spider Reactor

The Spider Reactor is a system of 16 continuous fixed bed parallel reactors, able to work up to 8 MPa and 700 °C [8,9,10]. Each reactor is fed independently by means of one liquid and one gas mass flow controller. The temperature and pressure are also measured in each catalyst bed. The simultaneous catalytic tests were carried out at 3 MPa total pressure (80 % H₂, 20 % N₂), temperature of 360 °C and the LHSV of 19 h⁻¹. Because of the inherent specificities of its hardware, we had to set the M_G/M_L ratio at 9. The amount of catalyst in each fixed bed reactor is 100 mg mixed with carborundum for a total bed volume of 2 mL and catalyst particle size 0.2 - 0.4 mm. Our reaction products were analyzed using an online gas chromatograph equipped with a FID and a PFPD.



Figure III.9: Catalytic reactor (Spider Reactor) for high throughput testing [8]

III.2.2. Tests preparation

For the first tests, we chose three catalysts of different composition but with a similar specific surface area and the commercial catalyst NM for the reference to evaluate the activity of our materials. The new bulk catalysts compared with the reference in this experiment were the ones that were developed with the highest S_{BET} on that time: MT1501, MT1405 and MT2001 (Table III.4).

“NiMo” catalysts classically prepared at ITQ by impregnation method on $\gamma\text{-Al}_2\text{O}_3$, as well as the reference catalyst, contain around 15 wt% of active phase. To be in the same weight proportion and to have higher amount of total material, we mixed our samples with SiO_2 supplied by Aldrich (nanopowder purity 99.5 %, 10 nm, $d = 2.2$, $M = 60.09 \text{ g.mol}^{-1}$). The preparation of the catalytic bed is the same than described in III.1.4.1.

When working with the Spider Reactor, the sulfidation of our catalysts is carried out in a different reactor and according to the protocol described in III.1.4.1.2. Unfortunately, this implies a slight re-oxidation of the catalysts during the transfer from one reactor to the other.

The specific surface areas (S_{BET}) given are those measured on the calcined powder before sulfidation of the samples. For those experiments, we used as references fresh NM (not sulfided) and NMS which is also a commercial catalyst that has been sulfided by the supplier and presents the same characteristics.

Table III.4: Sample tested for the preliminary experiments

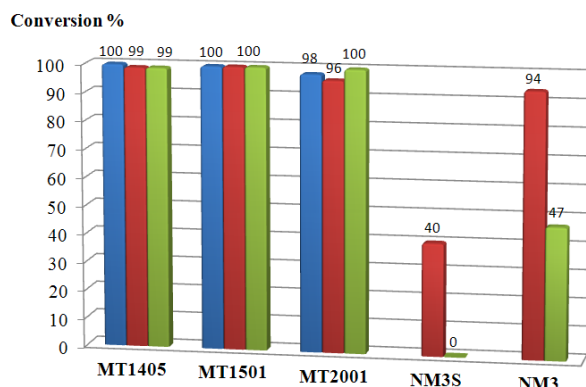
Samples	at% Ni	at% Mo	Ni/Mo (molar ratio)	S _{BET} (m ² .g ⁻¹)
MT1501	53	47	1.1	26
MT1405	55	45	1.2	25
MT2001	57	43	1.3	25
NM	36	64	0.6	200
NMS	36	64	0.6	200

III.2.3. Results

The results obtained for the conversion of the most refractory sulfur compounds are schematized on [Figure III.10](#). Regarding dibenzothiophene (DBT), the three bulk catalysts showed a high conversion rate close to 100 % with almost no deactivation after 32 h TOS. Their activity was even higher than the one of the commercial catalyst NM (94 % after 24 h TOS down to 47 % after 32 h TOS), and its sulfide equivalent NMS (40 % after 24 h TOS down to 0 % after 32 h TOS). This tendency was also observed for the other sulfur compounds present in the feed (Thiophene, M-Thiophene, THT and BT) and were therefore not considered in this part of the study.

Concerning 4,6-Dimethyldibenzothiophene (4,6-DMDBT), MT1501 reaches a conversion of 73 % after 8 h TOS that falls down to 48 % conversion after 32 h TOS. MT1405 displayed 68 % conversion and MT2001 56 % after 8 h TOS. Both fell below 20 % conversion after 32 h TOS. Although in this case the two commercial catalysts showed better activity than our new materials (80 and 82 % for NMS and 75 % down to 54 % for NM), it was shown that they all presented activity for hydrodesulfurization of sulfur compounds within the model feedstock.

DBT



4,6-DMDBT

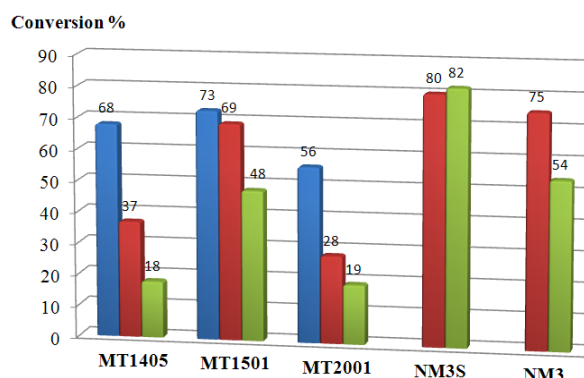


Figure III.10: Conversion vs. TOS (8 h, 24 h, 32 h)

Our materials present an activity toward the HDS reaction and show good performances regarding the sulfur compound of reference, 4,6-DMDBT, even diluted in SiO₂. We thus decided to go on with the project, continuing to upgrade our material and switch to the reactor dedicated to HDS reaction.

III.3. Experiments with HDS-specific reactor

In this second part of the catalytic study, the setup used for the catalytic tests will be the one described in III.1.1. The materials tested are no longer diluted with SiO₂ (pure bulk catalysts) and the sulfidation takes place in the reactor right before starting the reaction. Blank reactions carried out under the different tested conditions showed that after 4 hour TOS, whatever the values of LHSV, temperature or M_G/M_L, we observe no conversion of any of our sulfur compounds which means we will not overestimate the conversion calculated for our experiments.

III.3.1. First tests: materials and experimental conditions

We chose three catalyst precursors of different composition and S_{BET} . MT040 and MT041 present similar S_{BET} what allows us to evaluate the influence of their composition. MT042 with a higher Ni content and a surface area more than double was used to study the influence of the M_G/M_L ratio. Table III.5 summarizes the materials and experimental parameters.

Table III.5: Sample description and experimental conditions

Sample	at% Ni	at% Mo	Ni/Mo* (molar ratio)	S_{BET} ($\text{m}^2 \cdot \text{g}^{-1}$)	LHSV (h^{-1})	Temperature ($^{\circ}\text{C}$)	M_G/M_L
MT040	42	58	0.7	45	19	320	5
						360	
						400	
MT041	18	82	0.2	51	19	320	5
						360	
						400	
MT042	66	34	1.9	110	19	320	5
						360	5
							8.17
						400	5
							8.17
NM	36	64	0.6	200	19	360	5
							8.17
						400	5
							8.17

* At that time of the PhD, materials were prepared on the basis of NiO/MoO₃ weight ratio, what explains those Ni/Mo molar ratios.

The conversion values obtained in our experimental conditions are very high, comprised between 90 and 100 % for all our sulfur compounds, including DBT and 4,6-DMDBT and independently of the catalytic material tested. Although concluding is therefore delicate, we can draw a general tendency of their catalytic behavior.

III.3.1.1. Influence of the M_G/M_L ratio

We evaluated the influence of this parameter focusing our attention on sample MT042. Its activity toward sulfur compounds is very high whatever the reaction conditions. The conversion is higher than 98 % for all sulfur compounds. However, other components of the model feed are also susceptible of conversion under HDS conditions, and their evolution with the experimental conditions can give us information regarding the catalytic systems. This is the case of the hydrogenation of aromatic compounds, such as benzene and naphthalene present in our model feedstock.

Cetane Number (CN) is a significant expression of diesel fuel quality, a measure of a fuel's ignition delay: the time period between the start of injection and start of combustion (ignition) of the fuel. In a particular diesel engine, the higher the CN, the shorter the ignition delay periods. Cetane values are closely related to the amount of aromatics contained in the diesel fraction: high aromatic content distillates have low cetane values and it is necessary to saturate aromatic rings through a deep hydrogenation process prior to performing the ring opening reaction (thus increasing CN). Hydrogenation of aromatics such as benzene and polyaromatics such as naphthalene is therefore an expected effect of hydrotreatment and since Deep-HDS catalysts present a high hydrogenation capacity, they are of particular interest toward this application [11,12].

In our experiments, benzene presents a conversion higher than 97 % for all catalysts, and therefore discussion is focused on naphthalene conversion. Under our reaction conditions, only one ring of naphthalene is hydrogenated and the product obtained is tetralin (1,2,3,4-tetrahydronaphthalene). Further hydrogenation would have given decalin. It has to be noted that conversion decreases with the increase of the reaction temperature, which is in agreement with the exothermic nature of the hydrogenation reaction: high temperatures inhibit it. As can be seen in Figure III.11, MT042 even shows a better activity than NM at the lowest M_G/M_L ratio. At higher H_2 partial pressure ($M_G/M_L = 8.2$), NM increases its hydrogenation activity and only then it gives conversion values close to those obtained with MT042. In other words, the bulk catalyst MT042 is able to achieve at the lowest M_G/M_L (of 5) the same hydrogenation levels obtained with the reference NM at a considerably higher M_G/M_L (of 8.2). Deep-HDS predominantly goes through the HYD path to hydrodesulfurize sterically hindered sulfur compounds - particularly 4,6-DMDBT - path that is hydrogen consuming, and therefore, this results has a considerable importance. As H_2 saving is one of the main priorities

in a refinery, a catalyst presenting good hydrogenation quality at low M_G/M_L will be relevant from an industrial perspective.

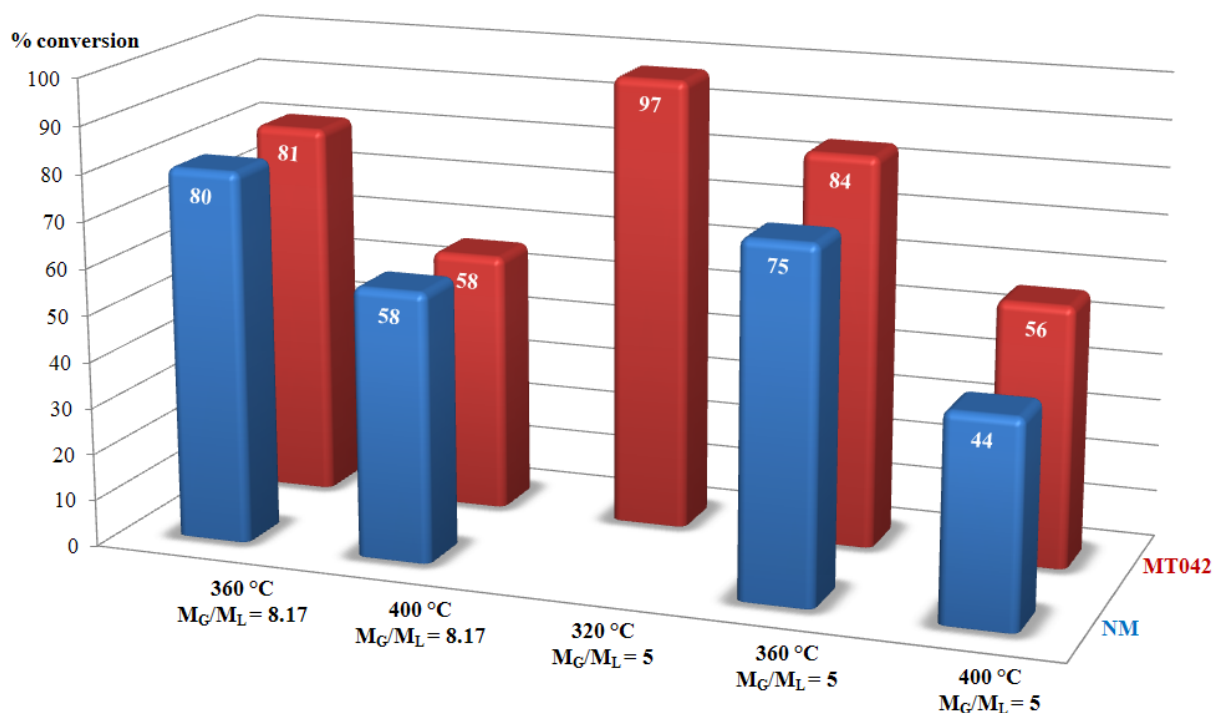


Figure III.11: conversion of naphthalene into tetraline

Our bulk material shows better aromatics hydrogenation activity than the commercial reference. This suggests that the HDS of 4,6-DMDBT should also perform better on our material since its HDS goes through the HYD path (cf. Chapter I).

III.3.1.2. Influence of the composition

When comparing the results obtained with bulk catalysts MT040 and MT041, with close S_{BET} but different chemical composition, again we obtain a very high conversion of all the sulfur compounds in all the conditions used, which renders difficult any conclusion at this time and no evident trend appears. Experiments at higher LHSV (shorter contact time between the feed and the catalyst) are requested to better discriminate between the different materials synthesized. However, what we can say so far is that our catalysts present efficiency similar to that of the commercial NM.

III.3.2. Higher LHSV

The previous experiments made us realize the need of refining our experimental conditions for the following tests. We fixed the M_G/M_L at 5, a condition that significantly reduces H_2 consumption compared to classical hydrotreating lab experiment, and in these conditions of feed partial pressure we tested three higher LHSV: 39 h^{-1} , 75 h^{-1} and 150 h^{-1} , in order to decrease the overall conversion and to better compare the intrinsic activity of our materials.

Under HDS condition, the low but gradual loss of catalytic activity is compensated by an increase in the process temperature. Since H_2S is the byproduct of HDS reaction, its presence in a hydrotreating reactor is unavoidable. Moreover, at low partial pressures, H_2S also plays a beneficial role in maintaining the sulfided state of the hydrotreating catalysts used in the hydrotreating process. H_2S may in some cases (i.e. under specific conditions) enhance hydrogenation. This has been observed with HDS of DBT on MoS_2 and $CoMo/Al_2O_3$ catalysts [13,14], and in the HDS of 4,6-DMDBT over $NiMo/C$ [15,16]. This could result from an increase in the surface SH groups formed by H_2S dissociation on the coordinately unsaturated sites. Therefore, at low H_2S pressures, its presence is beneficial, and even necessary. The problem is its inhibiting nature at higher concentrations. An HDS feedstock contains enough sulfur compounds to keep an adequate H_2S concentration within the reaction media. In deep-HDS however, the amount of sulfur in the feedstock is not enough to regenerate the catalyst and industrials usually artificially add sulfur in the stream either by adding dimethyldisulfide (DMDS) into the feedstock to be treated or by using a mixture of H_2S and H_2 as reactant gas. In our case, we did not add any DMDS to our feed or H_2S to the H_2 stream and for this reason we might see a stronger decrease of activity with TOS compared to industrials data.

Since we already work with the minimum flows the liquid pump and the gas flow-meter can deliver, we increased the LHSV value by using lower amount of catalyst precursor to prepare the catalytic bed but keeping the same total bed volume, always according to (eq. 1) and Table III.2. Decreasing the contact time between the catalyst and the feed logically induces a decrease in the conversion of our sulfur compounds.

III.3.2.1. Tested materials

Table III.6 (for “NiMo”) and **Table III.7** (for “CoMo”) summarize the materials and experimental conditions used. The bulk catalysts were compared according to their composition, S_{BET} and promoter nature criteria. We have seen in chapter II that powders with an excess of nickel contain the β -phase of NiMoO_4 , the most active phase toward HDS. For this reason, we choose to work with Ni-rich materials since we believe they are more efficient catalyzing this reaction. All of the materials present high S_{BET} but somehow lower than what have been announced in chapter II since this study was performed in parallel with our attempts to increase S_{BET} . MT071 was used as fresh powder in order to verify the relevance of calcination in the case of our material. CM is the equivalent of NM, and is our commercial reference concerning the “CoMo” catalyst precursors (3 wt% CoO , 14 wt% $\text{MoO}_3/\text{Al}_2\text{O}_3$), and the precursor bulk catalyst we decided to test is the stoichiometric CoMoO_4 (MT081).

Table III.6: Sample description and experimental conditions (“NiMo” type)

Sample	at% Ni	at% Mo	Ni/Mo (molar ratio)	S_{BET} ($\text{m}^2 \cdot \text{g}^{-1}$)	M_G/M_L	Temperature ($^{\circ}\text{C}$)	LHSV (h^{-1})
NM	36	64	0.56	200	5	320	39 - 75 - 150
						360	
						400	
MT043	69	31	2.2	115	5	320	150
						360	
						400	
MT044	54	46	1.2	110	5	320	39
						360	
						400	
MT071	61	39	1.6	97	5	320	39 - 75 - 150
						360	
						400	
MT072	62	38	1.6	80	5	320	39 - 75 - 150
						360	
						400	

Table III.7: Sample description and experimental conditions (“CoMo” type)

Sample	at% Co	at% Mo	Co/Mo (molar ratio)	S_{BET} ($\text{m}^2 \cdot \text{g}^{-1}$)	$M_{\text{G}}/M_{\text{L}}$	Temperature ($^{\circ}\text{C}$)	LHSV (h^{-1})
CM	29	71	0.4	200	5	320	150
						360	
						400	
MT081	50	50	1	40	5	320	150
						360	
						400	

III.3.2.2. Influence of the composition

The influence of the composition will be performed by comparing MT043, MT044 and MT072 that present different Ni at% and relatively close S_{BET} . To compare the effect of the powder composition in the most relevant way minimizing the contribution of other factors such as S_{BET} , we must normalize the conversion by the total surface area of the tested powders. Yet, this is relevant only if all the catalysts show a conversion percentage below 100 % for the considered reactants. As conversion is varied by increasing the reaction temperature, it is preferred to work with marked conversion differences between the different temperatures. If not, we may be underestimating the activity per square meter.

At a LHSV of 39 h^{-1} (Figure III.12), only the conversion of naphthalene, DBT and 4,6-DMDBT permit to make such a comparison. The rest of the sulfur compounds display conversions close to 100 % and the olefins are fully converted into their corresponding paraffins, even at the lowest reaction temperature. When we focus on the conversion of naphthalene (hydrogenation of one aromatic ring) and 4,6-DMDBT (HDS via hydrogenation of one of the aromatic ring (HYD path)), both bulk catalyst MT044 (54 at% Ni) and MT072 (62 at% Ni) display better or equivalent results than NM (absolute conversion and conversion per square meter). Our materials present better hydrogenation activity than NM, showing thus better activity toward the HDS of 4,6-DMDBT. Concerning DBT, the three studied catalysts show a similar activity, MT072 being the less active. However, this sample presents also the lowest surface area, so when we consider conversions per surface units, even though they are close in value, MT072 is the most active material toward HDS of DBT and 4,6-DMDBT, and MT044 also present higher activity than NM.

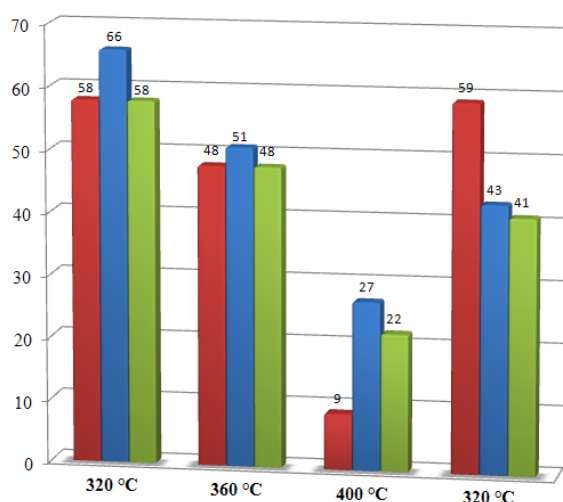
For similar conversion under similar operating conditions, we need a lower mass of our material than of the commercial reference NM.

We also highlight that for HDS of 4,6-DMDBT, we obtain the same absolute conversion % with MT044 and MT072 than with NM but at a temperature 40 °C lower.

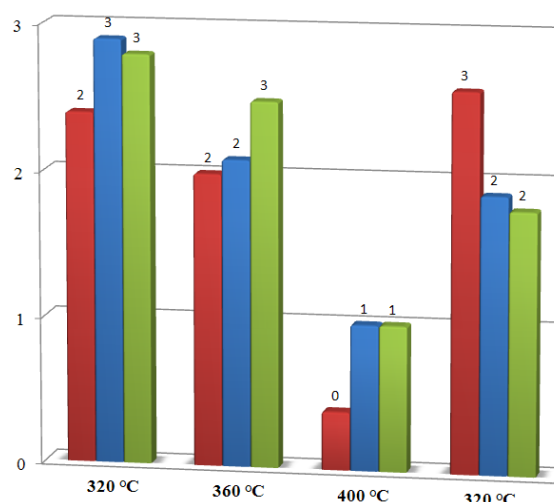
For similar conversion with similar amount of catalysts, we can work at lower temperature with our materials than with NM.

The results represented in [Figure III.12](#) also give information concerning the possible deactivation of the catalysts. Conversion level, as stated before, is varied by operating at increasing temperatures. As mentioned in [III.1.4.2](#), in order to verify if the catalyst has been deactivated along the different experiments a final test is performed at the lowest temperature, in the same conditions as the first test of the series. If results are reproduced, no deactivation has occurred, as in the case of NM. However, in the case of MT044 and MT072, conversion obtained in the final experiment is lower than the one obtained in the same conditions with the fresh catalyst, indicating that they deactivate more than NM. A more complete deactivation study is needed in future work on this project.

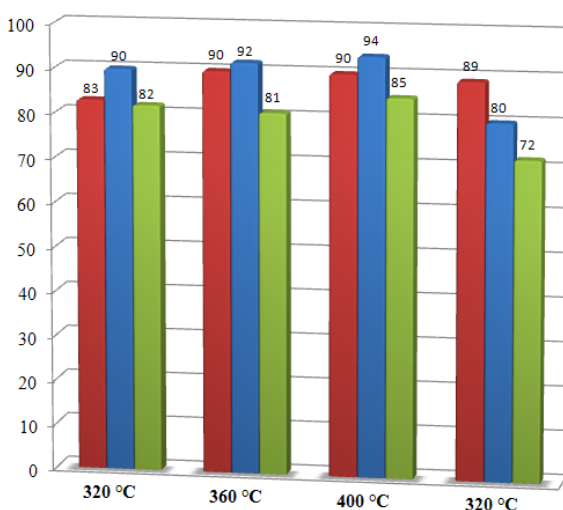
Naphthalene (conversion %)



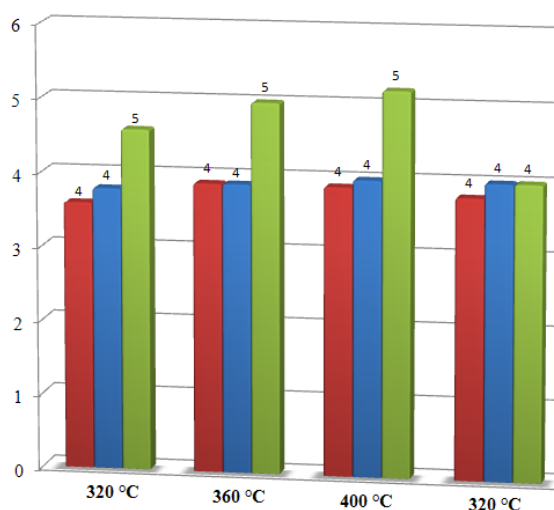
Naphthalene (conversion %.m⁻²)



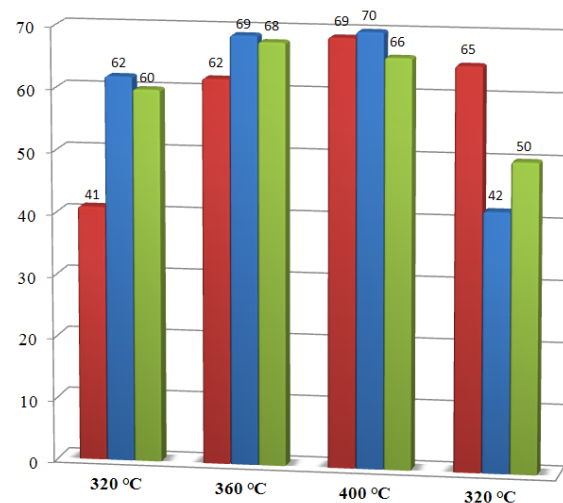
DBT (conversion %)



DBT (conversion %.m⁻²)



4,6-DMDBT (conversion %)



4,6-DMDBT (conversion %.m⁻²)

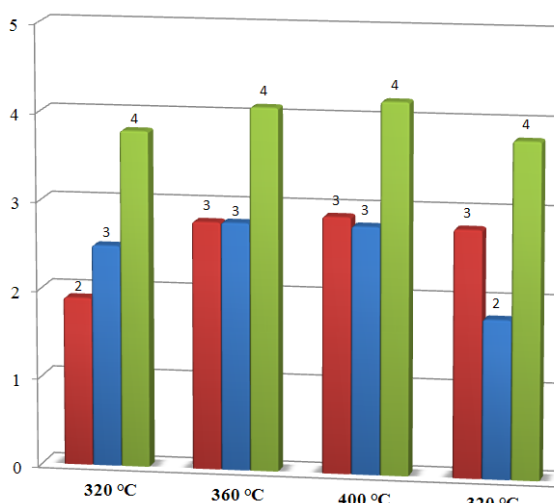
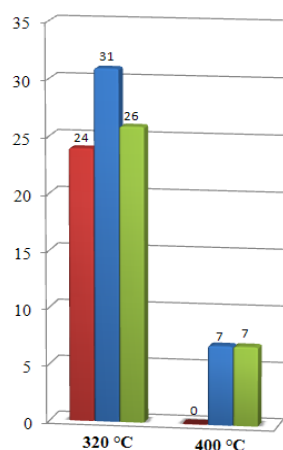


Figure III.12: Influence of the composition on the catalytic activity (NM, MT044 = 54 at% Ni, MT072 = 62 at% Ni, LHSV = 39 h⁻¹)

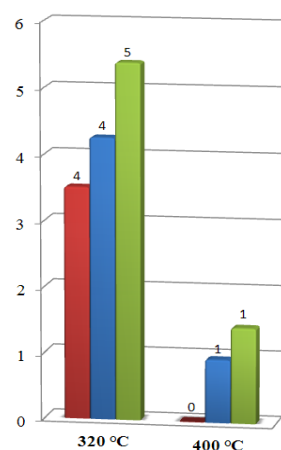
With the aim at obtaining larger differences among the catalysts, LHSV was increased to 150 h^{-1} (Figure III.13, note that only 320°C and 400°C were carried out at 150 h^{-1} for MT072). Comparing MT043 (69 at% Ni) and MT072 (62 at% Ni), it can be seen that MT043 is better regarding absolute conversion of naphthalene and DBT than MT072 and the reference NM, but when it comes to conversion per surface, the values are very close and it is difficult to assess any statement. However, MT072 appears as the best catalyst for naphthalene conversion, what we can relate to a higher hydrogenation activity. This is confirmed by its better activity for the conversion $\%.\text{m}^{-2}$ of 4,6-DMDBT over the other samples. Concerning DBT, MT072 shows bad activity compared to MT043 and NM by mean of absolute conversion, but the three of them behave similarly after normalization and it is more difficult to draw a tendency for the conversion of this compound.

Naphthalene

(conversion %)

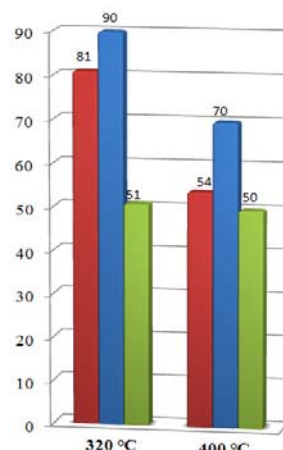


(conversion $\%.\text{m}^{-2}$)

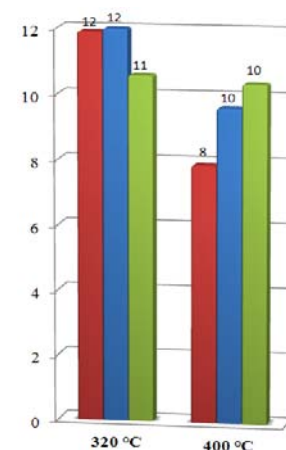


DBT

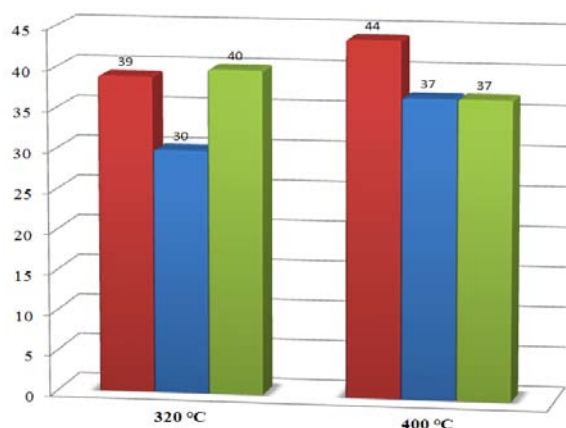
(conversion %)



(conversion $\%.\text{m}^{-2}$)



4,6-DMDBT (conversion %)



4,6-DMDBT (conversion $\%.\text{m}^{-2}$)

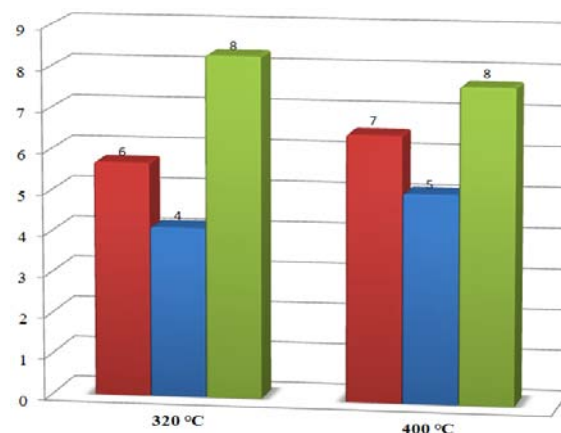


Figure III.13: Influence of the composition on the catalytic activity (NM, MT043 = 69 at% Ni, MT072 = 62 at% Ni, LHSV = 150 h^{-1})

Combining the results of the two studies at different LHSV we have the following trend in activity: MT072 (62 at% Ni) \geq MT044 (54 at% Ni) and MT072 (62 at% Ni) \geq MT043 (69 at% Ni). This suggests that it exists an optimum atomic percentage of Ni in the material for which the conversion of sulfur compounds is maximized, leading in this way to the highest catalytic activity (Figure III.14). The hypothesis we propose to explain this phenomenon is that the higher the Ni content in the bulk material, the higher the proportion of β -NiMoO₄ phase present in our HDS catalyst precursor. As we now know, when sulfided, this is the most active phase toward HDS (chapter II, II.2.1 [17]). It is known for long that the active sites are MoS₂ [18,19] whereas Ni has a promoting effect. An excess of Ni will cover the MoS₂ surface and may reduce the accessibility of sulfur compounds to the active sites. There should be a maximum value of Ni at% above which having the β -phase does not compensate the diminishing of active sites. If so, this maximum is comprised between 54 and 69 at% of nickel.

We assume that there is an optimum nickel content for our material corresponding to a maximum catalytic activity for the HDS reaction.

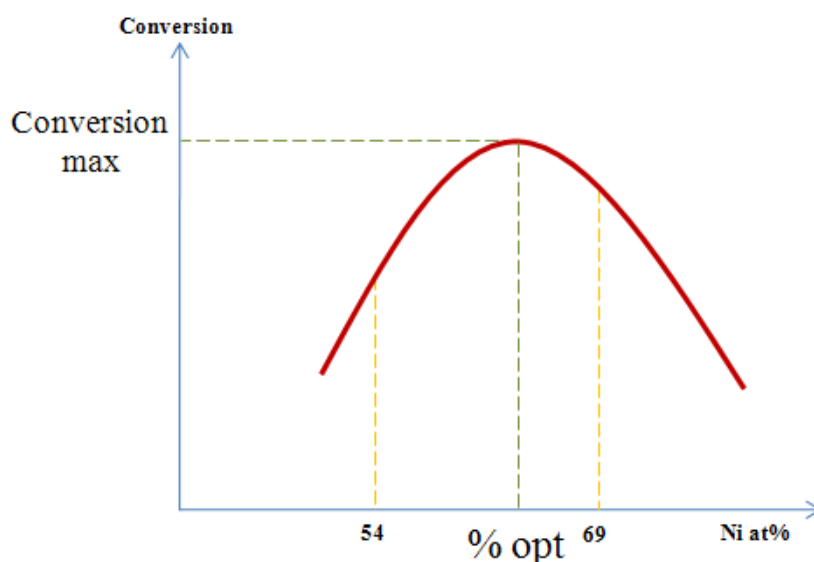


Figure III.14: Possible relation between Ni content and catalytic activity

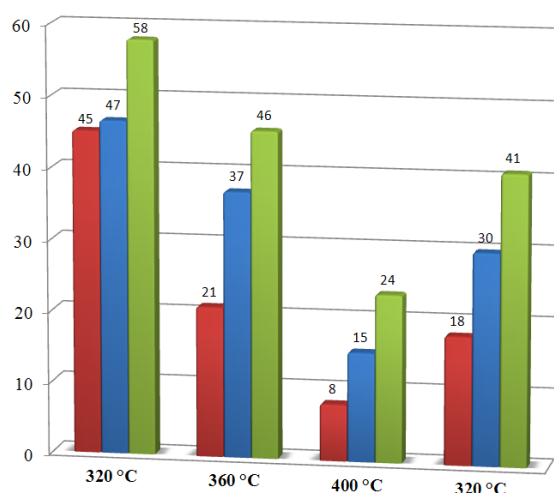
III.3.2.3. Influence of the calcination

The two powders MT071 and MT072 present a similar composition and relatively close S_{BET} . Since MT071 was not pre-calcined before sulfidation and catalytic tests, those two materials can be used to verify whether our powders really need a pre-calcination or not.

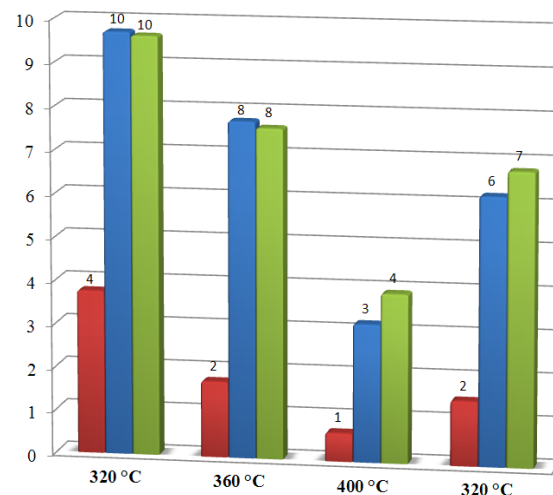
We know from chapter II that our fresh powders are clean from carbon and nitrogen that would poison the catalyst and calcination does not remove significant amount of them. Moreover, it induces a decrease in S_{BET} while our primary objective is to obtain the highest possible one, avoiding calcination should prevent from this inconvenient (cf. ID cards of the powders and Figure II.21). Moreover, we know that our fresh powders evolve toward the β -NiMoO₄ when heating at 400 °C (Figure II.16). Our sulfidation program is carried out at this temperature and therefore the idea also aimed at working directly with the β -phase: we would obtain this phase during the heating step before introducing H₂S in the reactor (the mixed oxide should not be reduced under the H₂ atmosphere).

We will consider for discussion the results from the experiments carried out at a LHSV of 75 h⁻¹ and we will compare the conversions of naphthalene, DBT and 4,6-DMDBT obtained with the two catalysts and with the reference (Figure III.15). Both MT071 and MT072 display better results than NM. They present a similar conversion (%.m⁻² of catalyst) of naphthalene into tetraline with slightly less deactivation for MT071 than for MT072. Regarding the sulfur compounds, both have similar activity toward DBT, with higher conversion per meter square than NM but not by mean of absolute conversion. However, when it comes to 4,6-DMDBT, MT071 appears to be the best catalyst. Moreover, its higher specific surface area permits to always have a better absolute conversion than MT072. Both catalysts outperform NM in this case.

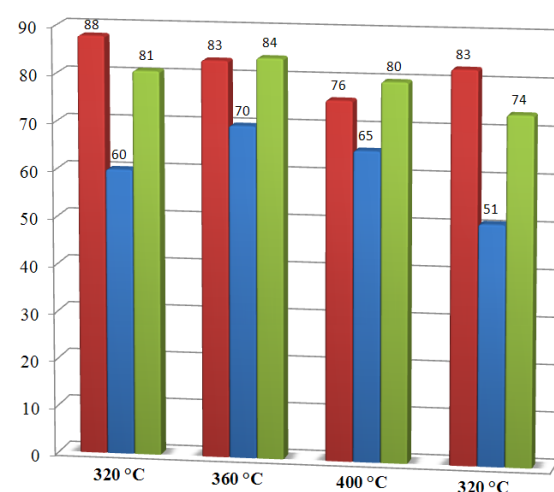
Naphthalene (conversion %)



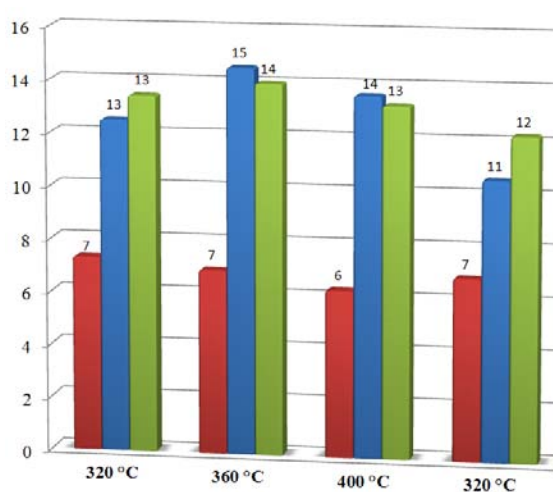
Naphthalene (conversion %.m⁻²)



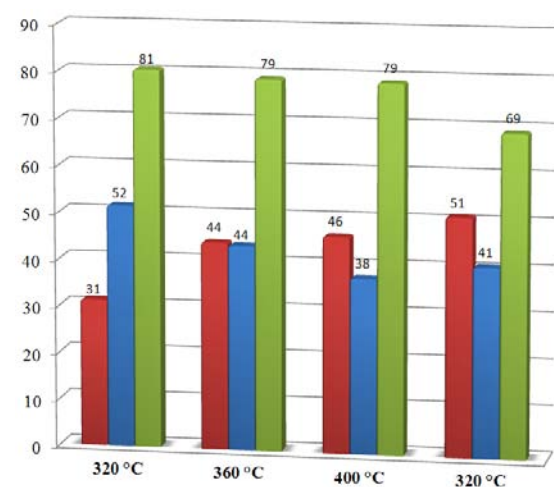
DBT (conversion %)



DBT (conversion %.m⁻²)



4,6-DMDBT (conversion %)



4,6-DMDBT (conversion %.m⁻²)

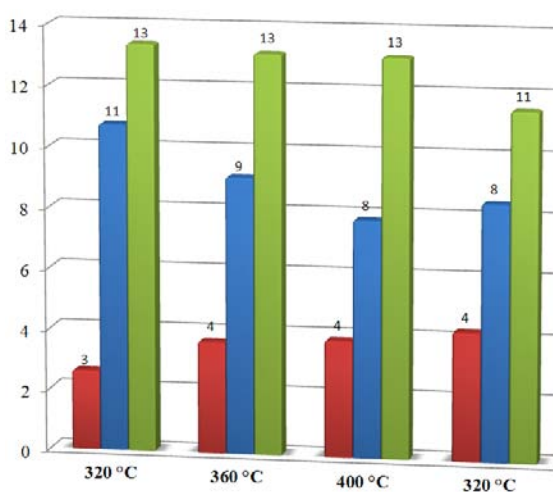


Figure III.15: Influence of the pre-treatment on the catalytic activity (NM, MT072 = calcined, MT071 = not calcined, LHSV = 75 h⁻¹)

Those results tend to confirm the fact that calcination of our catalyst precursors previous to catalytic reaction does not provide us with the best catalyst precursor and on the contrary deprives us from higher S_{BET} that permit higher absolute conversion percentage. Regarding the activity of those materials toward 4,6-DMDBT, we believe that our hypothesis that the sulfidation is realized on $\beta\text{-NiMoO}_4$ is reinforced.

Calcination of our materials previous to catalytic reaction lowers their activity toward the HDS reaction.

III.3.2.4. Influence of the promoter nature

We wanted to compare our “CoMo” bulk catalyst precursor to a commercial reference CM. Even if the CoMo based catalysts are rather preferred for HDS than for Deep-HDS, interesting conclusions can be drawn from the results. We will focus again on naphthalene, DBT and 4,6-DMDBT.

The experiments were carried out at a LHSV of 150 h^{-1} . Concerning the conversion of naphthalene into tetraline, the results clearly lead to the conclusion that our bulk CoMo materials have no hydrogenation activity neither has CM. Regarding the sulfur compounds, our catalyst presents a better activity than the commercial one and seems particularly efficient for the conversion of DBT compared to 4,6-DMDBT but also compared to “NiMo” catalyst when we refer to conversion $\%.\text{m}^{-2}$ of catalyst. Indeed, DBT conversion mainly occurs through direct desulfurization (80 – 90 %) as explained in [1.1.2.2.2. \[20,21\]](#), and this pathway is privileged by the “CoMo” catalyst.

The HDS of 4,6-DMDBT occurs preferably via the hydrogenation pathway (HYD) and the poor hydrogenation activity of “CoMo” renders it more difficult than with the use of “NiMo” that favors this pathway [\[22\]](#). However, our “CoMo” shows better performance than our “NiMo”. This can be due to the fact that hydrogenation of aromatics (benzene and naphthalene in our study) is in competition with HDS via HYD. Therefore, their presence decreases the efficiency of “NiMo” toward HDS. As “CoMo” does not show any hydrogenation activity, all his active sites are available for HDS via DDS and even if this pathway is less efficient concerning 4,6-DMDBT, “CoMo” seems to be a better catalyst toward our application in our specific experimental conditions.

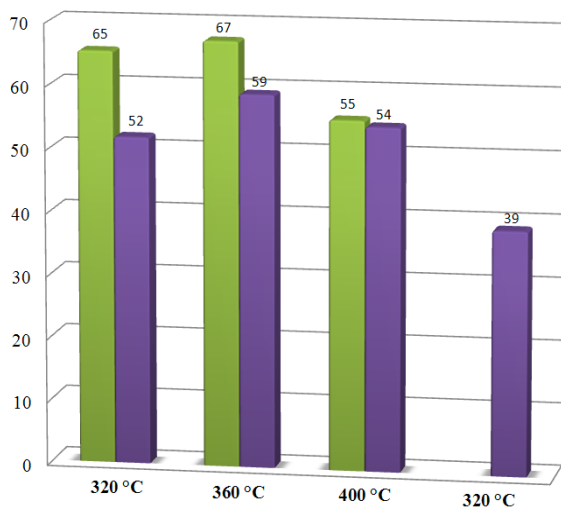
Naphthalene (conversion %)

No conversion detected

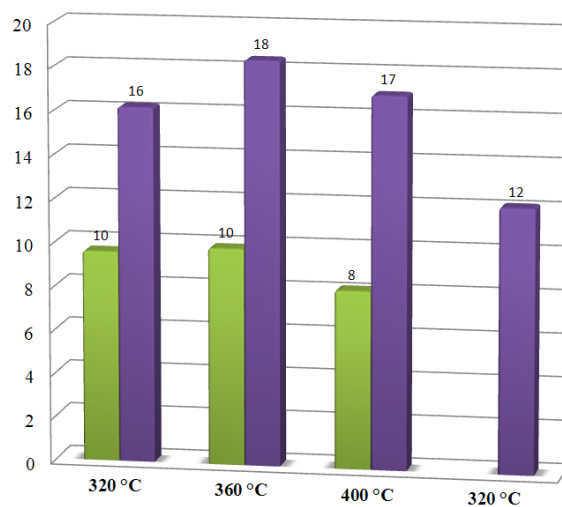
Naphthalene (conversion %.m⁻²)

No conversion detected

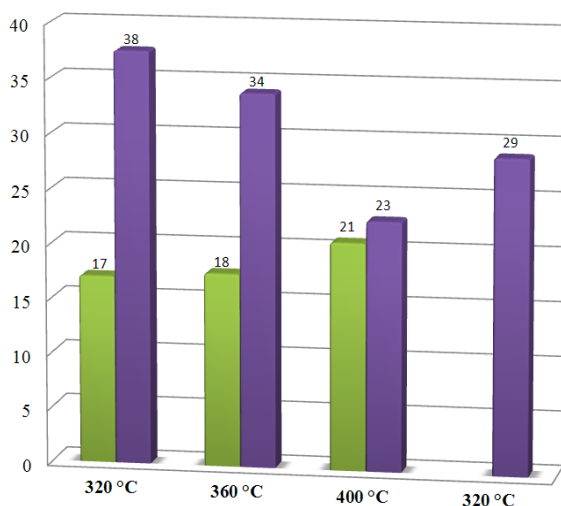
DBT (conversion %)



DBT (conversion %.m⁻²)



4,6-DMDBT (conversion %)



4,6-DMDBT (conversion %.m⁻²)

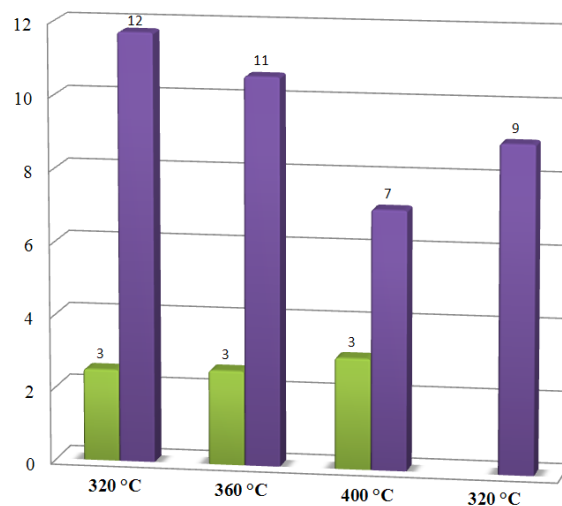


Figure III.16: Influence of the promoter on the catalytic activity (CM, MT081, LHSV = 150 h⁻¹)

With this study, we could highlight the different behavior of the HDS catalysts whether their promoter is Ni or Co. With materials containing nickel, HDS of 4,6-DMDBT encounters a strong competition with the hydrogenation of aromatics over the active sites of the catalysts. Using an aromatic-free feedstock would have show that NiMo based catalysts are actually more active toward HDS of 4,6-DMDBT than CoMo catalysts are. This also proves that our “bulk” catalyst shows better performances than his commercial equivalent.

III.3.2.5. Conclusion

At this point of the work, the second important objective of this project is successfully achieved: under our experimental conditions and for a model feedstock taking at best the “matrix effect” into account, our materials proved to be efficient and in an overall consideration better than the commercial reference we used.

Moreover, we also show that our NiMoO_4 outperforms the reference NM in hydrogenation reaction, being better at considerably lower M_G/M_L , what implies a non negligible H_2 saving for the industrials. It also proves to be better at lower temperature, both for aromatics hydrogenation (CN upgrading) and Deep-HDS, proving thus to be less energy consuming than the commercial reference for similar or better results.

“Bulk” HDS catalysts synthesized in supercritical fluids, be it NiMoO_4 or CoMoO_4 , perform better than the commercial references used during this work. The second important objective is fulfilled: our material catalyzes the hydrogenation reaction and the Deep-HDS reaction at lower temperature and with lower amounts of H_2 than the considered commercial reference.

We wanted to go further by testing our material on a real Deep-HDS feedstock. The work presented below presents the first experiment carried out on a Light Cycle Oil (LCO).

III.4. Tests on real feed

Since the final objective of this project is the possible commercial application of our bulk “NiMo” precursors as catalysts for Deep-HDS in petrol refinery plants, we started a set of runs with a real petrol-derived fraction to have an idea of the behavior of our bulk catalysts with real feedstock. This feed is a Light Cycle Oil (LCO), one of the product fractions recovered from the Fluid Catalytic Cracking process in the refinery that contains a high percentage of aromatics and which among the most difficult to hydrodesulfurize. The sulfur content of this fraction, not pre-hydrotreated, is close to 5000 wppm S, higher than one could expect for a Deep-HDS feed. However, a good catalytic performance in converting this

fraction, richer in S, will be a clear indication of the viability of these catalysts to be used in Deep-HDS processes.

Only a few preliminary tests have been performed, in order to confirm the potential interest of our materials from an industrial point of view. Therefore, the reaction conditions were not optimized in this part of the study: we kept a very high LHSV (150 h^{-1}) that implies a low contact time between the sulfur compounds and the catalysts surface, and the equipment in the lab does not permit higher H_2 pressure higher than 3.5 MPa when industrial processes go to pressure higher than 10 MPa to treat this kind of feedstock. Therefore, under the conditions used, the conversion should be quite low. Still we can present some results.

III.4.1. Description of the Light Cycle Oil

To describe our LCO, we used Simulated Distillation which is a well established chromatographic technique used to characterize petroleum fractions and crude oil which have a wide range of boiling point distribution. It roughly consists in correlating the retention time of reference compounds (n-paraffins) with their boiling points and applying this correlation to the analyzed product (a complex mixture of hydrocarbons). Within our LCO we have considered three fractions with the following cut-points: the naphtha fraction (from C_5 to 216.1°C) represents 7.1 wt% of the LCO (+ 1 wt% corresponding to heptane that we added to serve as internal standard), the diesel fraction (from 216.1 to 359°C) represents 74.5 wt% and the heavy ends ($359+$) represents 17.4 wt% (Table III.8). The distillation curve of the LCO determined by means of the D86 correlation is given in (Table III.9). Its density is of 0.889 g.mL^{-1} .

Analysis of the LCO feedstock by gas chromatography and applying the response factors determined by means of previous calibrations, gave a sulfur concentration of 5200 wppm.

Table III.8: Cut-points of our LCO

Fraction	Weight %
Naphtha	8.1
Diesel	74.5
Heavy ends	17.4

Table III.9: Distillation Curve according to D86 Correlation of our LCO

% Off	Temperature (°C)
IBP	187
10	239
20	252
30	263
50	286
70	318
80	336
90	359
FBP	390

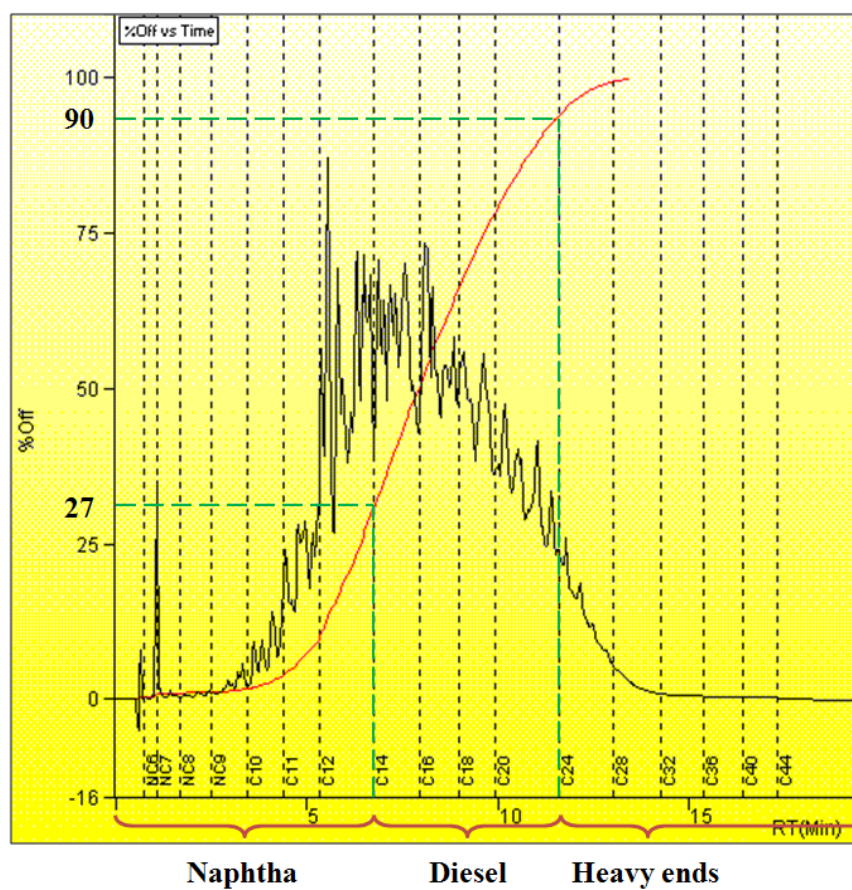


Figure III.17: Simulated Distillation chromatogram of our LCO

III.4.2. HDS test

We carried out the catalytic tests using the commercial reference NM and sample MT072, the most efficient bulk catalyst we had at the time. As the main advantages of our bulk catalysts toward NM were obtained at low temperature and low H_2 partial pressure, we decided to work at a temperature of 320 °C and M_G/M_L ratio of 5. The catalysts characteristics and the operation conditions are summarized in Table III.10.

Table III.10: Experiments carried out with our LCO

Sample	at% Ni	at% Mo	Ni/Mo (molar ratio)	S_{BET} ($m^2.g^{-1}$)	M_G/M_L	Temperature (°C)	LHSV (h^{-1})
NM	36	64	0.6	200	5	320	150
MT072	62	38	1.6	80	5	320	150

III.4.2.1. Cut points

Simulated Distillation performed on the products of the catalytic reactions gave us a product distribution very similar to the ones of the initial LCO (Table III.11). This proves that the reaction did not change noticeably the physical properties of the LCO and particularly cracking did not happen since the weight percentage of the light fraction does not increase.

Table III.11: Cut-points before and after treatment of the LCO

Fresh LCO		LCO treated on NM		LCO treated on MT072	
Fraction	Weight %	Fraction	Weight %	Fraction	Weight %
Naphtha	8.1	Naphtha	7.9	Naphtha	7.6
Diesel	74.5	Diesel	74.5	Diesel	74.4
Heavy ends	17.4	Heavy ends	17.6	Heavy ends	18

No undesirable side effects on the feedstock are observed after Deep-HDS reaction over our catalysts: boiling point distribution of the fraction is not modified.

III.4.2.2. Sulfur compounds conversion

When processing real feedstocks, the analysis of the reaction products becomes a difficult task. As it is more difficult to separate and therefore to identify the individual sulfur molecules in a real feedstock as compared to our model feedstock, we have to proceed differently for their analysis. Instead of analyzing each compound of the feedstock separately, a specific method of the chromatograph software permits classifying them into groups thanks to adequate calibrations: BT and its alkylated derivatives in a group we call BTs, and DBT and its alkylated derivatives in another group we call DBTs (Figure III.18). 4,6-DMDBT is included in this last group but we could not isolated from the rest of the isomers. In this way, we can estimate an overall conversion for the benzothiophene-like molecules and the dibenzothiophene-like ones over our bulk catalysts and the commercial reference.

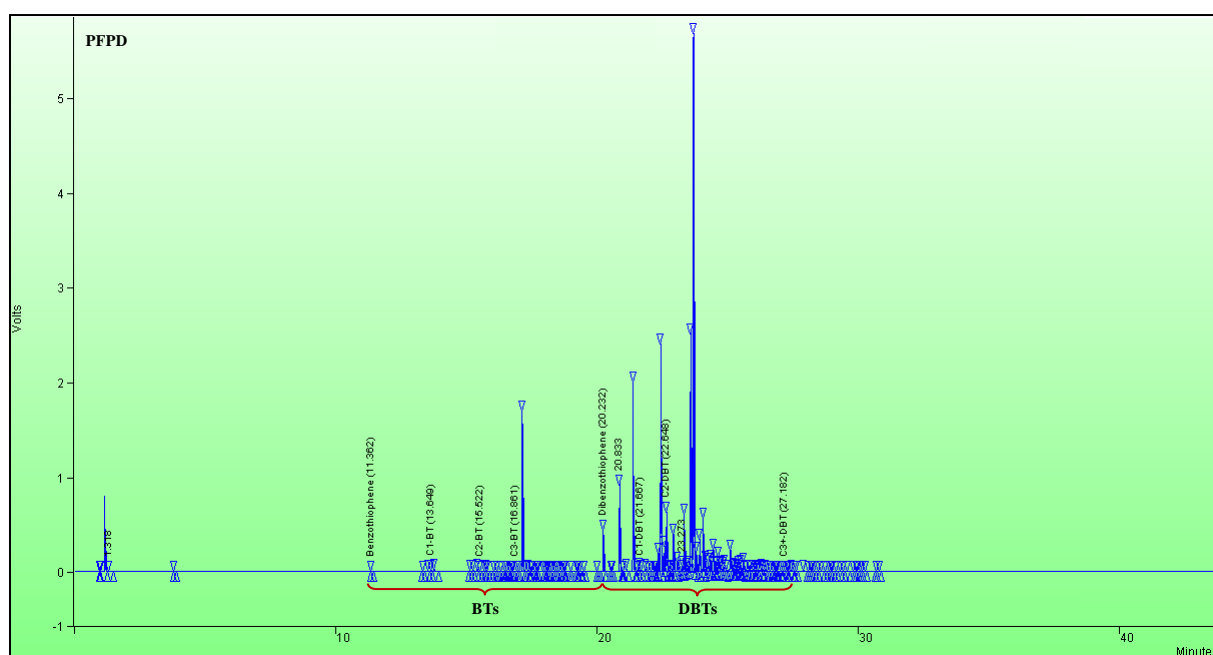
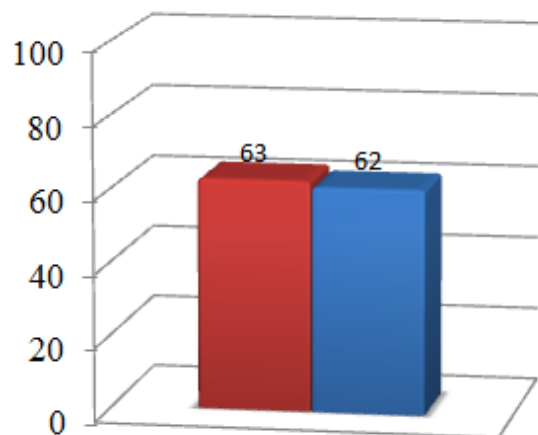


Figure III.18: Chromatogram obtained with the PFPD of our LCO

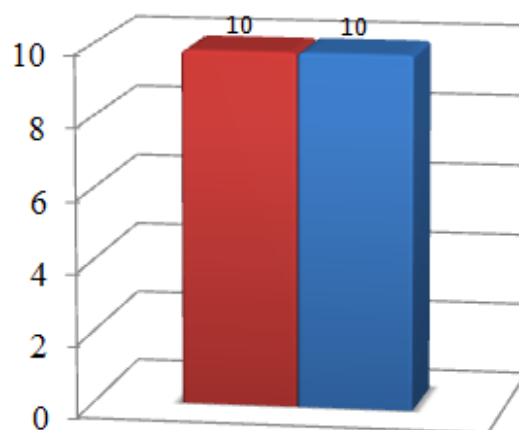
The results obtained with the “bulk” catalysts are compared to those of the commercial reference NM catalyst in Figure III.19. It can be seen that although the reference supported NiMo catalyst performs slightly better when looking at the absolute conversions, the conversions obtained with our bulk material are in the same range and therefore comparable. The differences are even lower when the conversions are given per square meter. Taking into account that the conditions are not the most favorable, these preliminary results are

remarkable and promising for our bulk catalyst, evidencing their potential as HDS bulk catalysts.

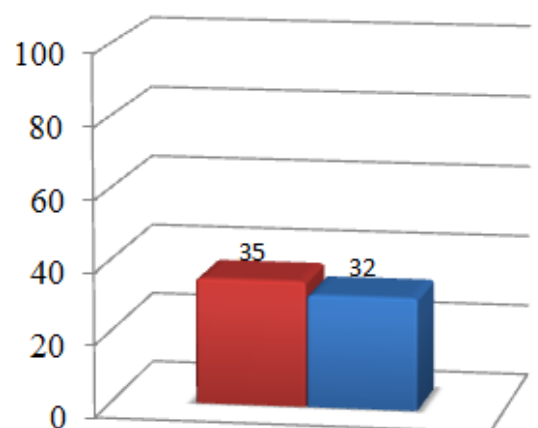
BTs (conversion %)



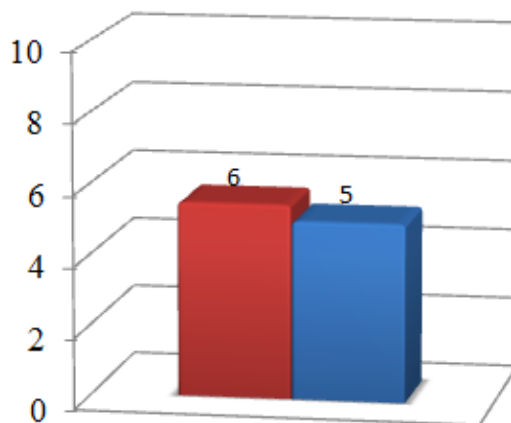
BTs (conversion %.m⁻²)



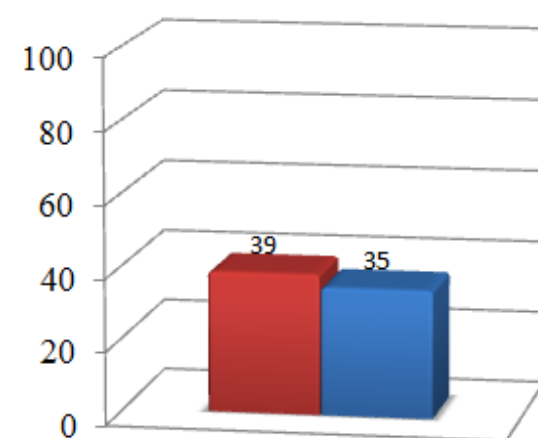
DBTs (conversion %)



DBTs (conversion %.m⁻²)



Total sulfur (conversion %)



Total sulfur (conversion %.m⁻²)

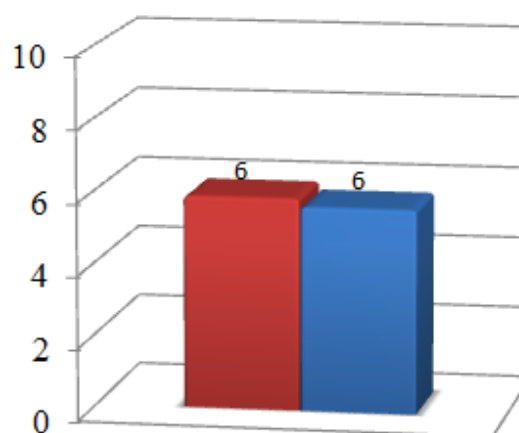


Figure III.19: Catalytic activity in the LCO (NM, MT072, T = 320 °C, LHSV = 150 h⁻¹)

Our bulk catalyst proves to be active for converting a real feedstock chosen among the most difficult to treat and with results comparable to the commercial reference.

III.5. Conclusion

Our bulk HDS catalysts obtained from NiMoO_4 and CoMoO_4 synthesized in supercritical fluids were tested and compared with two commercial references (NM for “NiMo” and CM for “CoMo”). A model feedstock was specifically thought for these experiments: it takes at best the “matrix effect” classically observed in real feedstocks into account by mixing different type of molecules encountered in petroleum fractions. Moreover, its concentration in sulfur was adapted to correspond with those measured in usual Deep-HDS feedstocks and sulfurs principally come from refractory compounds such as dibenzothiophene and 4,6-dimethyldibenzothiophene, two molecules we used as reference compounds.

Our bulk catalysts show better activity for hydrogenation of aromatics than the commercial reference what can be related to a better HDS of 4,6-DMDBT which occurs preferentially through the hydrogenation of one of its aromatic rings. Moreover, an additional and appreciable property of our bulk catalysts is the possibility to increase the Cetane Number of the feedstock in the mean time it is hydrosulfurized.

We showed from the different results exposed that for similar conversion under similar operating conditions we need a lower mass of our material than of the commercial reference, or with similar volume of catalysts, we can work at lower temperature with our materials.

The second important objective is fulfilled: our material catalyzes the hydrogenation reaction and the Deep-HDS reaction at lower temperature and with lower amounts of H_2 than the considered commercial reference.

Finally, promising results were obtained on the conversion of a real feedstock, a Light Cycle Oil. No undesirable side effects on the feedstock are observed after Deep-HDS reaction over our bulk catalyst and it proved to be active for HDS with such a feedstock chosen among the most difficult to treat and with promising results evidencing their potential as HDS bulk catalysts.

III.6. References

- [1] Frye, C. G. and Mosby, J. F. "Kinetics of hydrodesulfurization." *Chemical Engineering Progress* **1967**. vol. 63, 66
- [2] Cheskis, S., Atar, E., and Amirav, A. "Pulsed-flame photometer: a novel gas chromatography detector." *Analytical Chemistry* **1993**. vol. 65, no. 5, 539
- [3] Atar, E., Cheskis, S., and Amirav, A. "Pulsed flame - a novel concept for molecular detection." *Analytical Chemistry* **1991**. vol. 63, no. 18, 2061
- [4] Schulz, H., Böhringer, W., Waller, P., and Ousmanov, F. "Gas oil deep hydrodesulfurization: refractory compounds and retarded kinetics." *Catalysis Today* **1999**. vol. 49, no. 1-3, 87
- [5] Farwell, S. O. and Barinaga, C. L. "Sulfur-selective detection with the FPD: current enigmas, practical usage, and future directions." *Journal of Chromatographic Science* **1986**. vol. 24, 483
- [6] Schulz, H., Böhringer, W., Ousmanov, F., and Waller, P. "Refractory sulfur compounds in gas oils." *Fuel Processing Technology* **1999**. vol. 61, no. 1-2, 5
- [7] Prins, R. 13.2. In: *Hydrotreating*, edited by G. Ertl. Wiley-VCH Verlag GmbH & Co. KGaA Weinheim, Germany, vol. 6 **2008** 2695–2718
- [8] Serra, J. M., Chica, A., and Corma, A. "Development of a low temperature light paraffin isomerization catalysts with improved resistance to water and sulphur by combinatorial methods." *Applied Catalysis A: General* **2003**. vol. 239, no. 1-2, 35
- [9] Corma Canos, A., Hernandez Fenollosa, J., and Serra Alfaro, J. M. "Catalytic test device and method for the use thereof in material tests." **2003**. EP1273919 (A1)
- [10] Corma Canos, A., Hernandez Fenollosa, J., and Serra Alfaro, J. M. "Catalytic test device and method for the use thereof in material tests." **2001**. WO0159463 (A1)
- [11] Arribas, M. A. and Martínez, A. "The influence of zeolite acidity for the coupled hydrogenation and ring opening of 1-methylnaphthalene on Pt/USY catalysts." *Applied Catalysis A: General* **2002**. vol. 230, no. 1-2, 203
- [12] Arribas, M., Corma, A., Díaz-Cabañas, M., and Martínez, A. "Hydrogenation and ring opening of tetralin over bifunctional catalysts based on the new ITQ-21 zeolite." *Applied Catalysis A: General* **2004**. vol. 273, no. 1-2, 277
- [13] Leglise, J., van Gestel, J. N. M., Finot, L., Duchet, J. C., and Dubois, J. L. "Kinetics of sulfur model molecules competing with H₂S as a tool for evaluating the HDS activities of commercial CoMo/Al₂O₃ catalysts." *Catalysis Today* **1998**. vol. 45, no. 1-4, 347
- [14] Farag, H., Sakanishi, K., Kouzu, M., Matsumura, A., Sugimoto, Y., and Saito, I. "Investigation of the influence of H₂S on hydrodesulfurization of dibenzothiophene over a bulk MoS₂ catalyst." *Industrial & Engineering Chemistry Research* **2003**. vol. 42, no. 2, 306
- [15] Farag, H., Sakanishi, K., Mochida, I., and Whitehurst, D. D. "Kinetic analyses and inhibition by naphthalene and H₂S in hydrodesulfurization of 4,6-dimethyldibenzothiophene (4,6-DMDBT) over CoMo-based carbon catalyst." *Energy & Fuels* **1999**. vol. 13, no. 2, 449

- [16] Sakanishi, K., Nagamatsu, T., Mochida, I., and Whitehurst, D. D. "Hydrodesulfurization kinetics and mechanism of 4,6-dimethyldibenzothiophene over NiMo catalyst supported on carbon." *Journal of Molecular Catalysis A: Chemical* **2000**. vol. 155, no. 1-2, 101
- [17] Mazzocchia, C., Aboumrar, C., Diagne, C., Tempesti, E., Herrmann, J. M., and Thomas, G. "On the NiMoO₄ oxidative dehydrogenation of propane to propene: some physical correlations with the catalytic activity." *Catalysis Letters* **1991**. vol. 10, no. 3, 181
- [18] Ho, T. C. "Hydrodenitrogenation catalysis." *Catalysis Reviews: Science and Engineering* **1988**. vol. 30, no. 1, 117
- [19] Prins, R., De Beer, V. H. J., and Somorjai, G. A. "Structure and function of the catalyst and the promoter in CoMo hydrodesulfurization catalysts." *Catalysis Reviews: Science and Engineering* **1989**. vol. 31, no. 1, 1
- [20] Girgis, M. J. and Gates, B. C. "Reactivities, reaction networks, and kinetics in high-pressure catalytic hydroprocessing." *Industrial & Engineering Chemistry Research* **1991**. vol. 30, no. 9, 2021
- [21] Alibouri, M., Ghoreishi, S. M., and Aghabozorg, H. R. "Effect of supercritical deposition synthesis on dibenzothiophene hydrodesulfurization over NiMo/Al₂O₃ nanocatalyst." *AIChE Journal* **2009**. vol. 55, no. 10, 2665
- [22] Zhang, Q., Ishihara, A., Yashima, H., Qian, W., Tsutsui, H., and Kabe, T. "Deep desulfurization of light oil (part 5) hydrodesulfurization of methyl-substituted benzothiophenes and dibenzothiophenes in light gas oil catalyzed by various sulfided Co-Mo/Al₂O₃ and Ni-Mo/Al₂O₃." *Journal of The Japan Petroleum Institute* **1997**. vol. 40, 29

Conclusion

Sulfur content of diesel fuel has been cut down to ultra low levels by environmental regulation in many countries with the aim of reducing diesel engine's harmful emissions and improving air quality. As a result, research on the production of ultra low sulfur diesel has gained enormous interest in the scientific community worldwide.

Although these new environmental regulations are beneficial from environmental and health point of view, meeting these required stringent specifications represents a major operational and economic challenge for the petroleum refining industry. Some refractory sulfur compounds such as 4,6-dimethyldibenzothiophene are difficult to remove under conventional desulfurization conditions and therefore, their hydrodesulfurization (HDS) represents a tough challenge. This situation asks for innovative and efficient solutions for oil desulfurizing. Numerous alternative to HDS are proposed, however, as they imply costly modifications of the existing equipments, solutions that improve hydrotreatment are preferred. Today's objective is to develop a new generation of catalysts to achieve Deep-HDS (HDS of feedstock containing less than 500 wppm of sulfur).

Two kinds of catalysts exist: i) supported catalysts which have high specific surface area (higher than $200 \text{ m}^2.\text{g}^{-1}$) but their active sites are diluted by the support and strong interaction between them lower their efficiency; ii) bulk catalysts which have more active sites and present advantages over the supported ones but they develop low specific surface area (lower than $30 \text{ m}^2.\text{g}^{-1}$, maximum $80 \text{ m}^2.\text{g}^{-1}$). In this context, this project aimed at addressing the issue refineries face toward deep-HDS by proposing a new and original method to synthesize of a new generation of "bulk" catalysts presenting high S_{BET} .

The first important objective of this project work was to propose and develop a new synthesis method of bulk catalysts based on supercritical fluids technology. The synthesis and characterization of these "bulk" catalysts were mainly performed in France within the group "supercritical fluids" of the Institut de Chimie de la Matière Condensée de Bordeaux (ICMCB-CNRS) based at the Université de Bordeaux I (UB1). We chose nickel promoted molybdenum based catalysts for their well known propensity for catalyzing the Deep-HDS reaction. With this work we showed that from metal precursors dissolved in a water/alcohol mixture with a molar ratio of 1:1 at 290°C and 23 MPa in a continuous mode, we can obtain contaminant-free NiMoO_4 of high specific surface area (S_{BET}). We showed that the nature of the alcohol has an important influence on this S_{BET} : from $79 \text{ m}^2.\text{g}^{-1}$ with methanol, $134 \text{ m}^2.\text{g}^{-1}$ with ethanol to $179 \text{ m}^2.\text{g}^{-1}$ with isopropanol (values measured on powders obtained directly

after synthesis). We assume this effect due to the lower critical coordinates of the mixture water/isopropanol compared to water/ethanol and water/methanol, inducing a faster saturation of the media and nucleation of the particles. The powders as obtained mainly contain the hydrate phase $\text{NiMoO}_4 \cdot 0.75\text{H}_2\text{O}$. When optimizing our calcination program (optimization based on XRD and TGA analysis, 3 h at 400 °C) we realize that at 400 °C, we form $\beta\text{-NiMoO}_4$, the high temperature phase, more active than the room temperature phase $\alpha\text{-NiMoO}_4$. When we cool the powders down to room temperature, we showed that it becomes a mixture of $\alpha\text{-NiMoO}_4$, $\beta\text{-NiMoO}_4$ and NiO when the ICP analysis reveals an excess of nickel and only $\alpha\text{-NiMoO}_4$ and $\text{MoO}_3 \cdot 2\text{H}_2\text{O}$ when the ICP analysis reveals an excess of molybdenum. Regarding the general objective of synthesizing an efficient catalyst for the reaction of hydrodesulfurization, a powder with an excess of nickel is the best material.

We manage to fulfill and even outperform our objectives from the French part of this project: we synthesize a new generation of HDS catalysts precursors presenting higher S_{BET} than commercially available “bulk” catalysts.

The second important objective of this project was of course to prove the efficiency of our catalysts in the reaction of deep-HDS. This whole work was therefore performed in parallel with catalytic tests at the Instituto de Tecnología Química (ITQ - Valencia) in Spain. A model feedstock was specifically thought for these experiments: it takes at best the “matrix effect” classically observed in real feedstocks into account using paraffins, olefins and aromatic compounds, and its concentration in sulfur (from dibenzothiophene and 4,6-dimethyldibenzothiophene, our compounds of reference, 100 wppm of sulfur each) corresponds with those measured in usual Deep-HDS feedstocks. Our “bulk” catalysts show better activity for hydrogenation of aromatics and hydrodesulfurization of sulfur compounds than the commercial reference we used in this work. This second objective is fulfilled: our material catalyzes the hydrogenation reaction and the Deep-HDS reaction at lower temperature and with lower amounts of H_2 than the considered commercial reference. Promising results were obtained on the conversion of a real feedstock, a Light Cycle Oil among the most difficult to treat and with results comparable to the commercial reference.

The objectives set for this thesis work are then accomplished and the results are patent-pending at the time these lines are written. Yet, we can think of further work on the global project, like an improvement of the catalysts synthesis, to attain even higher specific surface area and refining the composition of the powders. Tests on various real Deep-HDS feedstocks with the best catalysts and under optimized conditions would complete the study. Finally, deactivation of these materials still need to be fully investigated.

Appendices

Appendices	219
Appendix I. Process families in a refinery plant	223
Appendix II. Process providing hydrotreatment feedstocks.....	224
A.II.1. Atmospheric distillation.....	224
A.II.2. Vacuum distillation	225
A.II.3. Fluidized-bed Catalytic Cracking (FCC).....	225
A.II.4. Coking	226
Appendix III. Hydrodesulfurization	228
A.III.1. Industrial process	228
A.III.2. Feedstock considerations for reaction conditions.....	229
A.III.3. Operating variables	231
Appendix IV. Characterization techniques.....	232
A.IV.1. X-ray Diffraction (XRD)	232
A.IV.2. Microscopy (Transmission Electron Microscopy (TEM), High Resolution TEM, Scanning Electron Microscopy (SEM))	238
A.IV.3. Inductively Coupled Plasma/Optical Emission Spectrometry (ICP-OES). 239	
A.IV.4. X-ray photoelectron spectroscopy (XPS).....	240
A.IV.5. Elemental analysis (CHNS-O)	241
A.IV.6. Specific surface area (BET)	242
A.IV.7. Thermogravimetric analysis coupled with mass spectrometry (TGA-MS) 242	
A.IV.8. Flame Ionization Detector (FID)	243
References	245

Appendix I. Process families in a refinery plant

Separation processes. The separation process is the first phase in petroleum refining operations. Crude oil is separated into its major constituents using three petroleum separation processes: atmospheric distillation, vacuum distillation, and light ends recovery (gas processing). Crude oil consists of a mixture of hydrocarbon compounds including paraffinic, naphthenic, and aromatic hydrocarbons with small amounts of impurities like sulfur, nitrogen, oxygen, and metals. Those processes separate these crude oil constituents into common boiling-point fractions.

Conversion processes. The conversion processes turn the heavy unfinished products from the crude distillation unit into more valuable lighter products such as high-octane gasoline, jet fuel, and diesel fuel. Cracking, coking and visbreaking processes are used to break large petroleum molecules into smaller ones. Polymerization and alkylation processes are used to combine small petroleum molecules into larger ones. Isomerization and reforming processes are applied to rearrange the structure of petroleum molecules to produce higher-value molecules of a similar molecular size.

Treating processes. Petroleum treating processes stabilize and upgrade petroleum products by separating them from less desirable products and by removing objectionable elements. Undesirable elements such as nitrogen, oxygen and more important in our work, sulfur are removed by hydrodesulfurization, hydrotreating, chemical sweetening, and acid gas removal. Treating processes, employed primarily for the separation of petroleum products, include such processes as deasphalting. Desalting is used to remove salt, minerals, grit, and water from crude oil feedstocks before refining. Asphalt blowing is used for polymerizing and stabilizing asphalt to improve its weathering characteristics.

Appendix II. Process providing hydrotreatment feedstocks

A.II.1. Atmospheric distillation

Atmospheric distillation is the first process crude oil encounters in refineries. Because hydrocarbons vaporize at different temperatures, crude oil is heated over $370\text{ }^{\circ}\text{C}$ and then is sent to a distillation tower. The temperature decrease as the vapors rise through the tower and the components of the crude oil condense and separate at different heights (Figure A.II.1).

In most cases, the distillation is operated at a continuous steady state. New feed is always being added to the distillation column and products are always being removed. Unless the process is disturbed due to changes in feed, heat, ambient temperature, or condensing, the amount of feed being added and the amount of product being removed are normally equal.

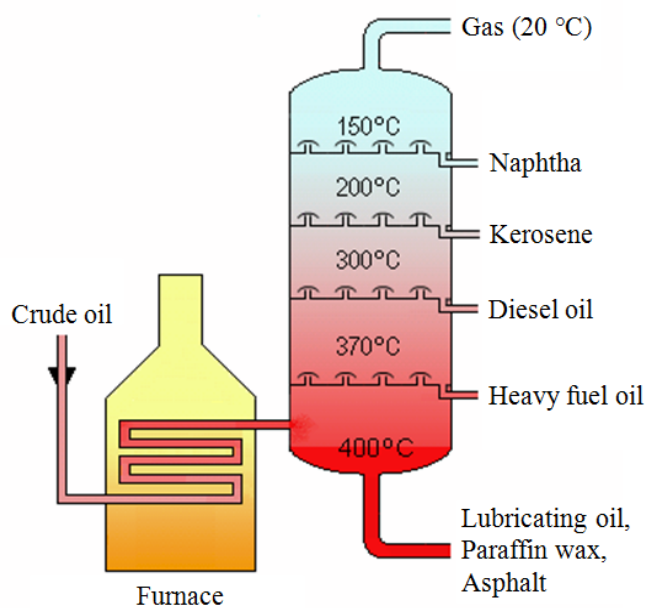


Figure A.II.1: Scheme of atmospheric distillation process

A.II.2. Vacuum distillation

Crude fraction withdrawn from the bottom of the atmospheric distillation column is composed of high boiling-point hydrocarbons. When distilled at atmospheric pressures, the crude oil decomposes and polymerizes and will foul equipment. To separate this crude fraction into components, it must be distilled in a vacuum column at a very low pressure and in a steam atmosphere.

In the vacuum distillation unit, the charge is heated with a process heater to temperatures ranging from 370 to 425°C. It is then flashed into a vacuum distillation column operating at absolute pressures ranging from 3.4×10^3 Pa to 1.4×10^4 Pa. The charge is separated into common boiling-point fractions by vaporization and condensation. Stripping steam is normally injected into the bottom of the vacuum distillation column to assist the separation by lowering the effective partial pressures of the components.

A.II.3. Fluidized-bed Catalytic Cracking (FCC)

Catalytic cracking, using heat, pressure, and catalysts, converts heavy oils into lighter products with product distributions favoring the more valuable gasoline and distillate blending components. Feedstocks are usually gas oils from atmospheric distillation, vacuum distillation, coking, and deasphalting processes. These feedstocks typically have a boiling range of 340 to 540°C.

The FCC process uses a catalyst in the form of very fine particles that act as a fluid when aerated with a vapor. Fresh feed is preheated in a process heater and introduced into the bottom of a vertical transfer line or riser with hot regenerated catalyst ([Figure A.II.2](#)). The hot catalyst vaporizes the feed, bringing both to the desired reaction temperature, 470 to 525°C. The high activity of modern catalysts causes most of the cracking reactions to take place in the riser as the catalyst and oil mixture flows upward into the reactor. The hydrocarbon vapors are separated from the catalyst particles by cyclones in the reactor. The reaction products are sent to a fractionator for separation.

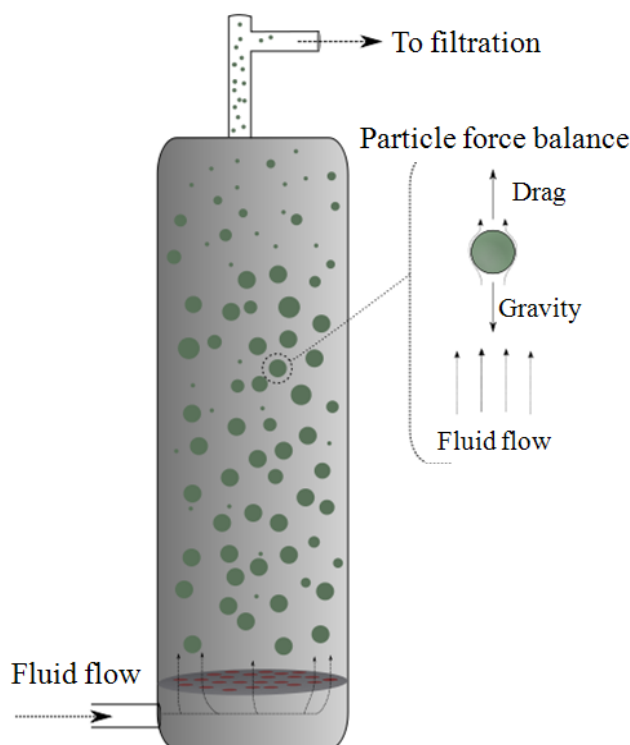


Figure A.II.2: scheme of a Fluidized-bed Catalytic Cracking reactor

A.II.4. Coking

Coking is a thermal cracking process used to convert low value residual fuel oil to higher value gas oil and petroleum coke. Vacuum residuals and thermal tars are cracked in the coking process at high temperature and low pressure. Products are petroleum coke, gas oils (diesel), and lighter petroleum stocks (naphtha). Two types of coking processes exist: delayed coking and fluid coking.

In the delayed coking process (Figure A.II.3), heated charge stock is fed into the bottom of a fractionator, where light ends are stripped from the feed. The stripped feed is then combined with recycle products from the coke drum and rapidly heated in the coking heater to a temperature of 480 to 590°C. Steam injection is used to control the residence time in the heater. The vapor-liquid feed leaves the heater, passing to a coke drum where, with controlled residence time, pressure (0.17 MPa to 0.2 MPa), and temperature (400 °C), it is cracked to form coke and vapors. Vapors from the drum return to the fractionator, where the thermal cracking products are recovered.

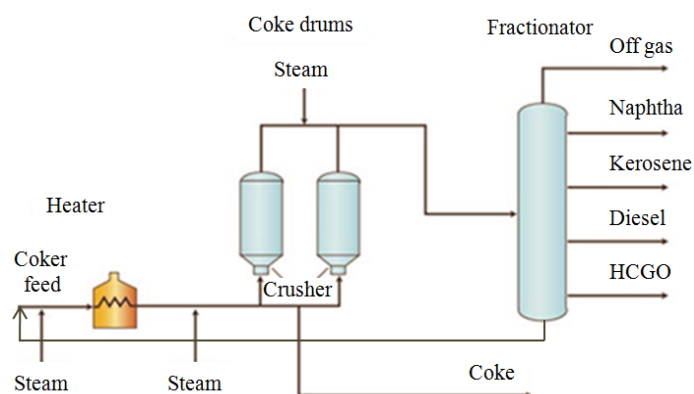


Figure A.II.3: Scheme of delayed coking process

In the fluid coking process (Figure A.II.4), residual oil feeds are injected into the reactor, where they are thermally cracked, yielding coke and a wide range of vapor products. Vapors leave the reactor and are quenched in a scrubber, where entrained coke fines are removed. The vapors are then fractionated. Coke from the reactor enters a heater and is pyrolyzed. The volatiles from the heater are treated for fines to yield a particulate-free gas. The pyrolyzed coke is circulated from the heater to a gasifier where 95 % of the reactor coke is gasified at high temperature with steam and air or oxygen. The gaseous products and coke from the gasifier are returned to the heater to supply heat for the pyrolyzation. These gases exit the heater with the heater volatiles through the same fines removal processes.

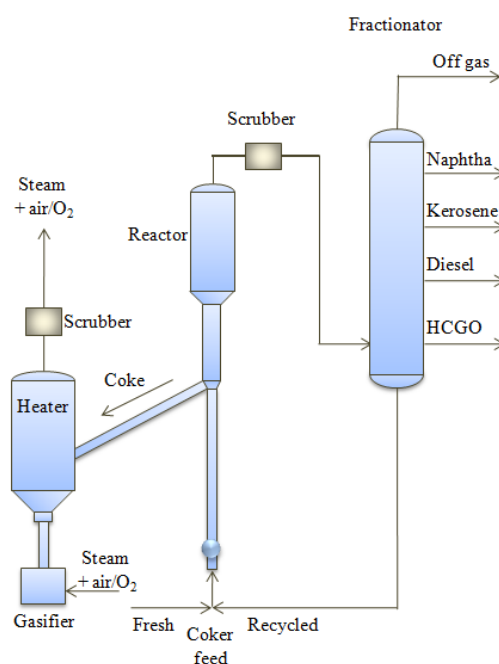


Figure A.II.4: Scheme of fluid coking process

Appendix III. Hydrodesulfurization

A.III.1. Industrial process

The liquid feed is pumped up to the required elevated pressure (1 to 20.7 MPa) and is joined by a stream of hydrogen-rich recycle gas. The resulting liquid-gas mixture is preheated by flowing through a heat exchanger. The preheated feed then flows through a fired heater where the feed mixture is totally vaporized and heated to the required elevated temperature (290 °C to 445 °C) before entering the reactor and flowing through a fixed-bed of catalyst where the hydrodesulfurization reaction takes place.

The hot reaction products are partially cooled by flowing through the heat exchanger where the reactor feed was preheated and then flows through a water-cooled heat exchanger before it flows through the pressure controller (PC) and undergoes a pressure reduction down to about 0.3 to 0.5 MPa. The resulting mixture of liquid and gas enters the gas separator vessel at about 35 °C and 0.3 to 0.5 MPa of absolute pressure.

Most of the hydrogen-rich gas from the gas separator vessel is recycle gas which is routed through an amine contactor for removal of the reaction product H_2S that it contains. The H_2S -free hydrogen-rich gas is then recycled back for reuse in the reactor section. Any excess gas from the gas separator vessel joins the sour gas from the stripping of the reaction product liquid. The recycle gas scheme is used to minimize the physical losses of expensive hydrogen. HDS reactions require a high hydrogen partial pressure in the gas phase to maintain high HDS reaction rates and to suppress carbon laydown that would lead to catalyst deactivation. The high hydrogen partial pressure is maintained by supplying hydrogen to the reactors at several times the chemical hydrogen consumption rate. Hydrogen is physically lost in the process by solubility in the desulfurized liquid hydrocarbon product, and from losses during the scrubbing or purging of hydrogen sulfide and light hydrocarbon gases from the recycle gas.

The liquid from the gas separator vessel is routed through a stripper distillation tower. The bottoms product from the stripper is the final desulfurized liquid product from hydrodesulfurization unit. The hydrogen sulfide removed and recovered by the amine gas treating unit is subsequently converted to elemental sulfur in a Claus process unit or to sulfuric acid in a wet sulfuric acid process or in the conventional contact process [1].

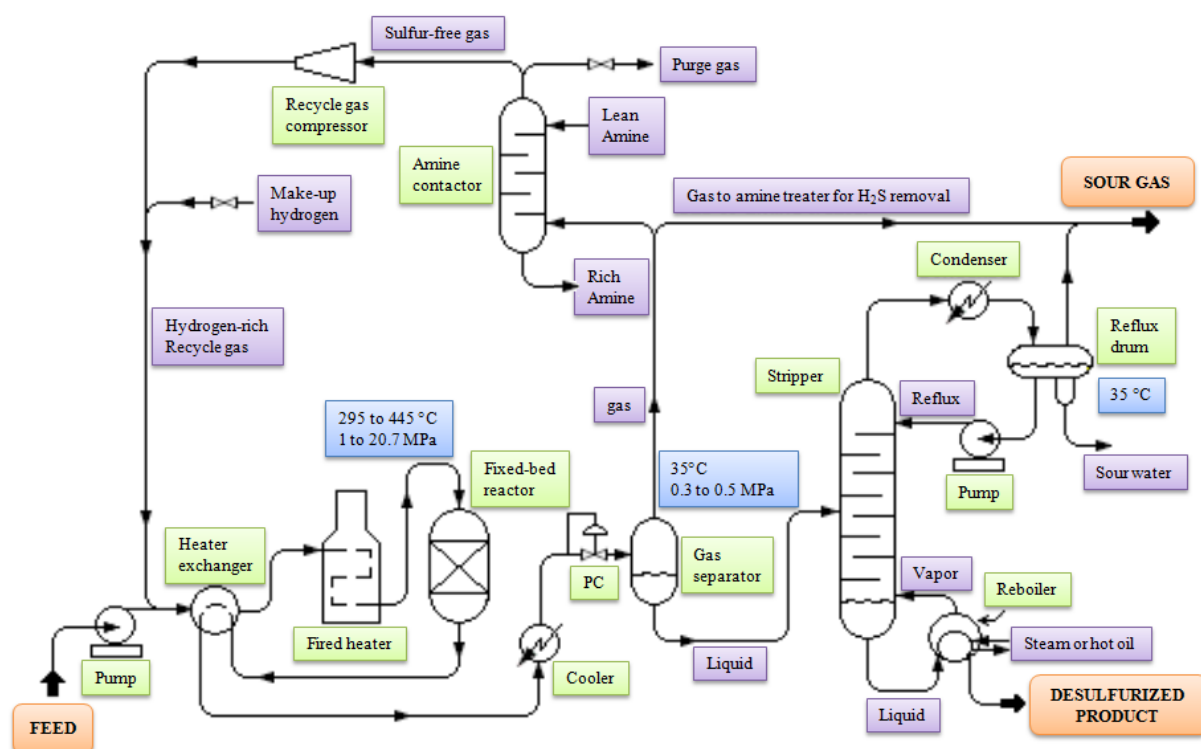


Figure A.III.1: Scheme of industrial HDS process

Kerosene and light gas oils are generally processed at mild severity and high throughput, whereas light catalytic cycle oils require slightly more severe conditions. Higher-boiling distillates, such as vacuum gas oils, require the most severe conditions. Those considerations are detailed hereafter.

A.III.2. Feedstock considerations for reaction conditions

The properties of the feedstock, especially its boiling range, have to be considered for the ultimate design of the desulfurization unit and process flow. In agreement, there is a definite relationship between the percent by weight sulfur in the feedstock and the hydrogen requirements. Moreover, the HDS reaction rate decreases rapidly with increasing average boiling point in the kerosene and light gas oil range, but much more slowly in the heavy gas oil range. This is attributed to the difficulty in removing sulfur from ring structures present in the entire heavy gas oil boiling range.

The HDS of light (low-boiling) distillate (naphtha or kerosene) is one of the more common catalytic HDS processes, as it is usually used as a pretreatment prior to further

processing. It can be achieved under relatively mild conditions. If the feedstock arises from a cracking operation, HDS will be accompanied with some degree of saturation, resulting in increased hydrogen consumption. This HDS is usually a gas-phase reaction and may employ the catalyst in fixed beds, and (with all of the reactants in the gaseous phase) only minimal diffusion problems are encountered within the catalyst pore system. It is, however, important that the feedstock completely gasifies before entering the reactor, as the possibility of pressure variations exists if part of the feed enters the reactor in the liquid phase and is vaporized within the reactor, leading to less satisfactory results.

The HDS of middle distillates is also an efficient process, and applications include predominantly the desulfurization of diesel fuel, jet fuel, and heating oil that boil over the general range of 250 °C to 400 °C. However, with this type of feedstocks, hydrogenation of the higher-boiling catalytic cracking feedstocks has become increasingly important, where HDS is accomplished alongside the saturation of condensed-ring aromatic compounds as an aid to subsequent processing. Under the relatively mild processing conditions used for the HDS of these particular feedstocks, it is difficult to achieve complete vaporization of the feed. Process conditions may dictate that only part of the feedstock is actually in the vapor phase and that sufficient liquid phase is maintained in the catalyst bed to carry the larger molecular constituents of the feedstock through the bed. If the amount of liquid phase is insufficient for this purpose, molecular stagnation (leading to carbon deposition on the catalyst) will occur.

High-boiling distillates, such as atmospheric and vacuum gas oils, merely serve as feedstocks to other processes for conversion to lower-boiling materials. For example, gas oil can be desulfurized to remove more than 80 % of the sulfur originally present in it with some conversion to lower-boiling materials. The treated gas oil (which has a reduced carbon residue as well as lower sulfur and nitrogen contents relative to the untreated material) can then be converted to lower-boiling products in, say, a catalytic cracker where an improved catalyst life and volumetric yield may be noted. The conditions used for the HDS of gas oil may be somewhat more severe than the conditions employed for the HDS of middle distillates, and in this case the feedstock will be liquid.

The operating conditions in HDS are strongly dependent upon the feedstock as well as the desired degree of desulfurization or quality improvement.

The principal variables that can be adjusted to operate at the required severity in distillate HDS, depending on the feedstock to be processed, are the hydrogen partial pressure, the space velocity, the reaction temperature. Their effects are explained in the following paragraph.

A.III.3. Operating variables

The important effect of hydrogen partial pressure is the minimization of cocking reactions. If the hydrogen pressure is too low for the required duty at any position within the reaction system, premature aging of the remaining portion of the catalyst will be encountered. In addition, the effect of hydrogen pressure on HDS varies with feed boiling range. For a given feed, there exists a threshold level above which hydrogen pressure is beneficial to the desired HDS reaction. Below this level, HDS drops off rapidly as hydrogen pressure is reduced.

To enhance the production capacity of the HDS unit, the space velocity of the feedstock flow can be increased. Yet, as the space velocity is increased, the extension of HDS is decreased, but increasing the hydrogen partial pressure and the reactor temperature can offset the detrimental effect of increasing space velocity.

A higher reaction temperature increases the rate of HDS at constant feed rate, and the start-of-run temperature is set by the design desulfurization level, space velocity, and hydrogen partial pressure. The capability to increase temperatures as the catalyst deactivates is built into most process or unit designs. Temperatures of 415 °C and above result in excessive cocking reactions and higher-than-normal catalyst aging rate. Therefore, units are designed to avoid the use of such temperatures for any significant part of the cycle life.

Industrial considerations are important to highlight the practical issues a refinery encounters and has to address. Hydrotreatment process is clearly an inevitable step in any refinery stream and it is now important to get to know better how hydrodesulfurization works.

Appendix IV. Characterization techniques

The following part briefly exposes the characterization techniques considered and their principle and utility in this work.

A.IV.1. X-ray Diffraction (XRD)

XRD experiments are carried out by Éric Lebraud and Stanislav Pechev in the “X-ray Diffraction” department of the ICMCB. The Rietveld refinements were performed with the help of Stanislav Pechev.

Equipment. Powder diffraction patterns are obtained at room temperature from Philips PW1820 and PANalytical X’Pert X-ray diffractometers (Bragg-Brentano geometry, $\lambda = 1.5418 \text{ \AA}$).

The diffractometer used to acquire XRD patterns for Rietveld refinements is a PANalytical X’Pert Pro MDD ($\theta - 2\theta$ Bragg-Brentano) with primary Ge (111) monochromator, Cu $K\alpha_1$ ($\lambda = 1.54059 \text{ \AA}$).

Crystal phase identification. X-ray diffraction first allows the identification of the crystal phase in the powders. Indeed, a XRD pattern could be compared to a fingerprint for the sample that can thus be identified through comparisons with the Powder Diffraction Files (PDF) database of JCPDS-ICDD. This investigation can easily be achieved with the help of the software DIFFRAC^{plus} EVA from Bruker AXS GmbH, Karlsruhe, Germany .

However, one must point out that the obtained XRD pattern actually results from two overlaid contributions, each one due to the $K\alpha_1$ ray (relative intensity of 100, $\lambda = 1.54059 \text{ \AA}$) and the $K\alpha_2$ one (relative intensity of 50, $\lambda = 1.54439 \text{ \AA}$). For low values of the θ angle, the two diffractograms merge, but their resolution power increase with θ which results in a splitting of the peaks. This also depends on the full width at half maximum (FWHM) of the peaks that can hide the splitting if it is too important. If we admit that “the resolution of the doublet” is obtained when its angle separation is equal to the FWHM, the angle 2θ (°) for which the splitting appears can be calculated from the equation (eq. 1):

$$\cot \theta = \frac{2 \cdot \Delta \lambda}{H \cdot \lambda} \quad (1)$$

With θ the diffraction angle (rad), $\Delta \lambda$ (Å) the deviation between $\lambda_{K\alpha 1}$ and $\lambda_{K\alpha 2}$ (0.00383 Å), H the full width at half maximum (rad) and λ (Å) the weighted mean wavelength (1.5418 Å). This is useful to make a difference between this splitting effect and an effect actually due to the structure of the material.

Crystalline rate estimation of the powders. The sharpness of the peaks could be related to the crystalline rate of the powders. Indeed, a well crystallized powder has a XRD pattern with thin diffraction peaks (Bragg reflection) whereas an amorphous substance presents a diffusion pattern. Consequently, the pattern of partially crystallized samples will present weakened broad peaks. The observed intensity of the diffraction peaks is thus proportional to the crystalline rate of the powder and it is possible to estimate it by comparing three patterns: the one from the amorphous material, the one from the fully crystallized powder and finally the one of the semi-crystallized powder.

Size of the crystallites. Providing that the peaks resolution allows it, this characterization technique also gives the possibility to access the size of the crystallites L (coherent domains of diffraction excluding edge effects) and the microstrains ε ($\Delta d/d$ characterizing the local variations of the reticular distance d due to non-uniform crystalline distortions) by analyzing the broadening of the diffraction peaks. Indeed, their integral breadth β (rectangle having the same surface area and of same height than the considered peak), is the resultant of the convolution of three types of contributions: instrumental function β_{inst} , Coherent domains size function β_L (for a reduced size of the crystallites) and microstrains function β_d .

β_{inst} is experimentally determined from the pattern of standard powder (Si, LaB₆...) for which the other factors of broadening are negligible.

β_L function is described by the Scherrer formula:

$$\beta_L = \frac{\lambda}{L \cos \theta} \quad (2)$$

with $\lambda = \lambda_{K\alpha}$ (Å), L the mean size of the crystallites (Å) and θ the diffraction angle (rad).

β_d is described by the expression:

$$\beta_d = 4. (\tan \theta). \varepsilon \quad (3)$$

with θ the diffraction angle (rad) and ε the mean rate of microstrains $\Delta d/d$

It is thus possible to access the size of the crystallites by measuring the integral breadth of the diffraction peaks (β_{obs}). A pseudo-Voigt function (convolution of Lorentzian and Gaussian functions) is usually used for the peak profile fitting. Then a Lorentzian approach is widely accepted to describe the microstructure of the material by simple subtraction of the instrumental broadening (β_{inst}) from β_{obs} (eq. 4):

$$\beta_{mat} = \beta_{obs} - \beta_{inst} \quad (4)$$

Two methods are then applied:

- (i) Use of the Scherrer formula

In this case, microstrains are neglected (generally, $\varepsilon < 10^{-3}$) and the size of the crystallites is obtained via the formula (eq. 2) with $\beta_L = \beta_{mat}$.

- (ii) Plot of the Williamson-Hall diagrams

The expression of β_{mat} (eq. 5) evolved toward the expression (eq. 6):

$$\beta_{mat} = \beta_L + \beta_d = \frac{\lambda}{L \cdot \cos \theta} + 4. \varepsilon \cdot \tan \theta \quad (5)$$

$$\beta_{mat} \cdot \cos \theta = A + B \cdot \sin \theta = f(\sin \theta) \text{ with } A = \lambda/L \text{ and } B = 4\varepsilon \quad (6)$$

The Williamson-Hall Diagrams correspond to the plotting of the curve described by equation (eq. 6) and thus give the mean size of the crystallites L (y-value = A at the origin) and a mean rate of microstrains (slop of the straight line B). When the samples present an anisotropic morphology of the crystallites (hkl dependent peak broadening) the Williamson-Hall diagrams present different straight lines corresponding to the different behavior associated with the family plans. When the microstrains are anisotropic as well, the straight lines present different slopes.

Crystal structure refinement (Rietveld method) [2,3]. In the late 70's, H.M. Rietveld proposed a method of refinement of the crystal structure from the global profile of a diffraction pattern. The idea is to compare an experimental pattern with a calculated one, not

only focusing on the diffracted intensities but in an overall view. At each point of the pattern, the observed intensity is considered as the sum of the intensity of all the individual peaks. Yet, the Rietveld method is a least squares method of structure refinement which is thus based on a starting structural hypothesis.

Realizing a structure refinement on powders requires a data acquisition of high quality. Not only the equipment but also the preparation of the samples is of high importance to get reproducible results of quality since those fundamental information are influenced by the sample:

- The position of the peaks
- Their intensity
- Their shape
- The background

There is of course no universal protocol to prepare the samples, yet here are some useful precautions (also applicable to more classical procedure):

As far as possible, the product must be of single phase to avoid the overlay of diffraction peaks with peaks from parasite phases, in sufficient quantity to fill deep sample carrier thus avoiding absorption in Bragg-Brentano geometry and with crystallites of small and homogenous size (use a sieve of 20 μm). The sample surface must be as plan as possible (Bragg-Brentano geometry) yet avoiding preferential orientations. During the acquisition the sample should rotate on itself to improve the statistic repartition of the crystallites.

The methodology to refine the diffractogram implies the following steps:

1. diffraction pattern indexing (Bragg relation),
2. refinement of the cell parameters and origin offset by the least squares method,
3. total profile refinement:

The profile refinement can be realized with the option “profile matching” of the software FULLPROF (Rodriguez-Carvajal J. 1995) which permits the refinement of the profile parameters without knowing the crystal structure (if we have at least an idea of the approximative lattice cell):

- The positions of the peaks,
 - The Full Width at Half Maximum (FWHM),
 - The shape of the peaks (gaussian, lorentzian, Pseudo-Voigt,...),
 - The asymmetry parameter,
 - The background noise,
4. Rietveld analysis.

Once the peaks profile parameters accurately determined, structural parameters must be cautiously refined, this means one by one. The following sequence proved to be rather efficient:

- Phase scale,
- Zero shift or specimen displacement,
- Lattice parameters,
- Coordinates of atoms,
- Profile parameters and asymmetry,
- Individual atomic displacement parameters in isotropic approximation,
- Occupation rate of the atoms,
- Individual atomic displacement parameters in anisotropic approximation,

In the structural refinement by the Rietveld method based on the least squares statistic principal, the value to minimize is:

$$\sum_i w_i (y_{iobs} - y_{ical})^2 \quad (7)$$

with y_{iobs} the measured intensity for an angle $2\theta_i$,

w_i the statistic weight of each measured intensity:

$$w_i = \frac{1}{\sigma^2(y_{iobs})} \text{ where } \sigma^2(y_{iobs}) \text{ is the variance,}$$

y_{ical} the calculate intensity for an angle $2\theta_i$,

$$y_{ical} = y_{iBF} + s \cdot \sum_h L_h \cdot F_h^2 \cdot \Omega(2\theta_i - 2\theta_h) \cdot A_h \cdot P_h$$

with y_{iBF} the intensity of the background (a degree 6 polynomial function of $2\theta_i$)

s the scale factor

L_h the Lorentz polarization correction and reflection multiplicity

F_h the structure factor

$\Omega(x)$ the profile function for the reflection h taking into account structural and instrumental parameters

$2\theta_i$ the diffraction angle for abscissa i

$2\theta_h$ the diffraction angle for the reflection h

A_h the asymmetric function

P_h the function describing the preferential orientation of the crystallites

A series of agreement factors calculated at each refinement cycle give an idea of the validity of this refinement. The comparison of both the calculated and observed patterns is the most relevant way to detect imperfections and deduce the corrections to be done.

The agreement factors are divided into two groups:

- The profile related:

$$R_P = \frac{\sum_i |y_{iobs} - y_{ical}|}{\sum_i y_{iobs}}, R_{WP} = \sqrt{\frac{\sum_i w_i \cdot |y_{iobs} - y_{ical}|^2}{\sum_i w_i \cdot y_{iobs}^2}} \quad (8), (9)$$

$$cR_P = \frac{\sum_i |y_{iobs} - y_{ical}|}{\sum_i |y_{iobs} - y_{iBF}|}, cR_{WP} = \sqrt{\frac{\sum_i w_i \cdot |y_{iobs} - y_{ical}|^2}{\sum_i w_i \cdot (y_{iobs} - y_{iBF})^2}} \quad (10), (11)$$

$$R_{exp} = \sqrt{\frac{N - P + C}{\sum_i w_i \cdot y_{iobs}^2}}, \chi^2 = \left(\frac{R_{WP}}{R_{exp}} \right)^2 \quad (12), (13)$$

- The structural related:

$$R_B = \frac{\sum_k |I_{kobs} - I_{kcal}|}{\sum_k I_{kobs}} \quad (14)$$

with I_{kobs} the integrated intensity of the peak k.

In the expression of R_{exp} , N is the number of points considered in the refinement, P is the number of variables and C the number of constraints which implies that $N - P + C$ represents the degrees of liberty of the system.

The agreement factors cR_P and cR_{WP} include a “background” correction which make them higher in value than R_P and R_{WP} but more realistic. R_B (or R_{Bragg}) is the best “crystallochemical indicator” since it is related to the structural model. Finally, for a gaussian type residuals distribution, χ^2 should converge toward the value 1.

A.IV.2. Microscopy (Transmission Electron Microscopy (TEM), High Resolution TEM, Scanning Electron Microscopy (SEM))

TEM acquisitions were carried out by Mélanie Majimel from the “supercritical fluids” group and Sonia Gomez from the "Thin films and interface center" of the ICMCB, High resolution TEM by Mélanie Majimel and Jérôme Majimel from the “Functionalized Materials: Fluorine, Hybrids, Nanoparticles” group of the ICMCB, and SEM micrographs were acquired by Sonia Gomez and Elisabeth Sellier from the CREMEM (Centre de Ressources en Microscopie Electronique et Microanalyse). Most of the interpretations were done in collaboration with either Mélanie Majimel or Jérôme Majimel.

With scanning and transmission electron microscopy, we can observe the shape and estimate the size of the particles and their size distribution. With high resolution micrographs we can confirm the size of the crystallites obtained by XRD and their crystalline structure. STEM mode (Scanning TEM) is used to make chemical X-ray mapping of our particles (distribution of the elements considered).

Equipment. Different microscopes localized at the CREMEM were used. Their characteristics are summed up in [Table A.IV.1](#):

Table A.IV.1: Characteristics of the equipments used in microscopy

Microscope	TEM JEOL 2000 FX	TEM JEOL JEM-2200FS	SEM JEOL 6700F
electron gun	Thermo-ionic LaB6	Field effect (FEG 1000 V)	Thermo-ionic W (FEG)
accelerating voltage	200 kV	200 kV	30 kV
resolution mode	Low resolution	high resolution	high resolution
additional equipment	EDX	EDX, EELS, STEM	EDX

Preparation protocol.

- TEM and HR-TEM: The nanoparticles are dispersed in ethanol with the help of an ultrasonic wave bath. A droplet of this suspension is then deposited on specific supports and the ethanol is evaporated at room temperature. The supports are made of

a 3 mm diameter copper grid of 300 mesh recovered of thin amorphous membrane of carbon.

- SEM: The samples must be conductive, that is why powders are metalized 10 to 30 s with Au, Pt, Pd or C before being stuck on a double-face carbon adhesive tape and fixed to the conductive sample carrier of the SEM (made of Al).

A.IV.3. Inductively Coupled Plasma/Optical Emission Spectrometry (ICP-OES)

ICP-OES analysis were performed either by Laëtitia Etienne from the “Energy: Hydrogen, Fuel Cells, Thermoelectrics” group of the ICMCB or the “chemical analysis” center of the ITQ.

ICP-OES is an analytical technique in solution that uses a plasma to obtain thermal dissociation of the molecules into atoms and ions, then to excite them. The equipment used is a Varian 720-ES. This technique permits to control the stoichiometry of the powders and verify the existence of pollutants.

Solutions of the powders to analyze are prepared by dissolving 10 mg of powder in a mixture of 3 mL of nitric acid and 3 mL of hydrochloric acid. Once the powder dissolved, distilled water is added up to 100 mL. This solution is then injected with a flow of argon in a nebulization chamber to create an aerosol. Spraying the solution on the chamber wall gives very small droplets that are then sucked in the plasma. The plasma is obtained by ionization of argon via a magnetic field. Once in the plasma, the sample is vaporized, atomized, ionized and excited.

Once the ion goes back to its ground state, it emits a photon which is collected and analyzed by a polychromator then a CCD detector (Charge-Coupled Device). The energy of the photon is typical of the emitting element. The results are expressed in mass percentage and the accuracy of measurement is of 2 % for each analyzed element (Ni, Co, Mo).

A.IV.4. X-ray photoelectron spectroscopy (XPS)

XPS analysis and interpretations were performed by Christine Labrugère from the “CeCaMA” center of the ICMCB.

XPS is a physical method allowing on one hand to identify chemical species (emitting atoms) and their different valence states or oxidation degree and to estimate the relative concentration (relative error of 5 %) of the different elements of a compound in the surface layers (3 – 5 nm).

This technique is based on the analysis of a sample placed in a high vacuum chamber irradiated by an X-ray source, commonly magnesium ($E = 1253.6$ eV) or aluminum anode ($E = 1486.6$ eV). The as emitted photoelectrons (from valence electrons and internal electrons, except for hydrogen and helium), characteristic from the present atoms, are sorted by mean of energy in a hemispheric analyzer and counted via a Channeltron type detector. The kinetic energy thus measured is closely related to the binding energy of the electrons on the specific orbitals. Each atom has its own signature by mean of electronic level, we can thus identify the nature of the elements on the surface of the sample. Moreover, this binding energy can present variations called “chemical shift” due to chemical environment changes.

An XPS spectrum is realized according to the following equation:

$$h\nu = E_C + E_b + \Phi_e \quad (15)$$

Where $h\nu$ is the energy of the source (eV, known value), E_C is the measured kinetic energy (eV), E_b the binding energy (eV) and Φ_e a constant inherent to the equipment. The spectrum displays the counts per second versus E_b .

A survey is firstly carried out to determine the elements present in the sample. The peaks are then indexed from energy values databases. Then, high energetic resolution spectra are recorded for each identified atoms. Those values compared to references give information on the oxidation state of the elements. As a general rule, the binding energy slightly increase (few eV) with the degree of oxidation. Fitting of those spectra also give information on the relative abundance of an oxidation state for a specific element.

Surveys realized on some of our product detect all the elements of our catalyst precursor (nickel, molybdenum, oxygen and carbon, [Figure A.IV.1](#)).

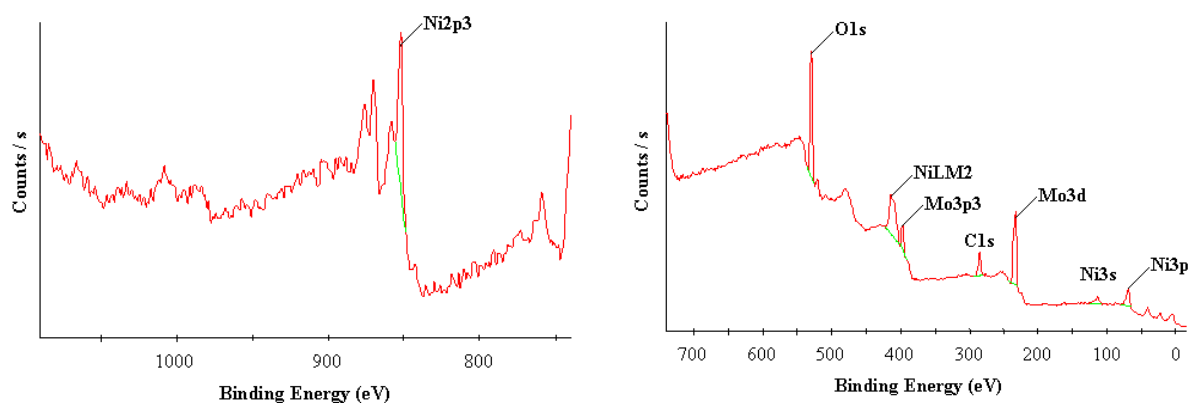


Figure A.IV.1: Surveys and elements present on the precursors surface

The XPS acquisitions were carried out on a VG ESCALAB 220-iXL apparatus equipped with a monochromatic $\text{Al}_{K\alpha}$ X-ray source (1486,6 eV). The spectra were collected via the ECLIPSE software. The analyzed spot correspond to a surface of 150 μm diameter for a 3 to 5 nm depth, with the following acquisition parameters:

- survey: $E_p = 150$ eV, 1 eV step,
- high energetic resolution spectra: $E_p = 20$ eV, 0.2 eV step

Deconvolutions were performed with the AVANTAGE software from ThermoFischer Scientific.

A.IV.5. Elemental analysis (CHNS-O)

CHNS-O analysis were interpreted by Patrick Rosa from the “Molecular Sciences: Photo, Piezo and thermo-sensible Materials” group of the ICMCB or by the “chemical analysis” center of the ITQ.

CHNS-O analysis, the most common form of elemental analysis, is accomplished by combustion analysis according to the Pregl-Dumas procedure. In this technique, a sample is burned in an excess of oxygen, and various traps collect the combustion products, namely carbon dioxide, water, and nitric oxide. The weights of these combustion products are used to calculate the composition of the sample and to detect carbon pollutions in our case. The equipment used is a Flash EH 1112 from Thermo Fisher.

A.IV.6. Specific surface area (BET)

BET measurements were done by Odile Babot from the Institute of Molecular Sciences (ISM) at the Université Bordeaux I, at the ITQ by Amparo Ferrero and Maribel Tadeo, and at the ICMCB.

BET measurements (named after the authors of the theory Brunauer, Emmett and Teller) permit to access the specific surface area of the powders (S_{BET}) [4].

Measurements were carried out with an Autosorb-1 from Quantachrome at the ICMCB, and an ASAP2010 from Micrometrics at the ISM as well as at the ITQ. After having been sufficiently outgased at low temperature (outgas pressure rise limit of 20 micron/minute) to remove surface pollutions, the apparatus injects precise volumes of nitrogen at 77.3 K (liquid nitrogen). The measured relative pressure P/P_0 gives an isothermal curve that is then transformed into a BET straight line (the software does all the transformation based on the BET theory and equations).

A.IV.7. Thermogravimetric analysis coupled with mass spectrometry (TGA-MS)

The acquisitions were carried out by Odile Babot at the ISM and by Dominique Denux from the “thermal analysis” center of the ICMCB.

Thermogravimetry is used to study chemical, physical or physico-chemical phenomenon related to temperature variation resulting in a mass variation. It is based on continuous recording of mass changes of a sample of material, as a function of a combination of temperature with time. The principal application is the study of reactions in which a solid sample undergoes a mass variation by releasing or fixing gases. When the TGA is coupled with a mass spectrometer, precise information on the nature of those gases is obtained since the released gaseous molecules are ionized and sorted by mean of weight. We thus can deduce the molar mass of the released molecules responsible for the mass variation of the sample [5].

At the ITQ, The acquisitions were carried out on the following equipment:

- a STA 409 Netzsch thermobalance equipped with a S-type thermocouple (T_{\max} : 1500 °C) for 50 μ L ceramic crucibles, under a 60 mL.min⁻¹ flow of nitrogen-oxygen I (Air Liquide). The temperature gradient programmed was a 5 °C.min⁻¹ ramp from 20 °C to 1000 °C.
- a Mass Spectrometer ThermoStar from Balzers (0-300 amu), a quadripole type MS which transfer line was heated at 190 °C.

At the ICMCB, they were performed on:

- a Setaram TAG 2400 symetrical thermobalance in DSC 1500 °C configuration for 100 μ L ceramic crucibles, under a 50 mL.min⁻¹ flow of Argon Alpha n°1 (Air Liquide). The temperature gradient programmed was a 3 °C.min⁻¹ ramp from 20 °C to 800 °C.

Mass spectrometry were performed with a Mass Spectrometer ThermoStar from Balzers (0-300 amu), a quadripole type MS which transfer line was heated at 190 °C in both laboratory.

A.IV.8. Flame Ionization Detector (FID)

Combined with the PFPD, our Chromatograph is also equipped with a Flame Ionization Detector (FID) (Figure A.IV.2). FIDs are best for detecting hydrocarbons and other easily flammable compounds. They are very sensitive to them and response tends to be linear across a wide range of concentrations [6].

As the name suggests, analysis involves the detection of ions. The source of these ions is a small hydrogen-air flame. Sometimes hydrogen-oxygen flames are used due to an ability to increase detection sensitivity, however for most analysis, the use of compressed air is sufficient. The resulting flame burns at such a temperature that it pyrolyzes most organic compounds, producing positively charged ions and electrons [7]. In order to detect these ions, two electrodes are used to provide a potential difference. The positive electrode is the nozzle head where the flame is produced. The negative one (called collector plate) is positioned above the flame or surrounds it and a relatively high voltage is applied between the two electrodes to collect the ions that are formed and upon hitting the plate, induce a current. This current is measured with a high-impedance picoammeter and fed into an integrator. It

corresponds roughly to the proportion of reduced carbon atoms in the flame. The response of the detector is determined by the number of carbon atoms (ions) hitting the detector per unit time. This makes the detector sensitive to the mass rather than the concentration, which is useful as the response of the detector is not greatly affected by changes in the carrier gas flow rate.

However, one thing to note - even if not of great importance in our specific case - is that the FID detects oxidized carbon atoms in ion form. In organic species that already have oxidized carbons via the presence of oxygen, a weaker signal is given when the sample enters the detector because the oxidized carbons are not ionized as effectively as compared to compounds solely made of carbon and hydrogen. Functional groups such as carbonyl, alcohol, halogens, or amines are sources of these oxidized carbons, sometimes causing few if any ions. This points out one of the main drawbacks of using a FID to detect effluent as it comes off a gas chromatograph column. Another drawback of FID is that the sample is destroyed, making it impossible to use for further measurements. For this reason the FID is stage in series with the PFPD in our chromatograph.

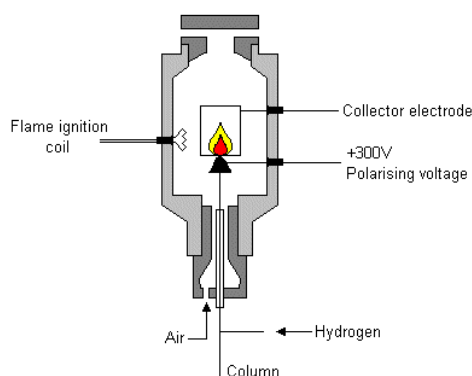


Figure A.IV.2: Scheme of a FID

The design of the flame ionization detector varies from manufacturer to manufacturer, but the principles are the same. The eluent exits the GC column and enters the FID. As the eluent travels up the FID, it is first mixed with the hydrogen fuel and then with the oxidant (Air). The effluent/fuel/oxidant mixture continues to travel up to the nozzle head where a positive bias voltage exists. This positive bias helps to repel the reduced carbon ions created by the flame pyrolyzing the eluent. The ions are repelled up toward the collector plate connected to a very sensitive ammeter (picoammeter) which detects the ions hitting the plates, then feeds that signal to an amplifier, integrator, and display system. The products of the flame are finally vented out of the detector through the exhaust port.

References

- [1] Speight, J. G. 20 – “Hydrotreating and desulfurization.” In: *The Chemistry and Technology of Petroleum*, Fourth Edition. CRC Press (Boca Raton, Fla.) **2006** 569–598
- [2] Grasset, F. “Propriétés structurales, magnétiques et catalytiques de nouveaux oxydes à base de ruthenium ou de platine à empilements mixtes dérivés de la structure perovskite.” Ph.D. thesis, Université de bordeaux 1 **1998**
- [3] Pecharsky, V. K. and Zavalij, P. Y. “Fundamentals of powder diffraction and structural characterization of materials.” Springer Science + business Media, Inc. **2005**
- [4] Rouquerol, F., Luciani, L., Llewellyn, P., Denoyel, R., and Rouquerol, J. “Texture des matériaux pulvérulents ou poreux.” *Techniques de l'Ingénieur - Techniques d'Analyse* **2003**. vol. P 1050, 1
- [5] Kaisersberger, E. and Post, E. “Practical aspects for the coupling of gas analytical methods with thermal-analysis instruments.” *Thermochimica Acta* **1997**. vol. 295, no. 1-2, 73 . “Coupling Thermal Analysis and Gas Analysis Methods”
- [6] McWilliam, I. G. and Dewar, R. A. “Flame Ionization Detector for gas chromatography.” *Nature* **1958**. vol. 181, no. 4611, 760
- [7] Holm, T. “Aspects of the mechanism of the Flame Ionization Detector.” *Journal of Chromatography A* **1999**. vol. 842, no. 1-2, 221

